

# **Local Buckling Response of Subsea Flexible**

## **Pipe**

By

©Alireza Ebrahimi

A thesis submitted to the

School of Graduate Studies

in partial fulfillment of the requirements for the degree of

**Doctor of Philosophy**

**Faculty of Engineering and Applied Science**

**Memorial University of Newfoundland**

**October 2016**

St. John's

Newfoundland and Labrador

## ABSTRACT

Applications of flexible pipe have been growing because of its characteristic features (i.e. low bending stiffness and high axial strength) which are because of various composite and steel layers have been used in the structure of this pipe. These characteristics make flexible pipeline capable to transfer oil and gas from wellhead to the fixed and floating platforms, or to inject water into the wells.

There are a number of technical and economic advantages for the use of flexible pipe with respect to conventional rigid line pipe. Rapid installation, typically 5 to 10 km per day, and special polymer material (i.e. elimination of needs for cathodic protection) suggest it may be used as a suitable option for installation in harsh environment fields. Furthermore, the pipe exhibits advantageous mechanical performance characteristics with respect to strength, collapse resistance, thermal expansion and vibration response, and fatigue and abrasion resistance.

Flexible pipe comprises of carcass and pressure armours which are interlocked layer wrapped with angle close to 90 degree and stand toward radial pressures; extruded polymer layers which prevents leakage of fluids to the other layers; high strength tape which are considered to prevent radial expansion of tensile armours; tensile armours which are rectangular cross section helical wires with pitch angle close to 35 degrees made by high strength steel to stand for axial and bending and torsional loads.

For deepwater flexible pipe systems, in response to local damage and loss of constraint, the tensile armour wires may exhibit two forms of local instability that includes radial buckling (i.e., birdcaging) and lateral buckling. These two failure modes may occur during installation or operational conditions due to pure axial compression and bending curvature.

Due to the complex mechanics for integrating the mechanical response of each layer and the corresponding interactions between adjacent layers, there are few analytical and numerical modelling studies addressing the mechanical performance of composite flexible pipe. These investigations are constrained by the underlying idealizations and assumptions used, and the available hardware and software technology. As the technology development and fabrication of flexible pipe is company-specific proprietary, intellectual property, there are few experimental studies available in the public domain. To improve knowledge, and potentially advance current engineering design and practice, it is important to develop a thorough understanding of the pipe mechanical response, strength performance limits and deformation mechanisms.

The main goals and major contributions in this thesis are the development and advancement of three-dimensional finite element modelling procedures investigating the local radial and lateral buckling of the tensile armour wires in flexible pipe. This investigation has provided new knowledge and insight, which is either incremental or unique, on these local instability mechanisms for tensile armour wires. The importance of using an implicit solver rather than the traditional use of an explicit solver has also been established. The simplifying assumptions of existing finite element and analytical models mostly have been improved and built sufficient reliability to be used for the different industrial practices.

The significance of pipe model characteristics (e.g., element type, topology, segment length), interlayer contact formulations, boundary conditions (i.e., natural, essential), interface friction, hydrostatic loads, damage condition, and curvature on the local instability mechanisms have been examined which is another unique step for consolidating the design standards.

## **Acknowledgement**

I would express my deepest gratitude to Dr. Shawn Kenny for his patient guidance, excellent advices and lessons which drastically improved my ability in researching and for his kind supporting in different aspects of my PhD program. I would like to thank him for allowing me to continue my study for three months in Iran and his unsparing financial support which helped me to have better focus in accomplishment of my PhD. I have learned invaluable points from him and benefited his knowledge and wise comments in every correspondence and meeting we had. He kindly spared his personal time to answer my questions and reviewing my documents in the shortest time.

Also, I would appreciate Dr. Amgad Hussein who supported me in different stages of my program as my co-supervisor. He has decent and kind nature and took care of all my concerns and facilitated my researching at MUN.

I appreciate Wood group Kenny for their financial support and providing expensive computational machines and software packages for our research group.

I am greatly indebted to my beloved family who gave me spiritual and material supports day and night and did not let me to feel alone even for a second. My family are the all asset I have and I am so proud of them.

To my mother Nasrin,

and

My father Mostafa.

## Table of Contents

1	Introduction .....	1
1.1	Background .....	1
1.2	Motivation and Objectives for Research.....	5
1.3	Methodology .....	6
1.4	Literature Review.....	8
1.5	Summary of Literature Review .....	13
1.6	Summary of Contributions.....	15
1.7	Thesis Outline .....	16
1.8	References .....	17
2	Finite element simulation of flexible pipe mechanical response- Challenges and solutions	24
2.1	Abstract .....	24
2.2	Flexible Pipe Technology.....	25
2.2.1	Overview.....	25
2.2.2	Analytical, Experimental and Numerical Modelling Studies .....	27
2.2.3	Motivation and Scope for this Study .....	30
2.3	Finite Element Modelling Procedures - Trials and Tribulations.....	30
2.3.1	Overview.....	30
2.3.2	Verification Basis.....	30
2.3.3	Modelling Constraints and Strategies .....	31

2.3.4	Material Behaviour .....	38
2.3.5	Contact Mechanics.....	39
2.3.6	Solution Procedures and Strategies.....	43
2.4	Preliminary finite element procedures – Radial buckling problem.....	46
2.4.1	Problem statement.....	46
2.4.2	Model parameters and numerical procedures .....	46
2.4.3	Results.....	49
2.5	Conclusions .....	55
2.6	References .....	56
3	Radial buckling of tensile armour wires in subsea flexible pipe – numerical assessment of key factors.....	61
3.1	Abstract .....	61
3.2	Introduction .....	62
3.3	Finite Element Modelling Procedures and Sensitivity Matrix.....	64
3.4	Results and Discussions .....	71
3.4.1	Global Comparison with Physical Model Data .....	71
3.4.2	Effect of Hydrostatic Pressure .....	77
3.4.3	Effect of Pipe Damage .....	86
3.4.4	Effect of Internal Hydrostatic Pressure.....	90
3.5	Conclusion.....	92

3.6	References .....	94
4	Elastic instability in tensile wires of subsea flexible pipe under axisymmetric loads.....	97
4.1	Abstract .....	97
4.2	Introduction .....	98
4.3	Finite Element Model.....	103
4.4	Results and Discussions .....	108
4.4.1	Pure Torsion with two different BCs .....	108
4.4.2	Friction coefficient assessment .....	116
4.4.3	Pure Tension .....	117
4.4.4	Torsion added to Tension.....	118
4.4.5	Effect of Internal and External Pressure .....	121
4.5	Conclusion.....	124
4.6	Reference.....	126
5	Combined mode shapes of lateral buckling and radial buckling-Parameters influencing birdcaging mechanism for subsea flexible pipe.....	130
5.1	Abstract .....	130
5.2	Introduction .....	131
5.3	Finite element modelling procedures and sensitivity matrix .....	133
5.4	Results and discussions .....	136
5.5	Conclusion.....	145

5.6	References .....	146
6	Lateral buckling of tensile armour wires in subsea flexible pipe- finite element assessment using Implicit solver .....	149
6.1	Abstract .....	149
6.2	Introduction .....	150
6.3	Finite Element Model.....	153
6.4	Results and discussions .....	159
6.4.1	Main model simulation and validation .....	159
6.4.2	Parametric study on initial curvature .....	167
6.4.3	Parametric study on friction coefficient.....	172
6.4.4	Critical curvature of flexible pipe .....	179
6.5	Conclusion.....	184
6.6	References .....	185
7	Conclusions and recommendations .....	188
7.1	Overview .....	188
7.2	Conclusions .....	188
7.2.1	Literature review.....	189
7.2.2	General modelling procedures .....	189
7.2.3	Radial buckling or birdcaging.....	189
7.2.4	Elastic instability.....	190

7.2.5	Lateral buckling .....	191
7.3	Recommendation for future studies .....	192
8	Appendix A: General Python Code .....	195

## List of Figures

Figure 1-1. General view of flexible flowline, Secher <i>et al.</i> [14].	3
Figure 1-2. Radial buckling (Birdcaging) in flexible flowline. Secher <i>et al.</i> [14].	4
Figure 1-3. Lateral buckling in flexible flowline, Secher <i>et al.</i> [14].	4
Figure 2-1. Cross section of unbounded flexible pipe.	26
Figure 2-2. Radial buckling (Birdcaging) in tensile wires of flexible pipe	28
Figure 2-3- Singularity caused by severe contact pressure.	36
Figure 2-4. Extremely deformed nodes close to boundary condition.	37
Figure 2-5. Accurate contact modeling performed by Implicit solver.	44
Figure 2-6. Inaccurate contact modeling performed by Explicit solver.	44
Figure 2-7. Global axial reaction force versus axial shortening in buckling of tensile armours of flexible pipe	45
Figure 2-8. Layers and element distribution in the cross section.	48
Figure 2-9. Coupling of the all layers to a reference node.	49
Figure 2-10. Smooth contact pressure around the birdcaging zone.	51
Figure 2-11. Contact penetration is avoided by means of Equilibrium check.	52
Figure 2-12. Stress concentration is avoided at the boundary condition by using a reference node.	52
Figure 2-13. Global axial force versus global axial shortening measured at the reference point.	53
Figure 2-14. Global axial force versus global twist measured at the reference point.	54
Figure 2-15. Global axial force versus global axial shortening (comparison between different models).	54
Figure 2-16. Global axial force versus global twist (comparison between different models).	55

Figure 3-1. Layers and element distribution in the cross section .....	67
Figure 3-2. Modeling wrapping of anti-birdcaging tape around the pipe.....	69
Figure 3-3. Contact pressure contour caused by anti-birdcaging tape wrapping procedure.....	70
Figure 3-4. The pipe after bird-caging (Radial buckling).....	72
Figure 3-5. Global axial force versus axial strain at the reference point. ....	73
Figure 3-6. Global axial force versus twist per unit length at the reference point.....	73
Figure 3-7. Global axial compression versus normalized axial stress in mid of the tensile armours. .....	76
Figure 3-8. Local compressive strain versus global axial shortening per unit length.....	77
Figure 3-9. Global axial force versus displacement per unit length at the reference point for different external pressures. ....	78
Figure 3-10. Global axial force versus twist per unit length at the reference point for different external pressures.....	78
Figure 3-11. Global axial force versus local radial expansion at the mid length of the pipe for different external pressures. ....	80
Figure 3-12. Local compressive strain versus global axial shortening per unit length.....	80
Figure 3-13. Global axial force versus local twist at the mid length of the pipe for different external pressures.....	82
Figure 3-14. Global axial compression versus axial stress in mid of the external armours. ....	83
Figure 3-15. Global axial compression versus axial stress in mid of the internal armours. ....	84
Figure 3-16. Influence of external hydrostatic pressure on axial buckling force, axial strain and torsional response.....	85
Figure 3-17. Influence of external hydrostatic pressure on the effective stiffness behaviour .....	86

Figure 3-18. Damaged area applied in the middle of pipe length.....	87
Figure 3-19. Global axial force versus axial shortening per unit length at the reference point for different damage lengths.....	89
Figure 3-20. Global axial force versus twist per unit length at the reference for different damage lengths.....	89
Figure 3-21. Global axial force versus global axial shortening under various internal pressures.	91
Figure 3-22. Global axial force versus global axial twist under various internal pressures. ....	92
Figure 4-1. Cross-section of flexible pipe [1].....	99
Figure 4-2. Layers and element distribution in the cross section. ....	106
Figure 4-3. Direction of positive twist moment which tend to untwist the external tensile armours. .....	108
Figure 4-4. Twist moment versus twist angle per unit length versus. ....	112
Figure 4-5. Twist moment versus local radial displacement in different layers.....	114
Figure 4-6. Twist moment versus local tangential displacement in two tensile armour layers..	114
Figure 4-7. Twist moment versus local axial displacement (end free to elongate BC).....	115
Figure 4-8. Twist moment versus normalized von Mises stress at the middle of tensile armours. .....	116
Figure 4-9. Twist moment versus twist angle per unit length for different friction factors. ....	117
Figure 4-10. Axial force versus axial deformation per unit length.....	119
Figure 4-11. Global axial force versus global axial rotation in end-free to rotate.....	119
Figure 4-12. Global axial force versus global axial reaction moment in end-constrained to rotate. .....	120
Figure 4-13. Torsion versus twist per unit length. ....	121

Figure 4-14. Torsion versus twist per unit length under 10 MPa of internal pressure. ....	123
Figure 4-15. Torsion versus twist per unit length under 5 MPa of external pressure.....	123
Figure 5-1. The introduced rupture in external plastic sheath and anti-birdcaging tape. ....	136
Figure 5-2. The flexible pipe after occurrence of birdcaging. ....	137
Figure 5-3. Tangential and radial buckling in external tensile armours. ....	138
Figure 5-4. Tangential and radial buckling in internal tensile armours.....	138
Figure 5-5. Global axial force versus global shortening in three different approaches.....	141
Figure 5-6. Global axial force versus global axial twist per unit length.....	142
Figure 5-7. Global axial force versus global axial shortening for different rupture length.....	143
Figure 5-8. Global axial force versus global axial bending.....	144
Figure 5-9. Global axial force versus global axial twist per unit length.....	145
Figure 6-1. Cross section of unbounded flexible pipe [2]. ....	151
Figure 6-2. Lateral buckling in tensile wires [3].....	151
Figure 6-3. Axial compression is applied on the initially curved pipe. ....	157
Figure 6-4. Cross section of the modeled flexible pipe. ....	158
Figure 6-5. FE model designed based on the analytical assumptions.....	162
Figure 6-6. Schematic comparison of buckling in analytical model and a real pipe. ....	163
Figure 6-7. Global axial force versus global axial shortening.....	165
Figure 6-8. Global axial force versus global axial twist per unit of length. ....	166
Figure 6-9. Global axial force versus aspect ratio of shear stress.....	167
Figure 6-10. Global axial force versus slip in external tensile wire. ....	167
Figure 6-11. Global axial compression versus strain in the 5-m length pipe with different initial curvature. ....	169

Figure 6-12. Global axial compression versus strain in the 1.25-m length pipe with different initial curvature. ....	170
Figure 6-13. Global axial compression versus twist in the 5-length pipe with different initial curvature. ....	171
Figure 6-14. Global axial compression versus twist in the 1.25-length pipe with different initial curvature. ....	171
Figure 6-15. Global axial force versus strain for different friction coefficients under no initial curvature. ....	174
Figure 6-16. Global axial force versus twist for different friction coefficients under no initial curvature. ....	175
Figure 6-17. Global axial force versus strain for different friction coefficients under R=11 m. ....	176
Figure 6-18. Global axial force versus twist for different friction coefficients under R=11 m. ....	176
Figure 6-19. Global axial force versus strain for the model with R=11, L=1.25 m and friction coefficient =0.025. ....	177
Figure 6-20. Global axial force versus twist for the model with R=11, L=1.25 m and friction coefficient =0.025. ....	177
Figure 6-21. Schematic comparison of lateral buckling of tensile wires in wet annulus condition, between a real pipe in field [3] and FE model (i.e. L=1.25m, R=11 m, wet condition, friction Cof.=0.025).....	178
Figure 6-22. Schematic of flexible pipe installation, [12]. ....	179
Figure 6-23. The boundary conditions of the bending limit analysis. ....	180
Figure 6-24. The pipe after imposing load condition. ....	182
Figure 6-25. Curvature versus axial twist in different load cases. ....	182

Figure 6-26. Curvature versus axial twist in load case 3..... 183

List of Tables

Table 2-1. Material and element specifications of each individual layers, [6]. ..... 46

Table 2-2. Time expense of each solution method. .... 55

Table 3-1. Characteristics of each individual layer. .... 65

Table 3-2. Buckling force in the FE model and model test. .... 74

Table 3-3. Buckling force in different designed damages. .... 90

Table 3-4. Rate of compression in respect to axial force and twist per unit length..... 90

Table 4-1. Characteristics of each individual layer. .... 104

Table 4-2. Torsional stiffness for the FE and analytical approach. .... 113

Table 4-3. Axial stiffness in two considered boundary condition for both experiment and FE model..... 120

Table 4-4. Torsional stiffness for the unpressurized pipe, internally and externally pressurized pipe. .... 124

Table 5-1. Characteristics of each individual layer. .... 134

Table 5-2. Buckling force in the FE model and model test. .... 140

Table 6-1. Characteristics of each individual layer. .... 154

Table 6-2. The boundary conditions of the pipe. .... 158

Table 6-3. Comparison of the axial stiffness between analytical model and FE model including assumptions..... 161

Table 6-4. Comparison between characteristic features of laboratory and FE analyses. .... 165

Table 6-5. Comparison between characteristic features of models with various initial curvature and lengths. .... 169

Table 6-6. Comparison between characteristic features of models with various initial curvatures and lengths. ....	173
Table 6-7. Comparison between axial stiffness of the model with $R=11$ , $L=1.25$ m and friction coefficient $=0.025$ . ....	173
Table 6-8. Load cases considered for bending limit analyses. ....	180
Table 6-9. Critical curvature (i.e. buckling point) at the different load cases. ....	183

# **1 Introduction**

## **1.1 Background**

Composite or hybrid offshore pipeline systems were first developed during the 1940's in support of military activities during the Second World War. This technology has been refined over the past 40 years for use as flexible riser systems, flowlines, offloading lines, fluid transfer lines, jumpers and umbilicals. The flexible pipe can be characterized by a low bending stiffness with high axial stiffness where a series of concentric metallic and polymeric layers build the pipe cross-section and define the mechanical performance Figure 1-1. The key advantages of flexible pipe include the ease of handling, storage transportation and installation, and operation performance with respect to permanent connections between subsea infrastructure and surface vessels with large motions. On the Grand Banks, these flexible pipe systems are used as flowlines on the Terra Nova and White Rose field developments.

Engineering assessment on the mechanical performance of these composite flexible pipe systems has been generally limited to idealized treatment of the cross-sectional behaviour through global structural analysis methods using analytical and computational frameworks [1-7]. The primary motivation for adopting this approach lies in the significant complexity to simulate the complex interaction between multiple layers, for static loading cases, and the intensive computational resources that would be required to conduct time domain and frequency domain analysis of risers systems subject to dynamic offshore environmental loads. Software programs (e.g. Flexcom, Abaqus) have developed numerical algorithms addressing this industry need.

The majority of flexible riser systems are less than 273 mm diameter within water depths less than 1000 m and operational conditions of less than 34.5 MPa design pressure and 80 °C design temperature [8]. Although the scope and use of flexible pipe systems in deepwater developments is expanding, the mechanical behavior for these environments is not fully developed. This is due to the complex response and interaction between multiple layers within the pipe system that introduces significant difficulties and constraints into the engineering analysis. As future developments look to extend the use of this technology to greater water depths and more harsh operating conditions there is a need to develop advanced computational tools that can evaluate the mechanical integrity of these complex hybrid pipe systems. Advancements in computational hardware and software have provided a platform to develop these simulation tools for combined loading, external pressure collapse and fretting [8-11]. For deepwater flexible pipeline systems, there is the potential for local failure mechanisms that include radial (i.e. “bird caging”) Figure 1-2 and lateral buckling modes [12-15], Figure 1-3.

The main target in this dissertation is the modeling of local buckling of tensile armours and providing an optimum model (i.e. model accuracy and time expense) which can be used for further study of which. The local buckling in wires is categorized into two main mode shapes. The first mode shape is called birdcaging or radial buckling in which anti-birdcaging tape is failed and the tensile wires are prone to have radial displacement under axial compression because of low moment of inertial in radial direction. The second mode happens when the anti-birdcaging is not damaged and it can still contain radial displacement. In this condition the wires move tangentially on supporting surface. This mode is called lateral buckling. Because of the complexity of the pipe structure, besides physical model test, the finite element method can be a potential way of precise modeling of buckling of tensile armours. Experimental approach is the most reliable solution,

although it is not doable to study physical model test or its parametric study, due to the test expense and manufacturers' authorization. Recent advancement on the finite element softwares (e.g. contact interaction modeling, accuracy check and material definition) and also improvement on the computing machines (e.g. multi-processor machine), make the finite element method as trustworthy and reasonable simulating method for analysis and design of a complex structure of flexible pipe.

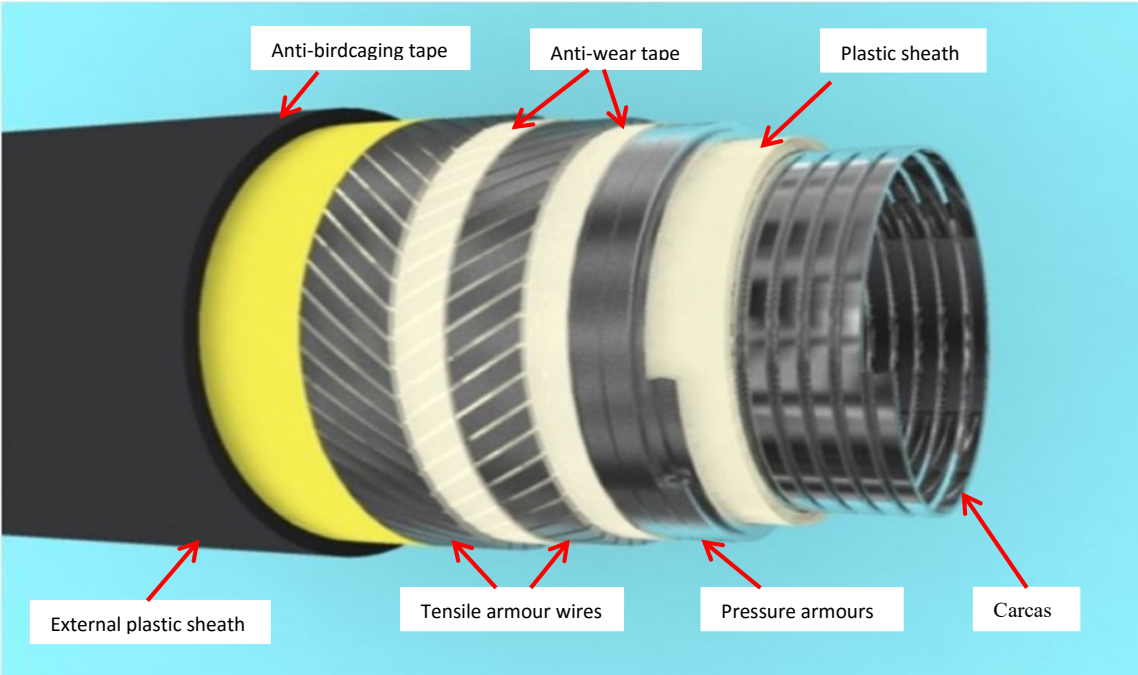


Figure 1-1. General view of flexible flowline, Secher *et al.* [14].



Figure 1-2. Radial buckling (Birdcaging) in flexible flowline. Secher *et al.* [14].



Figure 1-3. Lateral buckling in flexible flowline, Secher *et al.* [14].

## 1.2 Motivation and Objectives for Research

Failure modes (radial and lateral buckling) in both operation and installation might happen due to excessive bending curvature and axial force while there are still many uncertainties with mechanical performance of flexible pipe and the critical circumstances in which local buckling in tensile armours happens. A reliable method is needed to provide simulation of local buckling with minimum of assumptions to improve design standards.

According to the background, it is obvious that flexible pipe mechanical response is not well known especially for case of local buckling in tensile armours. Besides few experimental studies, which due to financial expenses, were implemented solely under specific conditions, without any evaluation on the key factors, most of the previous studies were analytical works including so many assumptions in order to facilitate the simulation of this complex structure. The necessity of knowledge on the mechanism of local buckling in tensile wires, asks for a method targeting both accuracy and financial expenses.

So this requires to have detailed nonlinear FE modeling of local buckling in which the idealization of analytical method are eliminated or minimized while the simulation can be extended to cover areas which have been unknown by now for physical model tests (e.g. material, imperfection and water depth).

The objectives of this thesis can be categorized into three main stages. In the literature review section, the author tries to give thorough understanding on the researches which were accomplished till now and elaborate the advantages and drawbacks of each individual method. In the next section, as the finite element modeling of flexible pipe possesses its own challenges, the challenges and solutions for them will be discussed through. In third section, an advanced

numerical modelling procedures will be developed to assess the potential for local failure mechanisms such as radial and lateral buckling in composite flexible pipe systems for deepwater applications. The numerical modeling will also be extended for assessment of the series of analysis under axisymmetric loading in which the tensile wires may not buckle, while the uncertainties of the mechanical performance still remain. The numerical modelling procedures can be extended to examine other mechanical integrity issues for flexible pipe systems such as external pressure collapse and effects of corrosion on fatigue life.

### **1.3 Methodology**

The literature review will assess existing practice and future trends for the use, analysis and design of flexible pipeline systems in offshore environment. The lessons learned, knowledge established, technology gaps, constraints and opportunities would be identified, distilled and disseminated. This will provide focus on the technical issues and directed outcomes from the research program. The input parameters, physical and material properties, viable technical approaches and solutions, and potential technical issues and constraints will also be established. The literature review will identify the geometric (e.g. diameter, thickness) and material properties (e.g. elastic modulus, ultimate strength) of the individual layers within the composite flexible pipe system that will provide the technical basis for developing the numerical modelling procedures. Having excellent understanding on material and geometry is so vital in this type of pipe, because of assumptions and idealizations that need to be integrated within the modelling procedures in order to reduce the effort, time and cost for these simulations.

The primary simulation tools will be Abaqus and Python. Guided by other studies, this task will examine the importance of element type (e.g. shell versus solid), mesh topology (e.g. fine versus coarse density) and simulation framework (e.g. static versus coupled Eulerian/Lagrangian). The

appropriate constitutive models (e.g. isotropic, anisotropic, orthotropic, nonlinear kinematic hardening) and interface properties (e.g. static and kinetic friction coefficients, maximum interface shear stress) for each layer will be evaluated. The main goal in developing detailed models is simulation of birdcaging and lateral buckling with minimum of assumptions. Simulation of these two modes of buckling by examination in wide range of key parameters will be presented. Besides, other models will be developed to evaluate some critical situations that may not lead to buckling, though those can cause other probable failure modes because of tension and/or other load combinations. This type of simulation will be carried out with same parametric study.

The integration of experimental modelling within this thesis study is not possible due to constraints on the lack of access to flexible pipe test segments that is associated with proprietary nature of the flexible pipe technology. Consequently, verification of numerical modelling procedures developed in this thesis will be established through comparison of elastic behaviour with vendor specification on flexible pipe mechanical performance for axial, bending and torsional loading conditions. Further confidence in the numerical modelling procedures developed in this study will be acquired through comparison with sparse data in the public domain literature, which includes analytical solutions, and limited experimental and numerical modelling simulations. The existing analytical results are the alternate option for validation. Through validation process of each study, a comprehensive discussion will be provided to explain the underlying reasons of any discrepancy and the uncertainty.

A sensitivity analysis will examine a range of practical design conditions to assess the effects of these parameters on the local buckling response (i.e. radial and lateral). Key factors influencing the response will be established, categorized within non-dimensional parameters and the load effects synthesized. Using nonlinear, multivariate regression analysis techniques, the development

of an engineering tool will be explored that may include the advancement of engineering design equations, charts and tables.

#### **1.4 Literature Review**

There are few studies examining the local buckling phenomenon of the tensile armour wire. These studies were accomplished through three main approaches, physical model tests (i.e. laboratory or deep immersion tests in sea), numerical approaches which mostly were implemented by FE (i.e. continuum or structural element methods), and analytical approaches. In this section, all literature which are relevant to the scope of current study are discussed through and advantages and drawbacks of which are elaborated. Since some of these studies investigated local buckling through two different approaches (i.e., for validating their main approach) the literature review is not categorized based on the methodologies.

Braga *et al.* [16] prefers to make a physical test at laboratory rather than deepwater immersion test which is too expensive. Some simplifications were used in test facilities which allow to produce equivalent axial pressure of 2000 m depth on the model without using hyperbaric chamber or watertight connectors. Two models which are a flexible riser and flowline were tested. Although, the paper presents a unique series and solid experimental tests, it lacks of enough results for readers.

Ostergaard *et al.* [17] presents an analytical approach for lateral buckling of tensile armour layers under cyclic bending and compression which may happen through installation procedure. This is such a solid analytical solution for lateral buckling. This paper is supported with experimental results as validation. Furthermore, it can calculate lateral buckling response for different imperfections in wires. It is mentioned in the paper that it is needed to have more physical tests to

evaluate friction factors which can trigger the lateral buckling. Tan *et al.* [18] presents an analytical solution by developing total strain energy for modeling buckling in tensile armour wires. This paper provides result and discussion of a series of DIP test, full scale deepwater immersion, implemented by Wellstream. This study was carried out to test flexible pipe for qualification in depth more than 2000 m. The driver for this series of tests was the development and evolution of some fields for depth of 2500 m and 2700 m.

In a numerical study, Vaz and Rizzo [19] developed finite element model procedures to examine the bird-caging phenomena. Their study included idealizations to address the computational effort and difficulties for modeling the discrete components of a flexible pipe cross-section. For example, only two wires, represented by spring elements, were used to represent the inward and outward radial deformation modes for the external and internal armour wires, respectively. A parameter study examined the effects of external pressure and interface friction on the potential for bird-caging mechanism to develop. Although, their study suffers many simplifications like lack of contact interactions between armour wires, it provides a sensitivity study on key parameters like external and internal pressures.

Experimental studies conducted by de Sousa [20] provide the basis for developing the numerical modelling procedures in this study. Physical tests on a 2.5 m length of 4” flexible pipe subject to axial compression were conducted. Continuum finite element modelling procedures were also developed using ANSYS software package. This study is as a significant step in modeling birdcaging behaviour both numerically and experimentally. The model includes most details of a real pipe. It is said that contact interactions are included. The results of numerical simulation show excellent consistency with results of physical tests. But, there are many ambiguities in the paper. Imperfection is essential for buckling of any structure, though it is not mentioned that what kind

of imperfection is imposed on neither in numerical model nor in real model. Also, the effect of key factors such as external or internal pressure is not studied.

Serta *et al.* [21] developed a full-3D finite element method in ABAQUS in which the inner layers are modeled as a homogenous layer while interacting with other layers. Tensile armours and exterior layers are separately modeled and Explicit solver is employed. This FEM study is supported by a laboratory test. The Explicit method is not supposed as unconditional stable solver. This might be the reason of significant discrepancy between the results of FE and experiments.

Many previous studies are implemented on the axisymmetric load conditions which do not target local buckling and those are mostly accomplished to address some severe loading conditions.

Torsional failure mechanism happens under pure axial torsion or combined with tension. Bahtui *et al.* [22] investigated 8" diameter pipe under separate load cases. In this study, the pipe is pre-stressed by internal and external pressure. In the next step, he examined the pipe under different load cases which are tension, torsion and bending. They employ explicit solver of ABAQUS to validate their analytical approach. The comparison shows high consistency, although the analyses are all in linear domains and does not include buckling phenomena. The other issue which comes to reader is that how the analytical approach can have high consistency with FE results while the pipe is unbounded and there are relative displacements between layers. De Sousa *et al.* [23] studied the response of flexible pipeline to the pure torsion in both experimental and numerical approaches. Also, he compared the results of pure torsion with tension to examine the effect of tension on torsional behavior. His work can be such a reliable resource for further study, as it is supported with all three methods. For further study, one can mimic all de Sousa has done and in addition complementary analysis's like assessment of friction factors in torsion and tension and also effect

of tension on torsion and vice versa or the other issues which worth to be considered. In another work by de Sousa [24], a 2.5” flexible pipe is examined under axisymmetric load conditions. Pure tension, tension combined with torsion and internal pressure are the load cases which are evaluated through his series of numerical works. He validates his FE model with a series of experiments for same those types of load conditions. Most of studies by de Sousa are valuable resources for further studies. The all of his studies can be extended and modified through analyses with more details or parametric studies like friction coefficients or external and internal pressure. De Sousa *et al.* [25] studies a finite element model of a flexible riser. The results of tensile load case in finite element model are compared with existing similar analytical one. Also, the finite element model is analyzed under compression. Ramos *et al.* [26] proposes an analytical method to estimate stress and deformation components in flexible riser which is imposed by combined loads, bending, twisting and tension. The results of the analytical approach are compared with previous experimental studies. Corre *et al.* [27] evaluates created moment under tension load case. This moment is named friction moment caused by friction between internal layers. The finite element model is compared with similar experimental work. Bahtui *et al.* [28] combines different analytical approaches for response of the flexible pipe under tension. Also, the paper compared the analytical results with results of finite element analyses using explicit solver of ABAQUS. Ramos *et al.* [29] presents main results of torsional-axial test on a 2.5” flexible riser implemented in Technological Research Institute of Sao Paulo and compares physical test results with analytical approaches. The other study on Bird-caging is carried out by Serta *et al.* [30]. In this study a finite element work is compared with physical test. Also, he developed a new approach of modeling, GUI customization for simple modeling, by simplification of outer layers like tensile armours, plastic sheath and anti-birdcaging tape. The finite element work is supported by experimental tests as validation, though

it uses explicit dynamic solver of ABAQUS. This solver takes more error into account in contact dominated simulation. In another study, Implicit and Explicit are employed by Edmans *et al.* [31] to calculate stress state in metallic and polymeric layers of pipe. The finite element results are validated by existing analytical solution. Bahtui *et al.* [32] validated his new analytical solution with explicit solver of ABAQUS. His analysis was carried out in three load cases, tension, torsion and bending. Studies of Edmans *et al.* [31] and Bahtui *et al.* [32] are mainly analytical works which to calculate different parameters in linear domain and those cannot be interpreted as new finite element solution for highly nonlinear issues. Leory *et al.* [33] considered three models by different approaches. In his first model, he used analytical solution in a simplified model, while for second model which has more details, he took advantage of Implicit solver of ABAQUS. In third model, he took all contact details of a full length model into account, and in this way used explicit solver of ABAQUS. In this study it is tried to model end-fitting in cyclic bending. The result of the FE simulation is compared with their experimental tests. Although, their model takes into account details of contact interactions and boundary conditions and it considers new parameter which is curvature of the pipe, it employs explicit solver. As it is explained earlier the explicit integration method cannot be completely successful in modeling of contacts. Some other studies have been carried out. De Sousa *et al.* [34] presents a 3-D finite element model of flexible riser response to loads imposed by hydraulic collar. The interaction between armours and hydraulic collar is modeled and stresses and strains are calculated.

Brack *et al.* [35] describes three main steps of the R&D program which are 1) improvement of computational tools, 2) new strategy for structural analysis under more realistic conditions, 3) review of implemented theoretical and experimental results.

## 1.5 Summary of Literature Review

The analytical solutions have provided a computationally efficient framework to examine the effects of combined, axisymmetric loading conditions (e.g. compression, tension, external or internal hydrostatic pressure, torsion) and predict the mechanical response of flexible pipe. Early studies extended engineering models simulating the behaviour of cables, ropes and strands. These approaches, however, were constrained by the underlying idealizations that limited the completeness and rigour of these prediction methods. For example, the methodologies assumed uniform geometry (e.g. homogeneous layers, no imperfections), simplified kinematics and boundary conditions (e.g. constant pitch angle or loxodromic configuration, slip occurs along loxodromic curve, no ovalization, uniform elongation and angle of twist for all layers), loading conditions (e.g. contact forces represented by uniform pressure), and mechanical response (e.g. linear elastic material properties with small strain behaviour) and contact mechanics (e.g. uniform contact pressure, no friction between layers, fully bonded interface without slip, no gaps or over-penetration). As shown later in this study, the idealizations incorporated within these analytical models cannot address local deformation mechanisms (e.g. opening and closing of the helical armour wires) when subject to loading conditions having the same amplitude but different sense. Some of these early studies, however, did recognize the importance of complex interactions that may influence mechanical response such as the influence of intra- and inter-layer contact mechanics (e.g. gap opening and closure, variable contact pressure and interface shear stress, interface friction) on nonlinear pipe response (e.g. stiffness, moment-curvature response due to relative slip) or lateral buckling mechanisms (e.g. transverse constraints and motion for behaviour based on single wire type models).

Experimental studies have been conducted to provide physical basis for understanding the complex mechanical response and interaction of flexible pipe for specific test conditions (e.g. loads, boundary conditions) and hypothesis (e.g. effect of damage on radial buckling), and the calibration of analytical and numerical models. Due to the proprietary nature of the flexible pipe technology, these experimental studies often lack the sufficient detailed information on the test configuration (e.g. boundary conditions, test frame and pipe stiffness), material and mechanical properties (e.g. stress-strain relationships), and pipe condition (e.g. damage state, imperfections). For example, in the study by de Sousa *et al.* [23], a 63.5 mm (2.5”) flexible pipe is examined under axisymmetric load conditions for pure tension, tension combined with torsion and internal pressure. The data was used to develop and calibrate finite element modelling procedures, however, there was insufficient data reporting (e.g. lack of local measurements or details on the solution procedures) where third parties could use this dataset for verification or calibration studies.

In comparison with the analytical methods, these numerical procedures provide an enhanced capability to simulate the mechanical response of flexible pipe. However, the modelling procedures developed may have inherent constraint or limitations depending on the element topology and geometric considerations (e.g. imperfections or damage), numerical procedures to model contact (e.g. springs, intra- and inter-layer frictional behaviour, distributed contact interactions, and gap or separation development), and algorithms to solve the nonlinear equations of motion (e.g. implicit or explicit solver).

Most numerical modelling studies, using finite element methods, investigating the mechanical response of flexible pipe have adopted an explicit scheme to solve the equations of motion. The explicit solution is generally selected for dynamic impulse and stress wave propagation problems where the solution is conditionally stable based on the minimum critical time step. The critical

time step is a function of the element size, elastic material properties and local changes in stiffness (e.g. variation in components, plasticity, incompressibility), and stress wave speed. For flexible pipe simulations, the critical time step is on the order of  $10^{-7}$  s to ensure unconditional stability of the solution (i.e. not encounter drift or divergence). The explicit solver can also be used to mitigate severe discontinuities associated with the large number of contact interactions between multiple element layers. However, one of the more significant issues is the explicit method does not enforce equilibrium conditions with respect to the balance of residual forces, which can be significant when examining nonlinear behaviour (e.g. plasticity, contact). Although implicit solvers are generally used to solve static, quasi-static and structural vibration problems, the explicit solver has been used to address numerical difficulties associated with complex nonlinear contact conditions. The implicit scheme, however, is unconditionally stable, performs equilibrium checks and updates the stiffness matrix due to nonlinear behaviour (e.g. geometry, material) following each iteration. In different stages of current study the use of an implicit scheme demonstrated an improved solution to predict the kinematics and bifurcation response of the tensile armour wires.

## **1.6 Summary of Contributions**

The major contribution of this thesis is the development of an improved three-dimensional nonlinear finite element model to investigate the local buckling (i.e. radial and tangential instabilities) in tensile wires of flexible pipe. This thesis will provide through understanding on the local buckling of flexible pipe by comprehensive investigation on the local instabilities in tensile wires; establish new insights in mechanism of flexible pipe through assessment of the new conditions and measurement of the local and global parameters; and introduce new terms (e.g. clamping area) which can help to have better understating over behavioural pattern in similar conditions. The underlying reasons of the importance of using implicit method in modeling

flexible pipe and particularly local buckling will be clarified and its advantage and drawbacks in respect to the traditional method (i.e. explicit solver) will be elaborated. This study will improve existing design standards for subsea flexible pipe by demonstration on the significance of pipe model characteristics (e.g., element type, topology, segment length), interlayer contact formulations, boundary conditions (i.e., natural, essential), interface frictions, hydrostatic loads, damage conditions, and curvatures on the local instability mechanisms.

## **1.7 Thesis Outline**

This thesis is compiled in seven chapters. The major outcome of this thesis will be presented as four journal papers and a conference paper which are brought in five different chapters separately (i.e. chapter 2 to 6), and in appendix a python code is provided that can be modified for any simulation of flexible pipe.

- Chapter 1 is spared to introduction over the topic of study, motivations for doing current study and also contributions and improvements which are made by this thesis.
- Chapter 2 describes challenges of FEM of flexible pipe in which the author tries to give well understanding upon the issues that an engineer might face through modeling of flexible pipe.
- Chapter 3 concerns the radial buckling (birdcaging) of tensile wires and assessments of key factors.
- Chapter 4 is an investigation of the pipe under axisymmetric load cases to spot instability in tensile wires. This chapter tries to highlight mechanical performance of the flexible pipe under tension, torsion and combination of these two load cases and assess any elastic or plastic instability in tensile wires.

- Chapter 5 is a conference paper which is supplementary study for chapter 2 and a pre-study on lateral buckling of flexible pipe (chapter 6). This chapter tries to give understanding on the role of bending on lateral buckling and produce a mixed mode shapes (i.e. radial and lateral buckling) by means of rupture in anti-birdcaging tape and plastic sheath.
- Chapter 6 comprises simulation of lateral buckling in tensile wires and a comprehensive study on key factors (i.e. friction coefficient and initial curvature) and simulation of lateral buckling of wires in installation procedure of the flexible pipe.
- In chapter 7, overall conclusion over different chapters and also recommendation for future study are presented.

Besides these publications which are presented as journal and conference research papers in different chapters of this dissertation, the compiled python script will be as a solid platform to facilitate further study whether concerning buckling issues or other phenomena as current model development possess capability and adjustability to be employed for other applications and load cases (e.g. VIV, fatigue analysis).

## **1.8 References**

- [1]. Behar, I. (1974). "Use of Coflexip flexible lines in the oil industry." Proceedings of OTC-1970, 8p.
- [2]. Oliveira, J.G., Goto, Y. and Okamoto, T. (1985). "Theoretical and methodological approaches to flexible pipe design and application." Proceedings of OTC-5021, 10p.
- [3]. Mahoney, T.R. and Bouvard, M.J. (1986). "Flexible production riser system for floating production application in the North Sea." Proceedings of OTC-5163, 10p.

- [4]. Sun, L. and Qi, D. (2011). "Global analysis of a flexible riser." *Journal of Marine. Science* 10: 478-484.
- [5]. Karve, S., O'Brien, P.J., McNamara, J.F. (1988). "Comparison of dynamic response of alternate flexible riser products." *Proceedings of OTC-5796*, 8p.
- [6]. Out, J.M.M. "On the prediction of the endurance strength of flexible pipe." *Proceedings of OTC-6165*, 10p.
- [7]. Connaire, A., O'Sullivan, E. Carr, T. and Witton, M. (2008). "Advancements in methods for quantifying energy dissipation in unbonded flexible pipe." *Proceedings of OTC-19705*, 19p.
- [8]. Bahtui, A., Bahai, H and Alfano, G. (2009). "Numerical and analytical modeling of unbonded flexible risers". *Journal of OMAE*, 134:13p.
- [9]. Neto, A.G. and Martins, C.de A. (2012). "A comparative wet collapse buckling study for the carcass layer of flexible pipes", *Journal of OMAE* 134:9p.
- [10]. Fernando, U., Leyland, J., Graham, G. and Sheldrake, T. (2011). "Prevention of fretting/wear damage in pressure armour layers of flexible pipes designed for high pressure applications." *Proceeding of OTC-22245*, 10p.
- [11]. Clevelario, J., Falcao, G. , Tan, Z., Lu, J. and Sheldrake, T. (2010). "Flexible pipe curved collapse behaviour assessment for ultra deepwater developments for the Brazilian pre-salt area." *Proceedings of OTC-20636*, 11p.
- [12]. O'Brien, P., Overton, C., Picksley, J., Anderson, K., Macleod, I. and Meldrum, E. (2011). "Outcomes from the SureFlex Joint Industry Project - An international initiative on flexible pipe integrity assurance." *Proceedings of OTC-21524*, 9p.

- [13]. Bectarte, F., Secher, P. and Fellix-Henry, A. (2011). “Qualification testing of flexible pipes for 3000 m water depth.” Proceedings of OTC-21490, 10p.
- [14]. Secher, P., Bectarte, F. and Fellix-Henry, A. (2011). “Lateral buckling of armor wires in flexible pipes: Reaching 3000 m water depth.” Proceedings of OMAE- 49477, 8p.
- [15]. de Sousa, J.R.M., Viero, P.F., Magluta, C. and Roitman, N. (2012). “An experimental and numerical study on the axial compression response of flexible pipes” Journal of OMAE, 134, 12p.
- [16]. Braga M. P., Kallef P., “Flexible pipe sensitivity to birdcaging and armor wire lateral buckling”, OMAE 2004, 23<sup>rd</sup> International Conference on Offshore Mechanics and Arctic Engineering, June 20-25, 2004, Vancouver, BC, Canada.
- [17]. Ostergaard, N.H., Lyckegaard, A., Andreasen, J. H., “On modeling of lateral buckling failure in flexible pipe tensile armour layers”, Journal of Marine Structures, Volume 22, 2012, p.age 64-81.
- [18]. Tan, Z., Loper, C., Sheldrake, T., Karabelas, G., “Behaviour of tensile wires in unbounded flexible pipe under compression and design optimization for prevention”, 25<sup>TH</sup> International Conference on Offshore Mechanics and Arctic Engineering, June 4-9, 2006, Hamburg, Germany.
- [19]. Vaz M.A, Rizzo N.A.S, “A finite elemet model for flexible pipe armor wire instability”, Journal of Marine Structures, Volume 24, 2011, page 275-291.
- [20]. De Sousa R.M, Viero. P.F, Magulta. C, Roitman. N., “An experimental and numerical study on the axial compression response of flexible pipe”, OMAE 2012, 31<sup>st</sup> International Conference on Ocean, Offshore and Offshore Engineering, Rio de Janiero, Brazil. July 1-6, 2012.

- [21]. Serta O., Connaire A., Tanaka R., Fumis R., Smith J., Barbosa T., “Prediction of armour wire buckling for a flexible pipe under compression, bending and external pressure loading”, Proceedings of the ASME 2012, 31st International Conference on Ocean, Offshore and Arctic Engineering, June 1-6, 2013, Rio de Janeiro, Brazil.
- [22]. Bahtui, A., Bahai, H., Alfano, G., “Numerical and analytical modeling of unbounded flexible risers”, 2009, Journal of Offshore Mechanics and Arctic Engineering OMAE 131(2): 1-13.
- [23]. De Sousa, J.R.M., Magluta, C., Roitman, N., Londono, T. V., Campello, G.C, “A study on the response of a flexible pipe to combined axisymmetric loads”, Proceedings of the ASME 2013 32<sup>nd</sup> International Conference on Ocean, Offshore and Arctic Engineering, June 9-14, 2013, Nantes, France.
- [24]. De Sousa J. R.M, Ellwanger, G. B., “On the tension-compression behavior of flexible risers”, 13<sup>th</sup> International Offshore and Polar Engineering Conference, May 25-30, 2003, Honolulu, Hawaii, USA.
- [25]. De Sousa, J.R.M., Magluta, C., Roitman, N., Londono, T. V., Campello, G.C, “A study on the response of a flexible pipe to combined axisymmetric loads”, Proceedings of the ASME 2013 32<sup>nd</sup> International Conference on Ocean, Offshore and Arctic Engineering, June 9-14, 2013, Nantes, France.
- [26]. Ramos, R., Pesce, C.P., “A consistent analytical model to predict the structural behavior of flexible risers subjected to combined loads”, 23<sup>rd</sup> International Conference on Offshore Mechanics and Arctic Engineering, June 20-25, 2004, Vancouver, Canada.

- [27]. Corre, V. L., Probyn, I., “ Validation of a 3-dimensional finite element analysis model of a deep water steel tube umbilical n combined tension and cyclic bending”,ASME 28<sup>th</sup> International Conference on Ocean, Offshore and Arctic Engineering, May 31-June 5, Honolulu, Hawaii, USA.
- [28]. Bahtui, A., Bahai, H., Alfano, G., “A finite element analysis for unbounded flexible riser under axial tension”, 27<sup>th</sup> International Conference on Offshore Mechanics and Arctic Engineering, June 15-20, Estoril, Portugal.
- [29]. Ramos, R., Martins, C. A., Pesce, C.P., “ A case study on the axial-torsional behavior of flexible risers”, ASME 27<sup>th</sup> International Conference on Offshore Mechanics and Arctic Engineering, June 15-20, 2008, Estoril, Portugal.
- [30]. Serta, O., Fumis, R., Connaire, A., Smyth, J., Tanaka, R., Barbosa, T., Godinho, C., “Predictions of armour wire buckling for a flexible pipe under compression, bending and external pressure loading”, OMAE 2012, 31<sup>st</sup> International Conference on Ocean, Offshore and Offshore Engineering, Rio de Janiero, Brazil. July 1-6, 2012.
- [31]. Edmans, B., Alfano, G., Bahai, H., Andronicou, L., Bahtui, A., 2012, “Local stress Assesment of Flexible Unbonded Pipes Using FEA”, Proceedings of the ASME 2012 31st International Conference on Ocean, Offshore and Arctic Engineering, Rio de Janero, Brazil.
- [32]. Bahtui, A., Bahai, H., Alfano, G., 2009, “Numerical and Analytical Modeling of Unbonded Flexible Riser”, Journal of OMAE, Vol. 131.
- [33]. Leory, J.M, Perdrizet, T., Le Corre, V., Estrier, P., 2010, “ Stress Assessment in Armour Layers of Flexible Riser”, ”, Proceedings of the ASME 2010 29th International Conference on Ocean, Offshore and Arctic Engineering, Shanghai, China.

[34]. De Sousa, J., Magluta, C., Roitman, N., Ellwanger, G., Lima, E., Papaleo, A., “On the response of flexible riser to loads imposed by hydraulic collars”, *Journal of Applied Ocean Research*, 31, 2009, p.157-170.

[35]. Brack, M., Troina, L.M.B, de Sousa, J.R.M, “Flexible riser resistance against combined axial compression, bending, and torsion in ultra-deep water depths”, *ASME 24<sup>th</sup> International Conference on Offshore Mechanics and Arctic Engineering*, June 12-17, 2005, Halkidiki, Greece.

## **Preface**

This journal research paper is an original study and the developing idea, planning and implementation of the whole technical parts of this research paper have been done by the candidate as the first author, and the regular supervision has been made by Dr. Shawn Kenny through advising on the planning of the research way, evaluation of the research merit and providing precious idea and experience on the discovered phenomena and technical parts. The compilation of the paper literature has also been implemented by the candidate and it has been continuously revised by Dr. Shawn Kenny to improve the quality of the technical part and the literature. Facilitation of the PhD program of the candidate and also final review of the paper has been made by Dr. Amgad Hussein as the third author. Wood Group Kenny Research Chair at Memorial University of Newfoundland has funded the whole PhD program study and provided the all facilities (cluster machine, Software and personal computer) for carrying out the study.

This journal research paper was published in Journal of Pipeline Engineering in December, 2015.

## 2 Finite element simulation of flexible pipe mechanical response- Challenges and solutions

*Alireza Ebrahimi<sup>(1)</sup>, Shawn Kenny<sup>(2)</sup>, Amgad Hussein<sup>(1)</sup>*

<sup>(1)</sup>Faculty Engineering and Applied Science, Memorial University of Newfoundland

St. John's, NL, Canada

<sup>(2)</sup>Department of Civil and Environmental Engineering, Faculty of Engineering and

Design, Carleton University

Ottawa, ON, Canada

### 2.1 Abstract

Flexible pipelines have found application in the offshore oil and gas industry due to inherent characteristics that includes low bending stiffness (i.e., flexibility), high axial strength, and resistance to collapse, fatigue and abrasion. These performance attributes are related to the unique features of the flexible pipe manufacturing processes that produce a composite pipe section through the integration of various material component including steel and polymeric layers. Each layer has a specific role to meet a functional design requirement and the composite section can be tailored to meet project specific needs.

The composite section may exhibit a complex mechanical response with respect to deformation mechanisms and local instability (e.g., radial or lateral buckling), fatigue, and material degradation or creep. There are a limited number of analytical solutions and numerical models addressing the mechanical behaviour of flexible pipe. These studies were constrained by idealizations and

simplifications in order to attain tractable solutions. Even fewer experimental modelling tests are available in the public domain to support these studies. Consequently, the development of a more robust computational model examining the mechanical response of flexible pipe was conducted. In this study, continuum finite element modelling procedures were verified, using the limited available public domain information and data, for a flexible pipe subject to combined loading of axial compression with external and internal hydrostatic pressure. The potential for local, radial buckling instability (i.e., Birdcaging failure mechanism) was also examined. The challenges, constraints, uncertainties and proposed solutions to successfully model the complex interaction between multiple composite layers are discussed. The outcomes from this study also provide guidance on the development and verification of these numerical simulation procedures where there limited guidance presently exists in the public domain.

## **2.2 Flexible Pipe Technology**

### **2.2.1 Overview**

Flexible pipeline are used in the offshore oil and gas industry to connect wellheads with subsea (e.g., flowline to manifolds) and surface (e.g., riser to floating platform) facilities, and interconnect subsea infrastructure (e.g., jumpers, PLEM, PLET). The flexible pipe comprises a cross-section with multiple layers having different materials (e.g., steel, thermoplastic) that are used to meet specific functional requirements (Figure 2-1). The cross-section geometry, number of layers, material selection and lay-up are prescribed and tailored to meet project specific design requirements.

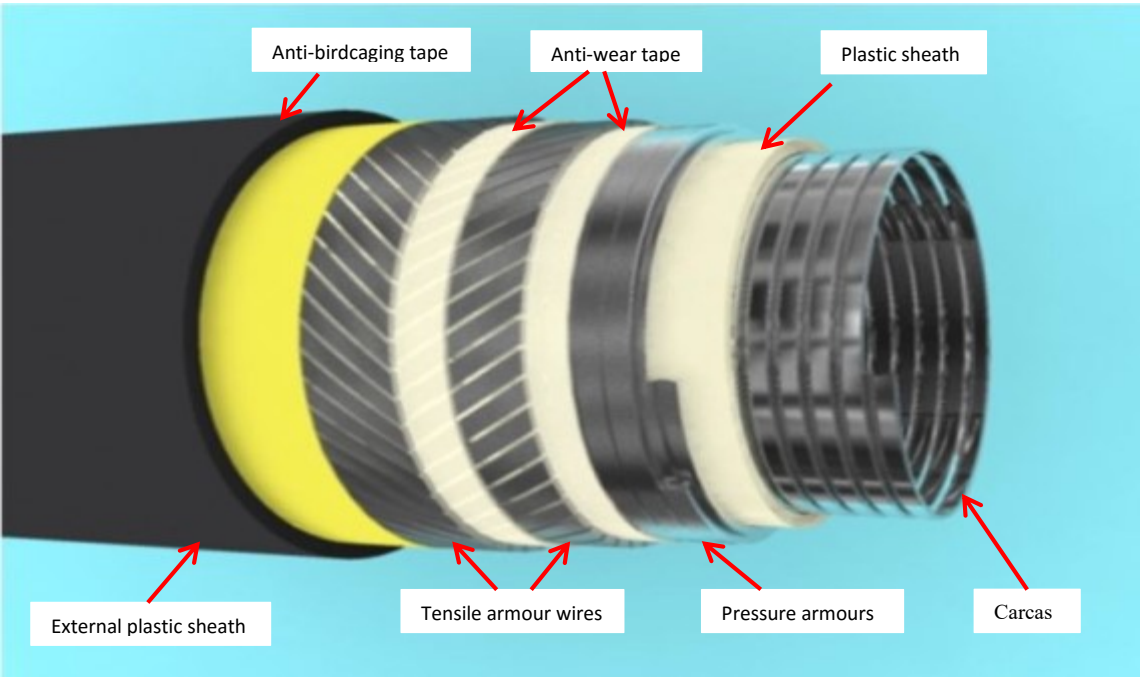


Figure 2-1. Cross section of unbounded flexible pipe.

There are a number of technical and economic advantages for the use of flexible pipe with respect to conventional rigid line pipe, particularly for fields located in deepwater that may have high pressure and high temperature requirements but not need long distance tie-backs or export transmission line [1]. In general, the pipe cross-section can be tailored to meet project specific requirements with inner pipe diameter ranging from 50 mm to 508 mm that can be wound on spools for rapid installation with rates as high as 5 km to 10 km per day.

The extruded thermoplastic layers (i.e., plastic sheath) provide corrosion resistance and thermal resistivity, and product containment with respect to mitigating leaks. The carcass and pressure armour provides circumferential resistance to hydrostatic loads exceeding 2,000 m water depth with recent development in flexible pipe technology being qualified for water depths exceeding 3,000 m. The helically wound armour wires provide longitudinal strength to axial tension loads

and flexibility in bending response. These armour wires can have different cross-sectional geometric configurations with the pitch angle approximately 35 degrees. High strength tape is used to prevent radial expansion of these tensile armour wires. This composite integration provides advantageous mechanical performance characteristics with respect to section collapse, combined loads and strength, and vibration response with excellent fatigue and abrasion resistance.

### **2.2.2 Analytical, Experimental and Numerical Modelling Studies**

The integrated composite structure hindered the early development of engineering models examining the mechanical response of flexible pipe where idealized analytical solutions and numerical modelling procedures were constrained by underlying assumptions and idealizations, and limitations in computational hardware and software.

Ostergaard *et al.* [2] presents an analytical solution for the lateral buckling of tensile armour layers due to cyclic bending and compression loads procedure, which was partially supported by experimental data. This local instability mechanism may occur during the installation process. The solution addressed the effect of initial imperfections, within the tensile armour wires, on the lateral buckling response; however, it is concluded that further study be conducted to assess the importance of interlayer friction on triggering lateral buckling events.

Braga *et al.* [3] conducted experimental studies simulating the effects of axial loading due to hydrostatic pressure, up to an equivalent 2000 m water depth, on the mechanical response of flexible pipe. This physical modelling approach was adopted due to the technical challenges and cost associated with deep-water hyperbaric chambers and connections. A flexible riser and flowline configuration was examined through a unique experimental program. Although the study was rigorous, the paper lacks detail that limits the value and leveraging by third parties.

Tan *et al.* [4] presents an analytical solution using total strain energy approach for modeling the buckling response of tensile armour wires. The results from a series of field test known as deep immersion performance tests (DIP), implemented by Wellstream are presented. This study was carried out to test flexible pipe for qualification in depth more than 2000 m. The driver for this experimental test program was the qualification for risers in water depths greater than 2000 m to address future deep-water field development opportunities.

Another local instability mechanism, known as birdcaging or radial buckling, that may occur with flexible pipe is the radial outward deformation mechanism due to a loss of circumferential constraint (i.e. damage to the pressure sheath or tape) subject to hydrostatic pressure and axial load

Figure 2-2.

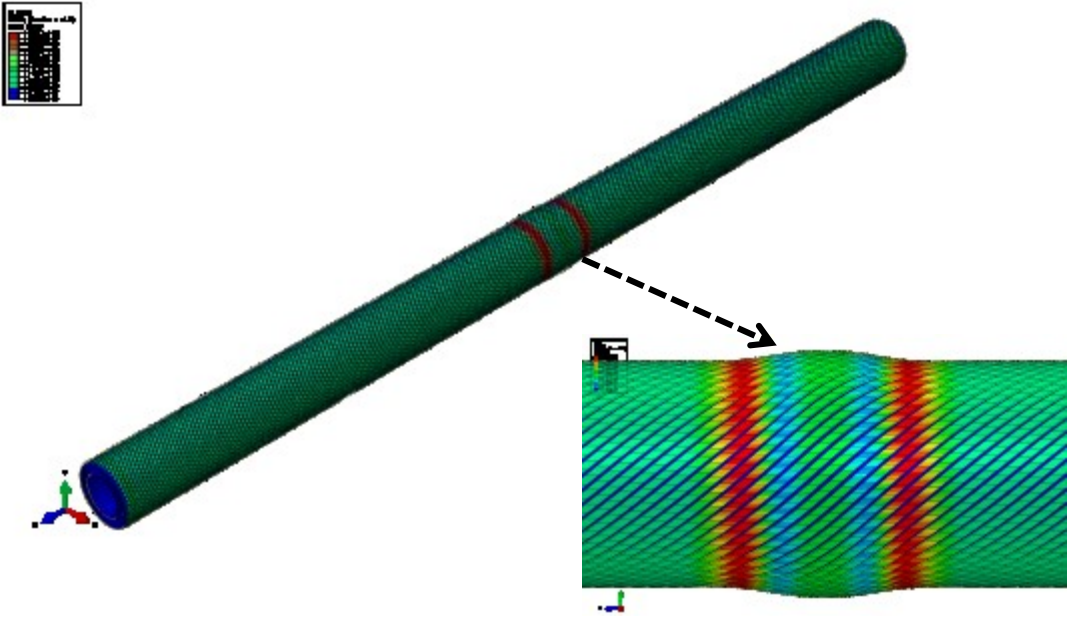


Figure 2-2. Radial buckling (Birdcaging) in tensile wires of flexible pipe

In a numerical modelling study, Vaz *et al.* [5] developed finite element modelling procedures to examine the effects of external pressure and interface friction on the potential for bird-caging mechanism to develop. Idealizations were incorporated in the modelling procedures where only two tensile armour wires, represented by spring elements without contact interaction, were used to represent the inward and outward radial deformation modes for the external and internal armour wires, respectively. A parameter study examined the effects of external pressure and interface friction on the potential for birdcaging mechanism to develop. The study highlighted key governing parameters, such as the effect of external and internal pressure, on radial instability.

Experimental studies conducted by de Sousa [6] provide the basis for establishing confidence in the numerical modelling procedures developed in his study. Physical tests on a 2.5 m length of 4” flexible pipe subject to axial compression were conducted. Continuum finite element modelling procedures were also developed using ANSYS. The use of physical and numerical modelling techniques was a significant step for improved understanding of the birdcaging (radial buckling) mechanism in flexible pipe. Although, correspondence between the results from physical and numerical investigations was demonstrated, uncertainties still remain on technical details (e.g., lack of reporting on the characterization of initial imperfections, damage state, or contact conditions). Although it is known the presence of initial geometric imperfections or damage state influences the buckling response and propagation of instabilities, details on the amplitude or distribution of initial geometric imperfections in the physical or numerical model were not provided. In addition, the effect of other key parameters, such as external or internal pressure, was not examined.

Another study on the bird-caging mechanism, conducted by Serta *et al.* [7], compared numerical simulations, using Explicit finite element methods, with physical test results. For the simulation

of birdcaging or lateral buckling mechanisms in the tensile armour wires of flexible pipe, where many layers may develop contact interaction, the use of Explicit methods is not recommended due to computational issues associated with large contact penetrations.

### **2.2.3 Motivation and Scope for this Study**

In this study, the development of continuum FE modelling procedures simulating the mechanical response of flexible pipe for local instability associated with bird-caging mechanism is presented. The motivation was to develop more robust computational tool, by reducing idealizations used in previous studies, promote confidence in the numerical modelling procedures through verification with available public domain data and to conduct a parameter study examining the key factors influencing potential local instability and failure of flexible pipe associated with radial birdcaging and lateral buckling mechanisms. The processes and requirements needed, challenges encountered and solutions developed to address this objective are discussed. In addition, the technical requirements to optimize these numerical procedures in terms of solution run time and model accuracy are also discussed.

## **2.3 Finite Element Modelling Procedures - Trials and Tribulations**

### **2.3.1 Overview**

In this section, the technical challenges encountered during development of the numerical modelling procedures are discussed. The observations that evolved during the study and the solutions generated are highlighted.

### **2.3.2 Verification Basis**

One of the significant hurdles was the limited number of studies in the public domain that could be used as verification basis. This issue was further compounded by the lack of specific

information or data not being reported within the literature source that was needed to develop the modelling procedures. This introduced uncertainty when qualifying these simulation tools, as developed in this study, and assessing the quality and significance of outcomes when comparatively critiquing studies.

Furthermore, the layup and cross-sectional characteristics of a composite flexible pipeline is dependent on the design service (e.g., pressure, temperature, product constituents) and environmental conditions (e.g., water depth, external force) [8]. The flexible pipe may have different characteristics (e.g. number of layers) with no unique encompassing design for all conditions. Thus, each individual flexible pipe configuration is “tailored for purpose”. This characteristic imposes constraints on the development of generalized finite element modelling procedures with respect to common formulations such as baseline characteristic response curves, and verification of numerical modelling procedures based on physical data that may not be transferable or scalable to other configurations. Consequently, a more detailed physical verification basis is seen as a current technical gap.

### **2.3.3 Modelling Constraints and Strategies**

Flexible pipe is an integrated composite section with individual components tailored for specific design and performance attributes. For example, the tensile armour wires provide axial strength but offer limited transverse stiffness and may experience local buckling (i.e., radial or bird-caging, lateral) instability mechanisms due to damage or loss of restraint. Other factors that may influence this local buckling mechanism include residual stress state and interface conditions, applied loading and boundary conditions, kinematic constraints and local damage state.

From a numerical modelling perspective, the complex pipe cross-sectional geometry, mechanical interactions and possible deformation mechanisms will promote the use of more simplified strategies (e.g., structural or line elements rather than continuum elements) while trying to preserve robustness, accuracy and computational effectiveness. These decisions impact other model attributes including the selection of model geometry (e.g., number of layers, mesh topology, segment length, element contact interaction definition), numerical procedures (e.g., non-linear geometric, material behaviour) and solution algorithms (e.g., equilibrium and solution convergence). As the model complexity grows, the frequency of numerical problems encountered will increase, and the need for more advanced computational hardware also increases.

To illustrate by example, de Sousa *et al.* [9] represented the carcass and pressure armour layers as orthotropic simple cylinders where the wrapping angles are close to 90 degrees. The wrapping angle plays a significant role in stability of helical layers and can be defined as Eq. (1).

$$L_p = \frac{2\pi R}{\tan(\alpha)} \quad (1)$$

Generally, when  $\alpha$  varies from 0 to 45 degrees, the pipe cross-section can withstand greater torsion loads, while the pipe segment tends to be more compliant with respect to bending or axial loading conditions.

The mesh topology (i.e. element type, order and density) plays a significant role in the idealization of flexible pipe mechanics (i.e. structural versus continuum behaviour), numerical procedures (i.e. nonlinear response, contact mechanics), debugging and solution quality (i.e. convergence rate, run time, accuracy). Each element type has its own advantages and drawbacks, which are discussed in the following paragraphs.

Line elements, such as spring, cable, and beam elements, and even solid and shell elements can be used to model the behaviour of tensile armour wire. Cylinders can be modeled using shell, continuum shell and solid elements. The element order (i.e., 1<sup>st</sup> or linear, 2<sup>nd</sup> or quadratic) and integration scheme (i.e., full, reduced) influences the mechanical response of the flexible pipe component (e.g. assumed displacement field, strain response and gradient) and solution convergence performance (e.g., shear locking, hour-glassing). This is dependent on the loading conditions, kinematic constraints and expected mechanisms.

In some studies on the behaviour of flexible pipe, the solid element was preferred for tensile armours and even cylinders. The main reasons of using solid for modeling are, 1) fewer degrees of freedom in each node while it can show 3-D stress and strain, [10], 2) in case of using contact pairs, the solid element can be better choice of modeling, as it does have more surfaces (six surfaces) for contact definition in comparison to shell (two surfaces). This is an advantage for particularly lateral buckling of tensile wires in which the wires move tangentially and might face lateral interactions with each other. However, the solid element does have drawbacks. If the flexible pipe is exposed to bending and torsion the solid element may not perform naturally, as the number of degrees of freedom is not enough. This can cause severe contact penetration between layers of flexible pipe. A possible way to address this problem is to use incompatible solid element in which an internal rotational degree of freedom is added to the solid element to reduce the shear stress for the first-order solid element.

As this pipe is nearly a slender structure with bending-dominated nature, it is highly suggested to avoid using full integration method neither solid nor shell element, particularly for first-order, linear elements. Shear locking can influence the buckling force prediction and affect the contact penetration and interaction between layers. Elements with reduced integration and hourglass

control should be selected with appropriate mesh topology strategies (i.e., h-, p and r- refinement) to improve the bending performance long the pipe segment length and through the individual layer depth (i.e. through the thickness). The use of higher order elements improves the curvature response but also the computational effort.

The integrated nature of multiple composite layers, inherent to the flexible pipe cross-section, introduces technical issues when developing the numerical modelling procedures. Each layer is relatively thin and is tailored for optimal performance with respect to specific loading and boundary conditions. These features may influence selection of modelling strategies to optimize computational efficiency and prevent solution divergence. Numerical singularities (i.e., may arise due to geometric effects (e.g., corners, edges), natural (i.e., force) boundary conditions, constraints (e.g., plane stress element, prescribed kinematic coupling).

Incorporating idealizations to the feature geometry (e.g., rounded edges, fillets) can transform singularities to stress concentrations. Using mesh refinement strategies (i.e., h-, p- and r-refinement) can mitigate singularities at the expense of increased computational effort. The stress singularity will have theoretical local infinite stress that does not converge, even with mesh refinement; however, the far field behaviour (i.e., St. Venant principle) will be captured adequately. For stress based finite element modelling procedures, the local displacement field and kinematics will not be affected and exhibit convergence at the stress singularity location.

Distributed loads or point loads acting on nodes may cause stress singularity that can be avoided using line elements (i.e., spring, truss, beam elements) or other structural elements (e.g., shell) when the load is applied perpendicular to the planar surface. The use of line elements, however,

does not capture local effects such as geometric imperfections (e.g., variation in diameter, ovality, lay-up angle) and stress effects.

The flexible pipe comprises layers of materials with different material and mechanical properties and roles or functions with respect to applied loads. Depending on the essential (i.e., geometric, kinematic) and natural (i.e., force) boundary conditions, which may also be mixed mode, then the finite element solution may encounter singularities or stress concentrations.

Stress concentrations (i.e., local stress greater than the nominal remote or far field stress state) will also develop when modelling the mechanical response of flexible pipe in regions with variations in stiffness and regions with contact interaction, Figure 2-3. Unlike the singularity problem, the stress field will exhibit convergence (i.e., tendency to approach a single finite value) when using mesh refinement strategies. To illustrate, the external plastic sheath (i.e., anti-birdcaging tape) layer has low stiffness material relative to the tensile armour wires and pressure armour. For combined loading conditions (e.g., hydrostatic pressure with axial force), the plastic sheath layer elements tend to exhibit out-of-plane bending and distortion Figure 2-4, which leads to numerical issues associated with contact penetration into adjacent layers. The use of kinematic coupling constraints help mitigate these difficulties encountered within the numerical simulation.

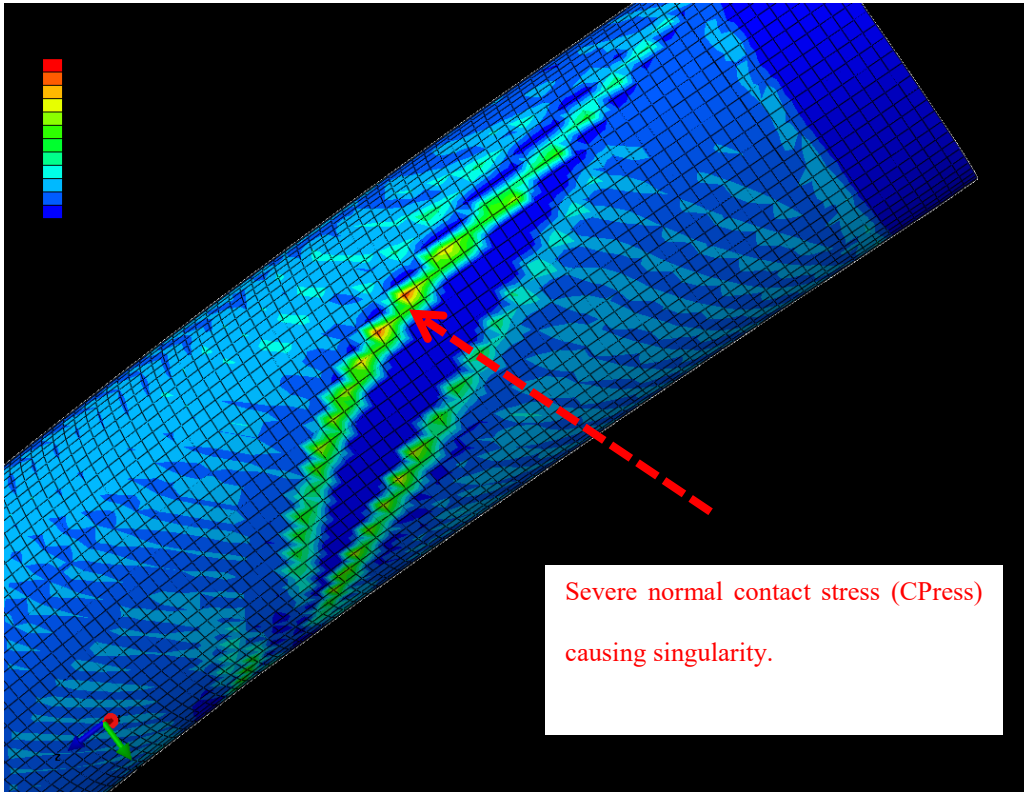


Figure 2-3- Singularity caused by severe contact pressure.

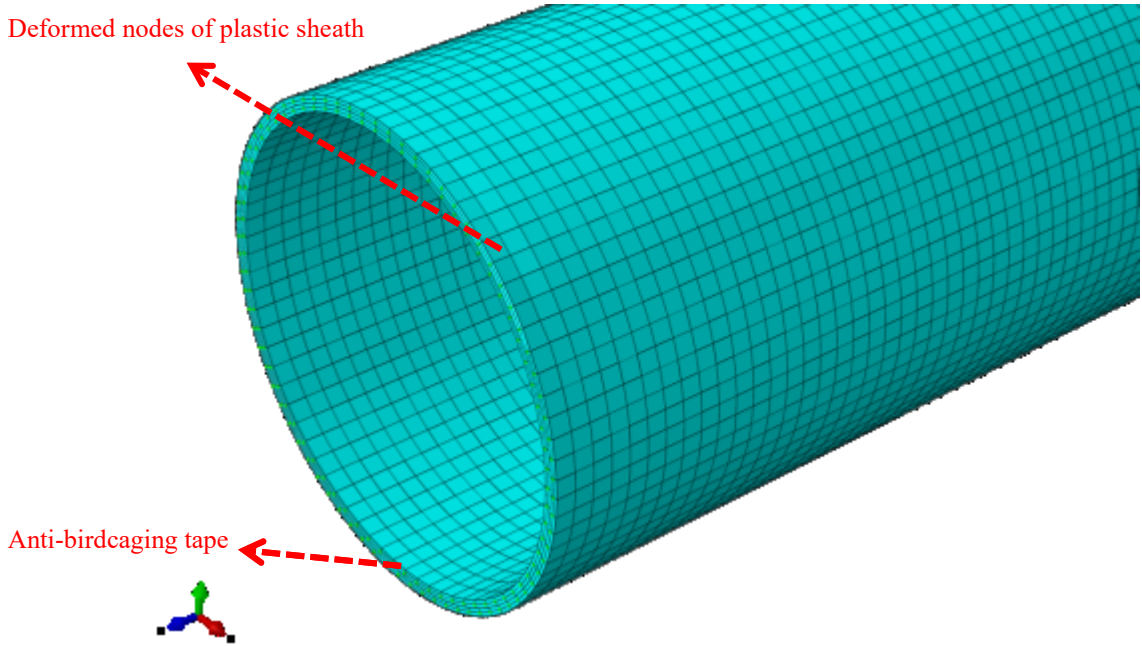


Figure 2-4. Extremely deformed nodes close to boundary condition.

The degrees of freedom for the elements associated with a boundary condition enforcing mixed-mode boundary conditions may also be influenced by the element type and interactions between layers. Depending on how the boundary condition is enforced there may be singularity in the stiffness matrix determinant due to rigid body motion in the structure. The boundary conditions may in turn influence the local and global mechanical response. For example, the global Euler buckling force, as defined by Eq. (2), is dependent on the boundary condition that influences the effective length. This is an important consideration when using experimental results to verify numerical modelling procedures, which may be incomplete in reporting all details of the investigation. Unlike conventional rigid pipe, the Euler buckling force for flexible pipe cannot be scaled due to the complex interactions and mechanical response of the composite unbonded structure.

$$F = \frac{\pi E I}{(KL)^2} \quad (2)$$

Furthermore, the relative movement between layers in the unbonded flexible pipe results in fluctuating and unequal reaction forces, which is related to the stick-slip condition defining the interlayer interface friction response.

### 2.3.4 Material Behaviour

Although design problems for flexible pipe primarily involve elastic behaviour, defining elastic-plastic material behaviour also provides a strategy to mitigate the effects of singularities and unrealistic stress concentrations. Material behaviour can have a knock-down effect on computational procedures used (e.g., implicit versus explicit) with respect to stress wave propagation and interference (i.e., numerical noise) within the flexible pipe model and time step stability requirements [11].

Simplifications in the mechanical and material behaviour of multiple layers are often used. For example, the pressure armour and pressure carcass are intertwined strips wrapped about the longitudinal axis with a lay-up angle of 90 degrees. These layers can be modelled as simple cylinders with orthotropic material behaviour. The compliance matrix must be consistent with material stability rules (Equations 4, 5, & 6) for three orthogonal directions, [12]:

$$E_i, G_{ij} > 0 \quad (4)$$

$$\frac{E_i}{E_j} > \nu_{ij} \quad (5)$$

$$1 - \nu_{12} \nu_{21} - \nu_{13} \nu_{31} - \nu_{23} \nu_{32} - 2\nu_{12} \nu_{23} \nu_{13} > 0 \quad (6)$$

### 2.3.5 Contact Mechanics

The multiple layers of a flexible pipe system have distinct roles (e.g., resistance to circumferential hydrostatic loads versus axial forces) and mechanisms (e.g., collapse versus lateral buckling). This results in numerical solution difficulties being encountered due to stress singularities and concentrations, as discussed, and problems associated with contact mechanics. The contact issues involve defining the interactions (i.e., contact geometry), kinematics (i.e., compatibility, penetration and over-closure) and forces normal (i.e., pressure, penetration) and tangential (i.e., friction, stick-slip or chattering) to the contact surfaces between adjacent layers [13]. This impacts the selection of numerical procedures when defining tolerances, and algorithm requirements to achieve equilibrium, iterate non-linear equations, and mitigate numerical instability and convergence issues.

The compatibility requirements must address not only issues related to degrees of freedom, as discussed, but also the interface between layers with respect to contact mechanics in terms of element size and distribution, and element order (i.e., kinematics and degrees-of-freedom). These factors may also be coupled with singularities associated with variation in material stiffness across element boundaries (e.g., plastic sheath interacting with the pressure armour). The more compliant layer may experience over-penetration through the adjacent layer that results in unrealistic interactions and contact forces.

Contact interactions may introduce numerical problems associated with severe discontinuity (i.e., contact discrepancy) and excessive contact penetrations (i.e., over-closure). The severe discontinuity can occur when the two layers or interfaces experience contact, stick together and then undergo relative slip or penetration with separation. The constraint enforcement methods may

include direct method, Penalty method and Lagrange, however, strict enforcement may lead to over constraint conditions and convergence issues.

In numerical computations, contact between two bodies may be defined using algorithms; such as Penalty, Lagrange multiplier and Augmented Lagrange methods, that have specific beneficial characteristics and constraints (e.g. [14-17]). In general, academic literature has focused on improving solution convergence for normal contact; whereas finite element codes have focused on refining the tangential behaviour and advancing applications for multi-body contact events.

The Direct method strictly enforces the load-displacement (i.e., pressure-overclosure) response, without approximation or use of augmentation iterations, through a Lagrange multiplier that should not be used for modeling hard contact.

The Penalty method is a stiff approximation of a hard contact, pressure-overclosure condition where the contact force is proportional with the penetration distance for equilibrium as defined in Equations (7) and (8), [18].

$$\min\{\cap (u)\} \tag{7}$$

Where  $\cap (u)$  is

$$\cap (u) = \frac{1}{2} k u^2 - mgu + \frac{1}{2} \epsilon [c(u)]^2 \tag{8}$$

where  $u$  is the penetration distance between the two surfaces and  $\epsilon$  is the penalty term, which can be defined by linear i.e., constant stiffness) and non-linear formulation.

The contact stiffness is generally defined by several orders of magnitude higher than the surrounding compliant elements. This may lead to an ill-conditioned system of equations that

results in solution convergence problems. The “interface spring” must also not be under-constrained where a low stiffness allows excess penetration during contact and errors in the simulation. These issues are further complicated by dependency on the mesh topology. Contact simulation using Lagrange multipliers, which represent contact forces, may be more accurate but are computationally more intensive due to the extra degrees of freedom and nonlinear solution iterations [14,19]. The penalty method can be implemented without using Lagrange multipliers that improves computational solver efficiency.

Contact interactions may involve chattering type mechanisms where the computational difficulties arise are compounded when the interface properties are governed near the stick–slip condition, which can be related to the abrupt change in kinematics, and loading conditions in response to stiffness estimates [e.g., 20]. This effect can be mitigated through a non-linear pressure-overclosure relationship by specifying an initially low stiffness with small displacement that adjusts according to condition the nature of the contact interaction.

The augmented Lagrange formulation adopts beneficial characteristics of the penalty and Lagrange multiplier methods with control on the relative penetration at the interface, contact forces and solution convergence rate [18,21]. The degree of over closure can be constrained by the penetration tolerance criteria. This method can mitigate over constraint issues and can improve solution efficiency by reducing the number of solution iterations required. the approach is mathematically described in Eq. (9) and (10), [22]. The computational effort should be considered through a trade-off analysis between the number of mesh seeds and the type of contact formulation.

$$\min\{\cap (u)\} \tag{9}$$

Where  $\Pi(u)$  is

$$\Pi(u) = \frac{1}{2} k u^2 - mgu + \frac{1}{2} \varepsilon [c(u)]^2 - \lambda c(u) \quad (10)$$

The method used to discretize the contact interaction (e.g., node-to-surface, surface-to-surface) must also be considered. Node-to-surface contact discretization tends to be more computational efficient, however may produce singular stress fields or large stress gradients. Surface-based discretization uses an average stiffness, on the surface of each element, that results in a smoothing of the stress and strain with less contact penetration between layers.

The contact stiffness of each layer is a function of the material properties (e.g., Young's modulus) and geometric properties (i.e., cross-sectional area, second moment of area). Incorporating a nonlinear stiffness function (Equation 10 & 11) would alleviate numerical issues where the contact stiffness should be as low as possible in first increment. The stiffness matrix components should have a suitable value to avoid unstable conditions associated with stress field singularity.

$$K_C = f(K_E) \quad (10)$$

$$K_T = K_E + K_C \quad (11)$$

Where  $K_T$  is the total stiffness matrix,  $K_E$  is the element stiffness of the structure and  $K_C$  is the contact stiffness of each layer. Definition of master and slave surfaces should also account for differences in the elastic material properties and element mesh topology of the contacting surfaces. In general, the master surface is selected based on the greater stiffness (i.e., geometric and material terms) or coarse element topology when having approximately equal stiffness.

### **2.3.6 Solution Procedures and Strategies**

The finite element procedures must integrate algorithms to iterate through non-linear equations (e.g., geometric, material, contact) to meet specified tolerance limits based on defined conditions (e.g., bending moment, over closure) and equilibrium (e.g., strain energy, work done, residual force).

The equations of motion can be addressed using implicit (i.e., unconditionally stable) methods and explicit (i.e., conditionally stable) integration methods. Implicit algorithms require iterations through each load increment for equilibrium check (e.g., residual force) Figure 2-5, and reformulation of the stiffness matrix for non-linear problems, which increases the computational effort but addresses solution stability in terms of predicted response. For explicit schemes, the minimum time step, which is a function of several parameters including material properties, element type and size, interface parameters, and loading conditions, controls the solution stability and accuracy, while no Equilibrium check is performed for it Figure 2-6. The inherent characteristics of flexible pipe create challenges when using explicit schemes.

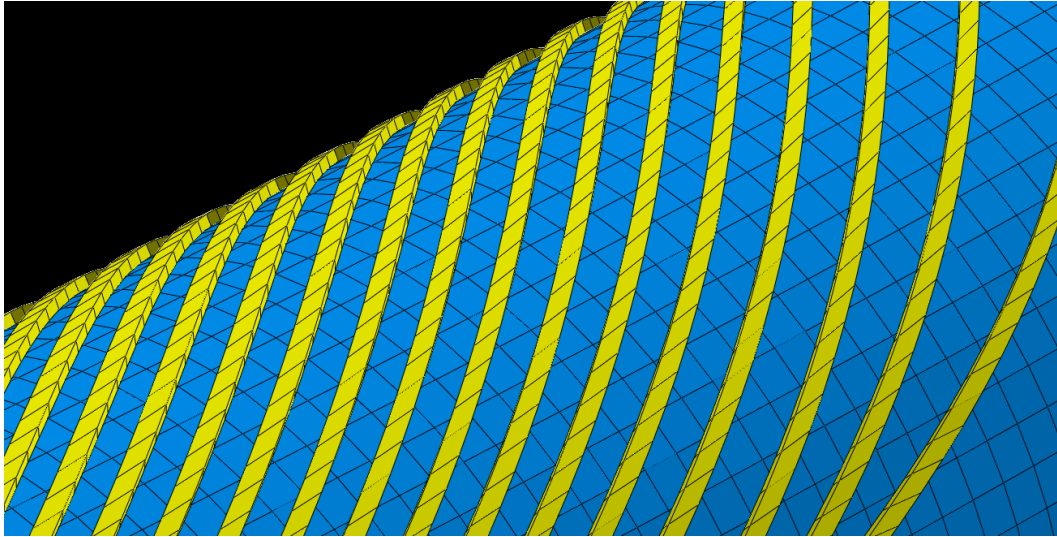


Figure 2-5. Accurate contact modeling performed by Implicit solver.

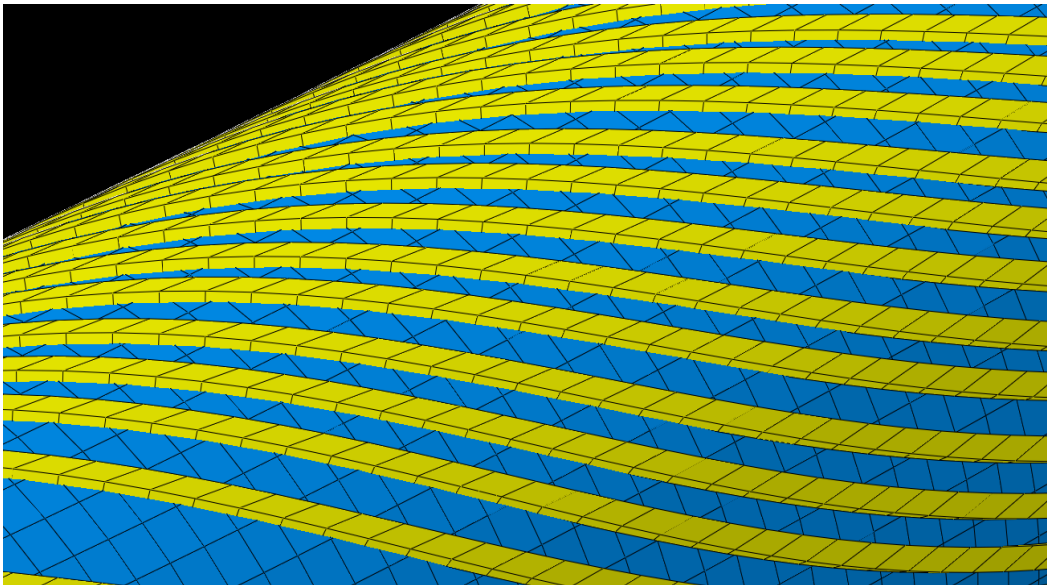


Figure 2-6. Inaccurate contact modeling performed by Explicit solver.

Flexible pipe may experience local failure mechanisms such as radial and lateral buckling. These problems are associated with the gradual development of stress and deformation within the

composite layers until a bifurcation point is reached. The load-deformation path then becomes unstable and requires tailored solution strategies depending on load or deformation controlled conditions.

Radial buckling (i.e., birdcaging mechanism) occurs when damage exists within the tape layer that allows the tensile armour wires to fail (i.e. unbounded radial growth) prior to global failure or global buckling. For load-control conditions, the analysis may have to address a snap-through problem, where the Riks method can be used to assess the local post-buckling response by controlling displacement and load parameters through an arc length method [10,23,24]. This is illustrated in Figure 2-7 for a flexible pipe subject to an axial load, where the Rik’s solver is needed to address the which, while the load-controlled method requires negative increments to pass the snap-through bifurcation point.

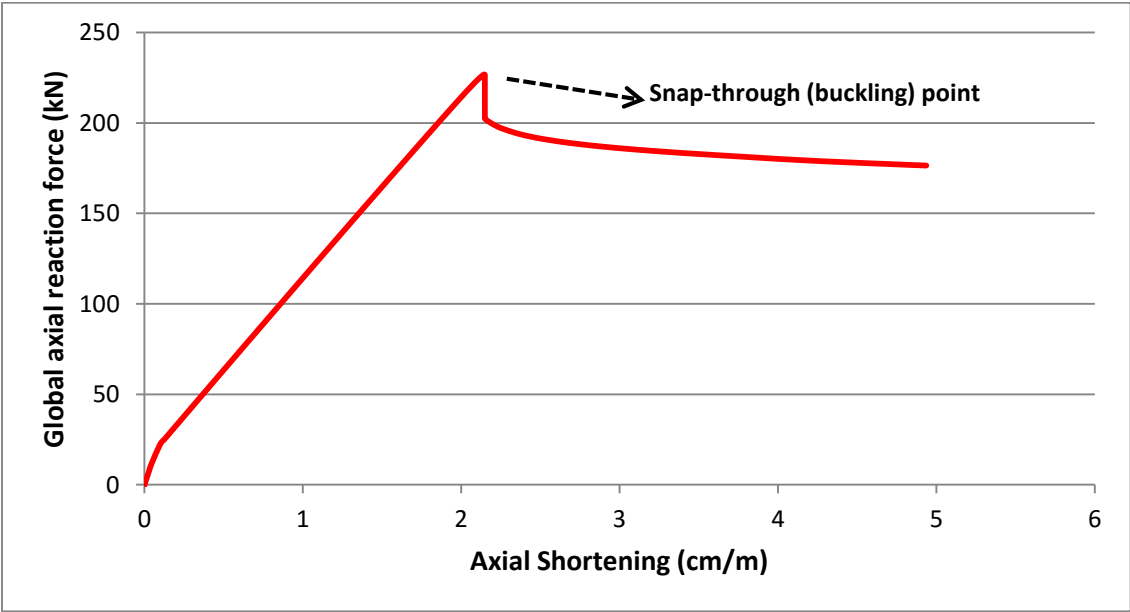


Figure 2-7. Global axial reaction force versus axial shortening in buckling of tensile armours of flexible pipe

## 2.4 Preliminary finite element procedures – Radial buckling problem

### 2.4.1 Problem statement

The technical issues discussed in previous sections are examined through a preliminary case study on the radial buckling of tensile armour wires. The model development, problems encountered, and results analysis can be used as a practical illustrative example.

### 2.4.2 Model parameters and numerical procedures

A 3-D continuum finite element model was developed with nine separate layers representing the flexible cross-section (Figure 2-1). The pipe geometry material properties, and element characteristics are summarized in Table 2-1 with some of the data adopted from the study by de Sousa [6]. The model segment length is equal 2.5 m (e.g. equal to de Sousa laboratory sample) and internal diameter of the pipe equals 4”.

Table 2-1. Material and element specifications of each individual layers, [6].

Layer	Material and Geometry	Element type
Carcass	Thickness = 4.0 mm Lay angle = 87.6 deg Young’s modulus = 193 GPa Poisson ratio = 0.3; Yield/Rupture stress = 320 MPa/640 MPa;	Shell
Plastic sheath	Thickness = 5.0 mm Young’s modulus = 345 MPa Poisson ratio = 0.3; Yield/Rupture stress = 20 MPa/20 MPa.	shell

Pressure armor	Thickness = 6.2 mm Lay angle = 87.0 deg Young's modulus = 205 GPa Poisson ratio = 0.3 Yield/Rupture stress = 900 MPa/1000 MPa	shell
Inner tensile armor	Thickness = 2.0 mm Number of wires = 47 Lay angle = 35.0 deg Young's modulus = 205 GPa Poisson ratio = 0.3; Yield/Rupture stress = 1260 MPa/1400 MPa	shell
High strength tape (Anti-bird caging tape)	Thickness=1.2 mm Young's modulus = 750 MPa Poisson ratio = 0.3	shell
Outer plastic	Yield/Rupture stress = 20 MPa/20 MPa	shell
Anti-wear tape	Young's modulus = 350 MPa	shell

In order to reduce computational effort, the carcass and pressure armour layers, which comprise interlocking profiled components, are modeled as simple cylinders, using shell elements, with orthotropic material behaviour [6]. The anti-wear and plastic sheath layers are also modelled as simple cylinders, using shell elements, with isotropic material properties. Surface-to-surface

contact discretization is used with hard normal contact having a low frictional coefficient ( $\mu=0.1$ ) in the tangential direction. The cross-section of the multi-layer pipe is shown in Figure 2-8 where the total number of nodes and elements are 129176 and 99119, respectively.

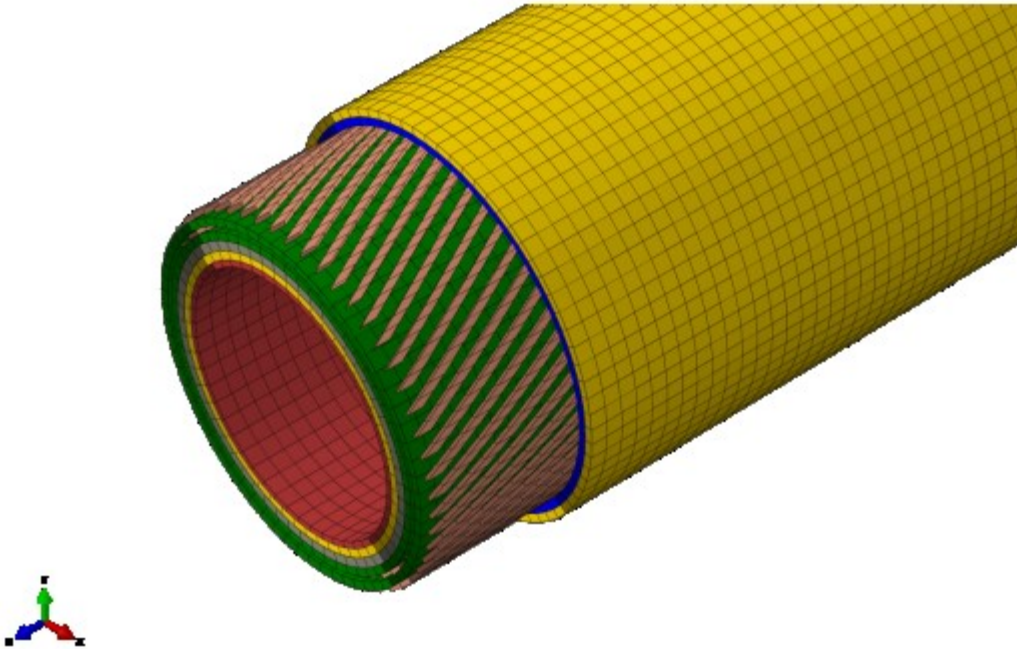


Figure 2-8. Layers and element distribution in the cross section.

The contact interaction between layers with different geometric properties, material characteristics, design functions, and large deformation response of the tensile wire during radial buckling requires the use of nonlinear solution techniques with precise mesh topology to achieve successful outcomes. Implicit type of solver is used because of highly reliable solution method (unconditionally stable), which can perform precisely in contact dominated problems by means of equilibrium check.

In order to model end-fitting for both extremities, the boundary conditions and loads are applied on two reference nodes which are fully coupled to the ends of layers Figure 2-9 . One of the

reference nodes is fully constrained while the other one is free to elongate and twist. The applied external load is imposed as pure compression force.

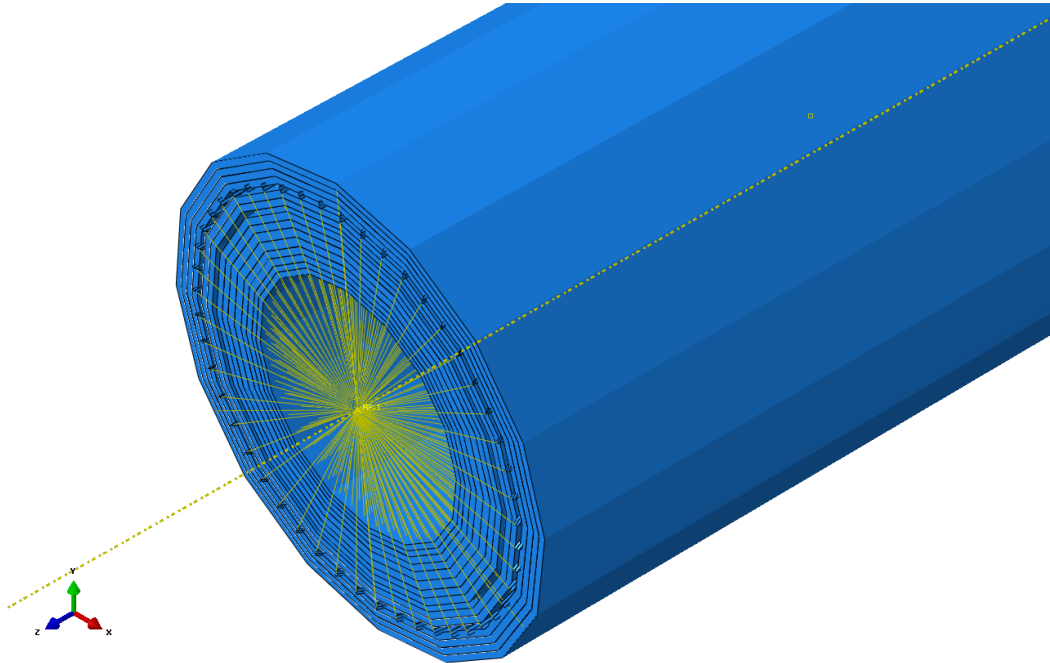


Figure 2-9. Coupling of the all layers to a reference node.

### 2.4.3 Results

The comprehensive report of the birdcaging analysis will be published soon (chapters 3-6), although in this section through some figures the accuracy of the model is illustrated. The accurate contact modeling can be seen in the Figure 2-10 in which the normal contact pressure does not show noise or discontinuity and Figure 2-11 proves that contact penetration is well avoided by the Equilibrium criterion even around birdcaging zone which is expected to have the most severe contact penetration. Another point which was discussed and makes a drastic influence on the contact interactions is element type, Figure 2-10 Figure 2-10. As it can be noticed, the shell element behaves well and natural in all critical areas (i.e. BC and birdcaging zone). The stress concentration is avoided, Figure 2-12, and proper combination of the options (i.e. element, solution method,

contact modeling, material modeling and BC) results in the well consistency of the numerical result with the similar experimental result [6], Figure 2-13 and Figure 2-14.

“In order to demonstrate the importance of application of implicit solver for running buckling simulation of flexible pipe, Figure 2-15 and Figure 2-16, are presented in which the accuracy of explicit solver in two different time increments is compared with implicit solver and physical model test results. Since the critical time step is a function of density, module of elasticity and element deterministic length, the minimum time step equal to  $1e-7$  should be considered to guarantee unconditional stability of the solution. In order to keep the kinematic energy as low as possible and improve the accuracy especially for the force-twist graph, the analysis was run with smaller time step equal to  $1e-8$ . As it can be seen in Figure 2-15, for the case that  $\Delta t = 1e - 8 s$ , the explicit solver mimics same force-strain pattern of experimental result and its accuracy for axial stiffness is acceptable but it can't predict bifurcation point as accurate as implicit solver. In Figure 2-16, the inaccuracy looks more severe. The explicit solver normally fails in precise prediction of bifurcation point and simulation of force-twist mechanism as it does not employ equilibrium criterion to check the results. Further analysis with smaller time step (e.g.  $\Delta t = 1e - 9 s$ ) is not practical as not only it takes much longer run time (i.e. around 18 days) but also due to too many executed time increments, the output file size exceeds the PC ram to be opened and its results be extracted (i.e. its ODB file exceeds 16 GB). Run time of explicit and implicit solver are compared in Table 2-2.

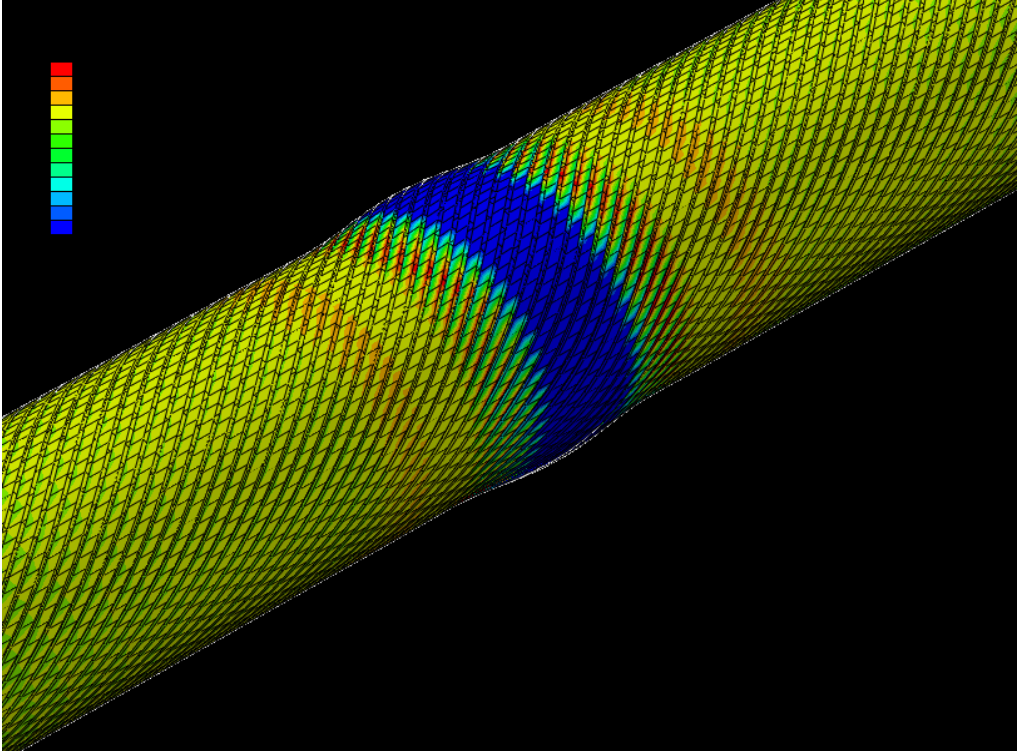


Figure 2-10. Smooth contact pressure around the birdcaging zone.

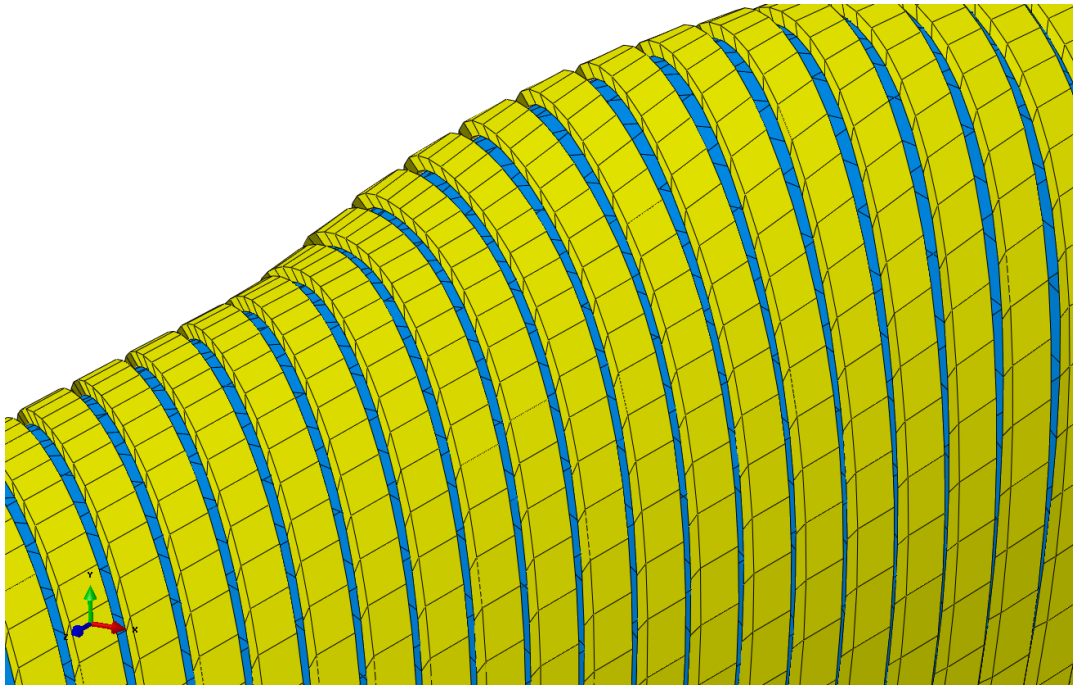


Figure 2-11. Contact penetration is avoided by means of Equilibrium check.

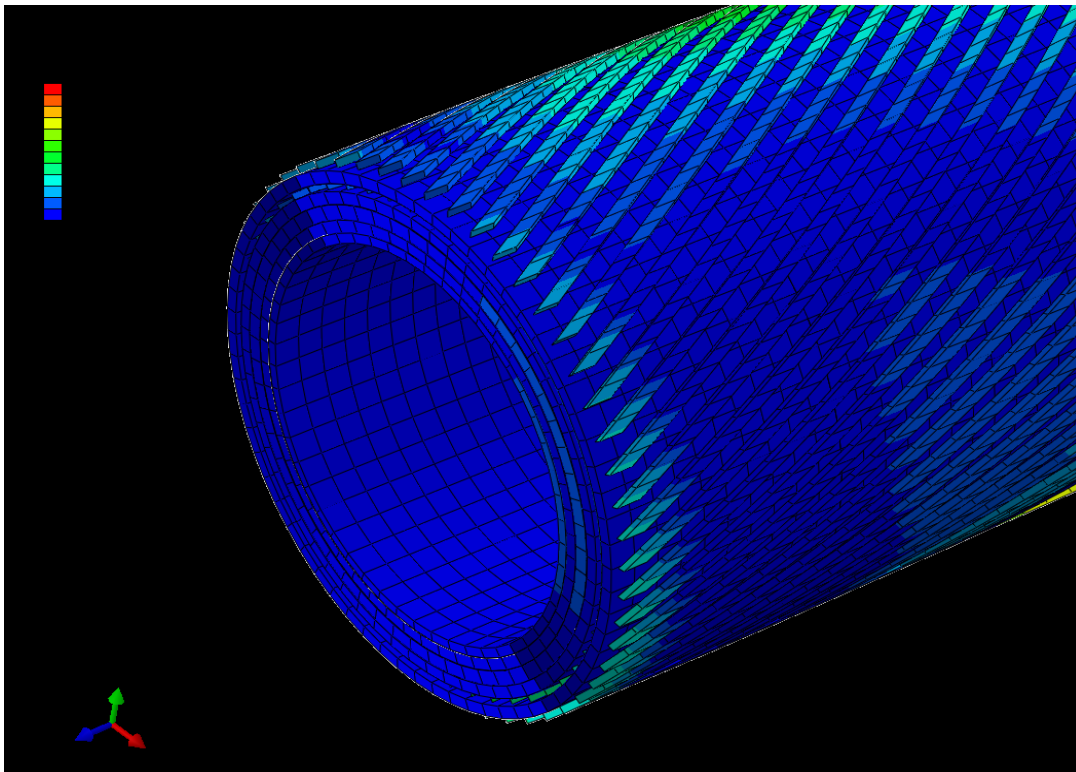


Figure 2-12. Stress concentration is avoided at the boundary condition by using a reference node.

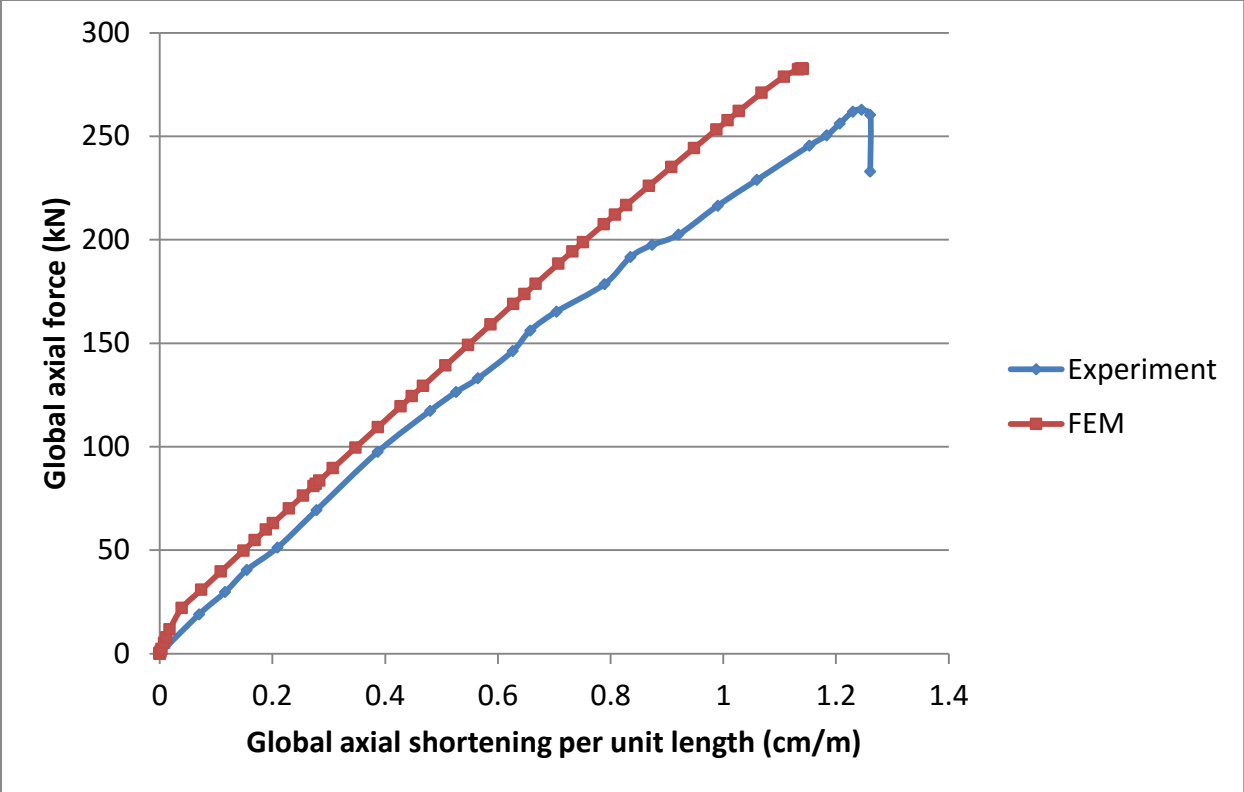


Figure 2-13. Global axial force versus global axial shortening measured at the reference point.

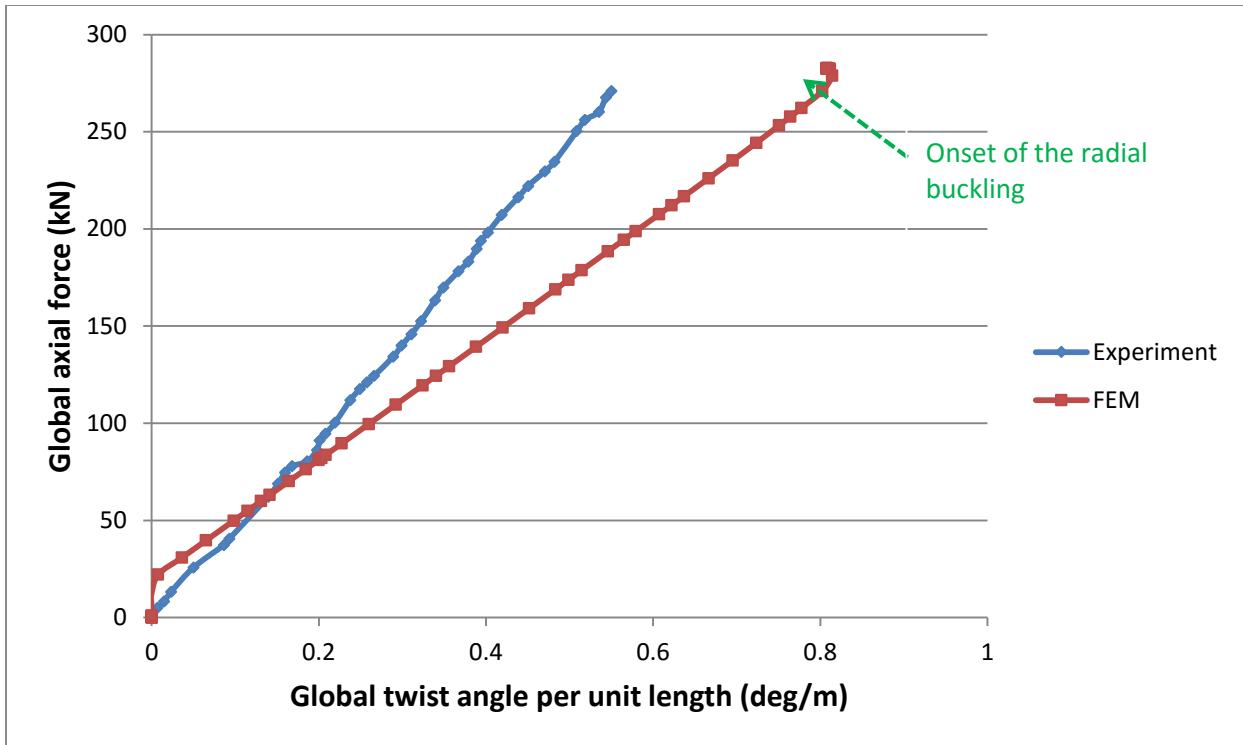


Figure 2-14. Global axial force versus global twist measured at the reference point.

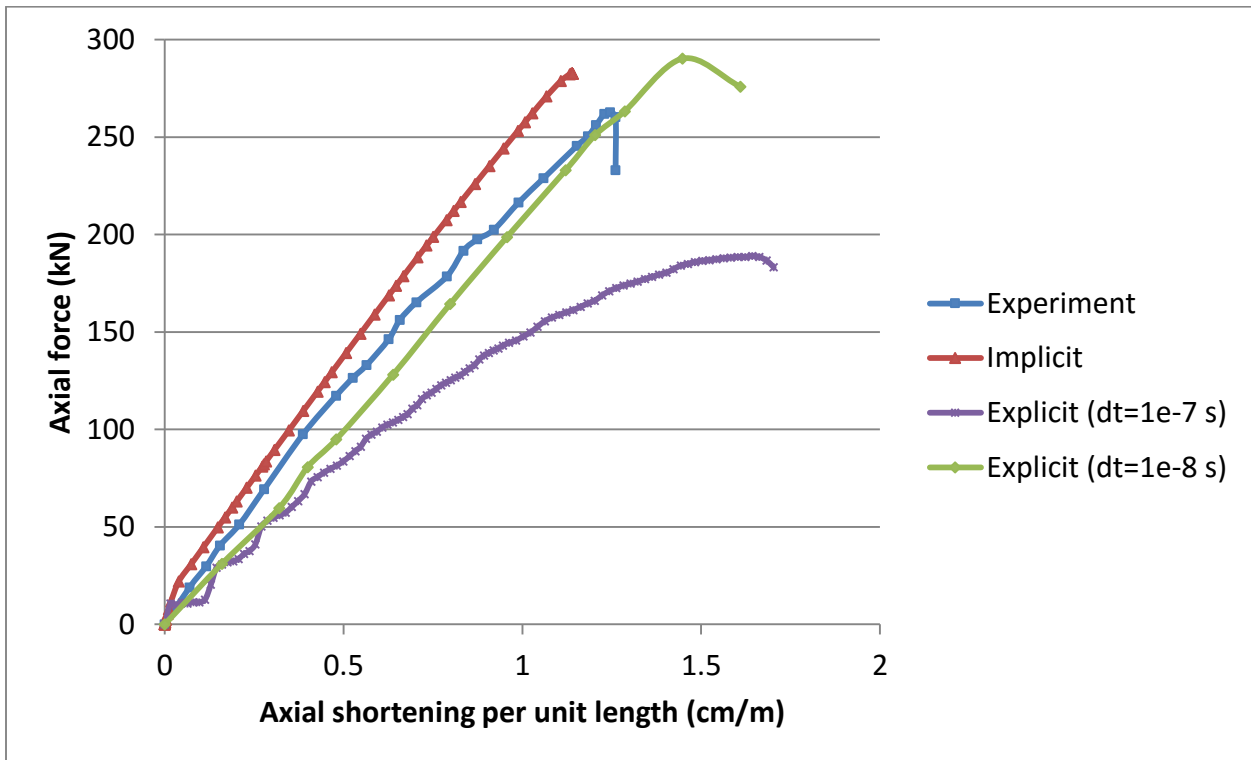


Figure 2-15. Global axial force versus global axial shortening (comparison between different models).

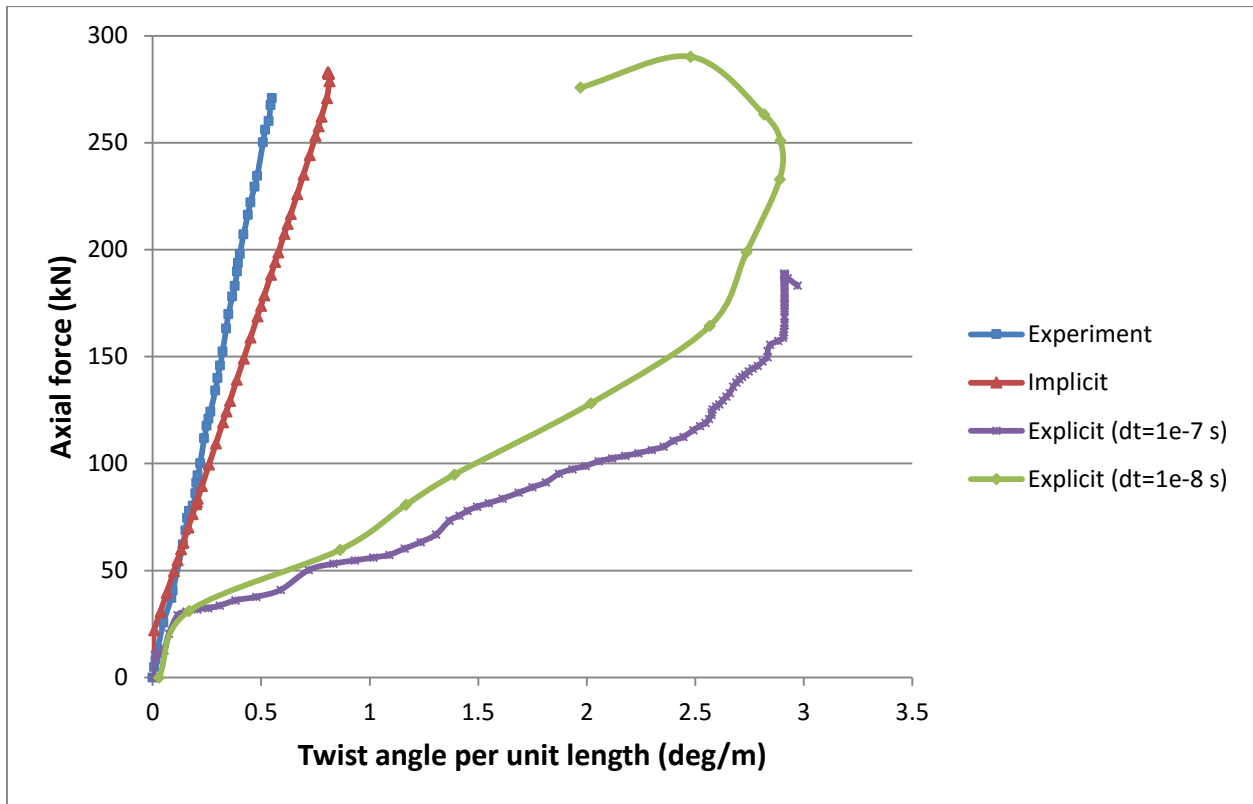


Figure 2-16. Global axial force versus global twist (comparison between different models).

Table 2-2. Time expense of each solution method.

<b>Solver</b>	<b>Implicit</b>	<b>Explicit (1e-7)</b>	<b>Explicit (1e-8)</b>
<b>Run time</b>	20 hrs	52 hrs	149 hrs

## 2.5 Conclusions

At the literature review of this paper by demonstration of the previous studies, the necessity of the current paper is highlighted. The literature review implies that analytical studies of the flexible pipe include numerous assumptions due to the complexity of the flexible pipe structure; finite

element simulations have to ignore many factors of a real model to overcome numerical issues; and physical model test are not always doable based on the constraints on the facilities. The challenges of the finite element simulation are elaborated through different sections (i.e. material modeling, contact interactions, solution method and etc.), and the solution for each individual section is provided through general terms of the elasticity and finite element method. At the end of this paper, a connection between all discussed sections of this paper is made by providing a finite element model for modeling radial buckling (birdcaging) of the flexible pipe. Although the full version of this simulation is going to be published in another work, the author tries to show that the discussions in this paper helps to have the best in-kind accurate model.

The author would recommend the readers to practice other types of the options (i.e. element type contact interaction and solver) to address the time efficiency without sacrificing the accuracy.

## **2.6 References**

- [1]. Technip, (2012), “Coeflexip-flexible steel pipe for drilling and service applications”, user guide, page 2-3.
  
- [2]. Ostergaard, N.H., Lyckegaard, A., Andreasen, J. H., “On modeling of lateral buckling failure in flexible pipe tensile armour layers”, *Journal of Marine Structures*, Volume 22, 2012, p.age 64-81.
  
- [3]. Braga, M.P., Kaleff, P., “Flexible pipe sensitivity to birdcaging and armour wire lateral buckling”, 23<sup>rd</sup> International Conference on Offshore Mechanics and Arctic Engineering, June 20-25, 2004, Vancouver, British Columbia, Canada.

- [4]. Tan, Z., Loper, C., Sheldrake, T., Karabelas, G., “Behaviour of tensile wires in unbounded flexible pipe under compression and design optimization for prevention”, 25<sup>TH</sup> International Conference on Offshore Mechanics and Arctic Engineering, June 4-9, 2006, Hamburg, Germany.
- [5]. Vaz M.A, Rizzo N.A.S, “A finite element model for flexible pipe armor wire instability”, Journal of Marine Structures, Volume 24, 2011, page 275-291.
- [6]. De Sousa R.M, Viero. P.F, Magulta. C, Roitman. N., “An experimental and numerical study on the axial compression response of flexible pipe”, OMAE 2012, 31<sup>st</sup> International Conference on Ocean, Offshore and Offshore Engineering, Rio de Janiero, Brazil. July 1-6, 2012.
- [7]. Serta, O., Fumis, R., Connaire, A., Smyth, J., Tanaka, R., Barbosa, T., Godinho, C., “Predictions of armour wire buckling for a flexible pipe under compression, bending and external pressure loading”, OMAE 2012, 31<sup>st</sup> International Conference on Ocean, Offshore and Offshore Engineering, Rio de Janiero, Brazil. July 1-6, 2012.
- [8]. Neto, A.G., Martins, D.A., “Flexible pipes: influence of the pressure armor in the wet collapse”, Journal of Offshore and Offshore Engineering, Volume 136, May 19, 2016.
- [9]. De Sousa, J., Magluta, C., Roitman, N., Ellwanger, G., Lima, E., Papaleo, A., “On the response of flexible riser to loads imposed by hydraulic collars”, Journal of Applied Ocean Research, 31, 2009, p.157-170.
- [10]. ABAQUS 6.13 documentation.
- [11]. Bathe, K.-J. (2007) Finite Element Procedures. ISBN 978-0979004902.
- [12]. Bower, A.F., “Applied mechanic of solids”, CRC press, page 83.

- [13]. Pike, K., Kenny, S., Kavanagh, K. K Jukes, P. (2012). “Pipeline Engineering Solutions for Harsh Arctic Environments: Technology Challenges and Constraints for Advanced Numerical Simulations.” Proc., OTC-23734, 9p.
- [14]. Wriggers, P., Simo, J.C. and Taylor, R.L. (1985). “Penalty and augmented Lagrangian formulations for contact problems.” Proc., NUMETA,
- [15]. Wriggers, P. and Zavarise, G. (1993). “Application of augmented Lagrangian techniques for non-linear constitutive laws in contact interfaces.” Comm. Num. Meth. Engg, 9:815–824.
- [16]. Wriggers, P. (2002). Computational Contact Mechanics. John Wiley & Sons, 441p.
- [17]. Zavarise, G. and Wriggers, P. (1999) “A superlinear convergent augmented Lagrangian procedure for contact problems” Eng. Comp. 16(1): 88-119.
- [18]. Wiggers, P.,” Computational contact mechanics”, Springer, 2<sup>nd</sup> edition, page 17.
- [19]. Simo, J.C. and Laursen, T.A. (1992). “An augmented lagrangian treatment of contact problems involving friction.” Comp. & Struct. 42(1):97-116.
- [20]. Benson, D.J. and Okazawa, S. (2003). “Contact in a multi-material Eulerian finite element formulation.” Comput. Methods Appl. Mech. Eng. 193:4277–4298
- [21]. Legrand, M., Batailly, A., Magnain, B. Cartraud, P., and Pierre, C. (2012). “Full three-dimensional investigation of structural contact interactions in turbomachines.” Journal of Vib and Sound, 331(11):2578-2601.
- [22]. Wiggers, P., “Computational contact mechanics”, Springer, 2<sup>nd</sup> edition, page 339.

[23]. Ahmed, M.B., Zu, S.X., “Arc-length technique for nonlinear finite element analysis”,  
Journal of Zhejiang University Science, 2004.

[24]. Crisfield, M. A., “A Fast Incremental/Iteration Solution Procedure that Handles ‘Snap-Through’,” Computers and Structures, vol. 13, pp. 55–62, 1981.

## **Preface**

This journal research paper is an original study and the developing idea, planning and implementation of the whole technical parts of this research paper have been done by the candidate as the first author, and the regular supervision has been made by Dr. Shawn Kenny through advising on the planning of the research way, evaluation of the research merit and providing precious idea and experience on the discovered phenomena and technical parts. The compilation of the paper literature has also been implemented by the candidate and it has been continuously revised by Dr. Shawn Kenny to improve the quality of the technical part and the literature. Facilitation of the PhD program of the candidate and also final review of the paper has been made by Dr. Amgad Hussein as the third author. Wood Group Kenny Research Chair at Memorial University of Newfoundland has funded the whole PhD program study and provided the all facilities (cluster machine, Software and personal computer) for carrying out the study.

This journal research paper was submitted to the Journal of Offshore Mechanics and Arctic Engineering (an ASME Journal) on May 20th, 2015 and it is accepted in December 2015.

### **3 Radial buckling of tensile armour wires in subsea flexible pipe – numerical assessment of key factors**

*Alireza Ebrahimi<sup>(1)</sup>, Shawn Kenny<sup>(2)</sup>, Amgad Hussein<sup>(1)</sup>*

<sup>(1)</sup>Faculty Engineering and Applied Science, Memorial University of Newfoundland

St. John's, NL, Canada

<sup>(2)</sup>Department of Civil and Environmental Engineering, Faculty of Engineering and  
Design, Carleton University

Ottawa, ON, Canada

#### **3.1 Abstract**

Flexible pipes can be used as risers, jumpers and flowlines that may be subject to axial forces and out-of-plane bending motion due to operational and environmental loading conditions. The tensile armour wires provide axial stiffness to resist these loads. Anti-birdcaging tape is used to provide circumferential support and prevent a loss of stability for the tension armour wires, in the radial direction. The anti-birdcaging tape may be damaged where a condition known as “wet annulus” occurs that may result in the radial buckling (i.e. birdcaging mechanism) of the tensile armour wires. A 3-D continuum finite element model of a 4” flexible pipe is developed using Abaqus/Implicit software package. As a verification case, the radial buckling response is compared with similar but limited experimental work available in the public domain. The modelling procedures represent an improvement over past studies through the increased number of layers and elements to model contact interactions and failure mechanisms. A limited parameter study highlighted the importance of key factors influencing the radial buckling mechanism that includes

external pressure, internal pressure and damage, related to the percentage of wet annulus. The importance of radial contact pressure and shear stress between layers was also identified. The outcomes maybe used to improve guidance in the engineering analysis and design of flexible pipelines and to support the improvement of recommended practices.

### **3.2 Introduction**

Tying subsea infrastructure to surface facilities (e.g., riser) and connecting subsea facilities (e.g., jumper) is one of the major applications for flexible pipes. There may be economic and technical advantages for using flexible risers or pipeline in comparison to conventional rigid line pipe [1]. The extruded external polymer sheath eliminates requirement for cathodic protection, which promotes reliability and maintenance expenses of the pipe. Over short distances, the installation rate of flexible pipe can be 5 km to 10 km per day; hence the installation cost of flexible pipes is lower than conventional line pipe installed using conventional S-lay or J-lay methods. Other beneficial mechanical properties include collapse strength and fatigue and abrasion resistance. In addition, the internal smooth surface minimizes heat loss and flow turbulence.

The wide spread use of subsea flexible pipes within more demanding operational conditions and harsh environments imposes demands on greater knowledge on the mechanical response and performance for this pipe. Subsea flexible pipes based on their applications can be exposed to axial compression, end-cap effect in short jumpers or axial movement in long pipes. For conditions with damage to the plastic sheath (i.e. “wet annulus”), the anti-birdcaging tape provides only resistance to radial expansion. As, the tensile armours have a low moment of inertia in the radial direction, the compression can separate layers that may result in radial buckling (i.e. bird-caging).

There are few studies examining the radial buckling phenomena for the tensile armour. In a numerical study, Vaz *et al.* [2] developed finite element modelling procedures to examine the effects of external pressure and interface friction on the potential for bird-caging mechanism to develop. The study by Vaz *et al.* [2] incorporated idealizations to addressing computational constraints on modeling discrete components of the flexible pipe cross-section. For example, only two tensile armour wires, represented by spring elements without contact interaction, were used to represent the inward and outward radial deformation modes for the external and internal armour wires, respectively.

Experimental studies conducted by de Sousa *et al.* [3] provide the basis for developing the numerical modelling procedures presented in this paper. Physical tests on a 2.5 m length of 4" (101.6 mm) flexible pipe subject to axial compression were conducted. Continuum finite element modelling procedures were also developed using ANSYS software package. The study provides many details of the pipe configuration with results from the numerical simulation, which included contact interactions, consistent with the physical test data and observations. However, there are some areas of uncertainty. Although it is known the presence of initial geometric imperfections or damage state influences the buckling response and propagation of instabilities, details on the amplitude or distribution of initial geometric imperfections in the physical or numerical model were not provided. In addition, the effect of other key parameters, such as external or internal pressure, was not examined. In this study, the influence of geometric imperfections and hydrostatic pressure on radial buckling is examined.

Another study on the bird-caging mechanism, conducted by Serta *et al.* [4], compared numerical simulations, using Explicit finite element methods, with physical test results. For the simulation of birdcaging or lateral buckling mechanisms in the tensile armour wires of flexible pipe, where

many layers may develop contact interaction, the use of explicit methods is not recommended due to computational issues associated with large contact penetrations.

Braga *et al.* [5] examined the response of a flexible riser and flowline subject to internal pressure and axial force, within an in-air physical test apparatus, that was used to represent equivalent conditions for 2000 m water depth. Although, the paper presents a unique series of experimental tests, it lacks detail for use by third-parties as a verification case study.

In this study, continuum finite element modelling procedures using the Abaqus/Implicit solver are developed to examine the radial buckling mechanism of the tensile armour wires. Factors influencing in the birdcaging mechanism of the tensile armour wires including percentage of wet surface area (i.e., damage zone), and the internal and external pressures are examined through a parameter study.

### **3.3 Finite Element Modelling Procedures and Sensitivity Matrix**

A 3D continuum finite element model was developed with nine separate layers to represent the flexible cross-section. A summary of the geometric and material properties, and element characteristics are presented in Table 3-1 with some of the data are adopted from the study by de Sousa *et al.* [3]. The total length of the modeled pipe is 2.5 m. In order to reduce computational effort, the carcass and pressure armour layers, which comprise interlocking profiled components, are modeled as a simple cylinder, using shell elements (S4), with orthotropic material behaviour [6]. The anti-wear tape and plastic sheath layers are also modelled as a simple cylinder, using shell (S4) elements, with isotropic material properties.

Table 3-1. Characteristics of each individual layer.

Layer	Mechanical Properties					Element Type
	Thickness (mm)	Elastic Modulus (GPa)	Poisson's Ratio	Yield Stress (MPa)	Rupture Stress (MPa)	
Carcass (Lay Angle 87.6°)	4.0	193	0.3	320	640	Shell (S4R)
Plastic Sheath	5.0	345	0.4	20	22	Shell (S4R)
Pressure Armour (Lay Angle 87.0°)	6.2	205	0.3	900	1000	Shell (S4R)
Anti-Wear Tape	2.0	350	0.4	20	22	Shell (S4R)
Inner Tensile Armour (Lay Angle 35.0° with 47 wires)	2.0	205	0.3	1260	1400	Shell (S4R)
Outer Tensile Armour (Lay Angle 35.0° with 48 wires)	2.0	205	0.3	1260	1400	Shell (S4R)
High Strength Tape	1.2	0.75	0.3	40	44	Shell (S4R)
Outer Plastic Sheath	5.0	215	0.4	20	22	Shell (S4R)

In Table 3-1, the properties of carcass and pressure armour layers are described in terms of isotropic properties. In order to calculate properties of the material in the three perpendicular axes, a six-by-six compliance matrix of orthotropic material in which all components due to symmetries are equal to zero except nine components as follow.

$$\begin{bmatrix} c_{1111} & c_{1122} & c_{1133} & 0 & 0 & 0 \\ 0 & c_{2222} & c_{2233} & 0 & 0 & 0 \\ 0 & 0 & c_{3333} & 0 & 0 & 0 \\ 0 & 0 & 0 & c_{2323} & 0 & 0 \\ 0 & 0 & 0 & 0 & c_{3131} & 0 \\ 0 & 0 & 0 & 0 & 0 & c_{1212} \end{bmatrix}$$

Based on isotropic properties of this layer, four components can be gained by straightforward calculations as follow.

$$c_{1111}=c_{3333}=\frac{1}{E} \quad (3-1)$$

$$c_{1133}=\frac{-\nu_{13}}{E} \quad (3-2)$$

$$c_{1133}=\frac{1}{2G_{13}} \quad (3-3)$$

The rest of the non-zero components were determined empirically. For this purpose, carcass layer was individually modeled and its behaviour was examined under tension and torsion. Based on these series of studies, due to the gap between interlocked profiled strip, the extent of other components are negligible in respect to the other components, Equation (3-1 to 3-3).

In comparison with the other polymeric layers (e.g., anti-wear tape), the anti-birdcaging tape layer has significantly greater elastic strength that was modeled as an extruded layer possessing orthotropic material. Determination of the elastic constants was established by adopting the same procedure used to calculate the elastic strength properties for the carcass and pressure armour layers.

Surface-to-surface contact discretization was used to have smooth contact and avoid stress concentration on nodes. In node-to-surface contact the master nodes may penetrate into the space between the slave surface nodes where there is no defined constraint between the slave nodes. This can be more severe in curved surfaces, when there is more probability of penetration under small loading. Hard normal contact with a low frictional coefficient ( $\mu=0.1$ ) in the tangential direction

was defined. The contact interaction between layers with different geometric properties, material characteristics and design functions, and large deformation response of the tensile wire during radial buckling requires the use of nonlinear solution techniques with precise mesh topology to achieve successful outcomes. The flexible pipe cross-section is shown in Figure 3-1 with 51 elements on the pipe outer circumference, and 250 elements along the pipe length for a total of 129,176 elements.



Figure 3-1. Layers and element distribution in the cross section

The implicit solver is used due to improved solution convergence rate and performance with respect to kinematics and over-closure penetration in non-linear contact dominated problems relative to the explicit solver. A static problem by nature does not depend upon time, so the equation of motion can be solved by Implicit (Backward Euler Method), [8]. Unlike explicit methods, implicit methods are an unconditionally stable method and consequently the static

problem can be solved with a few large increments. Besides faster convergence, the implicit methods employ equilibrium check after each increment to calculate the residual forces. This is a crucial check for finding snap-through points in the response of the structure. Also, equilibrium check improves contact interaction modeling in cases of using the penalty method. Penalty methods are generally framed in terms of the displacement variable with the contact stiffness defined as several orders of magnitude higher than surrounding elements. This may lead to an ill-conditioned system of equations and issues that may result in difficulties with solution performance. Furthermore, if the interface stiffness is under-constrained (i.e., low stiffness) then excessive penetration during contact is allowed that may lead to errors in the predicted interaction response with respect to local relative stiffness, and predictions of local displacement, velocity and acceleration [9-11]. This issue is further complicated through the interdependence on mesh density and stick-slip mechanisms [12]. These factors ultimately affect solution performance and, potentially, accuracy. Once implicit solver is used with Penalty method, the contact penetrations and forces must be within the defined contact penetration and force tolerances as well as the resultant forces caused by contact interaction are taken into account and checked by equilibrium criterion.

In order to model end-fittings for both pipe ends, the boundary conditions and loads are applied on two reference nodes. The reference nodes are fully coupled to the end section of each layer through a tied multi-point constraint to enforce compatibility and promote solution convergence for equilibrium iterations. One of the reference nodes is fully constrained while the other one is free to elongate and twist. The applied external load is imposed as pure compression force.

One of the major features of this study is that the pre-tension which is applied for wrapping the anti-birdcaging tape around the pipe, was taken into account to take into account one of the initial

condition caused by manufacturing process. The process of wrapping the tape around the pipe is modeled as Figure 3-2, in which one end of anti-birdcaging tape is fixed while the other end is pulled by 200 kN of force.

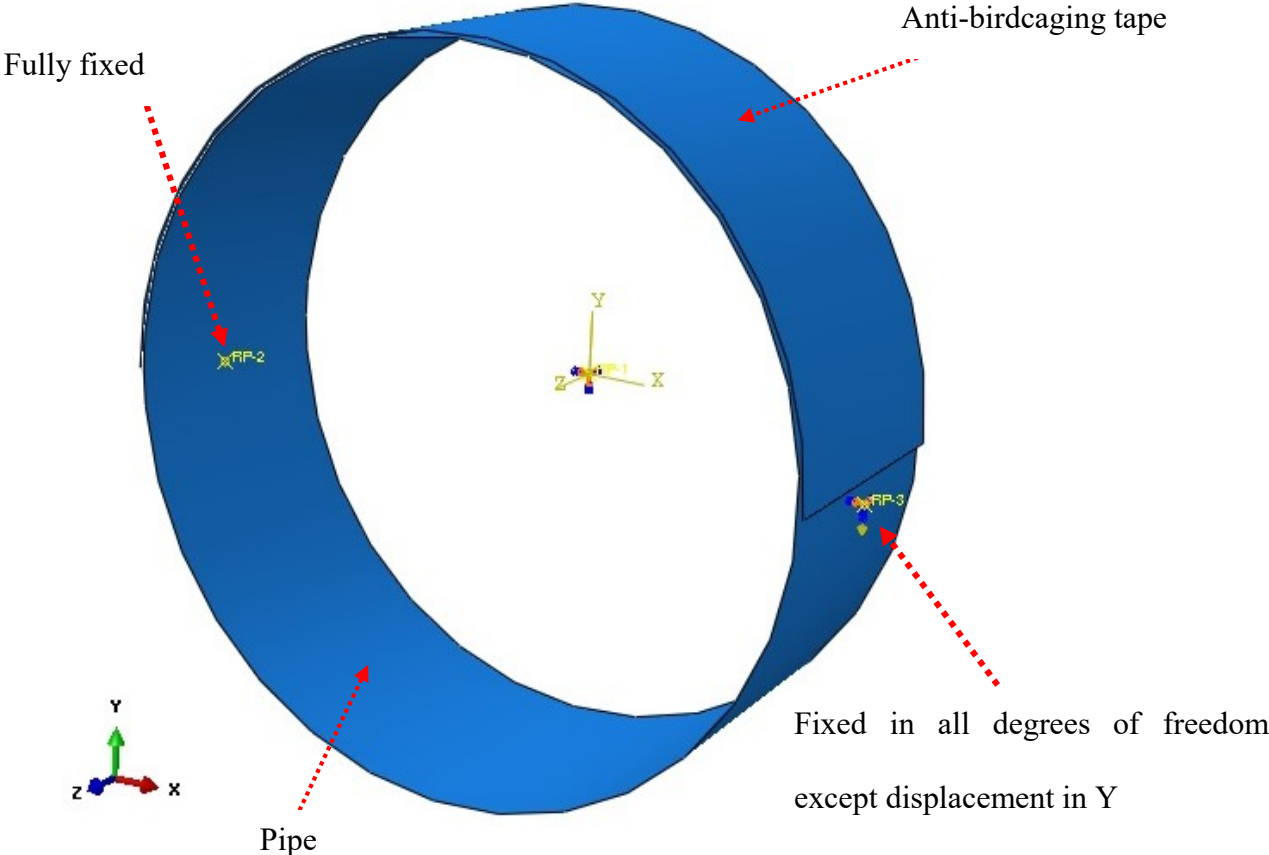


Figure 3-2. Modeling wrapping of anti-birdcaging tape around the pipe.

Results of modeling of wrapping procedure is shown in Figure 3-3, in which a uniform contact pressure equal to 0.1 MPa was caused at the interaction between the anti-birdcaging tape and the pipe. This contact pressure was considered as an initial condition for all models (all chapters) of this thesis. Therefore, even if the pipe was considered as laboratory condition (0 MPa of external and internal pressures) this initial condition was considered to cause the initial stress between layers of the flexible pipe.

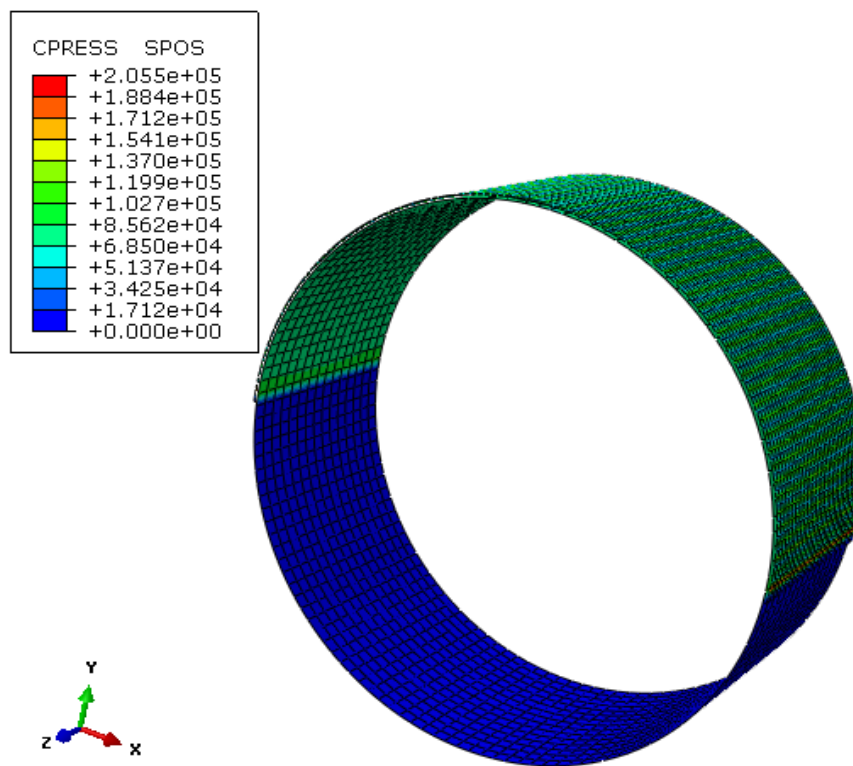


Figure 3-3. Contact pressure contour caused by anti-birdcaging tape wrapping procedure.

Due to the effects of inter-layer friction, it is hypothesized that the external and internal pressure may have significant role in the local radial buckling mechanisms by influencing the normal contact pressure and tangential shear stress. The effect of external hydrostatic pressure (0, 2.5, 5, 7.5 & 10 MPa), with no internal pressure (0 MPa), on the radial buckling response was examined

with an assumed interface friction coefficient ( $\mu = 0.1$ ). Another parameter study on the radial buckling response examined the effects of internal pressure (0, 10 & 20 MPa), with no external pressure (0 MPa) and an assumed interface friction coefficient ( $\mu = 0.1$ ).

The bird-caging mechanism is due to the presence of a damaged plastic sheath and leakage of seawater inside the annulus (i.e. wet buckling). It is hypothesized that the area of “wet surface” may influence the critical buckling load. In wet surface the external pressure is neutralized and the seawater pressure does not act as a constraint on the most exterior layer anymore. The damaged zone was located within the mid-length of the pipe on the circumference of the external plastic sheath and in the sensitivity study, the length of wet surface was varied as a percentage of the total pipe length (0.04, 0.08, 0.12 & 0.16).

### **3.4 Results and Discussions**

#### **3.4.1 Global Comparison with Physical Model Data**

In the first stage of this study, the finite element (FE) modelling procedures were calibrated with available physical modelling data presented by de Sousa [3]. The load conditions included no internal and external pressure with an imposed axial compressive force. Based on numerical simulations conducted in this study, the pipe deformation response due to the bird-caging mechanism is shown in Figure 3-4. The plastic sheath and anti-birdcaging tape is not shown for visual clarity.

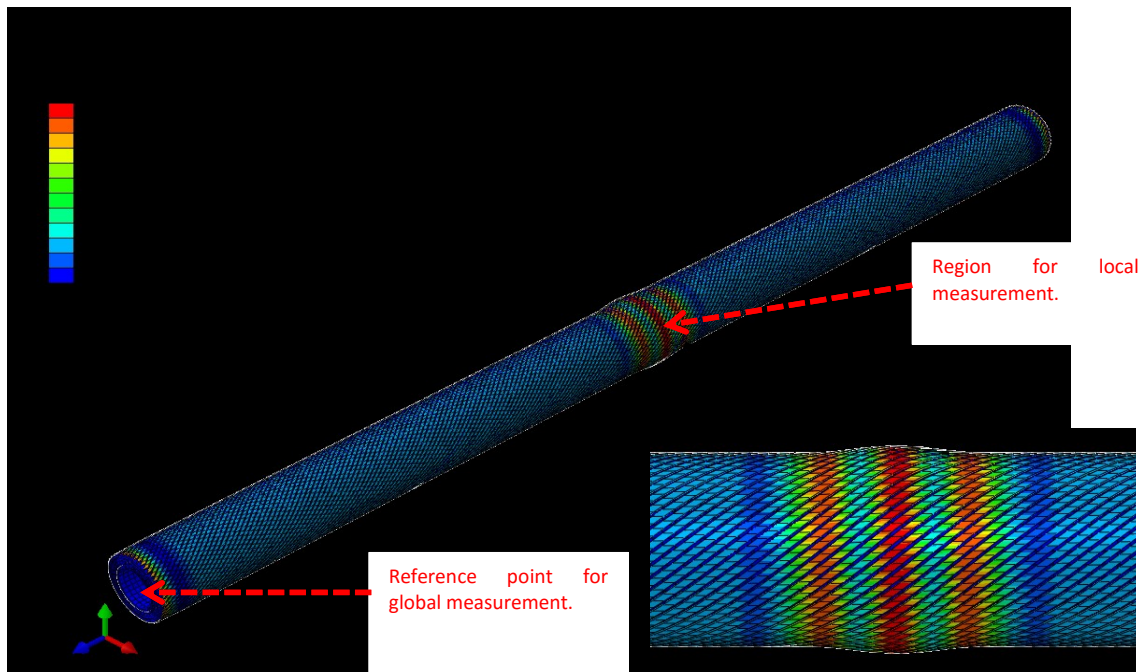


Figure 3-4. The pipe after bird-caging (Radial buckling).

Figure 3-5 and Figure 3-6 provide the predicted global axial reaction force versus global axial shortening per unit length and twist per unit length respectively, which are compared with the experimental results by de Sousa *et al.* [3]. The predicted global force, axial displacement and angle of twist for the finite element simulations were monitored at the reference point, which was positioned at the end of the pipe as shown in Figure 3-4. The confidence on occurrence of buckling in tensile armours is built by monitoring force-twist mechanism, Figure 3-6, as flexible pipe is a torsional-balanced structure which means if any instability gets started in the tensile armour wires, the instability is shown in form of either severe change in rate of twist or variation in twist direction. As it can be seen in the chapter 5 and 6 of this thesis, the form of torsional instability (i.e. change in twist rate or twist directions) is basically a function of different parameters like external pressure and friction force between layers. These parameters are the key factors for changing boundary conditions of tensile wires and local instability mode shapes.

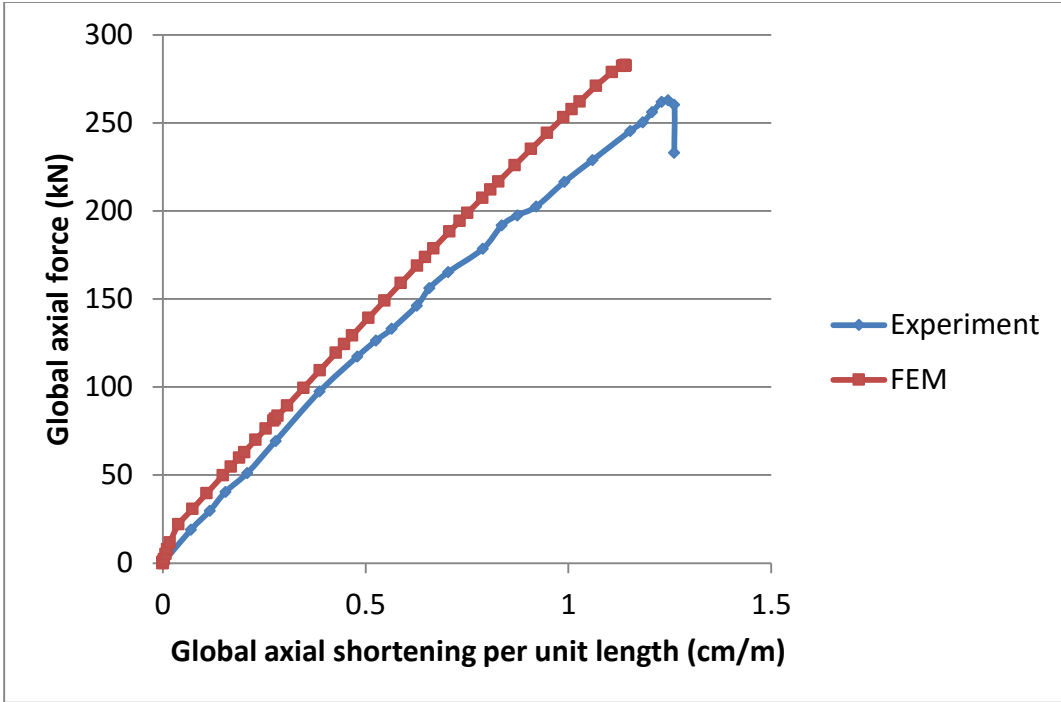


Figure 3-5. Global axial force versus axial strain at the reference point.

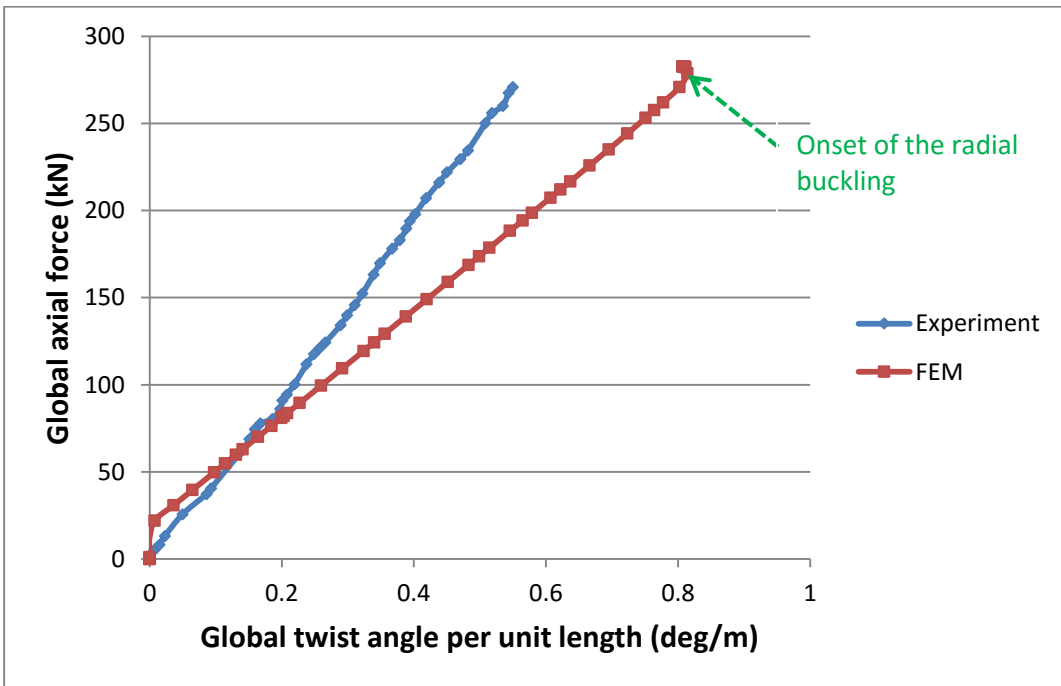


Figure 3-6. Global axial force versus twist per unit length at the reference point.

As it is shown in Figure 3-5 and Figure 3-6, and highlighted in Table 3-2, the FE model exhibits general consistency with the experimental tests for the axial force and displacement response but less correspondence with respect to the global torsional behaviour. Table 3-2 summarizes the global axial force, axial strain and angle of twist measured at the reference point.

Table 3-2. Buckling force in the FE model and model test.

Models	Buckling Force (kN)	Axial strain (cm/m)	Twist per unit length (deg/m)
FE model	282	1.14	0.81
Model test (Lab test)	263	1.24	0.53
% Difference	7%	-8%	42%

As highlighted in Table 3-2, there is better correspondence between the FE predictions and physical test for the axial force (i.e., equilibrium conditions) and axial strain (i.e. compatibility conditions) for the end reference point of the pipe segment. There is greater discrepancy for the angle of rotation (i.e., twist), which was attributed to the greater sensitivity and coupling effects with the birdcaging mechanism, and the need to measure local rather than averaged global response. It is expected to observe greater differences with the compatibility parameters (i.e., strain, angle of twist) that requires derivatives of the field variables (i.e. displacement) to be evaluated (e.g., Ugural *et al.* [7]).

The observed discrepancy, between the numerical simulation performed in this study and physical modelling conducted by de Sousa [2], may be due to differences in the material properties of the carcass and pressure armour layers, frictional forces between layers and contact interaction. This

data uncertainty was attributed to the limited information provided by de Sousa *et al.* [3] on the test procedures and measurements. For example, the magnitude and distribution of initial geometric imperfections and damage state in the pipe section was not reported, which would influence the peak load and any bifurcation path. Furthermore, as shown in this numerical study, global measurements, averaging the mechanical response over the pipe segment length, are not sufficient to capture local mechanisms and propagation of instabilities such as birdcaging. There is a need to characterize local parameters (e.g., geometric imperfections, material properties) and measure the local mechanical response. This data can be used to calibrate and verify modelling procedures and promote confidence in the numerical predictions.

Figure 3-7 illustrates the global axial force versus local compressive stress which is created in the middle section of the pipe in external and internal tensile armours (birdcaging place). The numerical simulation suggests the birdcaging mechanism occurs while the stress level in the tensile armour is below yield. The mechanical response of the pipe without external pressure can be interpreted from the stress variation in the tensile armour wires (Figure 3-7) as two different mechanisms. In the first stage, there are relative movements between the layers. The wires become compressed under the global axial force with no significant axial stress in the tensile armour wires until the gap between these tensile armour wires are reduced. In the second stage, exhibited by the horizontal plateau, the helixes have already been compressed with the gaps being reduced where the axial stress starts increasing due to increased constraint effects. Examination of the kinematic behaviour, with respect to the local compressive strain and global axial shortening per unit length (Figure 3-8), supports this hypothesis on the governing mechanisms. The local axial strain is measured within the external tensile armours at the location (Figure 3-4) where the birdcaging mechanism occurs. The global axial shortening compresses the tensile armour wires from one end

of the pipe, and reduces the gaps. Global axial shortening of 0.7 cm/m is needed to compress the gaps between one end and the middle section of the pipe without building up significant strain energy in external armours at the birdcaging location. Once the global axial shortening exceeds 0.7 cm/m, axial strain energy raises remarkably until the anti-birdcaging tape loses its radial resistance and the axial strain energy of external tensile armours turns into severe radial displacement and buckling (birdcaging). Propagation of this instability mechanism is a complex non-linear event.

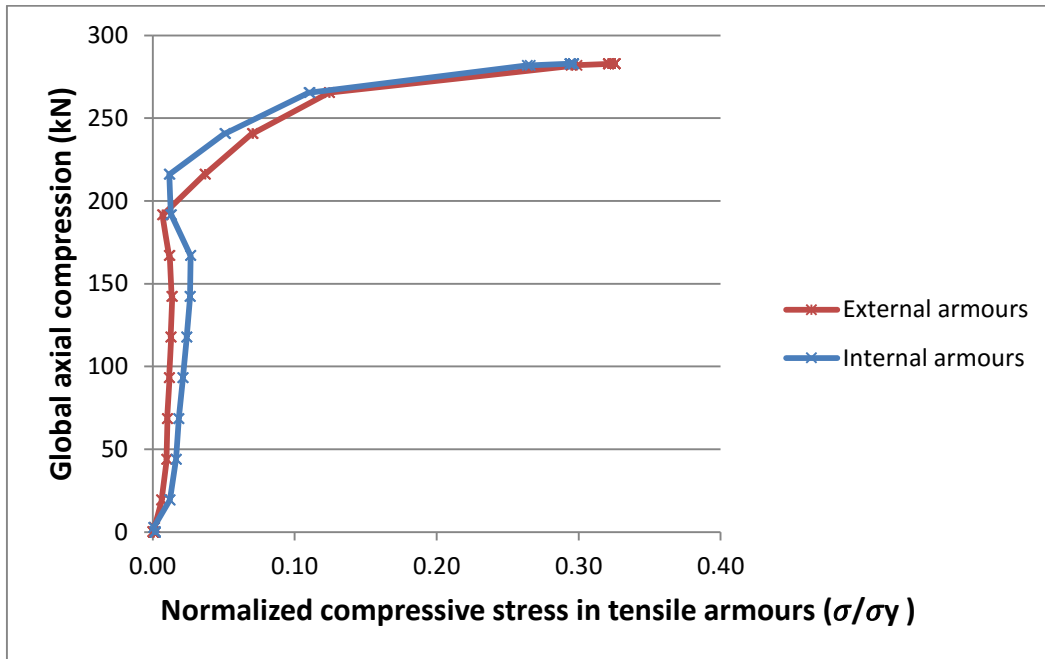


Figure 3-7. Global axial compression versus normalized axial stress in mid of the tensile armours.

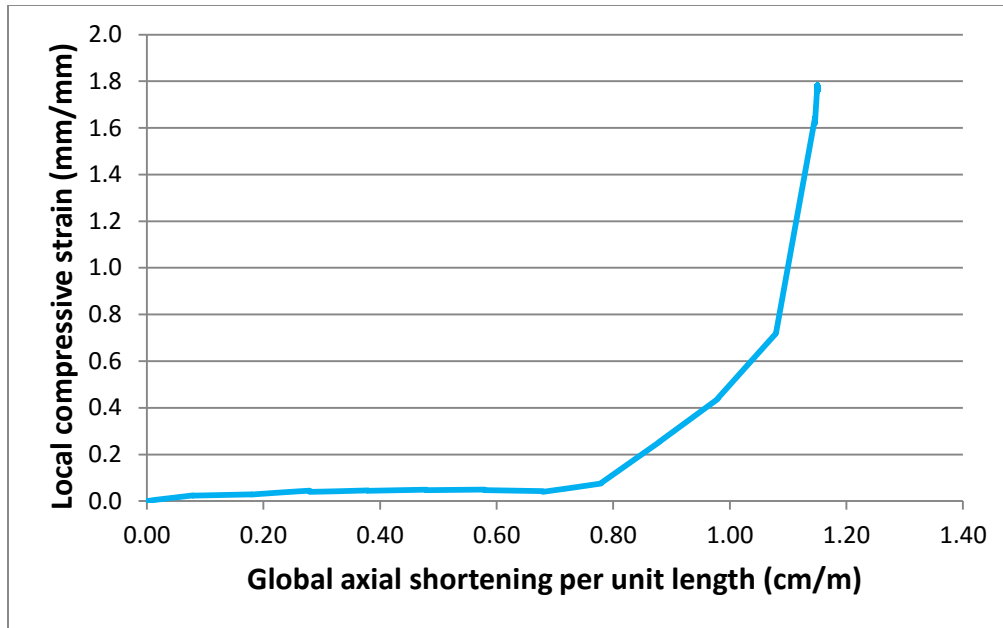


Figure 3-8. Local compressive strain versus global axial shortening per unit length.

### 3.4.2 Effect of Hydrostatic Pressure

In the next stage, the effect of external hydrostatic pressure (0, 2.5, 5, 7.5 & 10 MPa) was examined. The hydrostatic pressure was imposed on the exterior surface of the plastic sheath except for the damaged zone, which was associated with a wet surface region. Figure 3-9 and Figure 3-10 illustrate the effect of external pressure on the birdcaging phenomenon with respect to the global axial force-displacement and global axial force-rotation response. The effect of increasing external hydrostatic pressure was to increase the global pipe axial stiffness (by a factor of 2) and global axial rotation stiffness (by factor 4.14) and reduce the global axial force (by a factor of 0.7 to 0.8), displacement (by a factor of 0.3 to 0.4) and rotation (by a factor of 0.07 to 0.09) magnitude associated with the radial buckling instability.

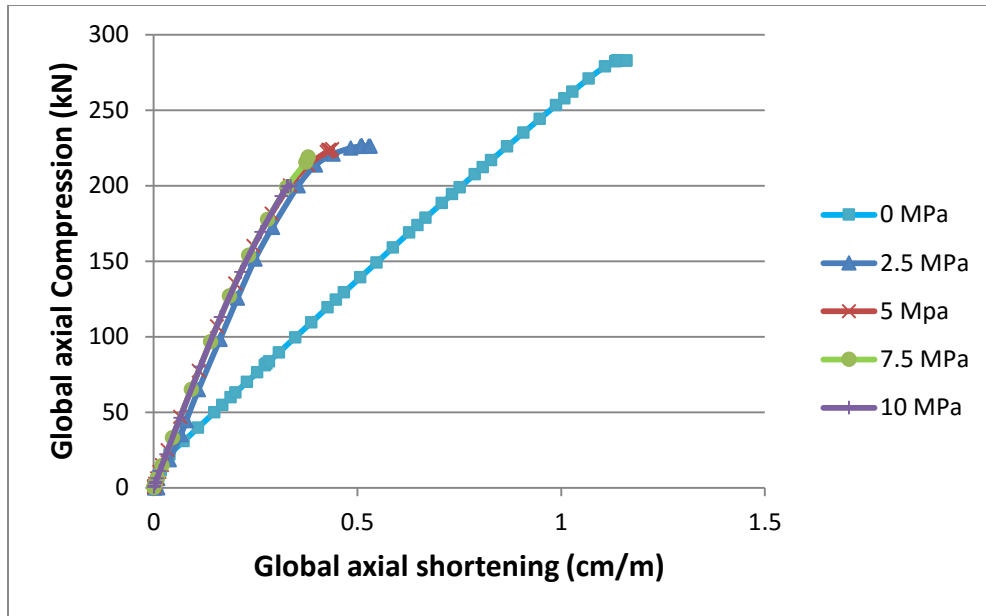


Figure 3-9. Global axial force versus displacement per unit length at the reference point for different external pressures.

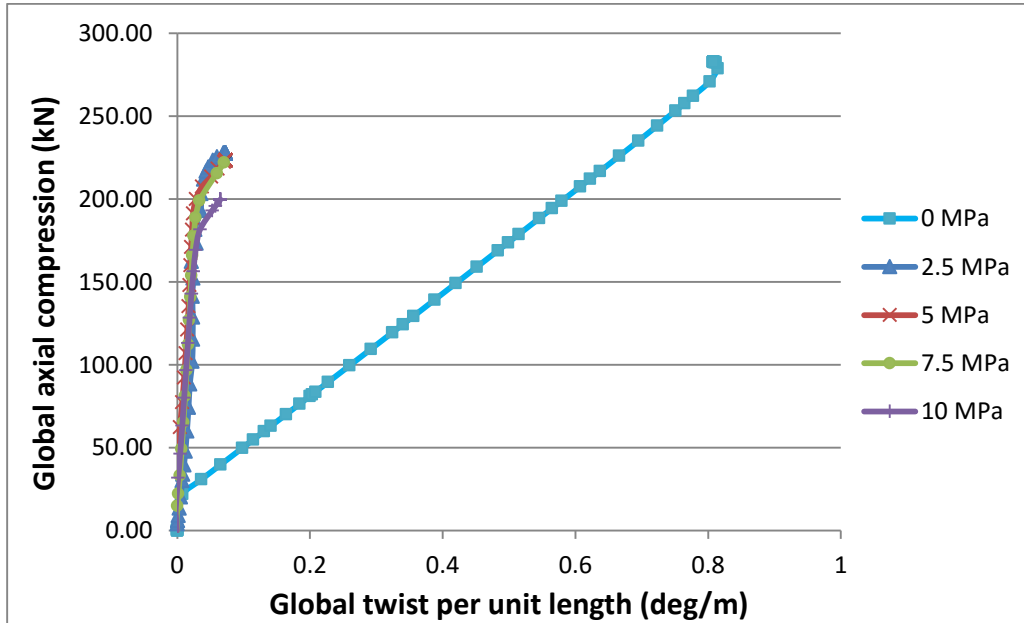


Figure 3-10. Global axial force versus twist per unit length at the reference point for different external pressures.

Through comparative examination of the local radial deformations (Figure 3-11) and axial strain response (Figure 3-12) with the global behaviour (Figure 3-9), the global axial force, measured at the pipe end reference node, is directly influenced by external hydrostatic pressure, and correlated with the development of local radial expansion and initiation of the birdcaging mechanism. For the zero external pressure load case, the tensile armour wires are relatively unconstrained, in comparison with the higher external pressure load cases, with the freedom to slip and translate along the longitudinal axis in response to the global axial force. The pipe experiences larger global axial forces and deformation prior to the initiation of buckling instability at the damage location. A critical strain of 0.7 cm/m is required to reduce or close the gap between tensile armour wires prior to the development of birdcaging mechanism and propagation of the instability. Introducing a small external hydrostatic pressure of 2.5 MPa provides sufficient constraint on the armour wires by reducing kinematic freedom on global axial motion (i.e., shortening) with greater magnitude of radial expansion achieved at lower global axial forces. Increasing the hydrostatic pressure tends to increase the constraint on the tensile armour wires that reduces the global axial shortening and axial forces required to initiate radial buckling instability.

The radial constraint caused by external pressure has another effect on the torsional mechanism (i.e. force-twist mechanism), Figure 3-10 . It was discussed earlier, for Figure 3-6, that the turn-back in the force-twist graph is the point which tensile armour wires buckle indeed. In condition that external pressure is imposed on the pipe, the turn-back almost fades as the interlocking caused by external pressure curbs the severe twist (i.e. tangential movement) of tensile wires.

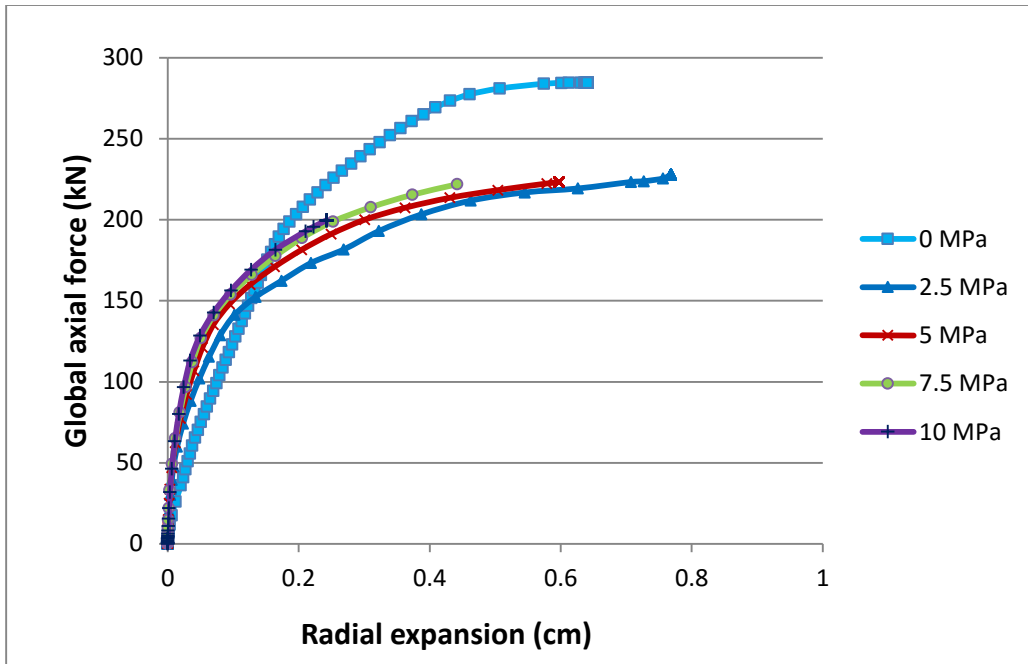


Figure 3-11. Global axial force versus local radial expansion at the mid length of the pipe for different external pressures.

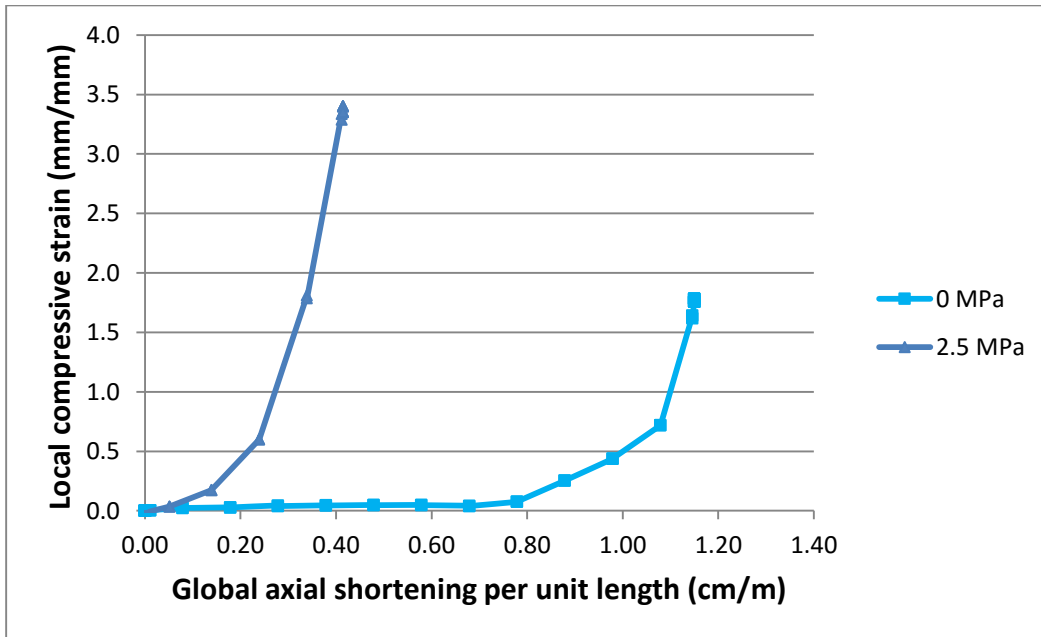


Figure 3-12. Local compressive strain versus global axial shortening per unit length.

Figure 3-13 shows global axial force versus twist at the middle of the pipe and in comparison with Figure 3-10 illustrates the effects of external pressure on the local twist deformation response within the location of birdcaging. The external pressure imposes a clamping force that constrains the armour wires from tangential movement (i.e., twist, displacement), as shown in Figure 3-10 and Figure 3-13 with respect to the significant increase in stiffness. The axial stress in the tensile armour wires starts to increase (Figure 3-14 and Figure 3-15) after axial shortening has started. In the presence of external pressure, a local buckling response occurs with greater stress and strain energy are accumulated in the tensile wires, Figure 3-14 and Figure 3-15, having less relative movement of wires in comparison with the zero external pressure load case. Differences between the global and local response are due to the reference scale where the global rotation response is measured per unit length, whereas the local rotation is an absolute value extracted at the mid of the pipe ( $L = 1.25$  m).

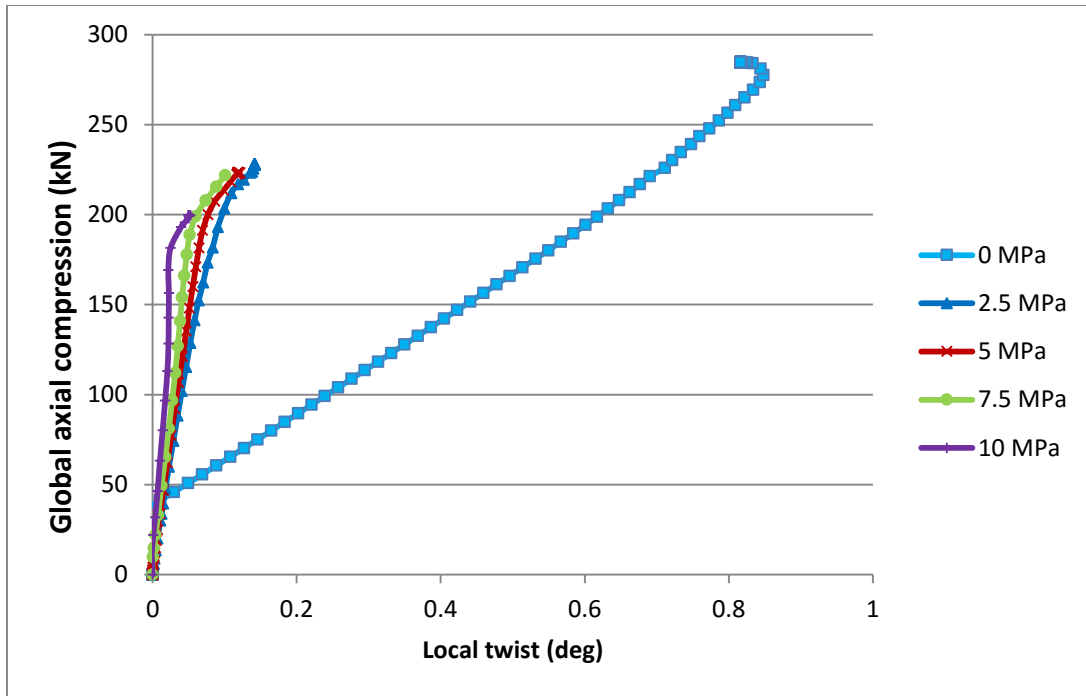


Figure 3-13. Global axial force versus local twist at the mid length of the pipe for different external pressures.

Figure 3-14 and Figure 3-15 illustrate axial stress level in external and internal tensile armours at the place of lateral instability due to birdcaging mechanism, respectively. As shown in Figure 3-14 and Figure 3-15, for the no external pressure load case, the global load increases with limited axial stress developing in the local armour wire response. The helical wires become compressed under the global axial force and move to fill existing gaps between adjacent wires. There is limited accumulation of axial stress and strain in the tensile armour wires during this response. Once the gaps are reduced and begin to close, the strain increases until the wires experience instability (i.e., bird caging or radial buckling). In the case of external pressure, the radial clamping force (interlocking) does not allow relative movements where the local axial strain and stress in the tensile armour wires increases as axial shortening is initiated. In this condition, the final level of the stress depends on the deformation mode, buckling force and instability mechanism. As illustrated in preceding Figure 3-9, Figure 3-10, Figure 3-11 and Figure 3-13 the tensile armour

mechanical behaviour (i.e. axial force, angle of twist, displacement) is significantly influenced by hydrostatic pressure that affects the contact mechanics (i.e. normal pressure, shear stress, layer interlocking) and kinematics (i.e. buckling instability and mechanism).

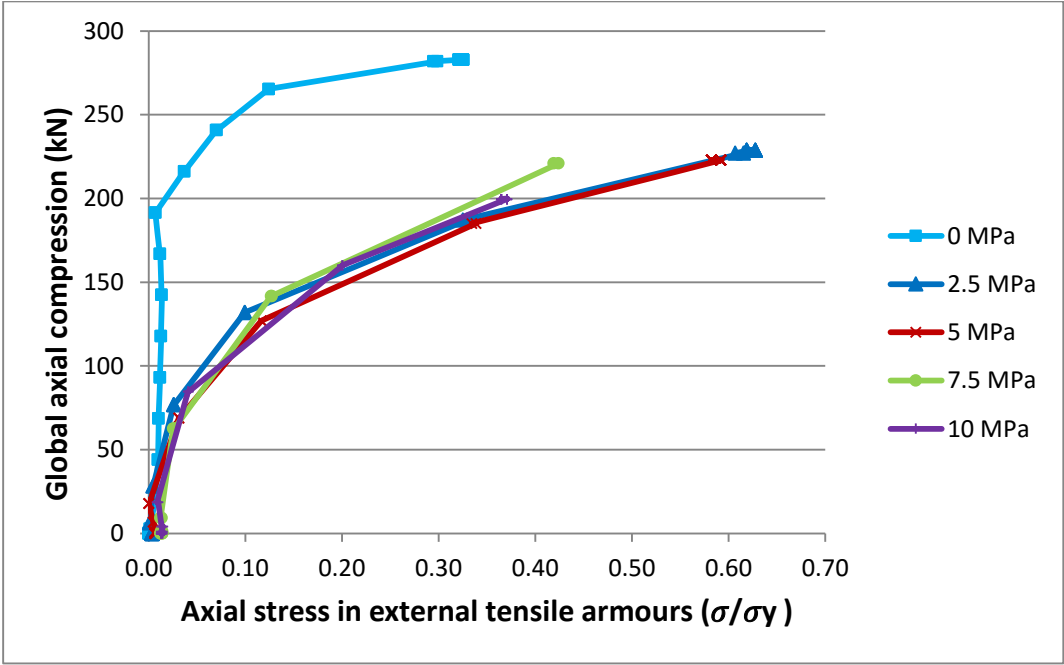


Figure 3-14. Global axial compression versus axial stress in mid of the external armours.

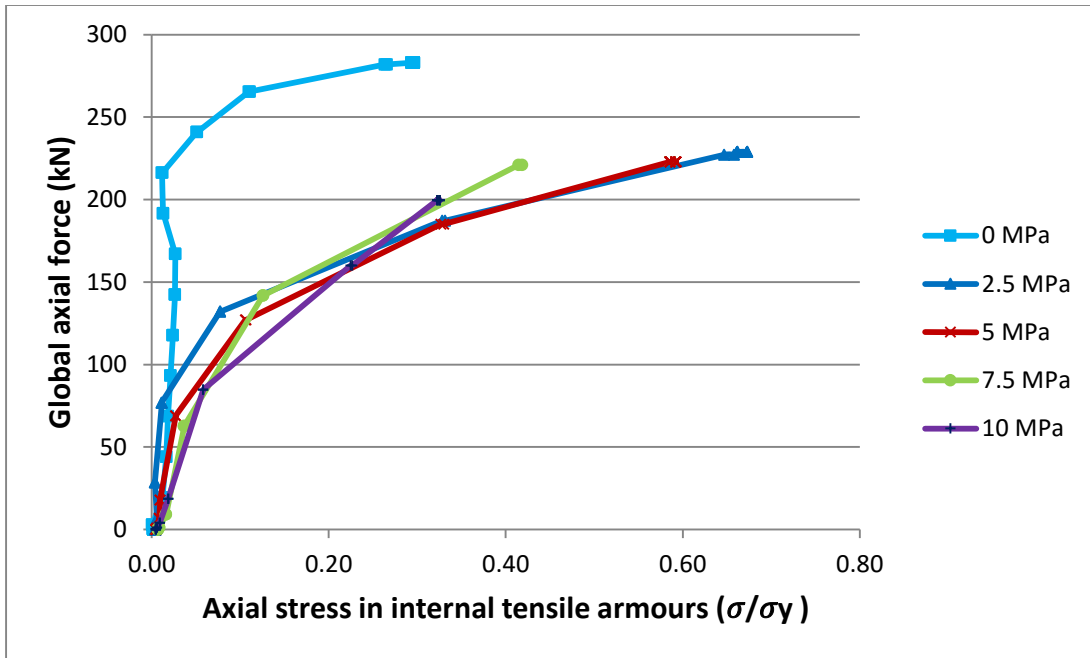


Figure 3-15. Global axial compression versus axial stress in mid of the internal armours.

Figure 14 illustrates the variation in the global buckling force, axial strain and angle of twist per unit length for the parameter study on the effects of hydrostatic pressure. The buckling force and axial strain exhibit a similar decrease (i.e. gradient related to stiffness) with a small increase in the external pressure from 0 MPa to 2.5 MPa. Further increasing the hydrostatic pressure does not significantly influence the mechanical response of the tensile armour wires with respect to axial force or strain. Increasing the hydrostatic pressure from 0 MPa to 2.5 MPa causes a reduction in the angle of twist per unit length by a factor of 0.1 without any significant influence with increasing pressure.

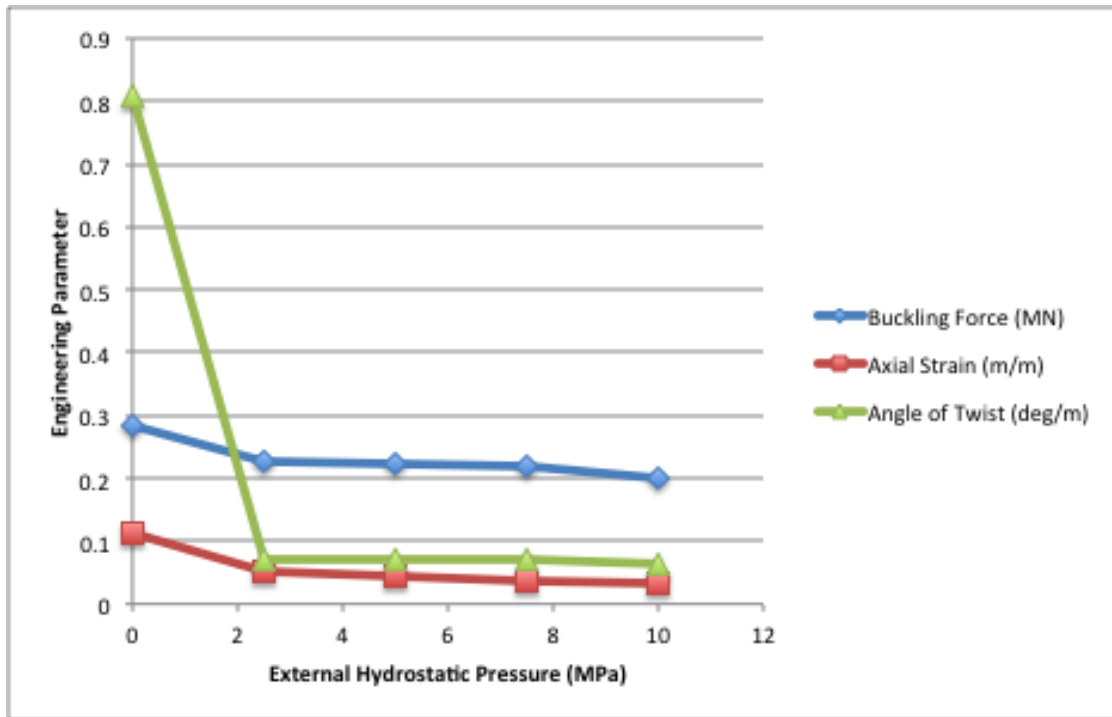


Figure 3-16. Influence of external hydrostatic pressure on axial buckling force, axial strain and torsional response

The mechanical response and buckling instability for the no hydrostatic pressure load case, in comparison with higher external hydrostatic pressure magnitudes, is due to the differences in the contact mechanics (i.e. normal contact pressure and tangential shear stress) that develops across the interface between layers, and the greater degree of kinematic freedom for the tensile armour wires during the loading event. Imposing greater external hydrostatic pressure increases the axial stiffness and effective torsional stiffness (Figure 15) that is related to an interlocking (i.e. sticking) mechanism between layers. Higher hydrostatic pressures limit the relative tangential movement between layers where the composite layered, flexible pipe mechanical response mimics a fully bonded interface. The change in axial stiffness was observed to be a non-linear function of the imposed external hydrostatic pressure, whereas the tangential shear stress response influencing relative slip was governed by the contact pressure and Coulomb friction model formulation.

Referring to Figure 3-9 and Figure 3-10, the buckling force tends to decrease with increasing external hydrostatic pressure, which initiates a radial buckling mode at lower buckling force or energy configuration (i.e. different bifurcation), even though the axial stiffness has increased, due to the interlocking mechanism.

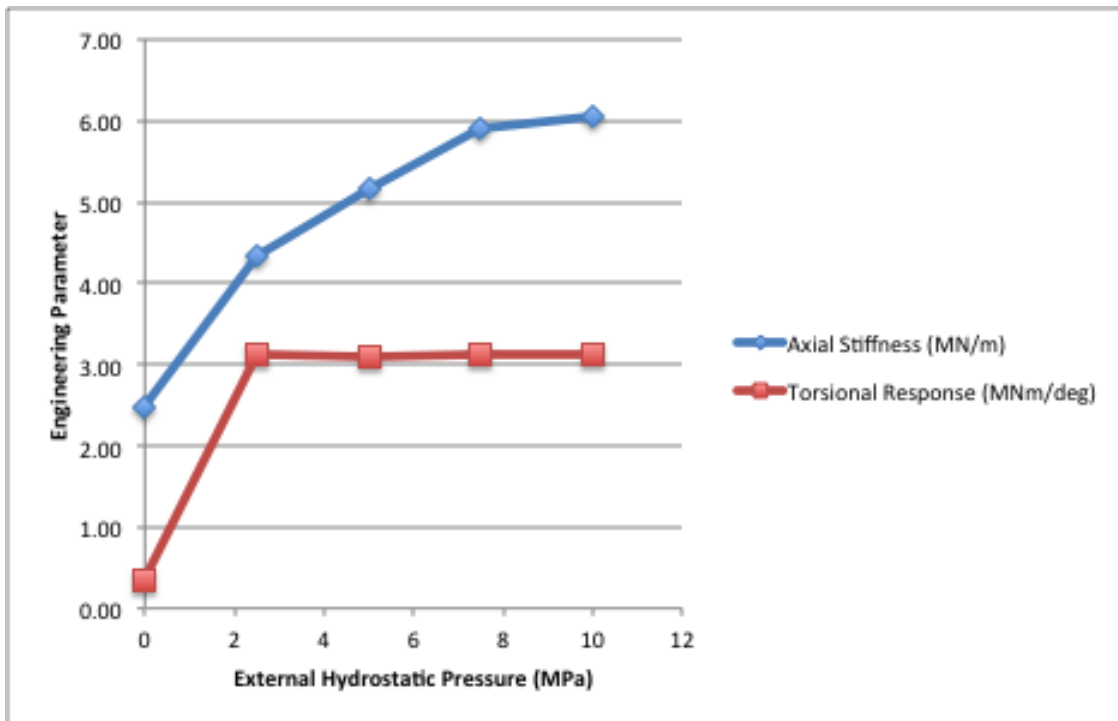


Figure 3-17. Influence of external hydrostatic pressure on the effective stiffness behaviour

### 3.4.3 Effect of Pipe Damage

The buckling load and mechanisms are typically influenced by the presence of geometric imperfections, which can be created in the pipe during the manufacturing, installation or operation. In this study, the wet annulus condition was defined as the ingress of sea water into the annulus and bounded by the adjacent leak-proof layer of the interior plastic sheath. Under this circumstance, the effects of hydrostatic pressure are neutralized for all layers (e.g. tensile wires)

except the carcass layers. Consequently, for the pipe layers subject to the wet annulus condition, the effects of hydrostatic pressure do not have to be accounted for in the natural (force) boundary conditions. The role of geometric imperfections on the local mechanical response of flexible pipes is studied below. The imperfection is characterized by a damaged condition in the plastic sheath and anti-birdcaging tape as defined by a reduced yield and ultimate strength. The damage length is defined as a percentage of pipe length with the damage location shown in Figure 3-18. The finite element simulations examined the laboratory condition damage state (4%) and damage lengths of 8%, 12% and 16% which were examined in this numerical study and centered in the pipe segment. In the study by de Sousa [3], the damage level or quantitative characteristics of the damage zone are not reported and thus a sensitivity analysis was conducted. In this FEA study, a 4% damage length was established as a representative damage condition relative to the available experimental data. Figure 3-18 shows the damaged area position in the pipe.



Figure 3-18. Damaged area applied in the middle of pipe length.

The influence of pipe damage on the pipeline mechanical response is illustrated in Figure 3-19 and Figure 3-20. The damage length does not significantly influence the load path to the bifurcation point, however, the amplitude of the buckling force and deformation at bifurcation is a function of the damage state. The FEA demonstrated greater confinement was observed with increasing external hydrostatic pressure and decreasing damage level in the anti-birdcaging tape. This condition would be similar to a defect free pipe imposed by higher external pressure. As the damage level decreases, the effects of greater shear stress and clamping effects were observed. In this condition, the pipe becomes slightly stiffer because the armour wires possess less freedom to move tangentially but the pipe buckle at lower axial force, Figure 3-19 and Figure 3-20. In other words, the smaller damage influences the same way as more external pressure does, in which once external pressure increases, the clamping area (e.g., interlocking) restrains the wire movements, while strain energy and stress start increasing and pipe buckles at lower axial force.

The turn-back in the force-twist mechanism, Figure 3-20, was discussed for Figure 3-6 Figure 3-10. This turn-back occur due to instability in tensile armour wires in which the wires manage to slip tangentially at the buckling point.

The global axial force, axial strain and angle of twist per unit length at the buckling point, is summarized in Table 3-3. In terms of percent difference relative to the laboratory test condition, the buckling force, axial strain and angle of twist per unit length for the 16% damage state was 16%, 18% and 23%, respectively. The rate of change or gradient in the axial force-displacement and axial force-angle of twist is presented in Table 3-4. In terms of percent difference relative to the laboratory test condition, the axial force-axial strain and axial force-angle of twist for the 16% damage case was 11% and 4%, respectively.

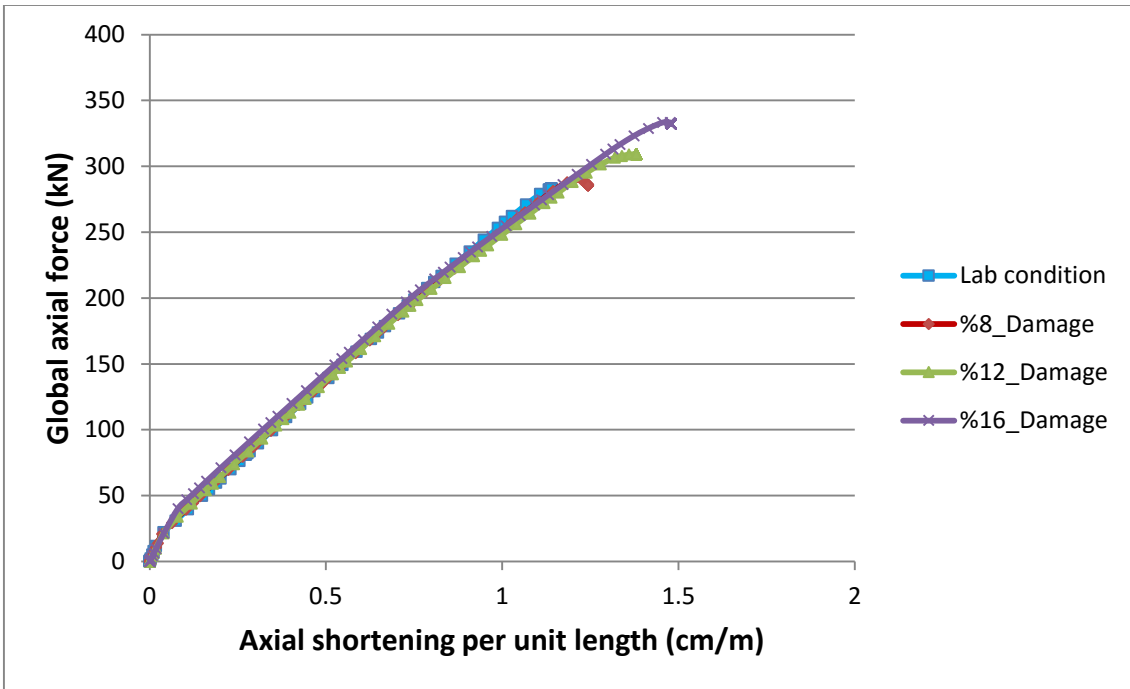


Figure 3-19. Global axial force versus axial shortening per unit length at the reference point for different damage lengths.

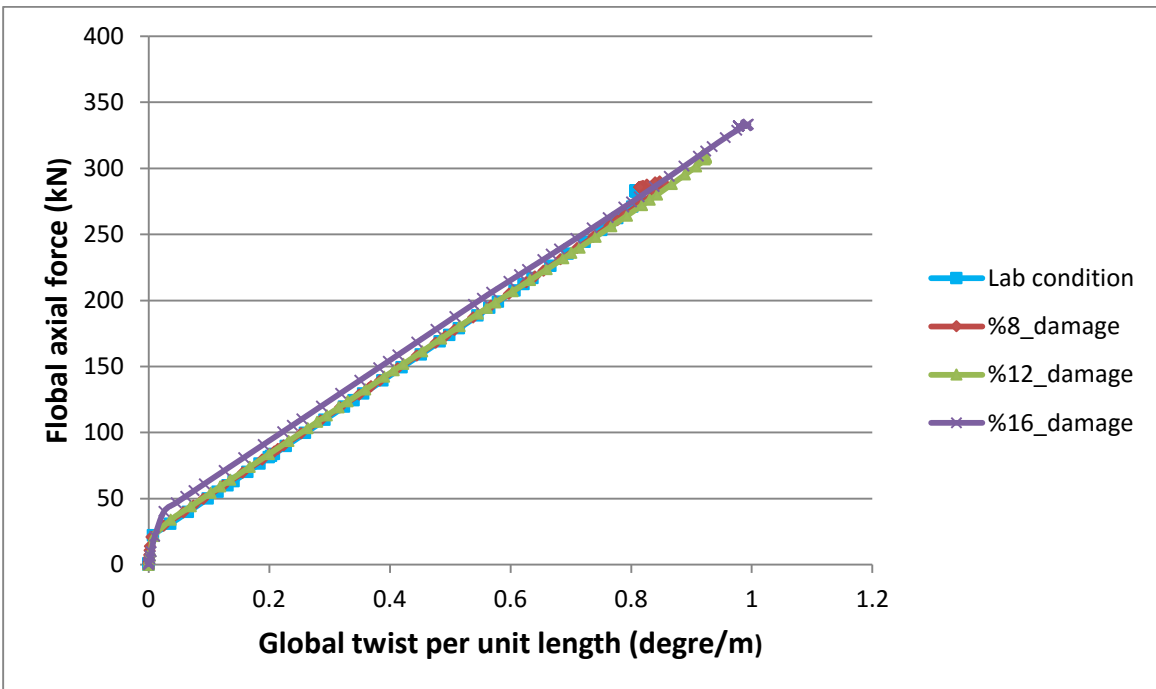


Figure 3-20. Global axial force versus twist per unit length at the reference for different damage lengths.

Table 3-3. Buckling force in different designed damages.

Damage percentage	Buckling Force (kN)	Axial strain (cm/m)	Angle of twist per unit length (deg/m)
Lab condition – 4%	283	1.14	0.807
8%	286	1.24	0.814
12%	309	1.38	0.918
16%	333	1.47	0.994

Table 3-4. Rate of compression in respect to axial force and twist per unit length

Damage percentage	Force/Axial strain (kNm/m)	Force/Twist per unit length (kNm/deg)
Lab condition – 4%	24345	33466
8%	22390	33491
12%	21821	32392
16%	21572	32196

#### 3.4.4 Effect of Internal Hydrostatic Pressure

Furthermore, the influence of internal pressure effects on bird-caging was examined through a numerical sensitivity study. The pipe under 20 MPa of internal pressure mimics the same behavior as the pipe tested under laboratory conditions de Sousa *et al.* [3], Figure 3-21 and Figure 3-22. Also, in terms of percentage of difference relative to the laboratory test condition, the global

buckling force, axial strain and angle of twist per unit length remain unchanged. That is because of high radial strength of pressure armours. The pressure armour is placed before tensile armours and so it stands for radial expansion caused by internal pressure (The pipe core under 20 MPa of internal pressure expand radially just as 0.02 mm) without letting any contact pressure be transferred onto the tensile wires. Consequently, the internal pressure cannot impose contact pressure between tensile wires and adjacent layers and layers do not stick together. So, the pipe remains unbonded and the mechanical response does not change through application of external pressure.

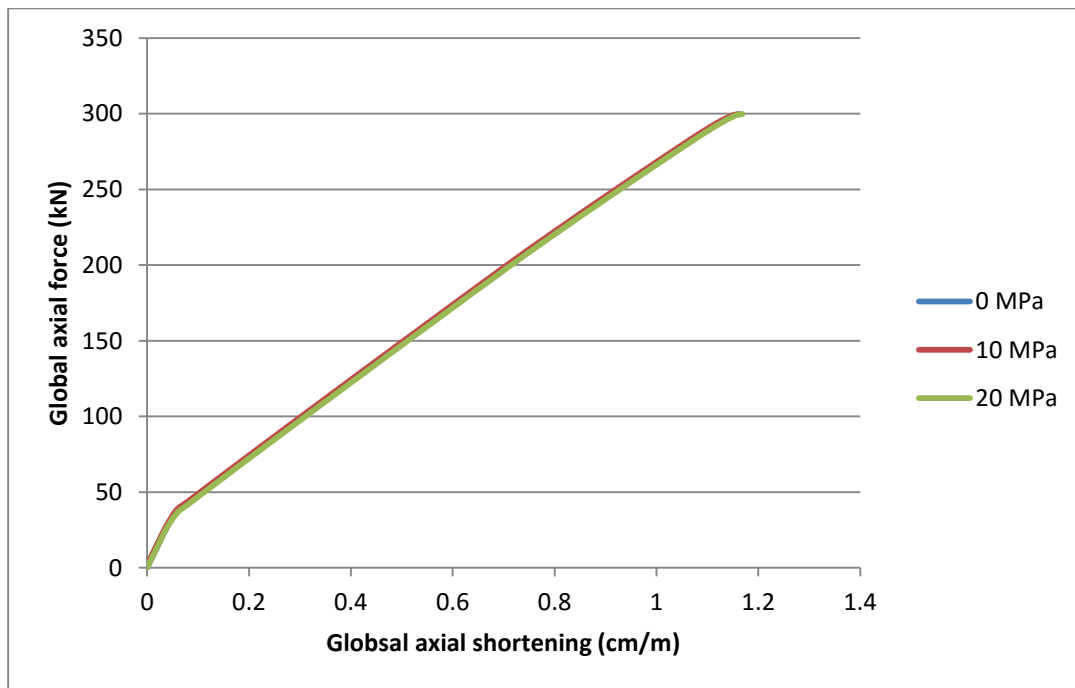


Figure 3-21. Global axial force versus global axial shortening under various internal pressures.

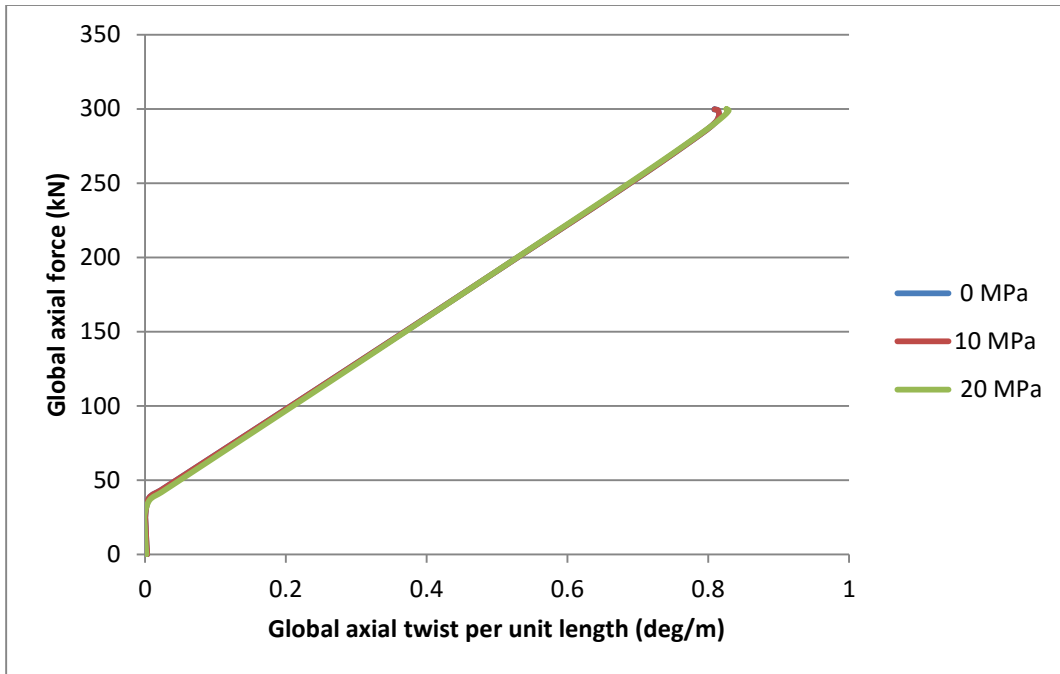


Figure 3-22. Global axial force versus global axial twist under various internal pressures.

### 3.5 Conclusion

Due to the complex mechanical response of each layer of flexible pipe and the corresponding interactions between adjacent layers, there are few analytical and numerical modelling studies addressing the mechanical performance of composite flexible pipe. These investigations are constrained by their underlying idealizations and assumptions. To improve knowledge, and advance current design standards, it is important to develop a thorough understanding of the pipe mechanical responses in the radial buckling failure by elimination of assumptions of previous studies.

In this study, radial buckling (i.e., birdcaging instability) of a 4-in flexible pipe is investigated through a finite element model which enjoys implicit solver for improving accuracy of contact interactions and run-time expenses. The numerical procedures are calibrated using experimental

data presented by de Sousa *et al.* [3]. Key factors influencing the radial buckling response, including internal and external pressure, and damage level in the anti-birdcaging tape and plastic sheath, were examined through a parameter study.

The results demonstrated the radial buckling mechanism and characteristic parameters (e.g., global or local force, deformation) was mainly influenced by the radial contact pressure and shear stress between the layers. The radial buckling occurs due to the rupture of plastic sheath and anti-birdcaging tape leading to sudden drop in axial stiffness and increase in radial expansion, while the tensile armour wires are still in the elastic region. The external hydrostatic pressure and level of damage influences the inter-layer contact stress state that affects the buckling mechanism with respect to the limit load, and the axial strain and angle of twist prior to the onset of local buckling instability (i.e., bird caging response). Also, it was concluded that the turn-back in the force-twist mechanism of the pipe is due to the instability of tensile wires. This turn-back is noticeable once the amount of radial confinement is small enough (i.e. pipe without external pressure). If the radial constraint increases by any factor (e.g. external pressure) this turn-back almost fades and the wires do not find chance to have severe twist (i.e. tangential movement) at the buckling point.

In future studies, experiments should be conducted to examine the effects of imperfection or damage level on the birdcaging mechanism. The use of a deep water immersion test facility to better simulate the combined stress state due to external pressure, axial force, bending and torsion should be investigated. On this basis, experimental data can be used to improve confidence in the numerical simulation tools, across a range of practical and realistic load case scenarios, to assess the effects of interlocking on the birdcaging mechanism. The significance of pipe effective length on radial buckling should also be examined in these experimental and numerical studies.

### 3.6 References

- [1]. Technip, “Coeflexip-flexible steel pipe for drilling and service applications”, 2014, page 2-3.
- [2]. Vaz M.A, Rizzo N.A.S, “A finite element model for flexible pipe armor wire instability”, *Journal of Marine Structures*, Volume 24, 2011, page 275-291.
- [3]. De Sousa R.M, Viero. P.F, Magulta. C, Roitman. N., “An experimental and numerical study on the axial compression response of flexible pipe”, *OMAE 2012, 31<sup>st</sup> International Conference on Ocean, Offshore and Offshore Engineering*, Rio de Janeiro, Brazil. July 1-6, 2012.
- [4]. Serta, O., Fumis, R., Connaire, A., Smyth, J., Tanaka, R., Barbosa, T., Godinho, C., “Predictions of armour wire buckling for a flexible pipe under compression, bending and external pressure loading”, *OMAE 2012, 31<sup>st</sup> International Conference on Ocean, Offshore and Offshore Engineering*, Rio de Janeiro, Brazil. July 1-6, 2012.
- [5]. Braga M. P., Kalef P., “Flexible pipe sensitivity to birdcaging and armor wire lateral buckling”, *OMAE 2004, 23<sup>rd</sup> International Conference on Offshore Mechanics and Arctic Engineering*, June 20-25, 2004, Vancouver, BC, Canada.
- [6]. De Sousa R.M, Magulta C., Roitman. N., Elliwanger G. B., Lima E.C.P., Papaeo A., “On the response of flexible risers to loads imposed by hydraulic collars”, *Applied Ocean Research* 31 (2009) 157–170.
- [7]. Ugural, A.C., Fenster, S.K., “Advanced strength and applied elasticity”, PTR Prentice-Hall, second edition, 1987, page 38.

- [8]. Bui, T., Choi, Y.S., “Explicit and implicit methods in solving differential equations”, 2010, honors scholar theses, paper 119.
- [9]. Cavalieri, F.J., Cardona, A., Fachinotti, V.D., and Risso, J. (2007). “A finite element formulation for nonlinear 3D contact problems.” *Mecanica, Computacional*, 26:1357-1372.
- [10]. Fourment, L., Chenot, J.L. and Mocellin, K. (1999). “Numerical formulations and algorithms for solving contact problems in metal forming simulation.” *Int. J. Numer. Meth. Engng.* 46: 1435-1462.
- [11]. Pike, K., Kenny, S., Kavanagh, K. K Jukes, P. (2012). “Pipeline Engineering Solutions for Harsh Arctic Environments: Technology Challenges and Constraints for Advanced Numerical Simulations.” *Proc., OTC-23734*, 9p.
- [12]. Benson, D.J. and Okazawa, S. (2003). “Contact in a multi-material Eulerian finite element formulation.” *Comp. Methods Appl. Mech. Engg.* 193:4277–4298

## **Preface**

This journal research paper is an original study and the developing idea, planning and implementation of the whole technical parts of this research paper have been done by the candidate as the first author, and the regular supervision has been made by Dr. Shawn Kenny through advising on the planning of the research way, evaluation of the research merit and providing precious idea and experience on the discovered phenomena and technical parts. The compilation of the paper literature has also been implemented by the candidate and it has been continuously revised by Dr. Shawn Kenny to improve the quality of the technical part and the literature. Facilitation of the PhD program of the candidate and also final review of the paper has been made by Dr. Amgad Hussein as the third author. Wood Group Kenny Research Chair at Memorial University of Newfoundland has funded the whole PhD program study and provided the all facilities (cluster machine, Software and personal computer) for carrying out the study.

This journal research paper was submitted to the Journal of Offshore Mechanics and Arctic Engineering (an ASME Journal) on July 11th, 2015.

## **4 Elastic instability in tensile wires of subsea flexible pipe under axisymmetric loads**

Alireza Ebrahimi (1), Shawn Kenny (2), Amgad Hussein(1)

(1) Faculty Engineering and Applied Science, Memorial University of Newfoundland

St. John's, NL, Canada

(2) Department of Civil and Environmental Engineering, Faculty of Engineering and Design,

Carleton University

Ottawa, ON, Canada

### **4.1 Abstract**

Flexible pipe are extensively used in subsea applications such as flowlines, jumpers, and risers for the transport of hydrocarbon products from production fields to local subsea infrastructure and offshore facilities. Advancements in the technical requirements for the design and operational performance envelope of flexible pipe are required to meet the demands of harsh environments such as deepwater and northern shallow water regions. Flexible pipe have a complex cross-section to address specific load components such as hydrostatic pressure and axial forces. Numerical modelling provides a framework to examine the mechanical response of flexible pipe subject to design loads for defined damage states or failure mechanisms.

In this study, continuum finite element modelling procedures were developed to evaluate nonlinear behaviour, associated with large deformations and contact mechanics, and kinematics, associated with deformation mechanisms and the potential propagation of instabilities. Idealized structural models, which may not account for these effects or interaction, may provide incomplete or

imprecise conclusions based on interpretation of the simulation results. The effects of axial tensile load, interface friction and hydrostatic pressure on torsional response are evaluated through a numerical modelling parameter study. The numerical predictions are in agreement with analytical studies and available experimental data.

Key words: Subsea flexible pipe, axisymmetric loads, sensitivity studies, elastic instability, lateral buckling.

## **4.2 Introduction**

Flexible pipeline has numerous applications in offshore oil and gas industry because of low bending stiffness and high strength in axial direction. This is because of various composite and steel layers are used in the structure of this pipe. This character makes flexible pipeline capable to transfer oil and gas from wellhead to the fixed and floating platforms, or to inject water into the wells.

Each individual layer of flexible pipe has its own duty in the pipe structure. The most inner layer is carcass which is profiled steel strips. This layer made to resist toward external pressure. The next layer is an internal plastic sheath made to prevent fluid leakage. Another profiled steel strip layer with Z-shape profile added to the other layers to withstand internal fluid pressure. Some anti-wear layers are considered in this pipe structure to reduce wear between metallic layers. High strength tapes are used to provide more radial strength. The layers which are made to stand toward tension, torsion, bending and even compression type of loading are the tensile armour layers. Figure 4-1 illustrates the cross-section of a flexible pipe considered in this study.

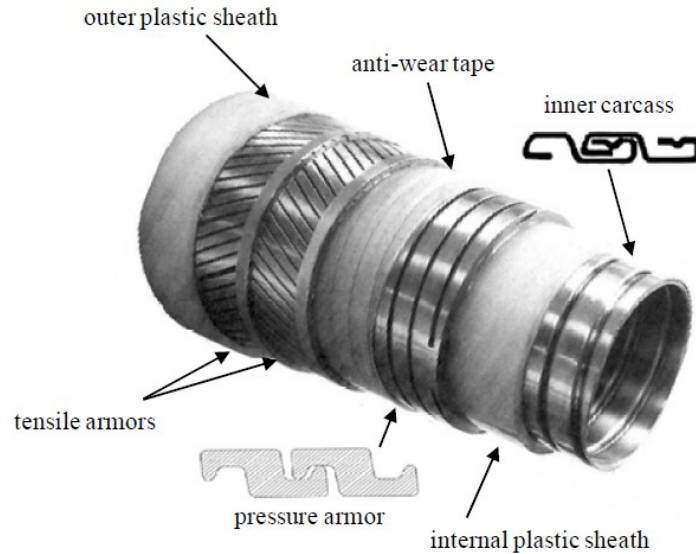


Figure 4-1. Cross-section of flexible pipe [1].

Previous studies concerning axisymmetric mechanical behavior of unbounded flexible pipe can be categorized into analytical, numerical and experimental approaches. While the analytical method enjoys computational efficiency, there are underlying idealizations that may influence predictions of the flexible pipe mechanical including:

Linear elastic, isotropic material properties with small strain behavior, lack of friction effect between layers, ignoring the separation between composite layers, elongation and angle of twist is equal for all composite layers, uniform loading along the pipe segment length or cross-section circumference, which ignores local effects due to distributed loading, and variable contact pressure and interface shear stress, and fully bonded interface (i.e. stick condition).

An early study by McNamara [2] presents an analytical solution for the mechanical response of flexible pipe but was limited to linear, small strain material behavior and did not account for the effects of interlayer friction and pipe section ovalization in the formulation. Ramos *et al.* [3] proposes an analytical method to estimate stress and deformation components in flexible riser,

which is imposed by combined loads, bending, twisting and tension. The results of the analytical approach are compared with previous experimental studies. This work examined the validity of these analytical idealizations, used in previous studies. Based on the work presented in this study, however, these simplifying conditions may not be realistic for some practical design conditions.

The advancement of numerical simulation procedures (e.g., finite element method) accounting for non-linear behavior (i.e., deformation, material, contact conditions) and computational hardware (e.g., parallel processors) provide a robust tool for the prediction of complex flexible pipe mechanical behavior and deformation mechanisms. This modeling framework is not constrained by the idealizations of the analytical solution that provides a more realistic simulation. In the following paragraphs, studies on the mechanical behaviour of flexible pipe using finite element methods are reviewed.

One common failure mechanism happens under pure axial torsion or combined with tension. Bahtui *et al.* [4] investigated 203 mm (8") diameter pipe under separate load cases. In this study, the pipe is pre-stressed by internal and external pressure. In the next step, he examined the pipe under different load cases which are tension, torsion and bending. The explicit solver was used, however, it is shown later in this study that implicit time integration schemes are more accurate. to validate their analytical approach. The comparison shows high consistency. The analytical solution is consolidated through three different formulations are used to account for the effects of layer separation, birdcaging mechanisms and interface sliding. Although the pipe was unbounded, the analytical solution was shown to be consistent with the FE simulations. The significance of variable loading conditions and non-linear kinematic effects (e.g., interlayer deformation, contact interactions) were not observed. The reasons for this observed response are uncertain..

Corre *et al.* [5] focuses on finite element analysis of umbilical to model more realistic tangential contact interaction and created moment caused by friction between internal layers. The finite element model is compared with similar analytical studies. Beam elements were used to model the tensile behavior, which improves solution efficiency but only accounts for stress and strain components in the axial direction.

Bahtui *et al.* [6] examined the tensile behavior of flexible riser using different analytical approaches to minimize assumptions of each individual method and have more realistic result for validation. An Explicit solver is chosen to address time expense due to many contact interaction, but as Explicit method does not enjoy equilibrium check, the time increment is specified so small,  $\Delta t=5e-7$ , to improve accuracy of the solver.

In a study by de Sousa [7], a 63.5 mm (2.5”) flexible pipe is examined under axisymmetric load conditions for pure tension, tension combined with torsion and internal pressure. The ANSYS FE model is validated with a series of experiments subject to the same load conditions. This work is a valuable resource to gain confidence in the development of numerical simulations and extend the knowledge base through parameter studies (e.g., effects of interface friction, external and internal pressure). This study, however, does not provide any local measurement data or details on the solution procedures used.

Although some of the previous researches both numerical and analytical might are compared by some experimental studies, there is a study by Merino [8] which is mostly dedicated to experimental facet. He studied the response of flexible pipeline to the pure torsion, tension combined with torsion experimentally which is compared with numerical and analytical approaches. His work can be such a reliable resource for further study, as it is supported with all

three. The analytical solution does not account for slip-stick phenomena. The solution method in finite element analysis plays significant role and it is not declared what kind of solution method is applied. Although, by considering theory of separation of layers the FE results look more sensible in respect to the analytical one, this might be noticed that there is no nonlinearity in torsional behavior of the pipe. Also, the decrease of torsional stiffness is justified by separation of layers while there is no quantitative report to prove this statement. This work can be supposed as a reliable method in experimental approach, while it needs complementary studies to improve solution method to highlight nonlinearity and improve accuracy, local measurement to prove separation of layers due to torsion, and further assessments on key factors (e.g. friction coefficient).

Most numerical modelling studies, using finite element methods, investigating the mechanical response of flexible pipe have adopted an explicit scheme to solve the equations of motion. The explicit solution is generally selected for dynamic impulse and stress wave propagation problems where the solution is conditionally stable based on the minimum critical time step. The critical time step is a function of the element size, elastic material properties and local changes in stiffness (e.g. variation in components, plasticity, incompressibility), and stress wave speed. For flexible pipe simulations, the critical time step is on the order of  $10^{-7}$  s to ensure unconditional stability of the solution (i.e. not encounter drift or divergence). The explicit solver can also be used to mitigate severe discontinuities associated with the large number of contact interactions between multiple element layers. However, one of the more significant issues is the explicit method does not enforce equilibrium conditions with respect to the balance of residual forces, which can be significant when examining nonlinear behaviour (e.g. plasticity, contact). Although implicit solvers are generally used to solve static, quasi-static and structural vibration problems, the explicit solver has been used to address numerical difficulties associated with complex nonlinear contact conditions.

The implicit scheme, however, is unconditionally stable, performs equilibrium checks and updates the stiffness matrix due to nonlinear behaviour (e.g. geometry, material) following each iteration.

In this study, FE method is used to examine the response of the flexible pipe to tension and torsion loading. The 3-D FE modeling procedures are calibrated based on the studies of de Sousa [7] and Merino [8]. The importance of the solution method (e.g., implicit versus explicit) and requirements for the interlayer contact algorithm are examined. Furthermore, the internal contact mechanism, (e.g. relationship between friction, normal contact and loading) is examined. Significant influencing factors in torsional behaviour of tensile armours like interaction and friction between layers and internal and external pressure are examined through a parametric study.

### **4.3 Finite Element Model**

A 3D continuum finite element model was developed with nine separate layers to represent the flexible cross-section. A summary of the geometric and material properties, and element characteristics are presented in Table 4-1 with some of the data adopted from the study by de Sousa [1]. The total length of the modeled pipe is 1.25 m. In order to reduce computational effort, the carcass and pressure armour layers, which comprise interlocking profiled components, are modeled as a simple cylinder, using shell elements (S4), with orthotropic material behaviour [1]. The anti-wear tape and plastic sheath layers are also modelled as a simple cylinder, using shell (S4) elements, with isotropic material properties.

Table 4-1. Characteristics of each individual layer.

Layer	Mechanical Properties					Element Type
	Thickness (mm)	Elastic Modulus (GPa)	Poisson's Ratio	Yield Stress (MPa)	Rupture Stress (MPa)	
Carcass (Lay Angle 87.6°)	4.0	193	0.3	320	640	Shell (S4R)
Plastic Sheath	5.0	345	0.4	20	22	Shell (S4R)
Pressure Armour (Lay Angle 87.0°)	6.2	205	0.3	900	1000	Shell (S4R)
Anti-Wear Tape	2.0	350	0.4	20	22	Shell (S4R)
Inner Tensile Armour (Lay Angle 35.0° with 47 wires)	2.0	205	0.3	1260	1400	Shell (S4R)
Outer Tensile Armour (Lay Angle 35.0° with 48 wires)	2.0	205	0.3	1260	1400	Shell (S4R)
High Strength Tape	1.2	0.75	0.3	40	44	Shell (S4R)
Outer Plastic Sheath	5.0	215	0.4	20	22	Shell (S4R)

Surface-to-surface contact discretization is used to have smooth contact and avoid stress concentrations at nodal points. In node-to-surface contact the master nodes may penetrate into the space between the slave surface nodes where there is no defined constraint between the slave nodes. This can be more severe in curved surfaces, when there is more probability of penetration under small loading. Unlike node-to-surface in which the slave nodes are just in contact with master surface, in surface-to-surface algorithm the contact constraint is also defined over regions around slave nodes. In other word, an average sense penalty stiffness is defined as well as each node of slave surface to avoid penetration of master surface into slave surface. This formulation

makes contact interaction smoother with less noise and decreases the possibility of penetration of master surface into slave one.

Concentric faceted (meshing discretized) cylinders are prone to have initial penetration into each other. Abaqus possesses capability to remove these initial over-closures automatically and render smooth surface which are adapted well onto each other. This important and beneficial feature is activated in this model to reduce contact discrepancy and equilibrium problem due to initial over-closure.

Hard normal contact with different frictional coefficients in the tangential direction, to be matched with validation results, were defined. The contact interaction between layers with different geometric properties, material characteristics and design functions, and large deformation response of the tensile wire during radial buckling requires the use of nonlinear solution techniques with precise mesh topology to achieve successful outcomes. In Figure 4-1, the cross-section of the multi-layer pipe is shown. The total number of elements and nodes are 187000 and 156000, respectively, in which 208 elements are distributed along the cylinder length and 62 elements around the cylinder circumference, Figure 4-2.

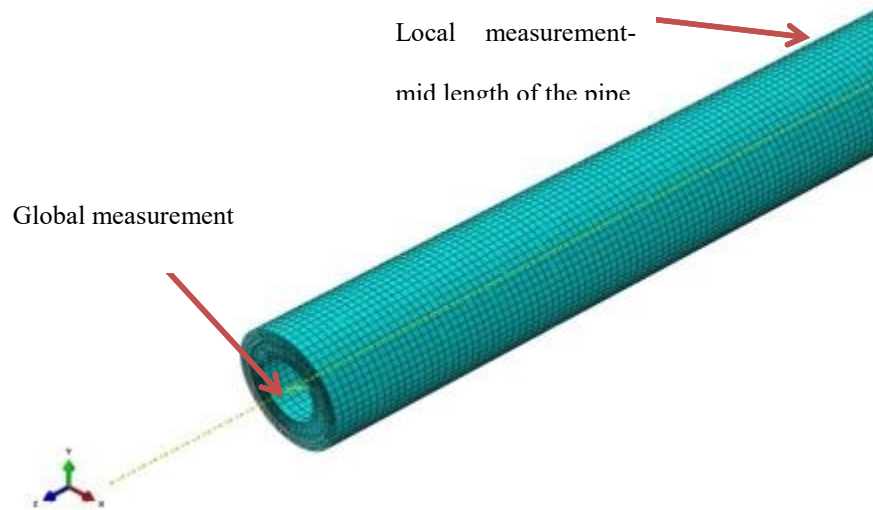


Figure 4-2. Layers and element distribution in the cross section.

Implicit type of solver is used because of highly reliable solution method by using Equilibrium check, which can perform well in contact dominated problems enjoying better accuracy. The equilibrium check benefits the accuracy of results in two different aspects. In each iteration, Abaqus Standard calculates residual force for entire nodes and degrees of freedom [9]. This criterion can drastically improve nonlinear problem accuracy, particularly for those kinds of problems which might include bifurcation and snap-through points. The another aspect in which equilibrium check benefits FEA is the contact interaction mechanism and once the problem suffers severe discontinuities including contact open-closure (normal direction) and slip-stick (tangential direction) status. In Abaqus Standard the contact penetration is supposed to fulfill two criteria, the contact penetration is considered small enough if it is within contact compatibility tolerant multiply incremental displacement, and the contact force due to penetration should be checked as well by equilibrium check and should be less than 5% of time average force. The opening between two layers is just checked with equilibrium check as the contact stress is set to zero. For tangential

contact interaction slip-to-stick status is handled like contact penetration while in stick-to-slip condition, the friction force is set to zero and is treated similar to opening.

Furthermore, unlike Implicit method exhibits faster convergence because of unconditional stable method, providing that the analysis does not encounter contact penetration problems [10], Explicit method demands for so small increment to compensate for conditional stability. As it is discussed earlier, almost all other similar studies used Explicit method to avoid strict check on contact interaction inconsistency, although it sacrifices accuracy and time expense.

In order to model end-fitting for both extremities, the boundary conditions and loads are applied on two reference nodes which are fully coupled to the ends of layers.

In case of pure torsional loading, two types of boundary conditions are assigned to the model. First, it is assumed that one end (end-fitting) is completely constrained while the other end-fitting is just allowed to rotate around axis of the pipe and torque =  $\pm 8000$  N.m is imposed on the end-fitting, Figure 4-3. Since the axial rotation of a helix is coupled with its axial displacement, in another case the one end-fitting is allowed to elongate axially.

This series of load cases helps to have well understanding on torsional performance of the pipe, axial displacement and twist, while the pipe is in linear elastic domain still. This series of torsional load case tests is complemented by examination of through different friction coefficients. A series of friction coefficients is chosen which are 0, 0.1, 0.3, 0.5, 0.7 and 0.9. This series of tests on friction factors is made to highlight effect of friction in possible friction factors between layers. The behavior of the pipe under pure tension itself can be crucial. It can be interesting to find out more with the effect of tension on torsional behavior of flexible pipe. In the third stage of this study, the model is analyzed under pure tension and then torsion is added in. The effect of tension

on torsion is examined by imposing tension=200 kN, while the tensioned pipe is followed by  $\pm 8000$  N.m torsion. At the last stage of this work, the effect of external and internal pressure on torsional behavior is provided. The torsional behavior of pressurized pipe is shown through investigation of the pipe in external pressure= 5 MPa and internal pressure=10 MPa.



Figure 4-3. Direction of positive twist moment which tend to untwist the external tensile armours.

## 4.4 Results and Discussions

### 4.4.1 Pure Torsion with two different BCs

The flexible pipe mechanical response is examined for pure torsional loading with one pipe end having either axial restraint or freedom, while the other pipe end is fixed. The modelling procedures were calibrated based on the analytical solution presented by Batista *et al.* [11].

As shown in Figure 4-4, the analytical solution exhibits a linear response for both an applied positive (i.e. counter-clockwise rotation, as per Figure 4-3) and negative (i.e. clockwise) torsional

moment. The magnitude of the applied torque was constant ( $\pm 8$  kNm). The positive torsional stiffness response was less than the negative torsional stiffness response, by a factor of 1/3 to 1/2, and was influenced by the axial boundary condition (i.e. free to elongate, axial restraint). Restraining the axial end displacement increased the torsional stiffness for an applied positive torque. The analytical model for the negative torsional response was not influenced by the boundary condition.

For the finite element predictions, the sense of the applied torque and axial restraint had similar influence on the global pipe mechanical response (Figure 4-4). For an applied negative torque (i.e. clockwise rotation), the predicted pipe response exhibited a linear relationship, with an increased stiffness by a factor of 1.5 relative to the analytical model, and the mechanical behaviour was independent of the imposed axial boundary condition. A bifurcation in the pipe response, at a torsional moment of 4 kN m, was observed when a positive (i.e. counter-clockwise) moment was applied, which was not captured by the analytical solution. Similar to the analytical solution, the finite element predictions for pipe mechanical response subject to positive torque was influenced by the axial boundary condition.

The bifurcation response was due to the separation of layers (i.e. opening) between the exterior tensile armour wire layer and the adjacent layer with a reduction in the torsional stiffness through the post-bifurcation response. In response to the applied torque, the external tensile armours become untwisted and experience radial expansion that results in bifurcation associated with the local behaviour of individual layers. The effect of layer separation was established by monitoring the radial displacement of the layers at mid-length of the pipe segment. The positive direction of torsional moment (i.e. anti-clock-wise) causes an opening between exterior tensile armour wire layer and adjacent tape layer below, whereas the interior layers (i.e. anti-birdcaging tape, interior

tensile armour wire and interior anti-wear tape) tightens up (i.e. experiences radial contraction). For applied negative torsional moment, the interior and exterior tensile armour wire layers exhibited slight radial expansion in comparison with the response to positive torsional moment with no observed bifurcation response or axial deformation coupling.

Separation of layers is shown in Figure 4-5 by examination the flexible pipe response at mid-length of the pipe segment. The reference frames for global and local measurements are shown in Figure 4-1. The negative (i.e., clockwise) torsional load causes the external tensile wire layer to contract radially that counteracts the radial expansion of the internal tensile wires. Positive (i.e., anti-clockwise) torsional loading causes the external tensile wires to expand radially and separate from underlying layer (i.e., external anti-wear tape), while contraction of the internal wires is moderated by the high radial strength core. The separation between external tensile wire and external anti-wear tape is initiated around 4 kN m torsional load and increases with increasing torsional moment. As the external tensile wires are not clamped or restrained by underlying layers, tangential instability occurs in the external tensile wires for torsional moment greater than 4 kN m (Figure 5). As the tensile armours provides axial stiffness, this tangential instability results in a decreased total axial stiffness. Figure 4-6 shows the global and local axial displacement (i.e., end free to elongate boundary condition). In this graph, response of the pipe changes after separation of layers and instability of tensile wires. These abrupt changes in axial displacement is due to separation of layers in which the tensile wires manage to displace tangentially and as result of this tangential displacement the axial stiffness gets softened.

Table 4-2 summarizes the torsional stiffness response for anti-clockwise loading with different end boundary conditions I.e., free to elongate, end constrained). The region between 0-4 kN.m torsion, which happens before bifurcation, is labeled A, and section B is dedicated to the region

after bifurcation, 4-8 kN.m, that torsional stiffness starts being softened. The torsional stiffness under anti-clock-wise torsion for end-free-to-elongate BC decreases 63% from section A to B and this is 47% for end-constrained-to-elongate BC under influence of the instability.

Separation of layers (created gap between external tensile armour layer and external anti-wear tape) shaped by positive (i.e., anti-clockwise) torsion, causes elastic-lateral buckling in tensile wires and softening in the axial tensile and torsional pipe stiffness. This response is different from observations on the radial instability of tensile wires as reported by Ebrahimi *et al.* [12,13]. In Ebrahimi *et al.* [12] a similar flexible including circumferential damage in anti-birdcaging tape is examined under pure axial compression. The introduced circumferential damage in anti-birdcaging tape reduces the radial confinement of tensile wires and pure compression triggers the radial instability (i.e. birdcaging) in them. The elastic instability is supposed for the monitored bifurcation under pure axial torsion loading, as it might fade and return to the initial configuration after unloading and it has not caused complete failure of the tensile wires.

Batista's analytical method [11] and the study by Merino in which the explicit solver was used for running the finite element model [8], showed linear responses for both directions of torsional moment, and do not account for the slipping mechanisms in the tensile wires for anti-clockwise loading conditions. Using an implicit integration scheme, the equilibrium check and contact interaction algorithms allows for the prediction of this slipping and bifurcation mechanism, while the analytical formulation solves the problem in global sense and explicit solver lacks enough precision in contact modeling interactions. Consequently, this slipping mechanism could not be captured by [11] and [8].

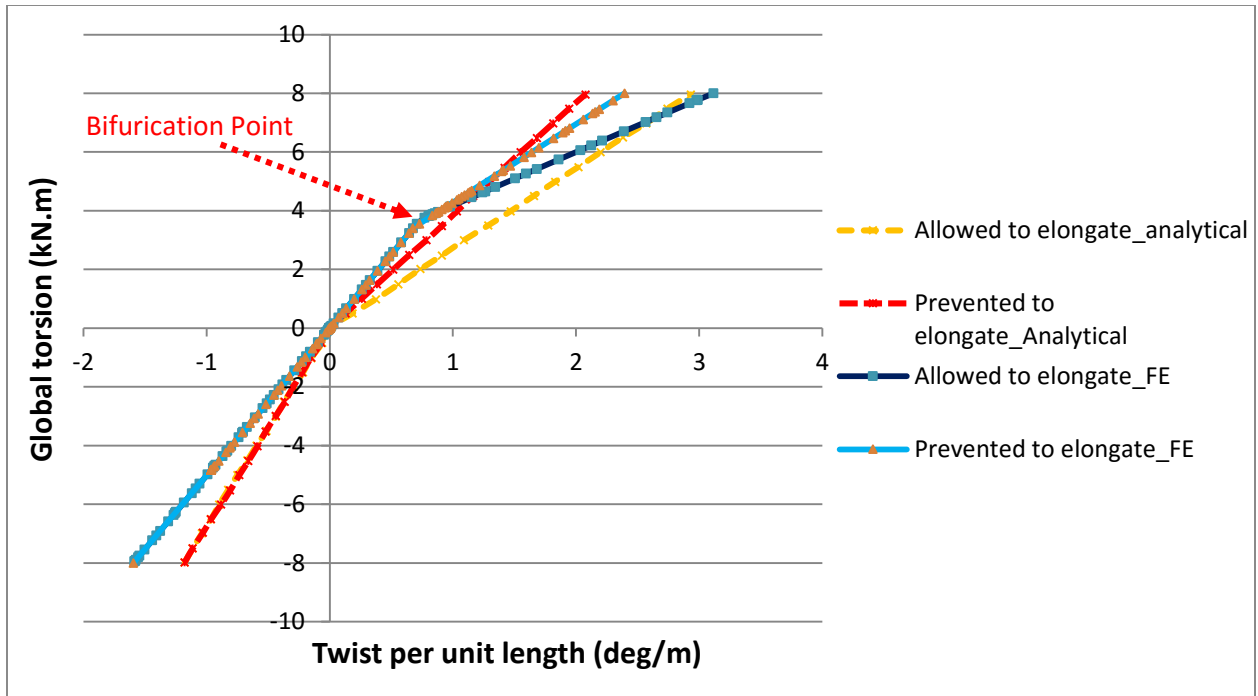


Figure 4-4. Twist moment versus twist angle per unit length versus.

Table 4-2. Torsional stiffness for the FE and analytical approach.

	Finite element method		Analytical method	
	Free to elongate	Prevented to elongate	Free to elongate	Prevented to elongate
Anti-clock-wise-part B <i>(N.m/rad)</i>	82378	122453	156085	220092
Anti-clock-wise-part A <i>(N.m/rad)</i>	230290	231134		
clock-wise <i>(N.m/rad)</i>	230218	230169	383935	388116

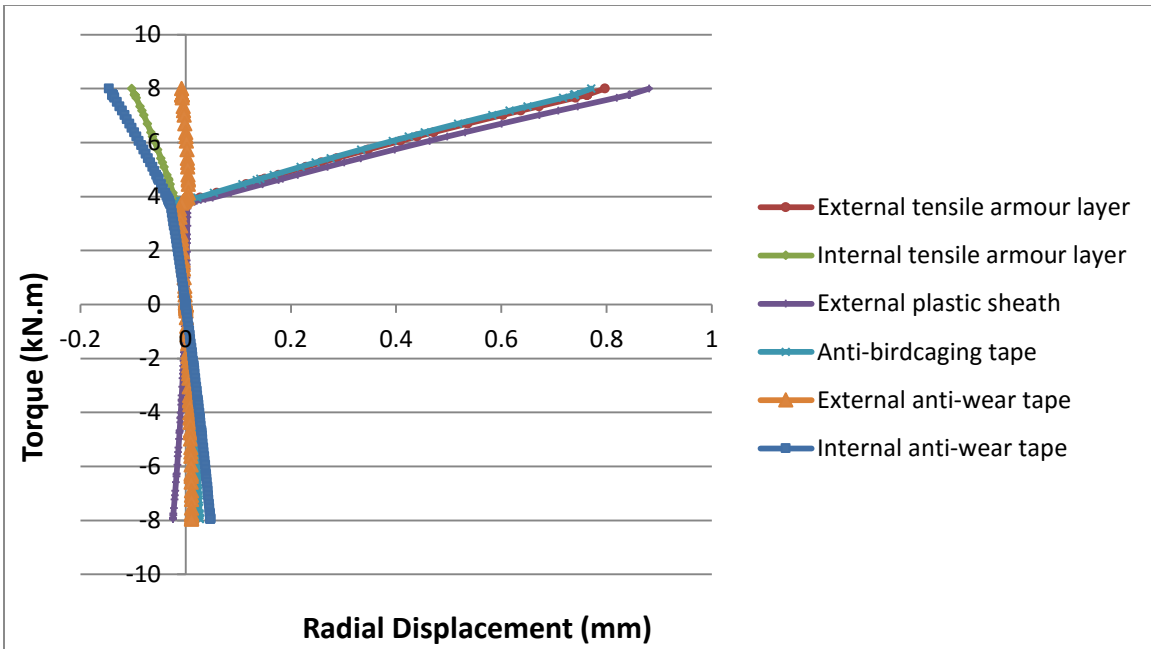


Figure 4-5. Twist moment versus local radial displacement in different layers.

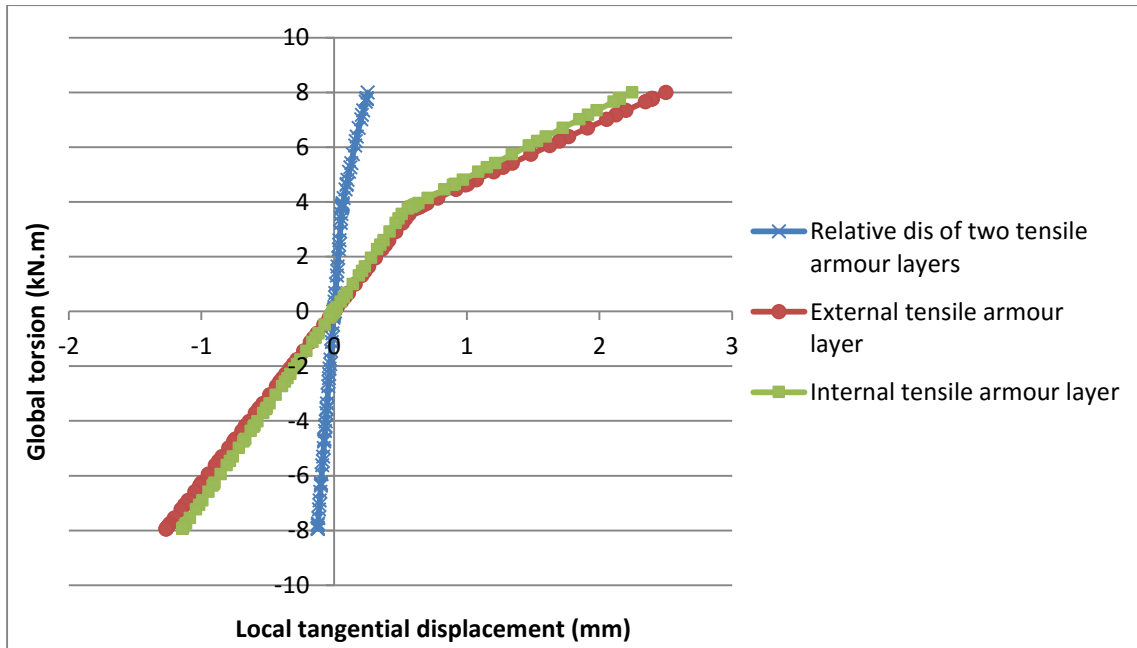


Figure 4-6. Twist moment versus local tangential displacement in two tensile armour layers.

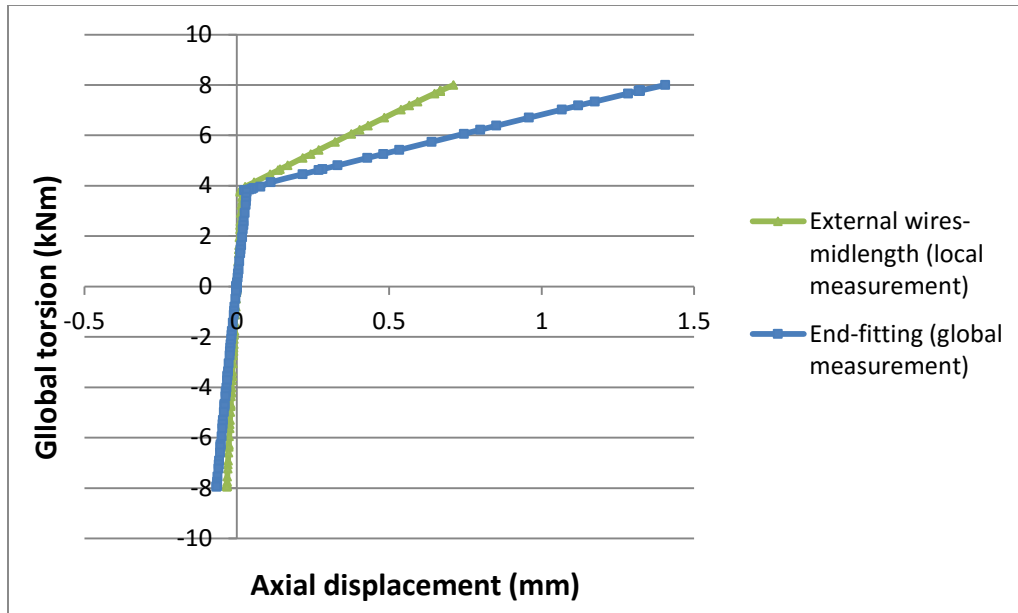


Figure 4-7. Twist moment versus local axial displacement (end free to elongate BC).

The relationship between global moment and von Mises stress (i.e. measured at an element node which is located at the mid-length of the pipe) (see Figure 4-2) is presented in Figure 4-8. Evaluating the local stress condition of the tensile armour wires demonstrates the significance of torsional loading direction (i.e. clockwise, anti-clockwise) on the flexible pipe response and development of the tangential instability mechanism. Under positive torsion, the external tensile wire layer is untwisted and starts expanding radially after the bifurcation point (i.e., torsional moment of 4 kN m). The wires buckle elastically under axial torsion (see also Figure 4-3) and axial compression (see Figure 4-6, and ) where the axial stiffness undergoes softening. For anti-clockwise torsional moments, after bifurcation the external tensile armour wires become unstable and shed load (i.e., stress) that is carried by the internal tensile wires. The internal tensile armour wires experience a greater stress magnitude for anti-clockwise torsional loading conditions than clockwise torsional moment loading due to the buckling instability and load shedding of the external wires.

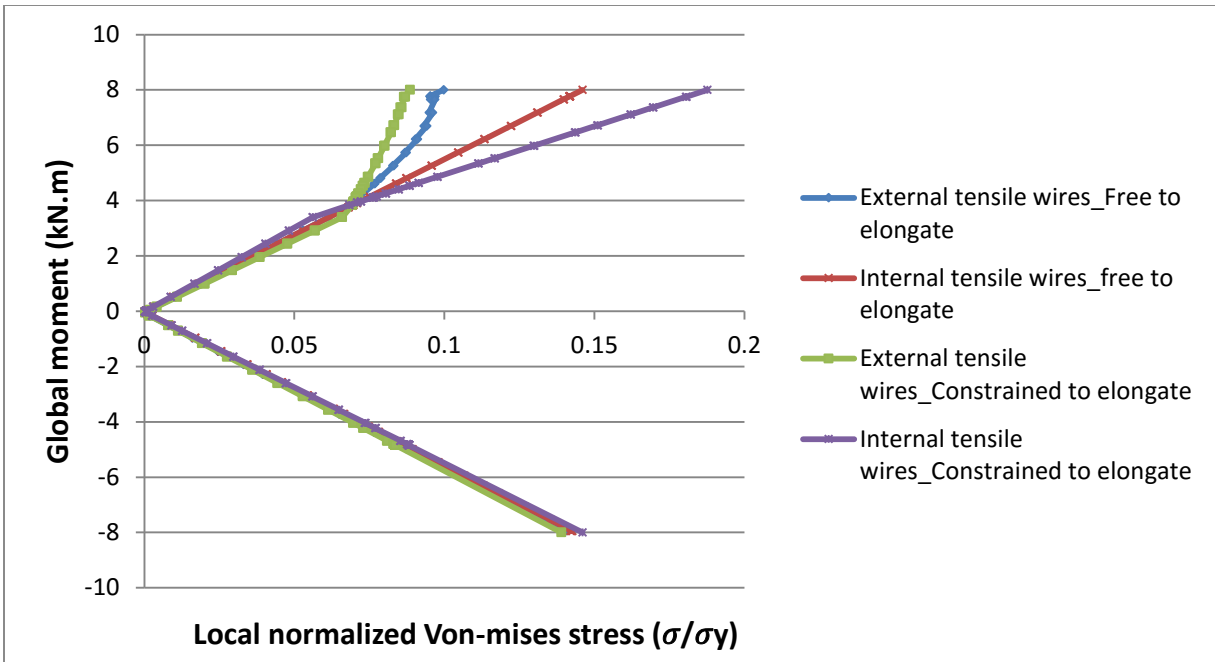


Figure 4-8. Twist moment versus normalized von Mises stress at the middle of tensile armours.

#### 4.4.2 Friction coefficient assessment

The influence of interface friction on the flexible pipe mechanical response was examined through a sensitivity study. A Coulomb friction model was used with a range of interface friction factors (0, 0.1, 0.3, 0.5, 0.7 & 0.9). Based on experience from previous studies, Ebrahimi *et al.* [12, 13], a small external hydrostatic pressure of 0.5 MPa was imposed to enforce normal contact across the layers. The kinematic (essential) boundary conditions include one end fixed with the other end free to elongate and rotate.

As shown in Figure 4-9, the interface friction coefficient did not influence the pipe mechanical response for either clockwise or counter-clockwise torsional moment. This is consistent with the conclusion by Muñoz *et al.* [15], where the tensile response of flexible pipe was found to independent of the friction coefficient between layers. For an applied negative torsional moment, the interior and exterior tensile armour wire layers experience slight radial expansion. This

mechanical response would negate any effects of internal friction due to the gap development and separation between layers. For the applied positive torsional moment, the bifurcation response and torsional-axial load coupling behaviour was observed, however, the mechanical response was not influenced by the interface friction coefficient Figure 4-9. The expansion and separation of the external tensile armour wire layer was not be influenced by the variation in the friction coefficient. The radial contraction of the interior tensile armour wire layer was governed by the normal contact force and was also not influenced by the interface friction factor.

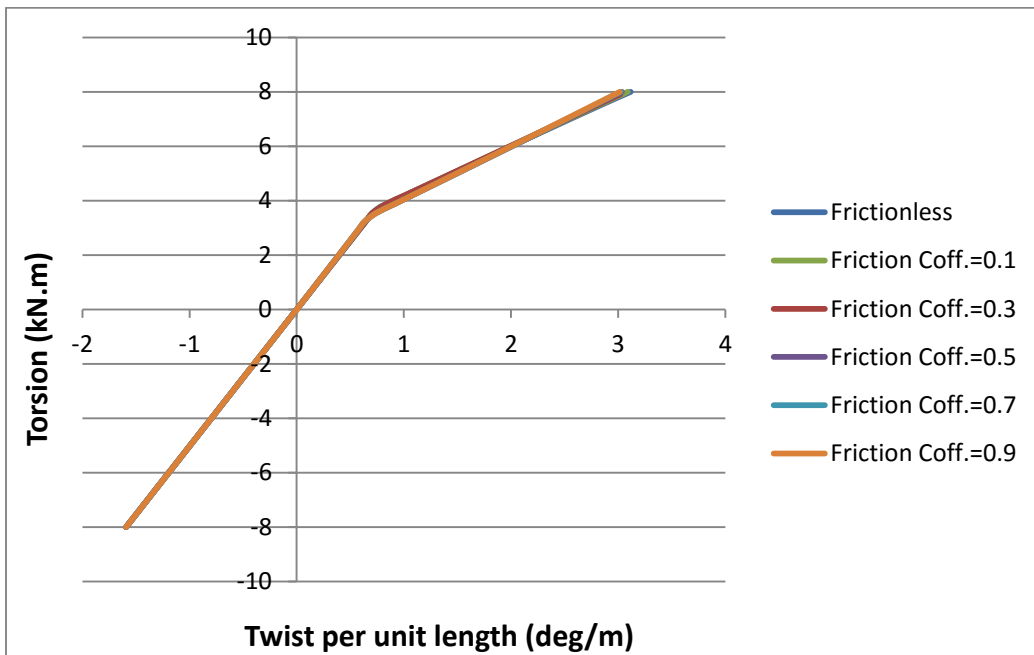


Figure 4-9. Twist moment versus twist angle per unit length for different friction factors.

#### 4.4.3 Pure Tension

Pure tension analysis is implemented here to prove pipe tensile response correctness and utilizing the pre-tensioned pipe for the previous torsional analyses to highlight effect of tension on torsion.

Two boundary conditions are considered in which the pipe is free to rotate in one case and in another one the rotation is constrained while the pipe is loaded by monotonic tension on one end

of the pipe. This examination provides force-strain curve which is compared to the experimental test by Merino *et al* [14]. Figure 4-11 shows force versus strain in FE simulation which possesses excellent consistency with available physical test result for the both considered boundary conditions. Figure 4-12 presents the rotation corresponding applied tension in end-free-to-rotate boundary condition, and Figure 4-13 shows the reaction moment under applied tension in end-constrained-to-rotate boundary condition. For better presentation of axial tensile stiffness and comparison with corresponding experimental results Table 4-3 provides axial stiffness of each individual case and error percentage of FE result with experimental one. The axial tensile stiffness in FE simulation becomes stiffer as 7% by changing BC from end-free to end-constrained, as the axial displacement of helices is coupled with their axial rotation and constraining each of these degrees of freedom restricts the other one as well.

#### **4.4.4 Torsion added to Tension**

In next stage, a monotonic tensile load 200 kN is applied and then superimposed by  $\pm 8000$  N.m of torsion. Figure 4-13 compares torsional response of the pipe with end-free-to-elongate and no pre-tension with the pipe which is pre-tensioned by 200 kN and possesses same boundary conditions. The comparison implies the fact that pre-tension causes a radial confinement for the pipe and precludes radial expansion of external tensile wires and separation of layers under anti-clock-wise torsion which consequently prevents lateral instability of wires in positive torsion and the pipe shows similar linear behavior like clock-wise torsion.

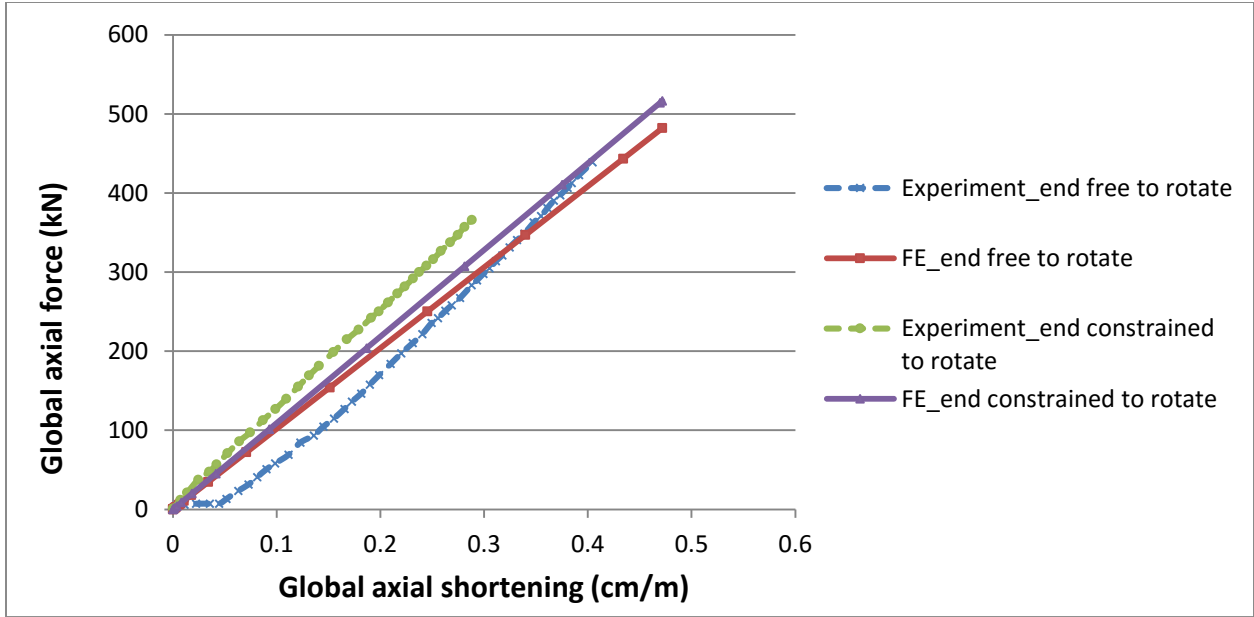


Figure 4-10. Axial force versus axial deformation per unit length.

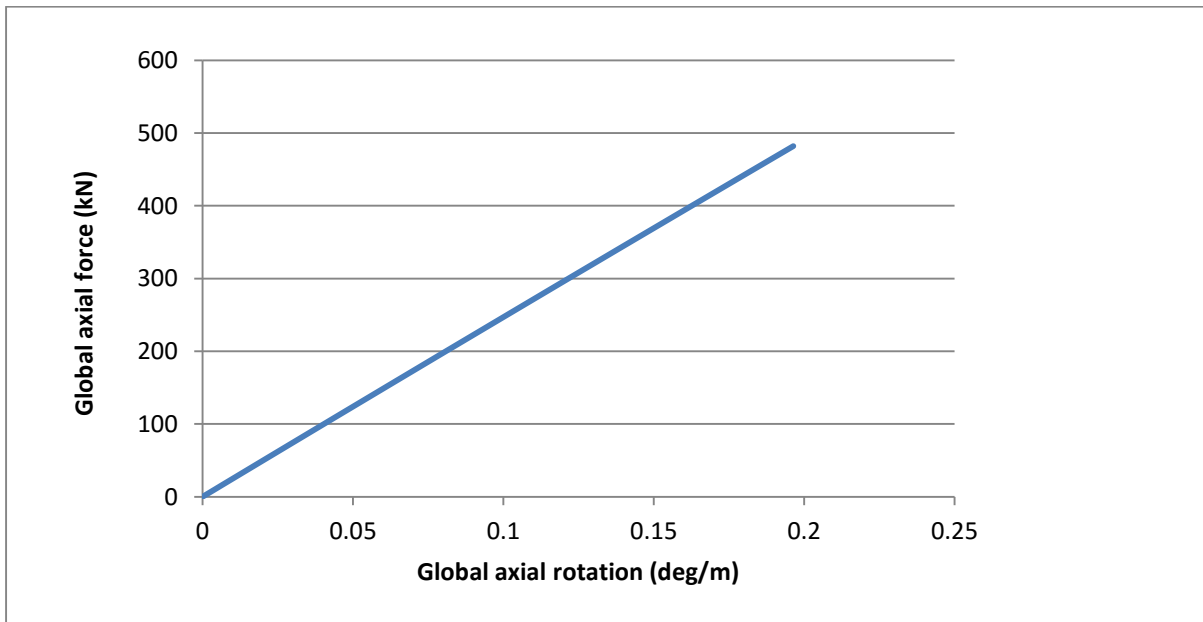


Figure 4-11. Global axial force versus global axial rotation in end-free to rotate.

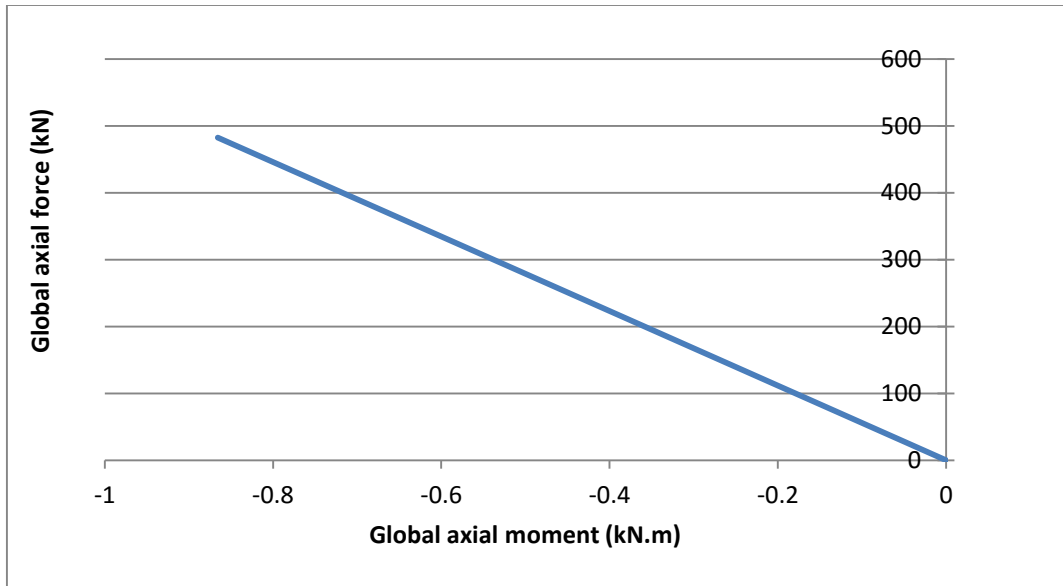


Figure 4-12. Global axial force versus global axial reaction moment in end-constrained to rotate.

Table 4-3. Axial stiffness in two considered boundary condition for both experiment and FE model.

	Finite element method (N/m)	Experiment (N/m)	Error %
End free to rotate	81745058	99539649	-17%
End prevented to rotate	87583335	101328710	-13%

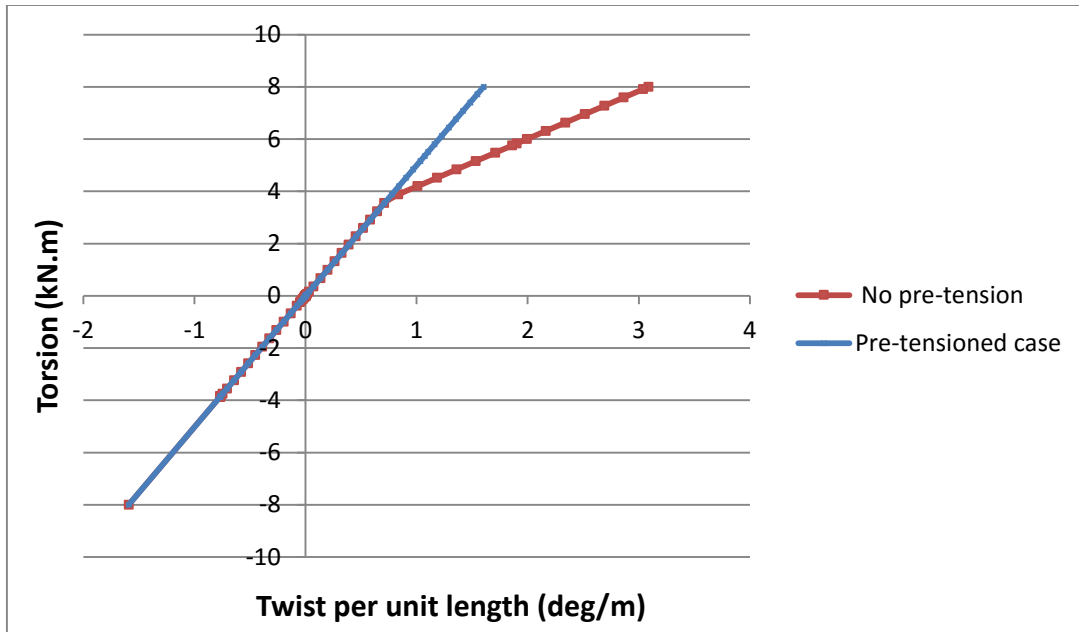


Figure 4-13. Torsion versus twist per unit length.

#### 4.4.5 Effect of Internal and External Pressure

The purpose of this section is to evaluate the role of contact pressure variation on torsional mechanisms by means of imposing external/ internal pressure while the other parameters are held constant in order to see solely the effect of contact pressure. In this way, while the pipe is initially exposed to external or internal hydrostatic pressure, the other load and boundary conditions follow the same condition of section 4.4.1 (i.e.,  $\pm 8$  kNm of axial torsion and no axial compression or tension). The analyses of pressurized pipe are accomplished in two steps, 1) first step is dedicated to imposition of internal or external pressure, and 2) the pressurized pipe is superimposed by torsion. In this way, the pipe is pre-pressurized by 10 MPa of internal pressure and then it is superimposed by  $\pm 8000$  N.m. Similar loading condition is repeated for external pressure while the 10 MPa of internal pressure is replaced by 5 MPa of external pressure. Figure 4-14 illustrates the response of the pipe under internal pressure and torsion and Figure 4-15 presents the effect of external pressure on the torsional behavior. Figure 4-14 implies that internal pressure of 10 MPa

does not play significant role on the torsional behavior of the pipe. This is because of high radial strength core which is designed to stand for high radial pressure of internal and external fluids. The internal core which enjoys the high radial strength and does not expand radially under 10 MPa of internal pressure, pressure armour radial expansion= $2.8 \times 10^{-2}$  mm, and so the pressure is not transferred to the tensile wires and the torsional behavior of pipe under internal pressure does not change significantly. The radial expansion of pressure armour ( $2.82 \times 10^{-2}$  mm) a bit increase contact pressure between above layers and layers separate a bit later than unpressurized pipe (4.8 kN.m of torsion). The behaviour of the pipe is even stiffer after bifurcation pipe according to Table 4-4. The torsional stiffness of internally pressurized pipe becomes 53% stiffer after instability in respect to unpressurized one.

Once the external pressure is imposed, the whole pressure is applied directly onto tensile wire layers, and the external pressure functions as a more confinement against separation of external tensile wires under anti-clock-wise torsion. Therefore, no gap and instability occur in an externally pressurized pipe even under anti-clock-wise torsion. Consequently, the pipe responds linearly for the both directions of rotation, Figure 4-15. Table 4 presents torsional stiffness for pressurized and unpressurized pipes.

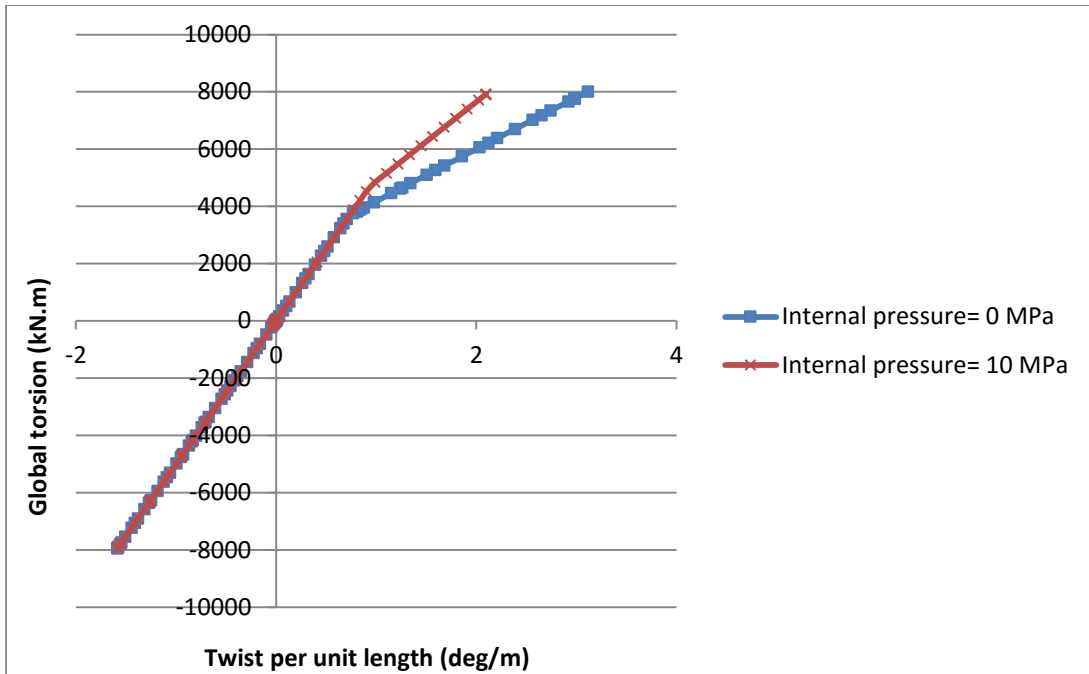


Figure 4-14. Torsion versus twist per unit length under 10 MPa of internal pressure.

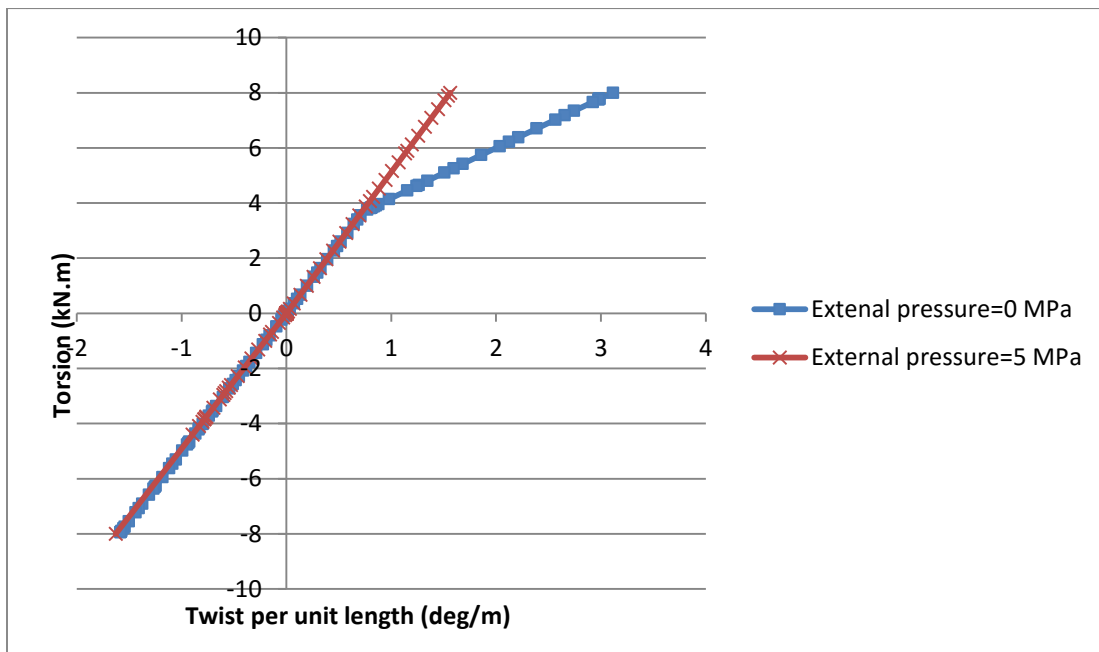


Figure 4-15. Torsion versus twist per unit length under 5 MPa of external pressure.

Table 4-4. Torsional stiffness for the unpressurized pipe, internally and externally pressurized pipe.

	Finite element method- Free to elongate BC		
	Unpressurized	Internal pressure=10 MPa	External pressure= 5 MPa
Anti-clock-wise-part B <i>(N.m/rad)</i>	82378	127349	234941
Anti-clock-wise-part A <i>(N.m/rad)</i>	230290	229875	
clock-wise <i>(N.m/rad)</i>	230218	230216	225159

#### 4.5 Conclusion

Finite element modelling procedures were developed to predict the mechanical response of flexible pipe subject to axisymmetric loading conditions through a numerical parameter study. The numerical predictions were consistent with available analytical solutions and experimental data. This study is conducted through four different stages, 1) examination of pure torsion in two different directions and two different probable boundary conditions, 2) assessment of pure tension in two different boundary conditions, 3) evaluation on the effect of tension on torsion, and 4) examination of key factors (friction coefficients, external and internal pressures). These stages are considered to highlight effect of each parameter and to provide improved understanding of flexible pipe mechanical behaviour for practical design scenarios.

The use of an Implicit integration scheme was shown to improve confidence in the simulations and detection of the bifurcation points (i.e., elastic lateral buckling) in the mechanical response, which may not be captured by analytical solutions or finite element procedures using Explicit schemes. This instability under torsion is due to separation of layers, which is caused by the direction of torsion trying to untwist external tensile armours. The parameter study demonstrates this lateral instability is independent of the interface friction coefficient.

Axial tension loads restrict the radial displacement of external tensile wires by tightening up both layers of tensile wires without the development of a gap between layers. This results in a linear pipe response for both directions of applied rotation.

The effects of internal pressure on the tensile armour wire response was negligible where the pressure load was carried by the high radial strength pressure armour with negligible radial expansion. The response was similar to the unpressurized pipe load case. External pressure, however, influences the torsional stiffness due to confinement of the external tensile wires to radial displacement, which is also constrained by the anti-birdcaging tape. The wire separation under external pressure is controlled, and thus no instability occurs under anti-clockwise torsional loading condition.

This necessity of this research was so urgent to cover the gap between development of the application of flexible pipe in harsh conditions and flaws of the existing numerical and analytical simulations. This paper provides a reliable series of parametric studies to improve design standards.

Physical modelling studies are needed to further validate the numerical modelling procedures and provide confidence in the observations and conclusions presented in this study.

## 4.6 Reference

- [1]. De Sousa R.M, Viero. P.F, Magulta. C, Roitman. N., “An experimental and numerical study on the axial compression response of flexible pipe”, OMAE 2012, 31<sup>st</sup> International Conference on Ocean, Offshore and Offshore Engineering, Rio de Janeiro, Brazil. July 1-6, 2012.
- [2]. McNamara, J. F., and Harte, A. M., 1989, “Three Dimensional Analytical Simulation of Flexible Pipe Wall Structure,” Proceedings of the Eighth International Conference on Offshore Mechanics and Arctic Engineering, Vol. 1, Issue No. 8, pp. 477–482.
- [3]. Ramos, R., Pesce, C.P., “A consistent analytical model to predict the structural behavior of flexible risers subjected to combined loads”, 23<sup>rd</sup> International Conference on Offshore Mechanics and Arctic Engineering, June 20-25, 2004, Vancouver, Canada.
- [4]. Bahtui, A., Bahai, H., Alfano, G., “Numerical and analytical modeling of unbounded flexible risers”, 2009, Journal of Offshore Mechanics and Arctic Engineering OMAE 131(2): 1-13.
- [5]. Corre, V. L., Probyn, I., “Validation of a 3-dimensional finite element analysis model of a deep water steel tube umbilical in combined tension and cyclic bending”, ASME 28<sup>th</sup> International Conference on Ocean, Offshore and Arctic Engineering, May 31-June 5, Honolulu, Hawaii, USA.
- [6]. Bahtui, A., Bahai, H., Alfano, G., “A finite element analysis for unbounded flexible riser under axial tension”, 27<sup>th</sup> International Conference on Offshore Mechanics and Arctic Engineering, June 15-20, Estoril, Portugal.
- [7]. De Sousa, J.R.M., Magluta, C., Roitman, N., Londono, T. V., Campello, G.C, “A study on the response of a flexible pipe to combined axisymmetric loads”, Proceedings of the ASME

2013 32<sup>nd</sup> International Conference on Ocean, Offshore and Arctic Engineering, June 9-14, 2013, Nantes, France.

[8]. Merino, H.E.M, De Sousa, J.R.M., Magulta, C., Roitman, N., “Numerical and experimental study of a flexible pipe under torsion”, Proceedings of the ASME 2010, 29<sup>th</sup> International Conference on Ocean, Offshore and Arctic Engineering, June 6-11,2010, Shanghai, China.

[9]. Abaqus documentation 6.13.

[10]. Ebrahimi, A., Kenny, S., Hussein, A., “Finite element simulation of flexible pipe: Challenges and Solutions”, Volume 14 (4), pages 275-287, 2015.

[11]. Batista, R. C., Bogarin, J. A. G., Ebecken, N. F. F., “Local Mechanical Behaviour of Multilayered Flexible Risers,” Proceedings of the 7th International Symposium on Offshore Engineering, pp. 494-510, 1989, COPPE/UFRJ,Rio de Janeiro, Brazil.

[12]. Ebrahimi, A., Kenny, S., Hussein, A., “Radial instability of tensile armour wires in subsea flexible pipe-numerical assessment of key factors”, Volume 138 (3), doi: 101115/1.4032894, 2015.

[13]. Ebrahimi, A., Kenny, S., Hussein, A., “Parameters influencing birdcaging mechanism for subsea flexible pipe”, ISOPE2015, 25<sup>TH</sup> Annual International Ocean and Polar Engineering Conference, June 21-26, 2015, Kona, Hawaii, US.

[14]. Merino, H.E.M, De Sousa, J.R.M., Magulta, C., Roitman, N., “On the coupled extensional-torsional response of flexible pipes”, Proceedings of the ASME 2009, 28<sup>th</sup> International

Conference on Ocean, Offshore and Arctic Engineering, May 31<sup>st</sup>- June 5<sup>th</sup> ,2009, Honolulu, Hawaii, US.

[15]. Muñoz, H.E.M., de Sousa, J. M. R., Magulta, C., Roitman, N., 2016, “Improvements on the Numerical Analysis of the Coupled Extensional–Torsional Response of a Flexible Pipe” *Journal of Offshore Mechanic and Arctic Engineering*, 138 (1):13p., doi: 10.1115/1.4032036.

## **Preface**

This journal research paper is an original study and the developing idea, planning and implementation of the whole technical parts of this research paper have been done by the candidate as the first author, and the regular supervision has been made by Dr. Shawn Kenny through advising on the planning of the research way, evaluation of the research merit and providing precious idea and experience on the discovered phenomena and technical parts. The compilation of the paper literature has also been implemented by the candidate and it has been continuously revised by Dr. Shawn Kenny to improve the quality of the technical part and the literature. Facilitation of the PhD program of the candidate and also final review of the paper has been made by Dr. Amgad Hussein as the third author. Wood Group Kenny Research Chair at Memorial University of Newfoundland has funded the whole PhD program study and provided the all facilities (cluster machine, Software and personal computer) for carrying out the study.

This conference research paper is published International Ocean and Polar Engineering Conference, Hawaii, USA, June 21-26, 2015.

# 5 Combined mode shapes of lateral buckling and radial buckling- Parameters influencing birdcaging mechanism for subsea flexible pipe

*Alireza Ebrahimi*<sup>(1)</sup>, *Shawn Kenny*<sup>(2)</sup>, *Amgad Hussein*<sup>(1)</sup>

<sup>(1)</sup> Faculty Engineering and Applied Science, Memorial University of Newfoundland

St. John's, NL, Canada

<sup>(2)</sup> Department of Civil and Environmental Engineering, Faculty of Engineering and Design, Carleton University

Ottawa, ON, Canada

## 5.1 Abstract

The influence of damage in the anti-birdcaging tape and plastic sheath on radial instability is examined through continuum finite element analysis. The numerical procedures are calibrated with physical tests on a flexible pipe subject to pure axial compression. An implicit solver is used in order to take advantage of contact modelling capabilities of ABAQUS software package. A parameter study is conducted to examine the effects of pipe damage, of the anti-birdcaging tape and external plastic sheath, on the potential for radial instability or bird-caging mechanism. Correspondence between the physical and numerical simulations provides confidence in the predicted outcomes.

Key words: Subsea flexible pipe; birdcaging; radial and tangential instability; finite element method; rupture.

## 5.2 Introduction

Tying subsea facilities to floating fixed facilities is the major application of flexible pipe. Flexible pipe can also be used as jumper. There may be economic and technical advantages for using flexible riser or pipeline with respect to conventional rigid line pipe Technip [1]. The extruded external polymer sheath eliminates requirement for cathodic protection, which promotes reliability and maintenance expenses of the pipe. Over short distances, the installation efficiency, which can be 5 km to 10 km per day, and cost of flexible pipe is lower than conventional line pipe installed using S-lay or J-lay methods. Other beneficial mechanical properties include collapse strength and fatigue and abrasion resistance. In addition, the internal smooth surface minimizes head loss and flow turbulence.

The wide spread usage of subsea flexible pipe asks for more knowledge of mechanical behavior and performance of this pipe. Subsea flexible pipe based on their applications can be exposed to axial compression, end-cap effect in short jumpers or axial movement in long pipes. This compression can separate layers. In case of any damage in plastic sheath and leakage of water into the annulus, “wet annulus” condition happens. In this condition, the anti-birdcaging tape just can stand toward radial expansion. As, the tensile armours do have low moment of inertia in radial direction, they are prone to buckle radially.

There are few studies examining the radial buckling phenomena for the tensile armour. In a numerical study, Vaz and Rizzo *et al.* [2] developed finite element modelling procedures to examine the bird-caging phenomena. In this study idealizations were used to address constraints with the computational effort for modeling the discrete components of a flexible pipe cross-section. For example, only two wires, represented by spring elements, were used to represent the inward and outward radial deformation modes for the external and internal armour wires,

respectively. A parameter study examined the effects of external pressure and interface friction on the potential for bird-caging mechanism to develop. Although, idealizations were incorporated within this study, such as the lack of contact interaction between armour wires, through a sensitivity study the results provided insight on key parameters influencing the mechanical response of flexible pipe; such as the effects of external and internal pressure.

Experimental studies conducted by de Sousa *et al.* [3] provide the basis for developing the numerical modelling procedures presented in this paper. Physical tests on a 2.5 m length of 101.6 mm (4") flexible pipe subject to axial compression were conducted. The pipe segment length to diameter (L/D) ratio is 25. Continuum finite element modelling procedures were also developed using the ANSYS software package. This study is as a significant step forward in modeling birdcaging behaviour both numerically and experimentally. Most details on the pipe configuration are presented with consistency observed between the numerical simulations and results from the physical tests. However, there are some areas of uncertainty. The presence of geometric imperfections plays an essential role in the buckling of structures, however, details on the amplitude or distribution of initial geometric imperfections in the physical or numerical model are not provided. In addition, the effect of other key parameters, such as external or internal pressure, was not examined. In this study, both the presence of geometric imperfections and influence of hydrostatic pressure are examined.

Another study on the bird-caging mechanism, conducted by Serta *et al.* [4] compared numerical simulations, using Explicit finite element methods, with physical test results. GUI customization of the numerical modelling procedures was also developed through simplification of the outer layers (e.g. tensile armours, plastic sheath and anti-birdcaging tape). Although the contact algorithms are almost the same in both Implicit and Explicit methods, Explicit method keeps

running the analysis, although it might have large contact penetrations. So for the birdcaging or lateral buckling in tensile wires of flexible pipe, where many layers may develop contact interaction, the use of Explicit methods is not recommended by Ebrahimi *et al.* [5]

Ebrahimi *et al.* [5] explores the challenges of modeling of flexible pipe buckling. A discussion on practical modelling approaches and possible solutions to address the technical challenges and complexities for numerical simulation of composite pipeline sections, deformation modes and mechanisms (e.g., tensile armour buckling) is presented.

In another recent study, Ebrahimi *et al.* [6] developed a 3D finite element model to simulate the development of radial (i.e., birdcaging) buckling response. This model utilizes an Implicit solver with detailed assessment of the contact mechanics. This study exhibits excellent consistency with the experimental results presented by de Sousa *et al.* [3]. Furthermore, the key factors influencing the radial buckling (e.g. sea hydrostatic pressure and damage on exterior layers) mode were assessed.

This current study is an extension of these investigations, (Ebrahimi *et al.* [6]) to further examine the radial buckling mechanism of the tensile armour wires under presence of imperfections. A rupture pattern was introduced on the exterior layers (plastic sheath and anti-birdcaging tape) and the effects on the composite pipe mechanical response was investigated through a parameter study.

### **5.3 Finite element modelling procedures and sensitivity matrix**

A 3D continuum finite element model was developed with nine separate layers to represent the flexible cross-section. A summary of the geometric and material property, and element characteristics are presented in Table 5-1 with some of the data adopted from the study by de Sousa *et al.* [7], The total length of the modeled pipe is 2.5 m. In order to reduce computational effort,

the carcass and pressure armour layers, which comprise interlocking profiled components, are modeled as a simple cylinder, using shell elements (S4), with orthotropic material behaviour (de Sousa *et al.* [3]). The anti-wear tape and plastic sheath layers are also modelled as a simple cylinder, using shell (S4) elements, with isotropic material properties.

Table 5-1. Characteristics of each individual layer.

Layer	Mechanical Properties					Element Type
	Thickness (mm)	Elastic Modulus (GPa)	Poisson's Ratio	Yield Stress (MPa)	Rupture Stress (MPa)	
Carcass (Lay Angle 87.6°)	4.0	193	0.3	320	640	Shell (S4R)
Plastic Sheath	5.0	345	0.4	20	22	Shell (S4R)
Pressure Armour (Lay Angle 87.0°)	6.2	205	0.3	900	1000	Shell (S4R)
Anti-Wear Tape	2.0	350	0.4	20	22	Shell (S4R)
Inner Tensile Armour (Lay Angle 35.0° with 47 wires)	2.0	205	0.3	1260	1400	Shell (S4R)
Outer Tensile Armour (Lay Angle 35.0° with 48 wires)	2.0	205	0.3	1260	1400	Shell (S4R)
High Strength Tape	1.2	0.75	0.3	40	44	Shell (S4R)
Outer Plastic Sheath	5.0	215	0.4	20	22	Shell (S4R)

Surface-to-surface contact discretization is used to have smooth contact and avoid stress concentrations on nodes. In node-to-surface contact the master nodes may penetrate into the space between the slave surface nodes where there is no defined constraint between the slave nodes. This can be more severe in curved surfaces, when there is more probability of penetration under small

loading. Hard normal contact with a low frictional coefficient ( $\mu=0.1$ ) in the tangential direction was defined. The contact interaction between layers with different geometric properties, material characteristics and design functions, and large deformation response of the tensile wire during radial buckling requires the use of nonlinear solution techniques with precise mesh topology to achieve successful outcomes. The total number of elements and nodes are 99119 and 129176, respectively.

The implicit solver is used because of highly reliable solution method, which can perform well in contact dominated problems (Ebrahimi *et al.* [6]). Implicit method exhibit faster convergence in case the analysis does not encounter contact penetration problems. Also, there is an equilibrium check criteria in Implicit method, which improves solution accuracy.

In order to model end-fitting for both extremities, the boundary conditions and loads are applied on two reference nodes which are fully coupled to the ends of layers. One of the reference nodes is fully constrained while the other one is free to elongate and twist. The applied external load is imposed as pure compression force.

Normally, the birdcaging mechanism is due to the presence of a damaged plastic sheath and leakage of seawater inside the annulus (i.e. wet buckling) or damaged anti-birdcaging and plastic sheath even though no external pressure is imposed. It is hypothesized the area of “wet surface” or rupture may influence the critical buckling load.

The imperfection type used in Ebrahimi *et al.* [6] was made by lowering yield strength of anti-birdcaging and plastic sheath possessing 4% of total length of the pipe and positioned at the center of the pipe length. Since there is neither experimental nor analytical results as validation of current study, the Ebrahimi *et al.* [6] FE model, which has already been validated, is modified and previous

type of imperfection is substituted (lowered yield strength) by a rupture with 4% of total length which lies in middle section of pipe and in axial direction. Figure 5-1 illustrates the whole pipe and the location of the applied rupture zone in mid-length of the pipe segment. Through a sensitivity study, the influence of local damage (i.e., ruptures) lengths (as a percentage of total pipe segment length) is examined through a numerical parameter study.

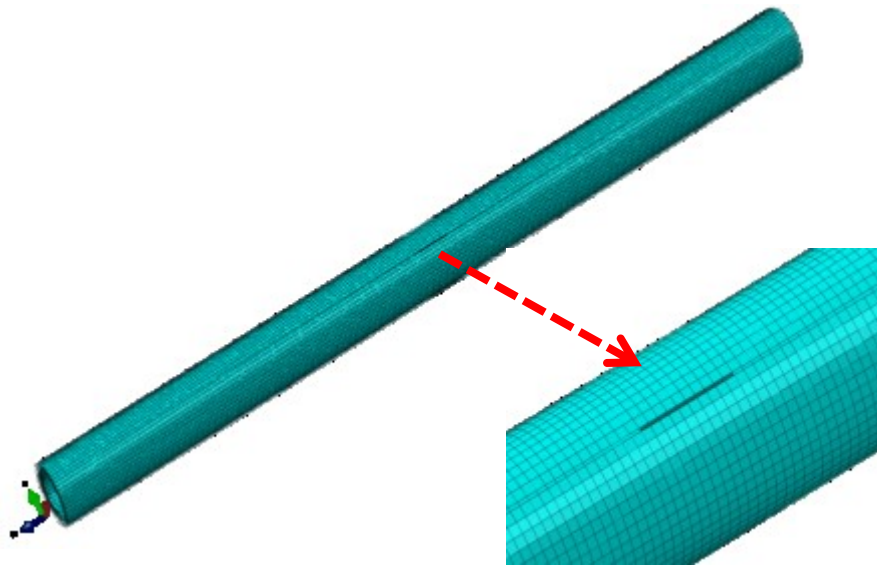


Figure 5-1. The introduced rupture in external plastic sheath and anti-birdcaging tape.

#### 5.4 Results and discussions

For a perfect flexible pipe segment (i.e., zero rupture length), the local radial instability (i.e., bird caging mechanism) does not develop. Normally, when the anti-birdcaging and external plastic sheath is not damaged the radial buckling is curbed. Under this circumstance, the lateral buckling is the only probable buckling mode shape of wires which needs for bending moment in addition to pure axial compression.

By imposing the rupture surface, local moments due to unsymmetrical bending occur in addition to the axial compression mode. Once the bending mechanism has been initiated, the local

deflection around the damage zone aggravates radial instability in the tensile wires, where the effect increases with greater rupture zone length. The bending moment created by the rupture causes the wires to move in both radial and tangential directions. Figure 5-2 illustrates form of the pipe and rupture after buckling. In overall, the bending moment reduces the buckling (radial buckling) force in respect to the model of Ebrahimi *et al.* [6]. The shaped bending moment, due to the ruptured surface, initiates a mixed mode instability (radial and lateral), but is mostly dominated by radial buckling (birdcaging) as shown in Figure 5-3. Figure 5-3 shows both radial and tangential displacement of the wires.

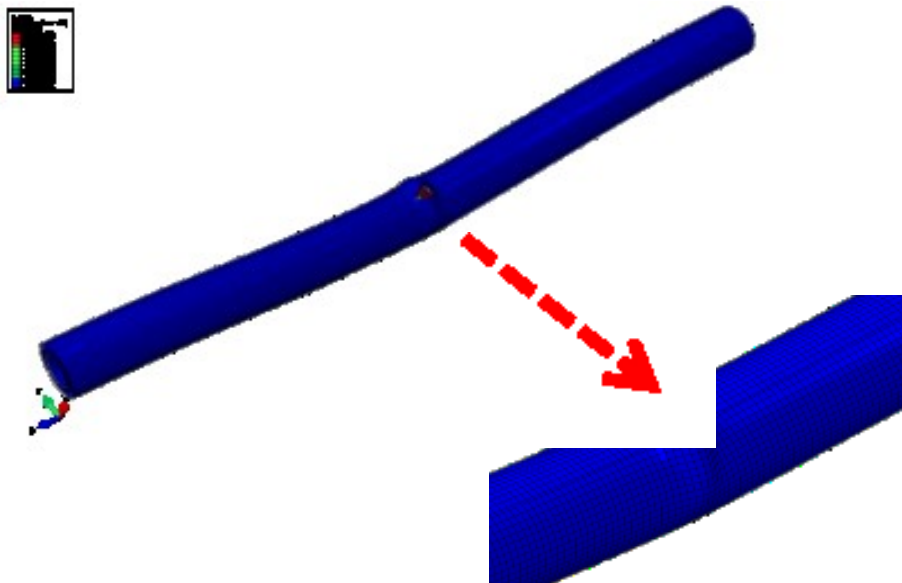


Figure 5-2. The flexible pipe after occurrence of birdcaging.

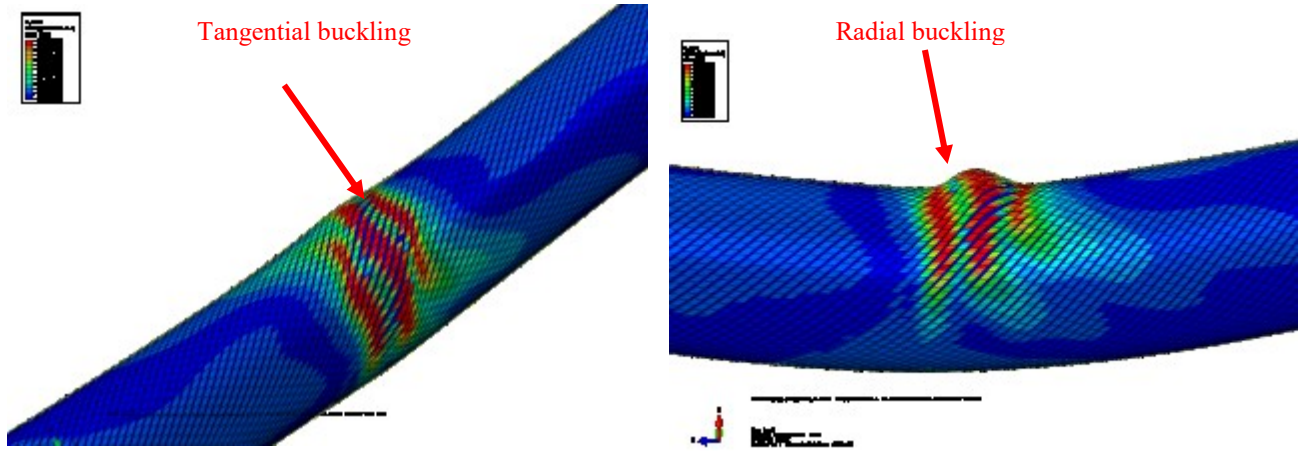


Figure 5-3. Tangential and radial buckling in external tensile armours.

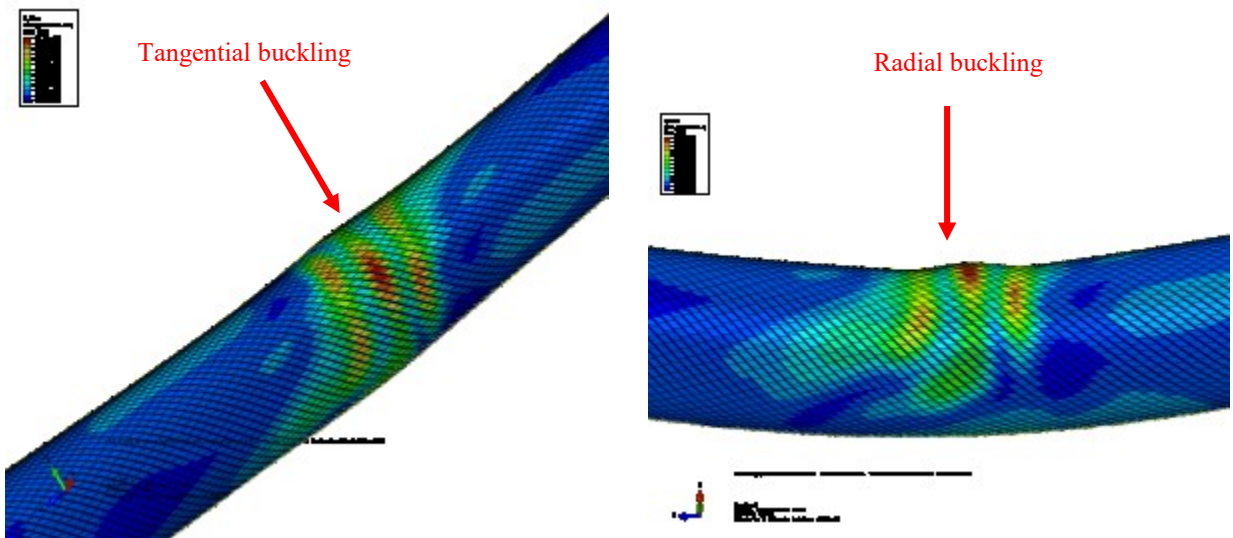


Figure 5-4. Tangential and radial buckling in internal tensile armours.

The global axial force as a function of the global axial shortening per unit length for three different studies (i.e., experimental test de Sousa's [5], FE model Ebrahimi *et al.* [6] and the current study) is shown in Figure 5-4. The model employed by Ebrahimi [6] has excellent consistency with the experimental model de Sousa *et al.* [6], as these two possess similar configurations and model of Ebrahimi *et al.* [6] is developed based on the physical model of de Sousa *et al.* [3] indeed. The little difference between these two models can be due to uncertainty with limited information on measurement and test procedure in de Sousa *et al.* [3]. In the physical model test there is no reported local measurement. Also, there are ambiguities associated with the type and magnitude of imperfection used on the exterior layers (anti-birdcaging tape and plastic sheath). The current model of pipe (the pipe including rupture) differs in two aspects with the model used by Ebrahimi *et al.* [6] which these two differences are the buckling point and elastic modulus. The ruptured pipe buckles at lower axial force as an opened-up rupture creates remarkable bending in the pipe which this bending moment causes a tangential movement of tensile wires in addition to the radial one which can be seen in Figure 5-3 and Figure 5-4. Combination of tangential and radial movement of the wires causes the pipe to buckle at lower axial force. Besides, the ruptured pipe shows a bit stiffer in Figure 5-4. Once the pipe does not include the imperfection in anti-birdcaging tape like what used in Ebrahimi *et al.* [6] except the rupture, the pipe remains stiffer in respect to Ebrahimi *et al.* [6] as far as no bending moment is shaped in the pipe. Once bending moment steeply starts growing in the pipe due to the rupture opening, the bending moment causes pipe to buckle, while the pipe shows stiffer in modulus of elasticity. The bending moment in the Ebrahimi *et al.* [6] is zero as the imperfection type which was used in Ebrahimi *et al.* [6] does not produce any kind of bending moment and pipe buckles axis-symmetrically.

A summary of the results is presented in Table 5-2. There is general consistency between the studies on the buckling force, with percent differences of 7% to 13%, and greater scatter on the kinematic variables (i.e., axial strain, twist per unit length), with percent differences of 3% to 42%. This variance is attributed to uncertainty in the pipe segment initial state (e.g., imperfections, characteristics of the damage state or rupture zone), boundary conditions (e.g., end coupling stiffness, out-of-straightness), material and mechanical properties (e.g., elastic modulus, section composition) and instrumentation (e.g., discrete global point data sources that does not measure local response).

Table 5-2. Buckling force in the FE model and model test.

Models	Buckling Force (kN)	Axial strain (cm/m)	Twist per unit length (deg/m)	Bending stiffness (kN.m)
Ebrahimi (2015b)	282	1.14	0.81	0
4% of rupture	231	0.84	0.545	1.37
De Sousa (2012)	263	1.24	0.53	Not Reported

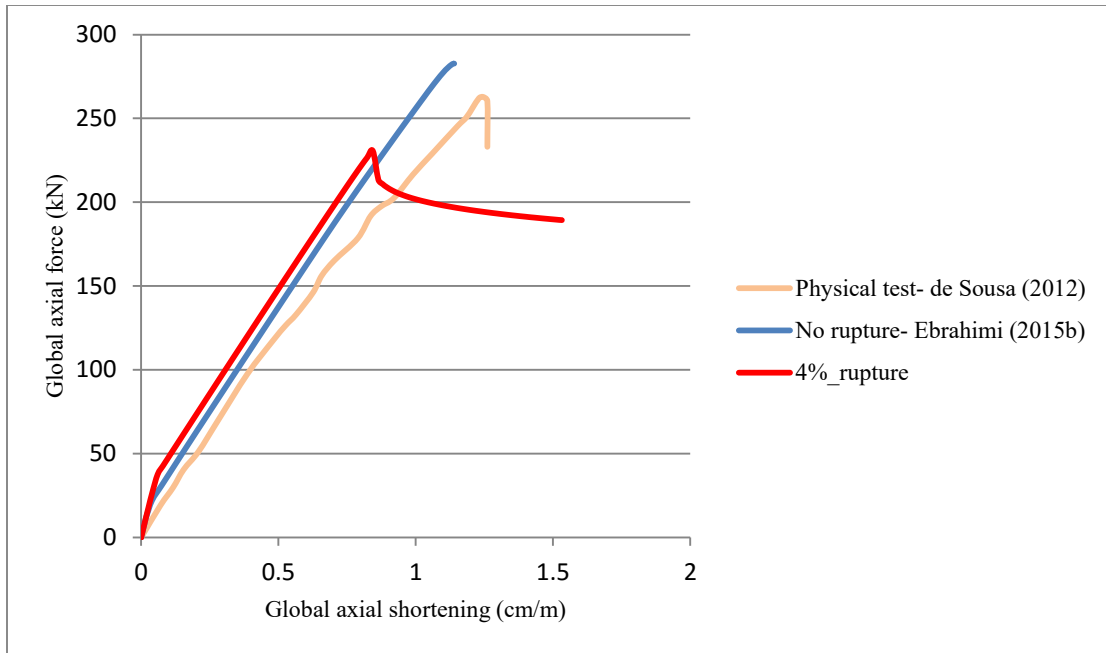


Figure 5-5. Global axial force versus global shortening in three different approaches.

The global axial force and axial twist per unit length response is illustrated in Figure 5-5. The reason of difference between the physical model test and FE model of Ebrahimi *et al.* [6] in Figure 5-5 is same reasons as explained for Figure 5-4 (limited information on measurement and laboratory configuration). In Figure 5-6, ruptured pipe shows a bit stiffer in rotational behavior in respect to Ebrahimi *et al.* [6]. This is because of the same reason which was stated for Figure 5-4. In ruptured pipe, the pipe shows stiffer both in axial shortening and axial rotation as far as the rupture does not start opening. Once the rupture opens, a sudden and remarkable bending is created in the pipe, Figure 5-7, and consequently pipe buckles at lower axial force. Also, it should be noted that as the rupture is completely opened just after buckling point, Figure 5-2, there is less constraint for the axial twist and it rotates significantly.

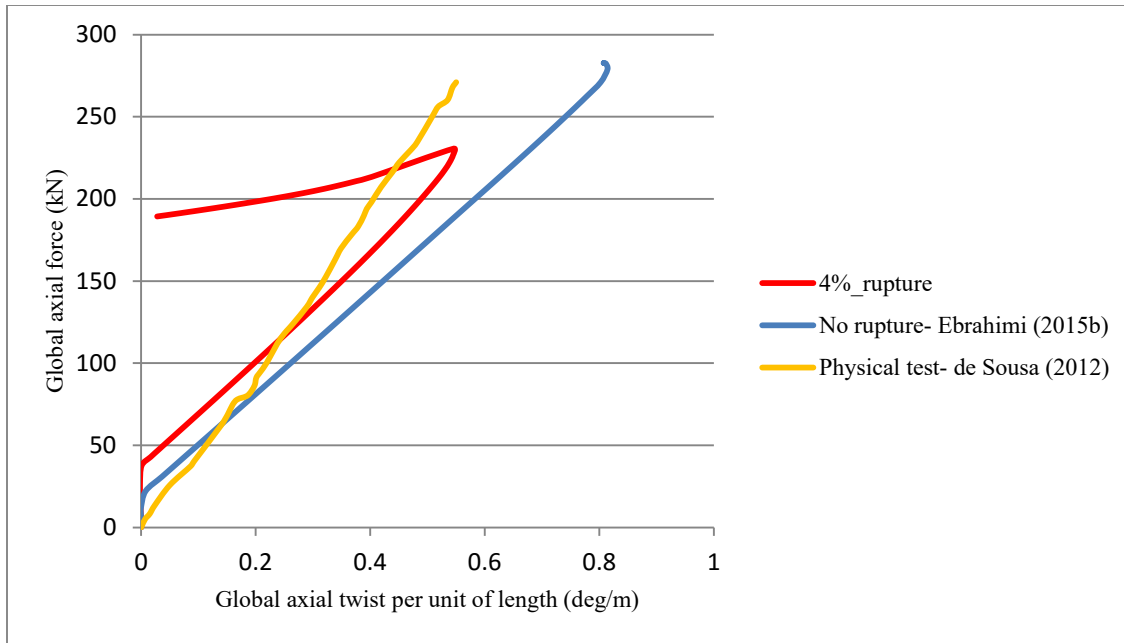


Figure 5-6. Global axial force versus global axial twist per unit length.

The peak load and strain at peak load decreases with increasing rupture zone length. The flexible section appears to change instability modes from a snap through type to more diffused local buckling with increasing rupture zone length, Figure 5-7. This is supported through examination of the global axial force and global bending moment relationship (Figure 5-8). The response is governed by three deformation modes associated with axial compression, local bending and radial instability. The pipe first experiences initial compression with no significant bending moment. As the pipe develops greater out-of-straightness due to rupture opening-up, the bending moment starts to increase and exhibits nonlinear response (Figure 5-8). A longer opened-up rupture creates a larger bending moment from axial compression in the pipe and this decreases buckling force. This mechanism initiates the radial instability (i.e. birdcaging) that limits the peak axial force and peak global moment. The axial resistance is significantly affected by this instability where the mechanisms is governed by the local moment and radial deformaitons. Once local moment is imposed on the pipe, the tangential instability in wires is added to the radial one and the pipe

buckles at lower axial force in respect to pure radial mode shape including a combination radial and tangential modes of buckling.

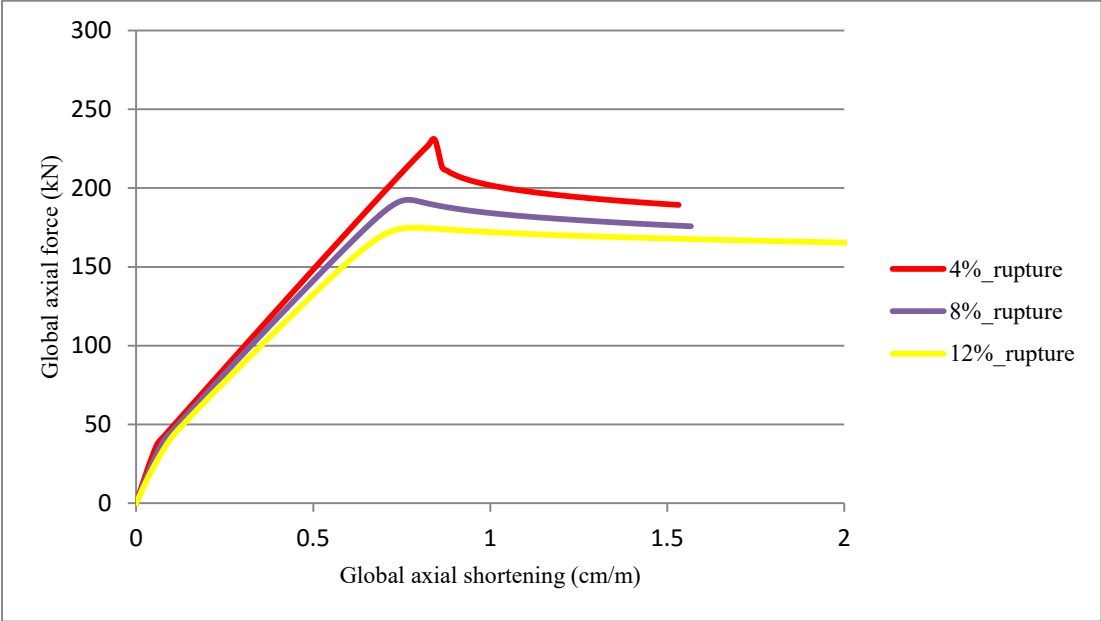


Figure 5-7. Global axial force versus global axial shortening for different rupture length.

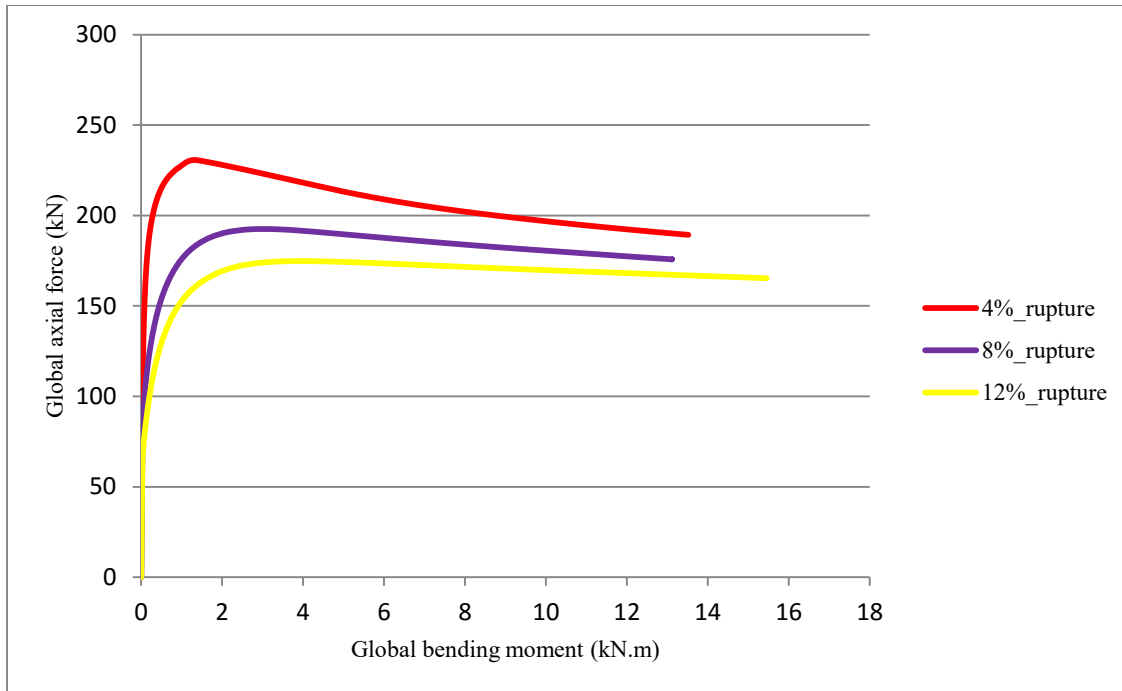


Figure 5-8. Global axial force versus global axial bending.

The relationship between global axial force and global axial twist for three different rupture lengths is illustrated in Figure 5-9. By raise of rupture length, the buckling shape pattern changes from snap through point to diffused local buckling and this changes the global twist response as matter of both twist direction and magnitude.

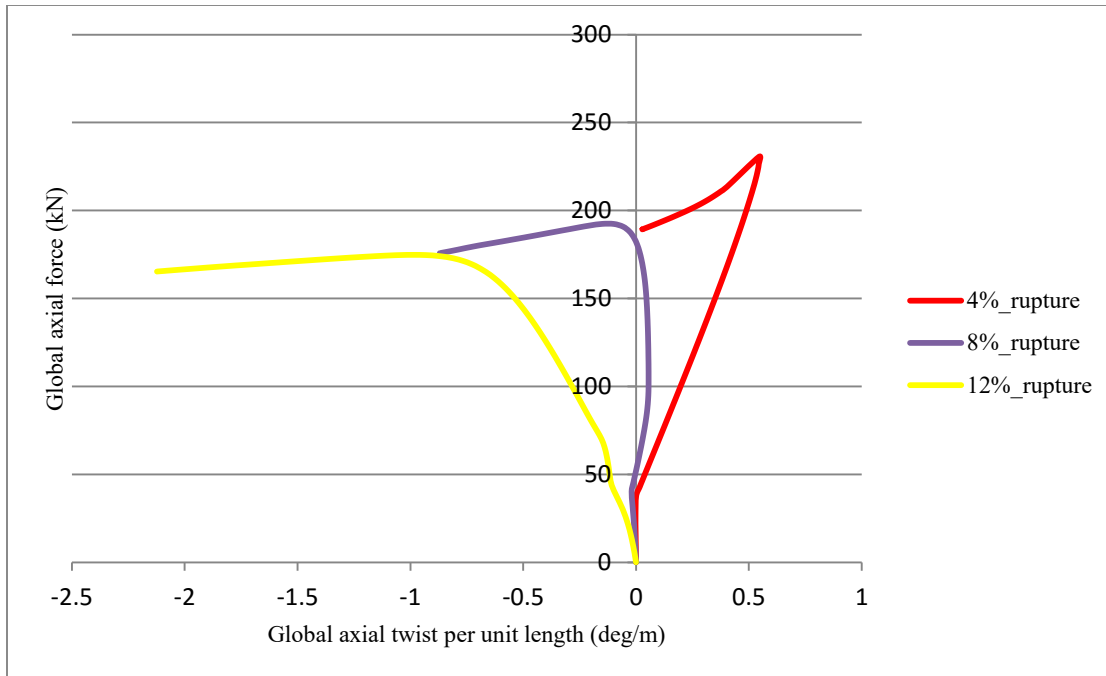


Figure 5-9. Global axial force versus global axial twist per unit length.

## 5.5 Conclusion

The aim of this investigation is evaluation of rupture effect on local buckling of tensile armours. A 3D continuum finite element model, which was calibrated based on available experimental data, examined the effects of rupture zone length on the global mechanical response (i.e., axial force, moment, angle of twist) and local deformation modes and failure mechanisms. The introduced rupture in anti-birdcaging tape and plastic sheath layers starts to open up after a certain point and creates bending moment from axial compression. Added bending moment to the imposed axial compression presents a combined buckling modes shapes in tensile wires (radial and tangential) and decreases the peak axial force and corresponding axial shortening. The ruptured pipe shows a bit stiffer in elasticity modulus, while it buckles at lower axial force. The longer opened-up rupture in the pipe presents larger bending moment and consequently the pipe buckles at lower axial force. Also, it is shown that rupture length influences global axial twist pattern. To promote further

confidence in the numerical modelling procedures, a series of physical tests is needed to verify the outcomes from this parameter study.

## 5.6 References

- [1]. Technip, (2012), “Coeflexip-Flexible steel pipe for drilling and service applications”, User guide, page 2-3.
- [2]. De Sousa R.M, Viero. P.F, Magulta. C, Roitman. N., (2012). “An experimental and numerical study on the axial compression response of flexible pipe”, OMAE 2012, 31<sup>st</sup> International Conference on Ocean, Offshore and Offshore Engineering, Rio de Janeiro, Brazil.
- [3]. De Sousa R.M, Magulta C., Roitman. N., Elliwanger G. B., Lima E.C.P., Papaeo A., (2009). “On the response of flexible risers to loads imposed by hydraulic collars”, Applied Ocean Research 31, 157–170.
- [4]. Ebrahimi, A., Kenny, S., Hussein, A., (2015). “Finite element simulation of flexible pipe: Challenges and Solutions”, Volume 14 (4), pages 275-287, 2015.
- [5]. Ebrahimi, A., Kenny, S., Hussein, A., (2015). “Radial instability of tensile armour wires in subsea flexible pipe-numerical assessment of key factors”, Volume 138 (3), doi: 10.1115/1.4032894.
- [6]. Serta, O., Fumis, R., Connaire, A., Smyth, J., Tanaka, R., Barbosa, T., Godinho, C., (2012). “Predictions of armour wire buckling for a flexible pipe under compression, bending and external pressure loading”, OMAE 2012, 31<sup>st</sup> International Conference on Ocean, Offshore and Offshore Engineering, Rio de Janeiro, Brazil.

[7]. Vaz M.A, Rizzo N.A.S, (2011), “A finite element model for flexible pipe armor wire instability”, Journal of Marine Structures, Volume 24, page 275-291

## **Preface**

This journal research paper is an original study and the developing idea, planning and implementation of the whole technical parts of this research paper have been done by the candidate as the first author, and the regular supervision has been made by Dr. Shawn Kenny through advising on the planning of the research way, evaluation of the research merit and providing precious idea and experience on the discovered phenomena and technical parts. The compilation of the paper literature has also been implemented by the candidate and it has been continuously revised by Dr. Shawn Kenny to improve the quality of the technical part and the literature. Facilitation of the PhD program of the candidate and also final review of the paper has been made by Dr. Amgad Hussein as the third author. Wood Group Kenny Research Chair at Memorial University of Newfoundland has funded the whole PhD program study and provided the all facilities (cluster machine, Software and personal computer) for carrying out the study.

This journal research paper was submitted to the Journal of Marine Structures on November 20th, 2015.

## **6 Lateral buckling of tensile armour wires in subsea flexible pipe- finite element assessment using Implicit solver**

Alireza Ebrahimi (1), Shawn Kenny (2), Amgad Hussein(1)

(1) Faculty Engineering and Applied Science, Memorial University of Newfoundland

St. John's, NL, Canada

(2) Department of Civil and Environmental Engineering, Faculty of Engineering and Design,

Carleton University

Ottawa, ON, Canada

### **6.1 Abstract**

Applications of flexible pipe has been growing as flowline, jumper and riser because of high axial stiffness and low bending stiffness that makes the pipe capable of making connection between fluctuating vessels (e.g. FPSO) and fixed structures (e.g. platform and PLEM) that due to harsh environment or type of application needs a low bending stiffness connection to comply with the harsh environment loading while it enjoys well resistance for axial loading, fatigue and collapse failures. Tensile armour wires are the components reinforce the pipe toward axial, torsional and bending loading condition. There are two mode shapes of buckling (i.e. radial and lateral buckling) can occur through severe conditions for tensile wires in which flexible pipe lose axial, torsional and bending stiffness. This paper studies the lateral buckling of tensile wires by 3D finite element modeling which simulate all probable contact interactions and nonlinearities with minimum of

assumptions, and employ the Implicit solver to target flaws of previous studies (i.e. time-efficiency and accuracy). This study uses Ostergaard's analytical simulation and experimental study [1] as validation and comparison. An assessment on length and friction coefficient of flexible pipe is carried out which demonstrates the effect of these parameters on buckling force, and mechanical behaviour. At last stage, the study is extended into determination of critical bending limit in installation procedure of flexible pipe as the most susceptible condition for lateral buckling of tensile armour wires.

## **6.2 Introduction**

High axial and low bending stiffness are two significant features of flexible pipes employed in numerous applications (e.g. jumper, riser and flowline) due to high mechanical resistance toward fatigue and collapse. This type of pipe consists of various layers in which each layer has its own role in mechanical or thermal behaviour. Tensile armours are the components designed to stand toward axial, torsional and bending loadings. A high strength anti-birdcaging tape is wrapped around the tensile armours to make circumferential constraint and prevent any radial instability. A typical section of a flexible pipe illustrating the multiple layers through the cross-section is shown in Figure 6-1, [2]. This tape is wrapped around the wire to avoid radial buckling of tensile armours, which is the most probable buckling mode shape of armours due to low moment of inertia of the wires. In case the radial movement is well constrained, a severe tangential movement might occur in the tensile armours due to out-of-plane bending and axial compression loading. For flexible pipe with local damage, sea water may leak inside the annulus that reduces the interlayer friction and releases the constraint on the tangential movement of tensile armours. The lateral (tangential) buckling of tensile armours may be considered a more critical failure mode, in comparison with

radial buckling, as it is difficult to be detected. Figure 6-2 illustrates the lateral buckling mode of tensile wires in flexible pipe [3].

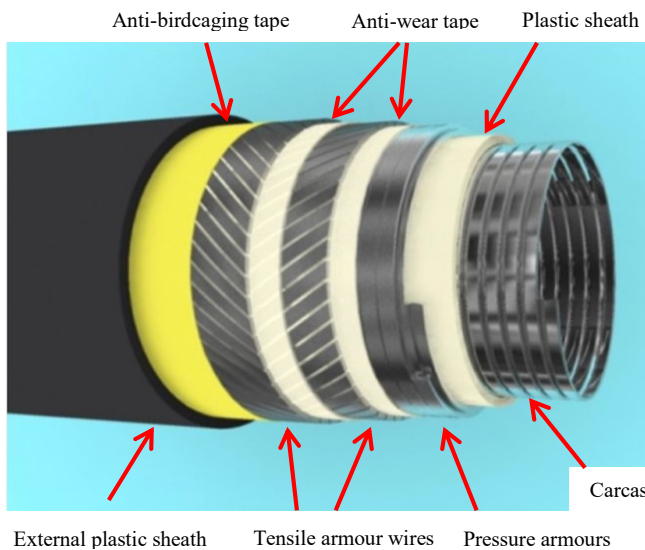


Figure 6-1. Cross section of unbounded flexible pipe [2].

Figure 6-2. Lateral buckling in tensile wires [3].

Braga *et al.* [4] conducted idealized experiments, in air at atmospheric pressure, to assess the effects of axial load, associated with deepwater conditions, on the mechanical response of a flexible riser and flowline test segments. Although the whole procedure of the physical model test is a valuable step in examination of the flexible pipe under a certain condition, the sole reported result is not a reliable data for development of numerical tools.

Ostergaard *et al.* [1] presents an analytical approach for lateral buckling of tensile armour layers subject to static and cyclic bending deformations with a superimposed axial compressive load, which may occur during installation procedures. Although the analytical solution was supported by physical modelling, the analytical result which was in form of an elastic-perfectly

plastic load-deformation response requires further investigation to address uncertainty. Furthermore, Ostergaard *et al.* [1], recommended additional test program to evaluate the significance of interlayer friction on the triggering of lateral buckling events. Tan *et al.* [5] presented an analytical solution predicting the lateral buckling in tensile armour wires based on total strain energy approach. A summary on implementation of series of deep immersion prototype (DIP) tests which were conducted for qualification of flexible pipe to water depths exceeding 2000 m, were presented without elaborating the test procedure and reporting the results.

Perdrizet *et al.* [6] developed 3D finite element modelling procedures, employing both implicit and explicit integration schemes, to duplicate the mechanical response of a physical model test of flexible pipe for specific loading conditions. The pipe was subject to internal pressure and axial tension with bending cycles of bending  $0^\circ$  to  $15^\circ$  and  $0^\circ$  to  $-15^\circ$ . The axial and transverse stress response of tensile armour wires was examined. Although lateral or tangential motion of the tensile armour wire was examined, the physical and numerical modelling investigations did not address the effects of axial compressive loading. In this study, however, the technical issues when using an explicit solver (e.g., time step for conditional stability, dynamic effects with stress wave propagation and contact) were highlighted and necessity for the implementation of the similar simulation with Implicit solver is emphasized. In a recent study, Ebrahimi *et al.* [7] also demonstrated the advantages for using an implicit scheme in investigation of radial instability in tensile wires of flexible pipe, due to the unconditionally stable time increment; better performance in determining equilibrium condition and snap through point due to equilibrium check.

The primary motivation for this study is the limited number of investigations, which includes analytical, experimental and numerical methods, and knowledge on the lateral buckling response

and failure mechanisms of tensile armour wires. A 3D finite element modelling, which accounts for nonlinear behaviour due to deformation response, material behaviour and contact interaction, is developed to investigate the lateral buckling response of tensile armour wires. The experimental study and analytical simulation by Ostergaard *et al.* [1] are used to assess and verify the computational procedures. A parameter study is conducted to assess the effects of model pipe segment length, diameter and interlayer friction on lateral buckling response. Critical bending limits for lateral buckling of tensile armour wires associated with installation procedures are also examined.

### **6.3 Finite Element Model**

The finite element modelling procedures adopted the test configuration used by Ostergaard *et al.* [1], which was 152.4 mm (6") diameter pipe with a 5 m segment length. The model accounted for 9 separate layers, through the pipe cross-section, with defined contact interactions between each layer. The name, geometric and material properties, and element type for each layer are summarized in Table 6-1.

Table 6-1. Characteristics of each individual layer.

Layer	Material and Geometry	Element Type and Order
Carcass	Thickness = 4.0 mm Lay angle = 87.6 deg Young's modulus = 193 GPa Poisson ratio = 0.3; Yield stress = 320 MPa Rupture stress = 640 MPa;	Shell
Plastic sheath	Thickness = 5.0 mm Young's modulus = 345 MPa Poisson ratio = 0.3; Yield stress = 20 MPa Rupture stress = 20 MPa.	Shell
Pressure armor	Thickness = 6.2 mm Lay angle = 87.0 deg Young's modulus = 205 GPa Poisson ratio = 0.3 Yield stress = 900 MPa Rupture stress = 1000 MPa	Shell
Tensile armor	Dimensions = 3.0 mm * 10 mm Number of exterior wires = 52 Number of exterior wires = 54 Lay angle = 26.0 deg	Shell

	Young's modulus = 210 GPa Poisson ratio = 0.3; Yield stress = 760 MPa Rupture stress = 850 MPa	
High strength tape (Anti-bird caging tape)	Thickness=1.2 mm Young's modulus = 750 MPa Poisson ratio = 0.3	Shell
Outer plastic	Yield stress = 20 MPa Rupture stress = 20 MPa	Shell
Anti-wear tape	Young's modulus = 350 MPa	Shell

As there are multiple layers with adjoining contact, the use of node-to-surface interaction results in ill conditioning due to excessive contact force or penetration associated with discontinuous surface normal to the element. In this study, a surface-to-surface discretization method was used to avoid the penetration of a master surface into slave by defining the constraint condition between slave nodes with a resultant smoother stress gradient. A circumferential geometric surface smoothing algorithm was used to better represent the contact between concentric cylinders in order to reduce interference fit and numerical noise that results in improved accuracy and convergence of contact interaction and estimates of contact stress during numerical simulations. This contact formulation accounts for the shell thickness, double sided surfaces, and self-contact. Hard normal contact was simulated using the Penalty method, which is an approximate method the pressure-overclosure response that is proportional with the penetration distance of the master surface into

the slave surface. Penalty method was specified for tangential contact with a friction coefficient of 0.1 (i.e., representing the dry annulus friction coefficient) between all layers.

Implicit solver was used, rather than an explicit solver, due to the improved performance to achieve equilibrium conditions for static or quasi-static problems with a large number of contact interactions and potential for snap-through response. The implicit method exhibits faster convergence due to unconditional stability method provided the analysis does not encounter contact penetration problems [10,11]. The explicit method demands a small time-step for conditional stability that is influenced by element geometry, material properties and contact interaction effects (e.g., dynamics, stress wave). The equilibrium check improves the precision of results in two different aspects. In each iteration, Abaqus/Standard (Implicit solver) calculates residual force for all nodes and each individual degrees of freedom and compares them with the calculated time average force [9]. This check significantly helps the Implicit solver to find equilibrium points especially for those problems including bifurcation and snap-through point in which the direction of equilibrium path of the structure abruptly changes. Furthermore, equilibrium check benefits FEM in the contact interaction mechanism and once the problem suffers severe discontinuities including contact open-closure (normal direction) and slip-stick (tangential direction) status. The predicted contact penetration must satisfy compatibility tolerance requirements and the contact force due to over-closure and also the residual force from opening or over-closure should be less than 0.5% of time average force. In the tangential direction, the stick condition should satisfy both penetration tolerance and equilibrium check, similar to the over-closure conditions, whereas the slip condition must satisfy the equilibrium criterion.

The boundary conditions are assigned at two reference points, located at each end of the pipe segment, with pipe layer edges coupled to them. The boundary conditions used in the FE modeling

procedures of this theses are consistent with the analytical simulation and physical model tests conducted by Ostergaard [1]. The first stage bending curvature (bending radius,  $R = 11$  m) is imposed at the reference points, while axial compression is imposed within the second loading stage using a pin-roller end boundary condition while the direction of compression is kept along the Z direction, Figure 6-3 and Table 6-2 .

Due to the non-linear response, associated with contact between multiple layers and local instability of tensile armour wire, a fine mesh discretization was required over the model domain, Figure 6-4. The total number of elements was 277,000 with more than 1,660,000 degrees of freedom (DOF). In order to reduce computational effort, the carcass and pressure armour layers, which comprise interlocking profiled components, were modeled as a simple cylinder, using shell (S4) elements, with orthotropic material behaviour [8]. The anti-wear tape and plastic sheath layers were also modeled as a simple cylinder, using shell (S4) elements, with isotropic material properties.

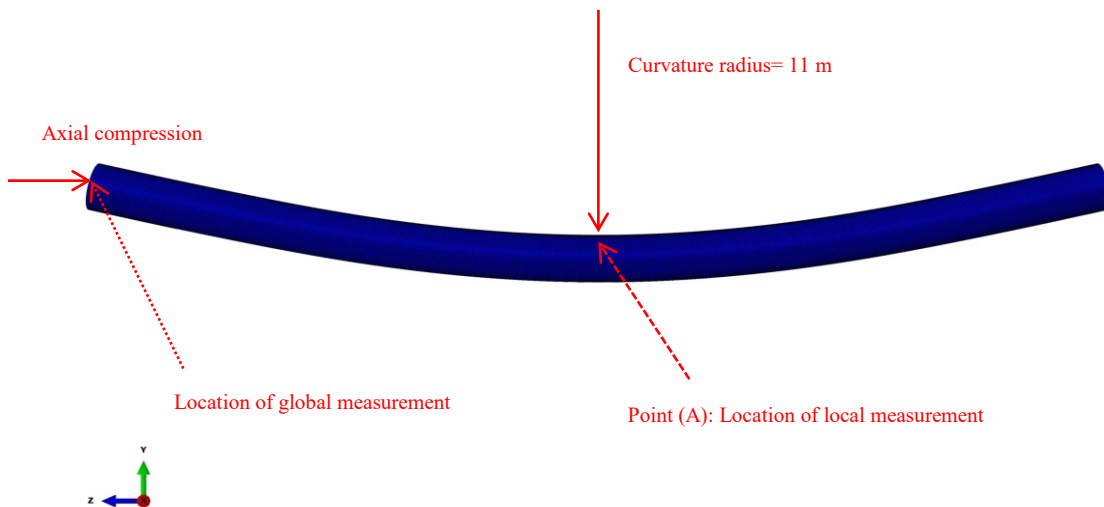


Figure 6-3. Axial compression is applied on the initially curved pipe.

Table 6-2. The boundary conditions of the pipe.

Step #	RF1	RF2
1	$U1 = UR2 = UR3 = 0$ $U2 = \partial y$ $UR1 = \partial \phi$ $U3 = \text{free to elongate}$	$U1 = U3 = UR2 = UR3 = 0$ $U2 = \partial y$ $UR1 = \partial \phi$
2	$U1 = UR2 = UR3 = 0$ $U2 = \text{fixed at } y$ $UR1 = \text{fixed at } \phi$ $U3 = \text{axial compression}$	$U1 = U3 = UR2 = UR3 = 0$ $U2 = \text{fixed at } y$ $UR1 = \text{fixed at } \phi$

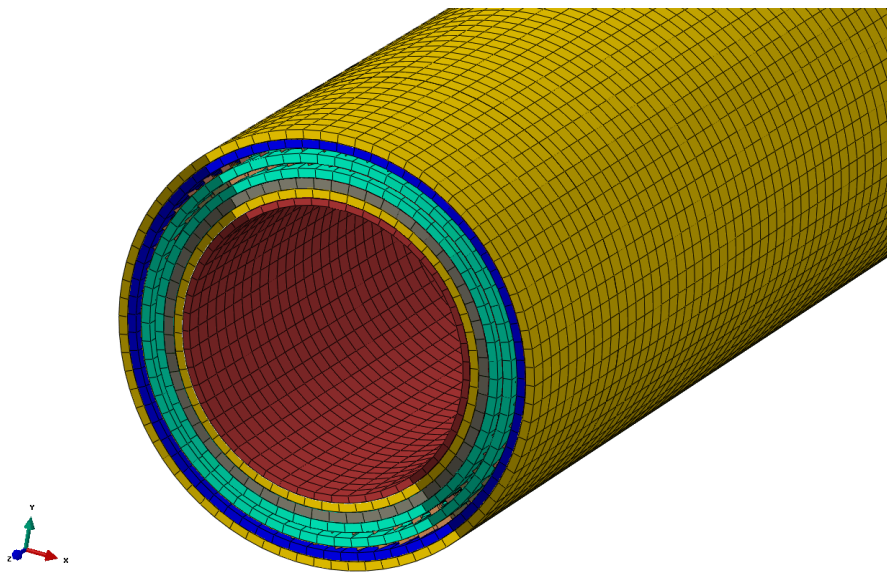


Figure 6-4. Cross section of the modeled flexible pipe.

## 6.4 Results and discussions

### 6.4.1 Main model simulation and validation

The lack of report on physical model tests of tensile wires tangential buckling in public domain which can be used by third party and existing constraints upon internally implementation of these series of tests due to company-specific proprietary nature of flexible pipe, made this study to use the Ostergaard's study as the main calibrating tool. Confidence on correctness of the calibrating procedure was established through two logical paces.

1. A finite element model incorporating Ostergaard's analytical model assumptions was developed and the influence of inclusion of the underlying assumptions was discussed, Figure 6-5,
2. The integrated hypotheses are replaced by realistic conditions (i.e. identical to a real pipe) and the FEM results (i.e. buckling forces) were calibrated with the few experimental tests by Ostergaard, Figure 6-7

As this was discussed earlier the Ostergaard's analytical formulation incorporated assumptions to facilitate the modeling of the flexible pipe complex structure, as follow.

- Simplified pipe cross-section geometry (e.g., no inclusion anti-birdcaging tape, external plastic sheath and internal core),
- Neglecting radial elastic deformation of the layers under axisymmetric loading.
- Idealization on pipe layer kinematics (e.g., external armour layer fixed in a loxodromic configuration with motion at a constant pitch angle without tangential displacement), and
- Idealized interlayer contact with no friction between internal tensile wire layer and adjacent layer.

These modelling hypotheses influenced the outcome for predicting the lateral buckling response of tensile armour wires. The consequence of first two assumptions (i.e. assumptions a and b) for analytical method was that, the tensile wires cannot possess natural behaviour through the interactions with adjacent layers. Combination of last two assumptions (i.e. external tensile wires are locked in their initial loxodromic configuration and no friction is assumed between other internal tensile wire layer and adjacent layer) caused the pipe to show higher axial stiffness with minor strain before bifurcation point (i.e. no tangential instability was accounted for the external tensile wires) and perfect-plastic failure after this point (i.e. no friction was taken into calculation). After buckling, the analytical solution has no axial resistance with infinite strain response in the post-buckling regime, Figure 6-5.

However, in a real pipe, it is expected that the constraint effects of adjacent multiple layers retains overall strength of the pipe to some extent even after that the bifurcation point is reached. Besides, the lack of interface friction in the analytical solution results in pipe buckling at lower axial forces without strain softening response. A schematic comparison of the analytical solution by Ostergaard *et al.* [1] and a real pipe response is shown in Figure 6-6. Later in this study, Figure 6-20, it will be shown and proved that external tensile wire layer shows tangential displacement under compression and should not be assumed as locked in initial loxodromic configuration.

The axial stiffness of the FE model, including the Ostergaard's analytical assumptions, possesses % 18 discrepancies, in respect to the analytical model and this provides confidence on the force-strain mechanism of the FE model to be developed to simulate the real pipe condition. There is an offset force (i.e. roughly 45 kN) in analytical model which was shaped in the process of bending pipe (i.e. loading step 1) while the finite element model was set free to elongate at one end in the process of bending to relax stress level.

Another type of validation is needed to enhance confidence about buckling force. In the next stage, the FEM was improved with the most similarity with a real model (i.e. analytical assumptions are removed) in which, the all layers are model and tensile wires can have natural interactions with other layers; the external tensile wires can have any tangential displacement; friction coefficient,  $\mu=0.1$ , is set for all layers. In this stage the buckling force is calibrated with the two samples examined in laboratory reported by Ostergaard, Figure 6-7.

Table 6-3. Comparison of the axial stiffness between analytical model and FE model including assumptions.

Approach	Axial stiffness (kN.m/m)
Analytical	362,000
FE method_ assumptions included	302,000

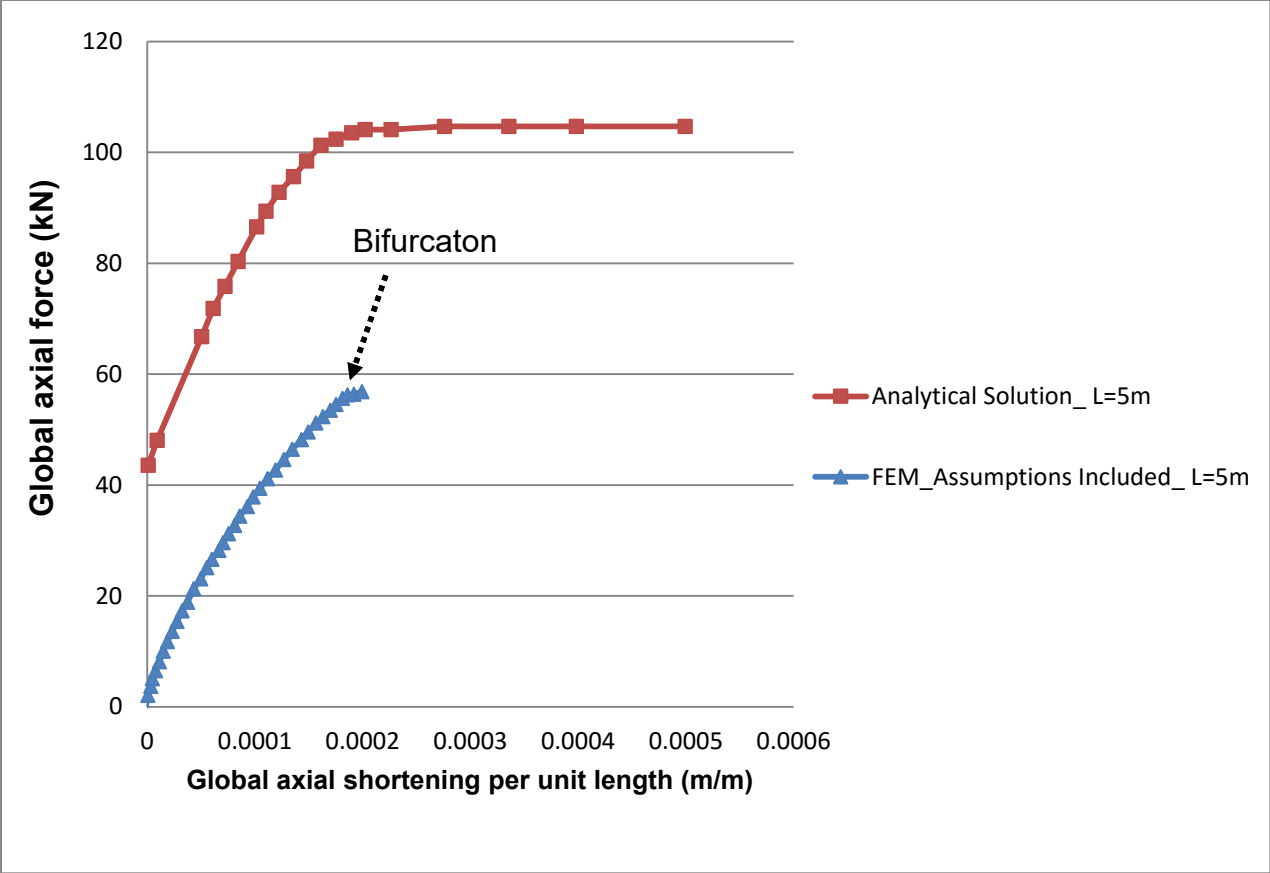


Figure 6-5. FE model designed based on the analytical assumptions.

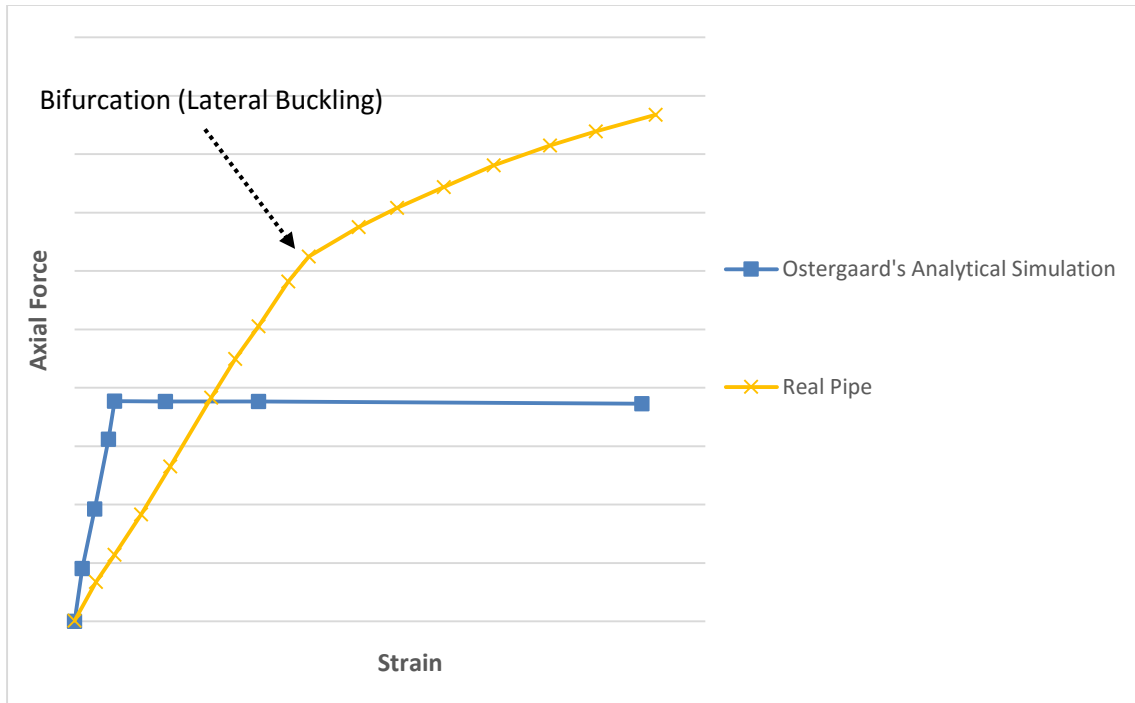


Figure 6-6. Schematic comparison of buckling in analytical model and a real pipe.

Regarding physical model test, as Ostergaard assumed his analytical model in frictionless condition, in order to be comparable with experimental results, in the physical model test, the constant curvature used in the analytical model was substituted by cyclic bending with the same radius of the curvature to reduce friction coefficient between layers. In this way, the experiment conditions could be as identical as possible to Ostergaard's analytical work (i.e. frictionless condition), while an uncertainty remains in experimental tests that whether this method could turn the original friction factor (i.e.  $\mu=0.1$ ) between layers to zero (i.e. frictionless condition). The current FE model, due to complexity of the model and computational time expense (i.e. 1.6 million degrees of freedom and more than a hundred active contact interactions), was not feasible to be examined under cyclic loading.

A comparison of the buckling force, between the experimental results [1] and the FE simulation from the current study (i.e. similar to a real pipe) are summarized in Table 6-4 and illustrated in

Figure 6-7. The data points represent the measured buckling force during the experimental studies [1], and the solid lines are the FE predictions (i.e. which is designed based on real pipe).

In the experiments conducted by Ostergaard *et al.* [1], two end-fittings were installed on the two ends of each 5 m-length test segment. All samples were initially subjected to a constant axial compression and then superimposed by cyclic flexural loading, with a maximum of curvature radius of 11 m over 100's of cycles to overcome internal friction effects. Two samples, experiencing axial force of 80 kN and 160 kN did not buckle, while tests samples subjected to higher compressive loads, 203 kN and 268 kN, exhibited buckling instability. As it can be expected, in the FE simulations, the global buckling force decreased (i.e., 55 kN, 104 kN and 212 kN) with increasing pipe segment length (i.e., 5 m, 2.5 m and 1.25 m). The 5-m length pipe in FE simulation buckled at 55 kN axial force less than the forces (i.e. 205 kN and 268 kN) in which the experimental samples buckled. In fact, the tested pipe in laboratory possesses 5 m of length, but two end-fittings which were installed at two ends of it, reduced its effective length. End-fitting normally caused circumferential clamping area (i.e. no-slip zone) for wires and this reduced the tensile wire effective length for tangential (lateral) buckling. Hence, this author examined the two shorter lengths of pipe, 2.5 m and 1.25 m, to take the end-fitting clamping areas into calculation. This method (i.e. estimation of effective length by reducing the total) was also used by Ostergaard's analytical model. It might be worth to say, at first, this author tried to simulate the end-fitting effect by another method like creating a radial confinement on the 5-m length pipe, but this method run into numerical divergence.

The 2.5 m-length simulated pipe buckled at 104 kN which was still below the experimental results, but 1.25 m-length pipe buckled in the axial force equal to 212 kN, in the area which two pipe samples buckled (i.e.  $F=203.7$  kN &  $F=268.77$  kN). Table 1 provides buckling forces of four

samples examined in laboratory, and mechanical response (i.e. force, strain and twist at the buckling point and axial stiffness) for three different segment lengths of analytical and FE models.

Table 6-4. Comparison between characteristic features of laboratory and FE analyses.

Sample	Buckling force (kN)	Buckling strain (m/m)	Buckling twist (deg/m)	Axial stiffness (kN/m)
Lab. sample #1	268.77	-	-	-
Lab sample #2	203.70	-	-	-
FE_ 5 m	55.32	0.0058	0.033	1890
FE_ 2.5 m	104.27	0.0016	0.06	24805
FE_ 1.25 m	212.21	0.002	0.114	63972

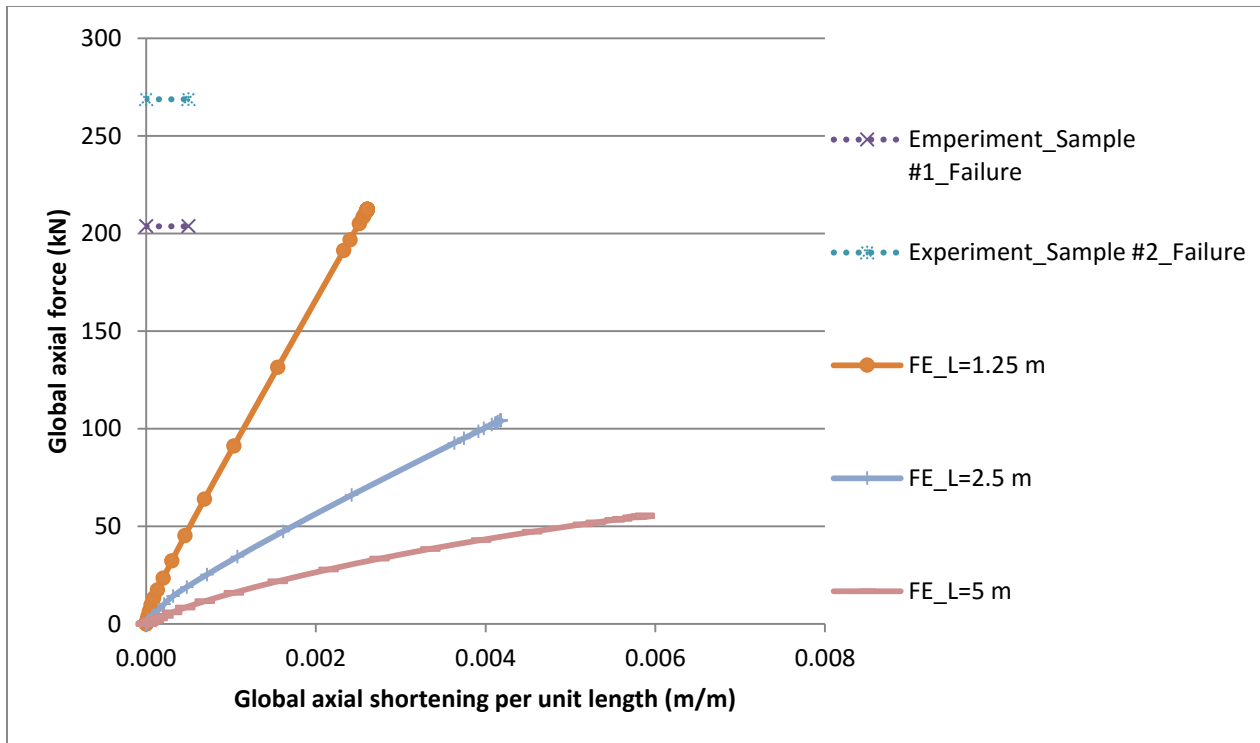


Figure 6-7. Global axial force versus global axial shortening.

During the lateral buckling event, tensile armour wires rotate and interact with adjacent surfaces that cause difficulties in the numerical solution with respect to contact penetrations and forces associated with local discontinuities, and equilibrium solution convergence through the bifurcation point. To establish confidence on the local buckling event (i.e. bifurcation point), the global axial force-axial strain and the global axial force-angle of twist response should be monitored simultaneously. Loss of lateral stability and onset of lateral buckling mechanisms in the tensile armour wires can be identified by changes in the torsional stiffness and angular twist response, . For more clarity on the occurrence of bifurcation point (severe twist), each graph is zoomed in at its end and these zoomed-in figures are included on the Figure 6-8.

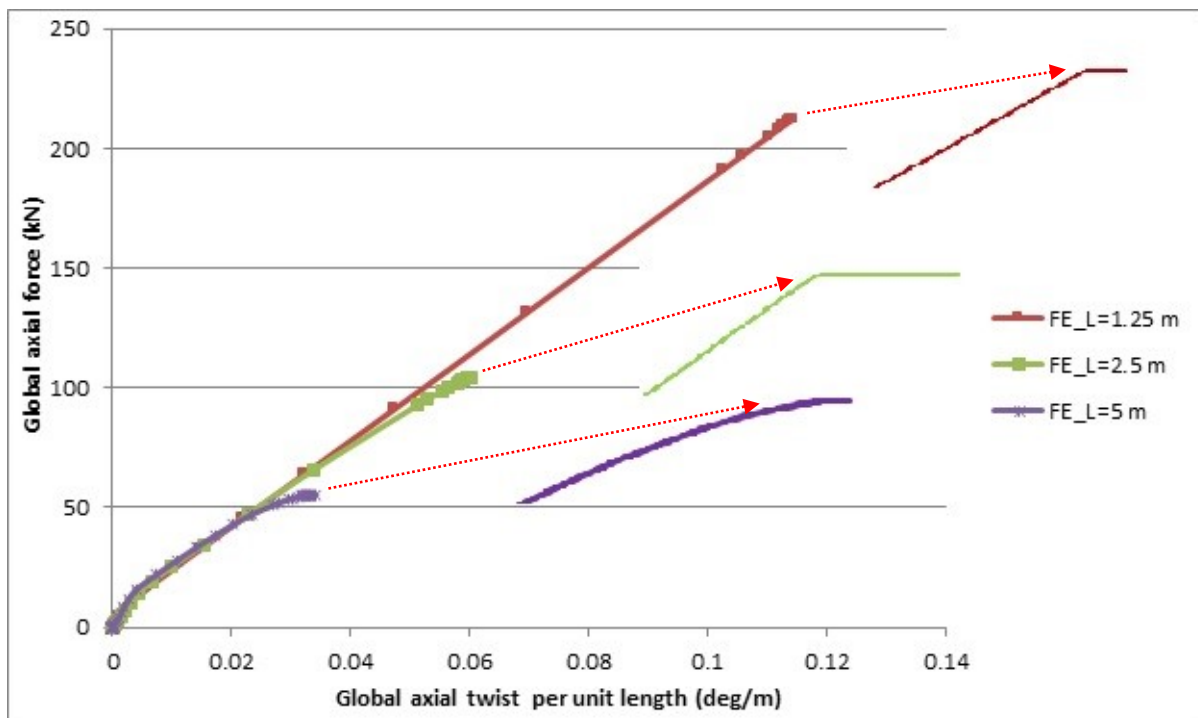


Figure 6-8. Global axial force versus global axial twist per unit of length.

In order to develop greater confidence on the FE prediction for lateral buckling and onset of local instability mechanisms, the local shear stress and slip displacement was examined at point A,

Figure 6-3. Once the normalized shear stress (i.e. ratio of shear stress to critical shear stress) equals one, the wires start slipping. The critical shear stress is defined in Equation 1.

$$\tau_{critical} = \mu_s \cdot P \quad (1)$$

where P is the normal contact pressure at the contact area and  $\mu_s$  is the static friction coefficient. As it is seen in Figure 6-9 except the initial increment of the axial compression, the normalized shear stress stays below one till axial force reaches 212 kN, in which normalized shear stress is equal one and the wires get slipping (i.e. lateral buckling), Figure 6-10. It should be noted that normalized shear stress at the first increment of the axial load step is equal one, since it remains from the previous loading stage (i.e. applying curvature).

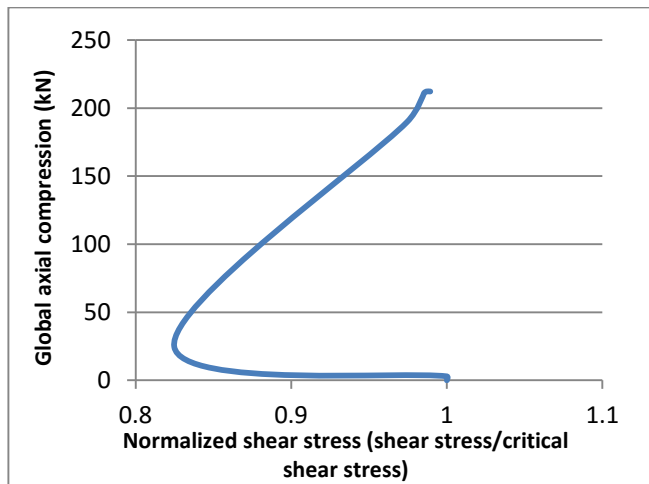


Figure 6-9. Global axial force versus aspect ratio of shear stress.

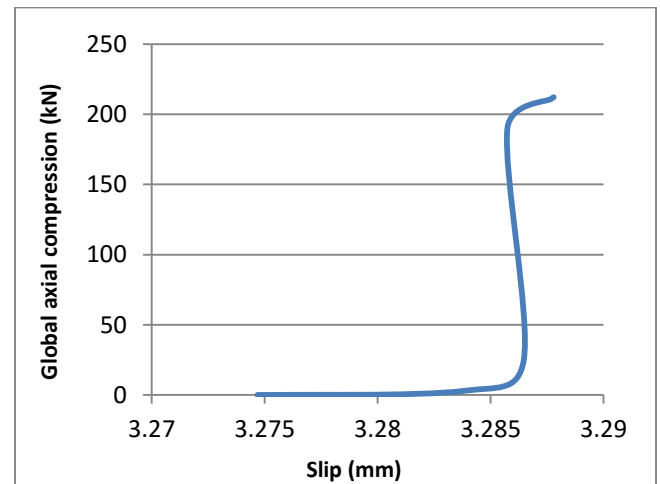


Figure 6-10. Global axial force versus slip in external tensile wire.

#### 6.4.2 Parametric study on initial curvature

During installation, the pipe may experience a range of axial force and bending curvature conditions that is related to parameters including pipe diameter and water depth. The effect of initial curvature on the local buckling response is examined through a parameter study assessing pipe segment length and radius of curvature, Table 6-5.

Force-strain and force-twist graphs of 5m-length pipe under  $R=11$  m, 13.5 m, and 16 m and a pipe with no initial curvature are provided in Figure 6-11 and Figure 6-13. The mechanical response of the 1.25 m length pipe is presented in Figure 6-12 and Figure 6-14.

Some points can be deduced from Figure 6-11 Figure 6-14. First, if no initial curvature is introduced in the models, there is no sign of buckling in the pipe neither in 5 m-length sample nor 1.25 m-length one, and 1.25-length sample reaches yield stress (i.e. 760 MPa) in internal tensile wire layer near the boundary condition zone. The axial stiffness for the 1.25 m-length sample is 61886 kN/m and it is 15348 kN/m for the 5 m-length one. The second point is that, although the curvature triggers the buckling in pipe, it does not alter the axial stiffness indeed. The 1.25 m-length pipe including curvature buckles at some point while the axial stiffness remains at the 61886 kN/m (i.e. axial stiffness of the pipe with no curvature). The last point to be notified is that, while the imposed curvature makes a bit of change in the 5 m-length model, the rotational stiffness sticks to the original amount (i.e. the pipe with no initial curvature) in both 1.25 m-length and 5 m-length samples.

Table 6-5. Comparison between characteristic features of models with various initial curvature and lengths.

Sample	Buckling strain (m/m)	Buckling force (kN)	Buckling twist (deg/m)	Axial stiffness (kN/m)
L=5m_R=11 m	0.0058	55.32	0.033	1890
L=5m_R=13.5 m	0.0057	63.03	0.035	2345
L=5m_R=16 m	0.0047	70.35	0.038	2944
L=5m_No curve	-	-	-	15348
L=1.25m_R=11 m	0.0026	212.21	0.114	61886
L=1.25m_R=13.5 m	0.0032	257.01	0.138	61886
L=1.25m_R=16 m	0.0036	287.54	0.156	61886
L=1.25m_No curve	-	-	-	61886

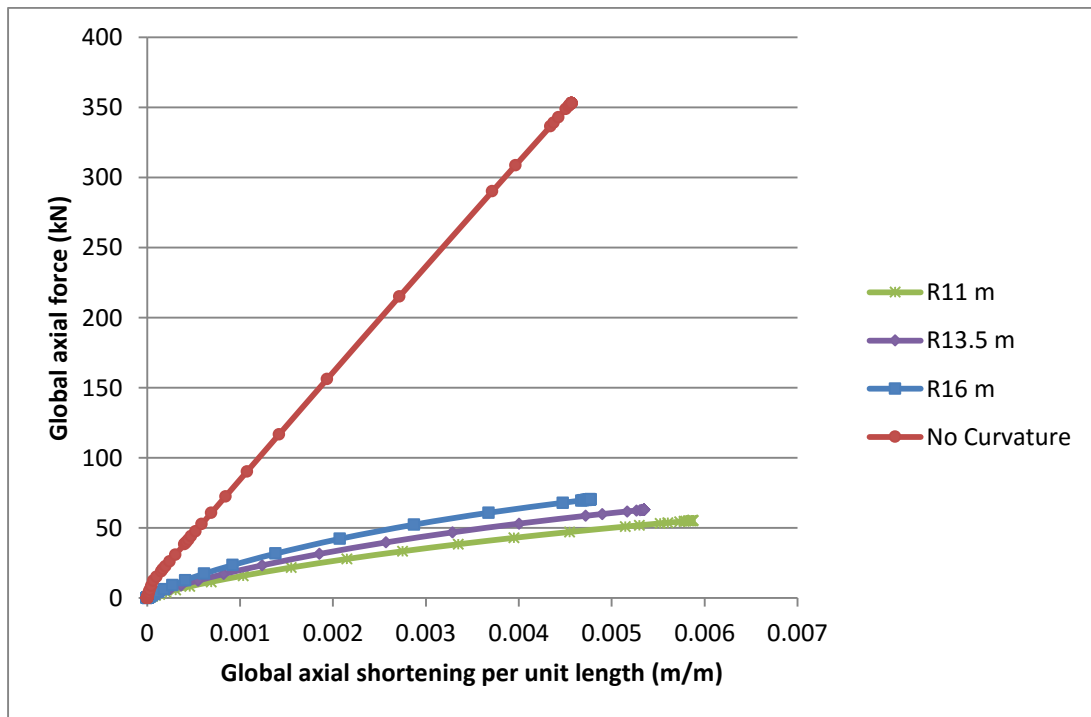


Figure 6-11. Global axial compression versus strain in the 5-m length pipe with different initial curvature.

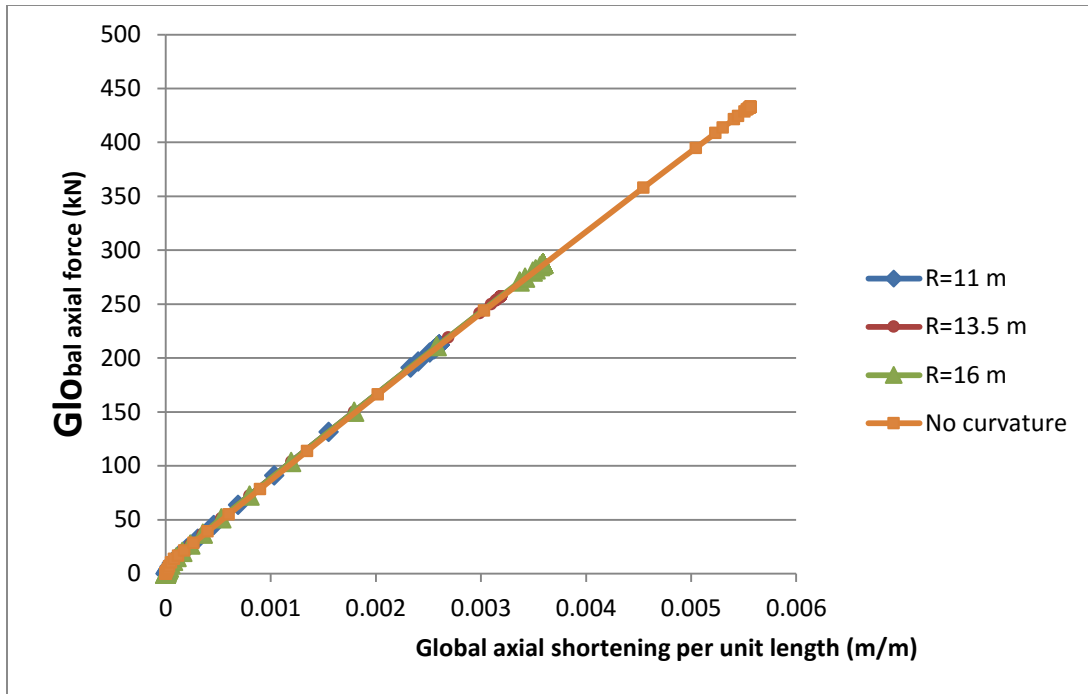


Figure 6-12. Global axial compression versus strain in the 1.25-m length pipe with different initial curvature.

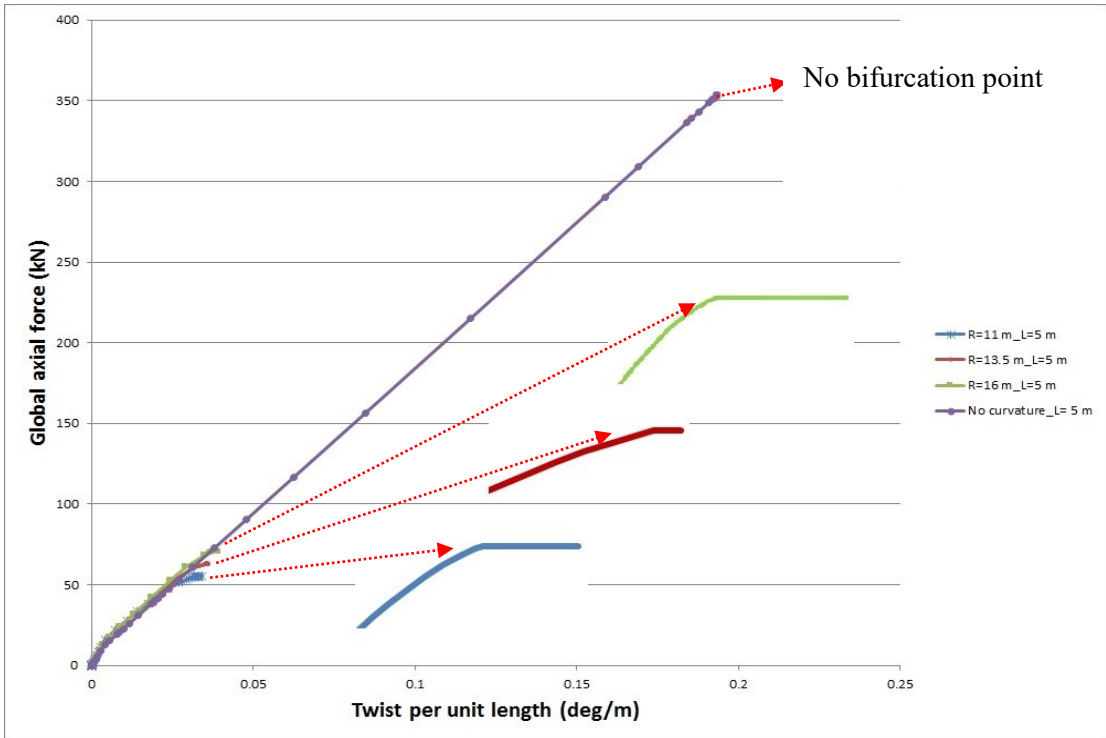


Figure 6-13. Global axial compression versus twist in the 5-length pipe with different initial curvature.

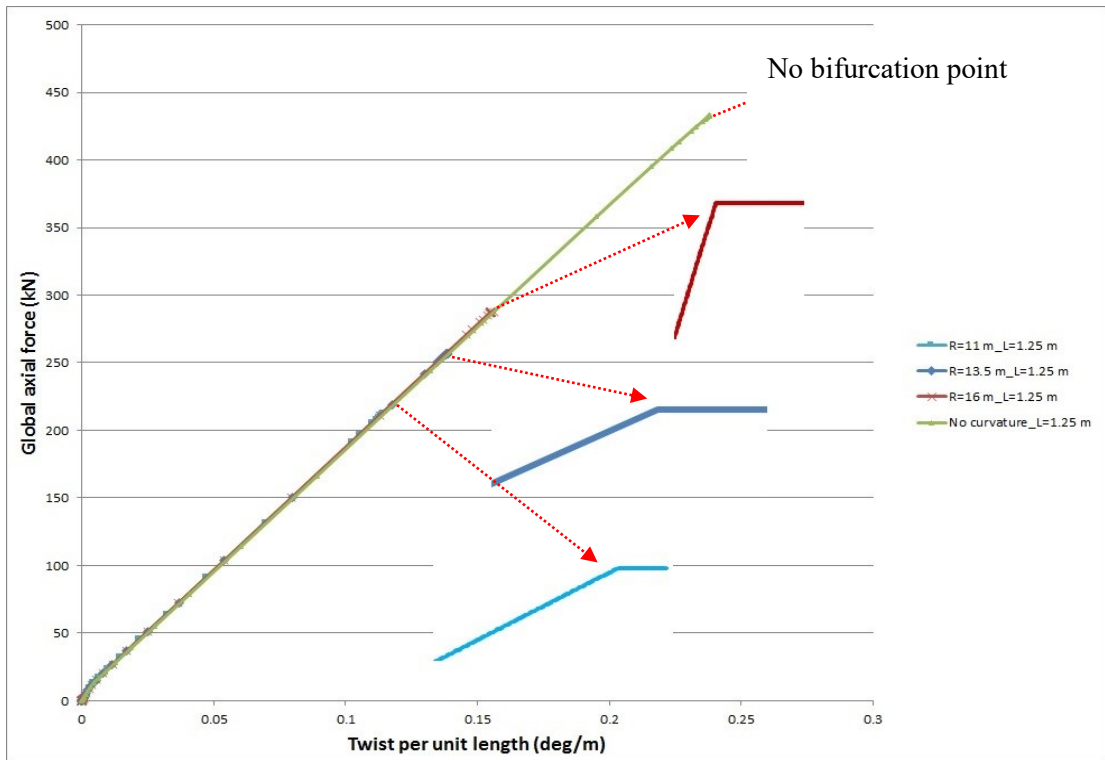


Figure 6-14. Global axial compression versus twist in the 1.25-length pipe with different initial curvature.

### 6.4.3 Parametric study on friction coefficient

If the external plastic sheath is breached and sea water leaks into the annulus, the friction coefficient is decreased and this condition is called “wet annulus”. Since friction force as the only factor which prevents lateral buckling is lowered, the tensile wires are likely to buckle laterally in lower axial compression in respect to dry annulus (i.e. the condition that external plastic sheath is intact and annulus is dry). To address time expense, the flexible pipe with 1.25 m of length which (i.e. representing the 5m-length pipe in laboratory with installed end-fittings) is chosen to be examined in wet annulus condition. A series of parametric study, including  $\mu=0.05$  and  $0.025$ , is carried out on friction coefficients as wet annulus condition, to be compared with dry annulus condition (i.e.  $\mu=0.1$ ). The Force-strain and force-twist mechanism in dry and wet annulus conditions of the  $R=11$  m are presented at Figure 6-15 and Figure 6-16, and for the straight pipe is reported at Figure 6-17 and Figure 6-18 . The noticeable point in these figures is that, at the first look, the flexible pipe with initial curvature  $R=11$  m and friction coefficient of  $0.025$  seems to have different pattern of behavior (i.e. force-strain and force-twist) in respect to the pipe with same initial curvature and friction coefficients of  $0.1$  and  $0.05$ . In fact, this model buckles at  $27$  kN of axial force, though it is successful to pass over buckling point (i.e. post-buckling scope) contrary to all other models which are not able to reach this scope because of harsh contact interactions (i.e. penetration in normal direction or slip-stick in tangential direction) caused by severe twist of the wires. This particular case is presented in Figure 6-19 and Figure 6-20, as this case is an excellent example to ascertain that although the axial stiffness (i.e. force-strain) of the flexible pipe varies after buckling point, though it does not lose axial strength totally. Table 6-6 provides features of mechanical response in different models and Table 5 presents the axial stiffness for before and after buckling point. In Figure 6-19 and Figure 6-20 the buckling force is highlighted to distinguish

the post-buckling zone. Figure 6-21 schematically compares the FE model in post-buckling stage with a lateral buckling in a real pipe which shows excellent resemblance.

Table 6-6. Comparison between characteristic features of models with various initial curvatures and lengths.

Sample	Buckling force (kN)	Buckling strain (m/m)	Buckling twist (deg/m)	Axial stiffness (kN/m)
No curve _ Cof=0.1	432	0.0057	0.238	65886
No curve _ Cof=0.05	273	0.0034	0.149	63397
No curve _ Cof=0.025	176	0.0021	0.1	62674
R=11 m _ Cof=0.1	212	0.0026	0.114	63810
R=11 m _ Cof=0.05	62	0.0006	0.033	63354
R=11 m _ Cof=0.025	27	0.0003	0.044	57110

Table 6-7. Comparison between axial stiffness of the model with R=11, L=1.25 m and friction coefficient =0.025.

Sample	Axial stiffness before buckling (kN /m)	Axial stiffness after buckling (kN /m)
R=11 m _ Cof=0.025	57110	20524

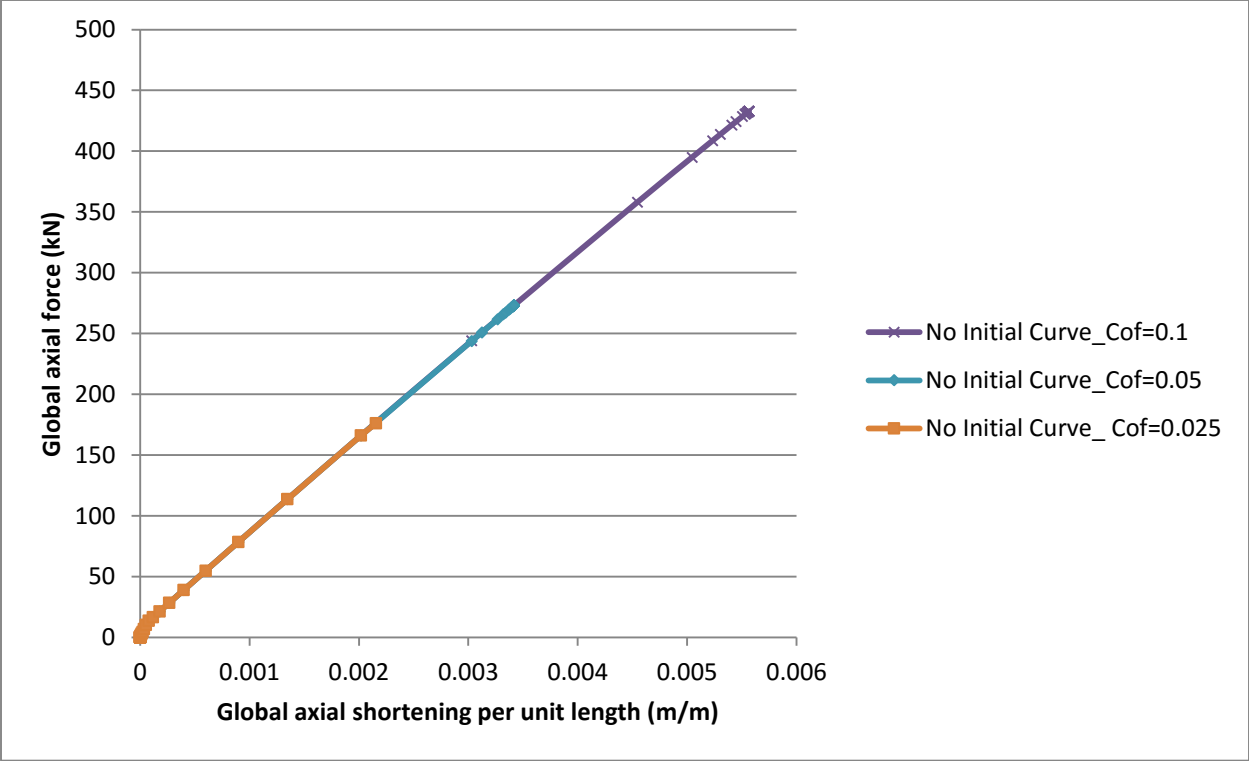


Figure 6-15. Global axial force versus strain for different friction coefficients under no initial curvature.

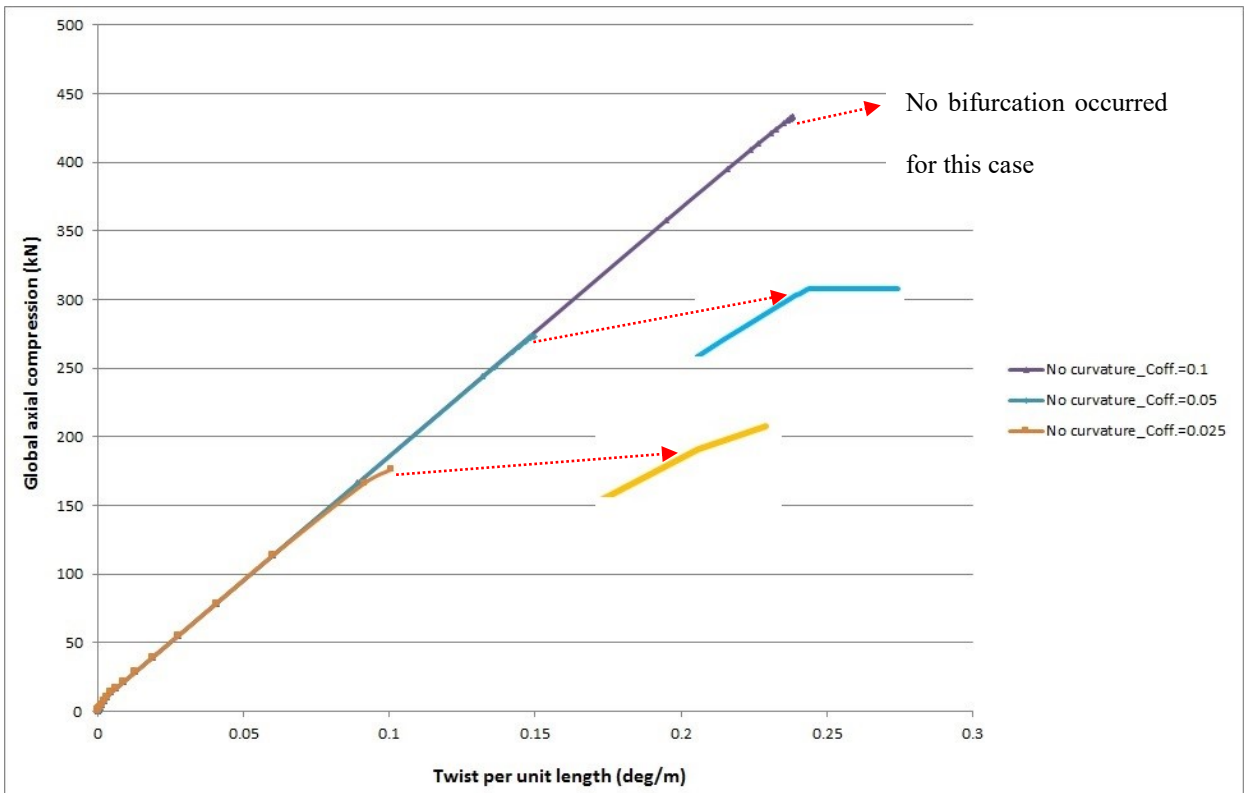


Figure 6-16. Global axial force versus twist for different friction coefficients under no initial curvature.

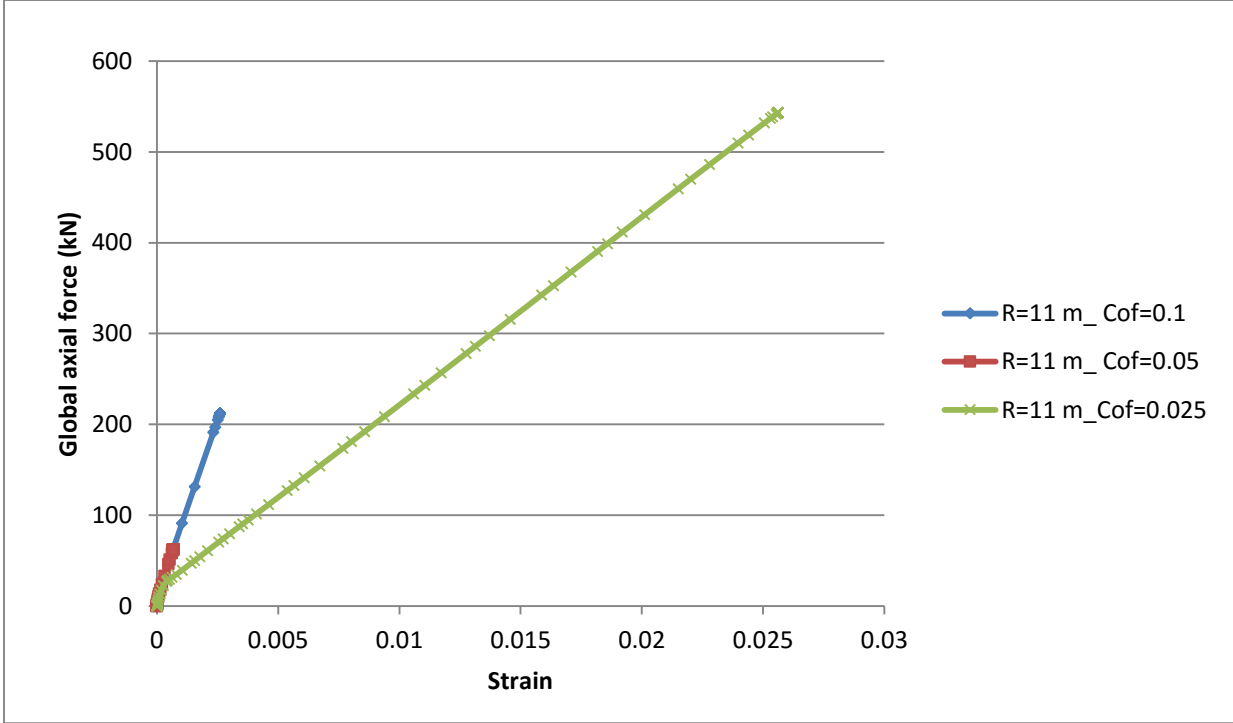


Figure 6-17. Global axial force versus strain for different friction coefficients under R=11 m.

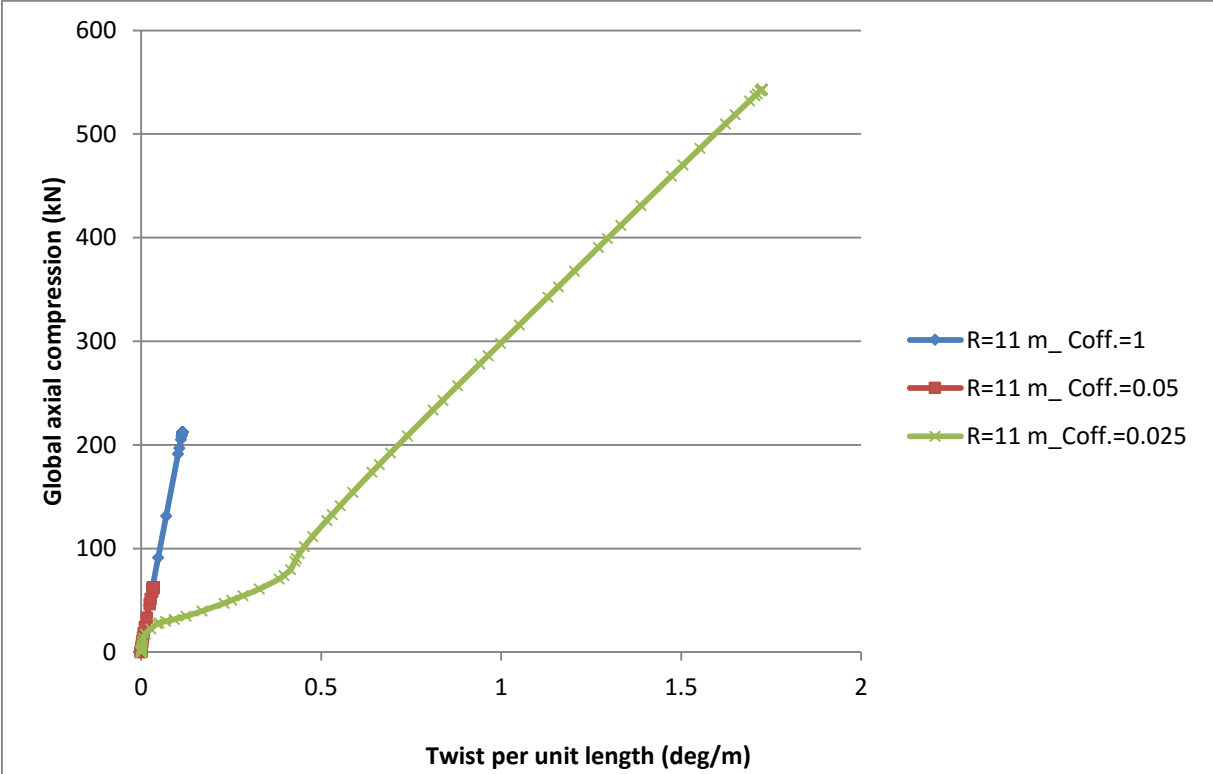


Figure 6-18. Global axial force versus twist for different friction coefficients under R=11 m.

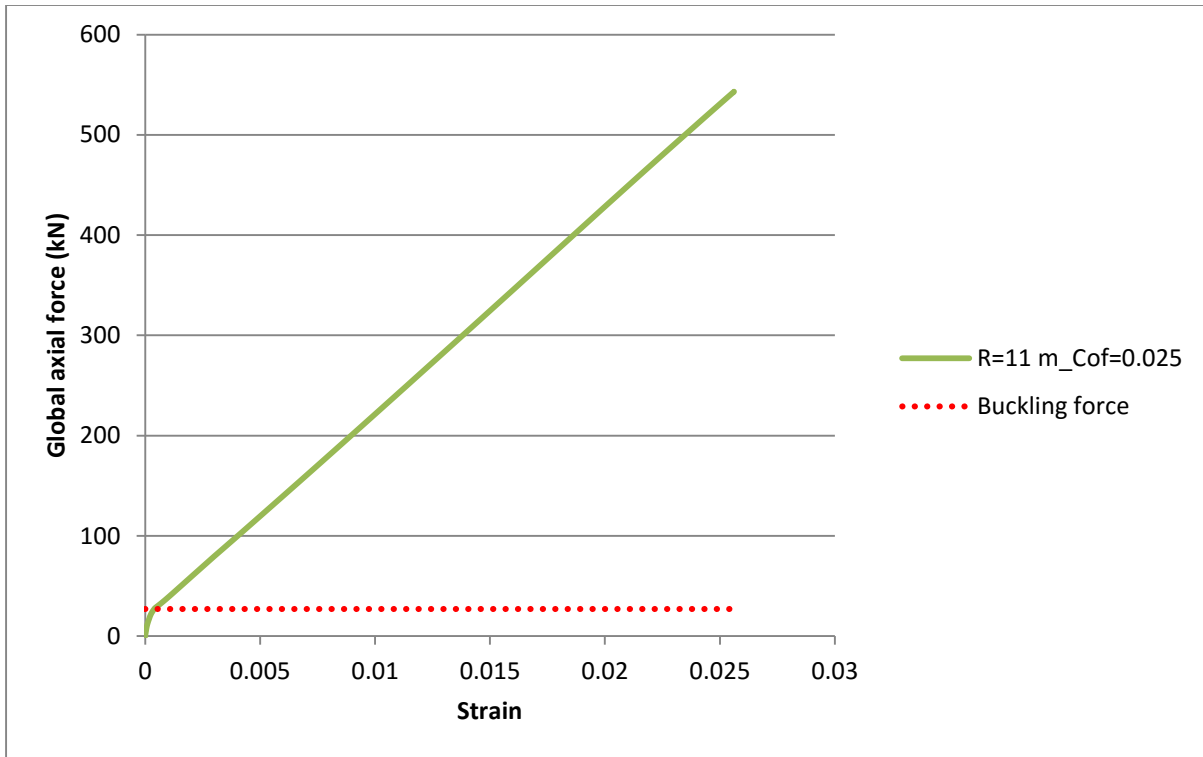


Figure 6-19. Global axial force versus strain for the model with R=11, L=1.25 m and friction coefficient =0.025.

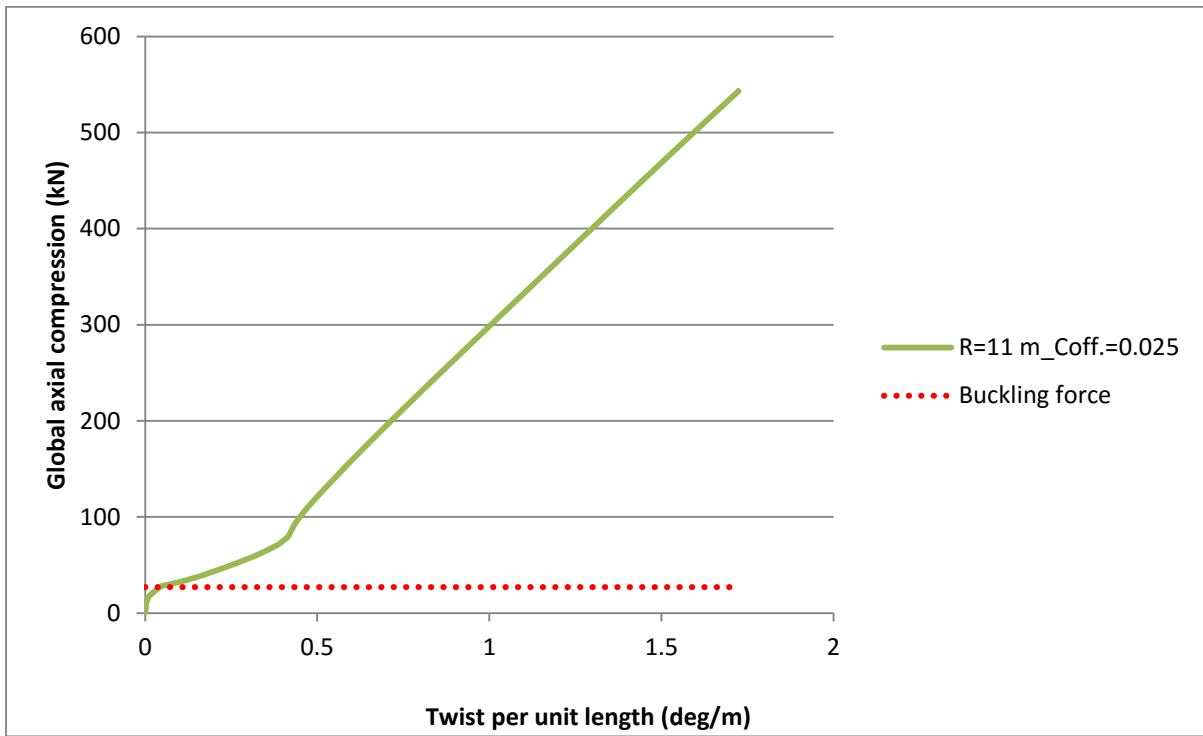


Figure 6-20. Global axial force versus twist for the model with R=11, L=1.25 m and friction coefficient =0.025.

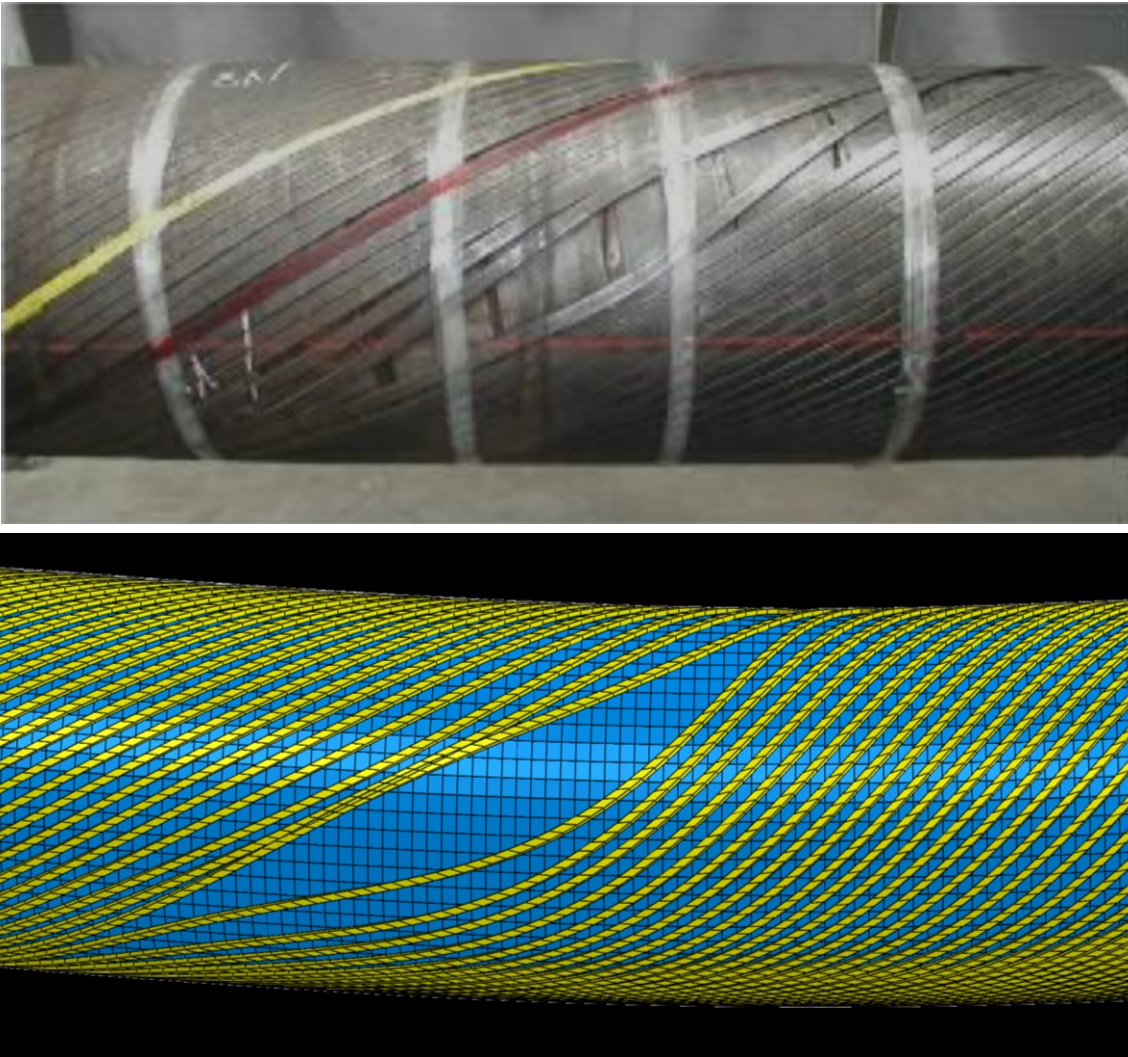


Figure 6-21. Schematic comparison of lateral buckling of tensile wires in wet annulus condition, between a real pipe in field [3] and FE model (i.e.  $L=1.25\text{m}$ ,  $R=11\text{ m}$ , wet condition, friction  $Cof.=0.025$ )

#### 6.4.4 Critical curvature of flexible pipe

Installation of flexible pipe is the most probable occasion that lateral buckling might occur as the pipe is empty and the sea hydrostatic pressure shapes axial compression force at the end-cap of the pipe. This scenario becomes more hazardous at the touch-down zone and departure angle as the two most susceptible over-bending (i.e. curvature) zones, Figure 6-22. This section is developed based on previous model to determine the critical bending curvature at the touch-down zone (TDP). The load cases and boundary conditions are described in Table 6-8 and Figure 6-23.

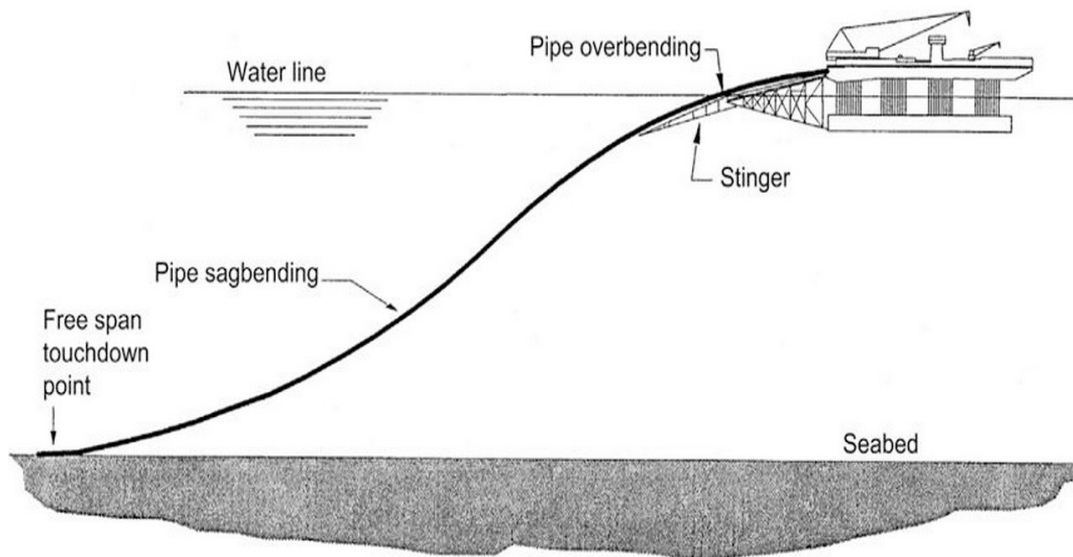


Figure 6-22. Schematic of flexible pipe installation, [12].

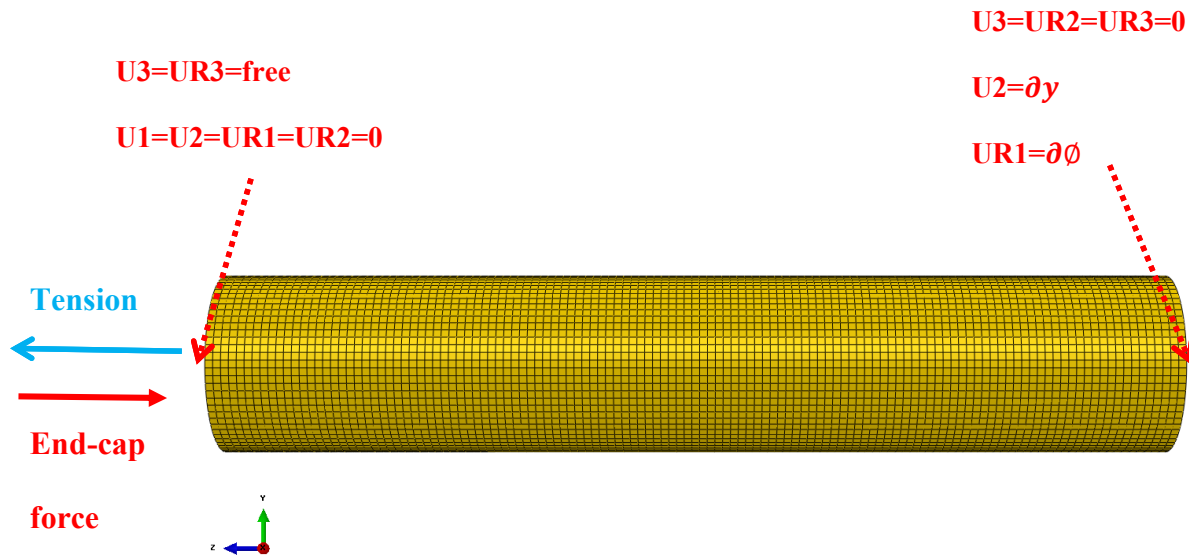


Figure 6-23. The boundary conditions of the bending limit analysis.

Table 6-8. Load cases considered for bending limit analyses.

Load case #	Depth of touch-down zone (m)	End-cap axial force (kN)	Axial tension force (kN)	External pressure (MPa)
1	0 (Lab condition)	0	0	0
2	80	35	0	0.8
3	80	35	70	0.8
4	160	70	0	1.6
5	160	70	140	1.6

These load cases are considered according to the depth of Hibernia platform (i.e. 80 m and two times of it, 160 m) to establish a guideline for installation procedure in the Grand Bank oil field

and to highlight the role of each of the imposed loads (i.e. axial end-cap force, tension and external pressure) onto the lateral buckling of tensile wires which determine the bending limit of flexible pipe. The pipe after loading is shown in Figure 6-24 and results are provided in Figure 6-25 and Table 7. The critical bending limit (i.e. the curvature that tensile wires buckle in it) is the curvature in which the axial twist becomes severe. In order to understand the mechanism of the pipe and the results in Table 6-9, the conclusion declared in the Ebrahimi *et al.* [11], which is an examination of flexible pipe toward axisymmetric load, should be noticed. It was declared that tension causes the both tensile wire layers to contract radially. Radial contraction of the layers naturally increases the normal contact pressure between layers, thereby raising friction between layers and hindering severe slip of wires (i.e. lateral buckling). In other words, the tension acts similar to sea hydrostatic pressure which increases the normal contact pressure. Axial compression (i.e. end-cap force in here) is a parameter which triggers instability (i.e. lateral buckling) in slender bodies and hence it decreases the critical bending curvature. The bottom line is that axial tension and sea hydrostatic pressure increase the critical curvature, while the axial compression lowers it down. Since the bending mechanism of each individual load case may not be apparent in comparison to others, in Figure 6-26 load case 3 is presented solely in order to give better understanding on the curvature-twist mechanism of the pipe through the installation procedure. The initial twists in Figure 6-25 and Figure 6-26 are the twist caused by end-cap force or tension.

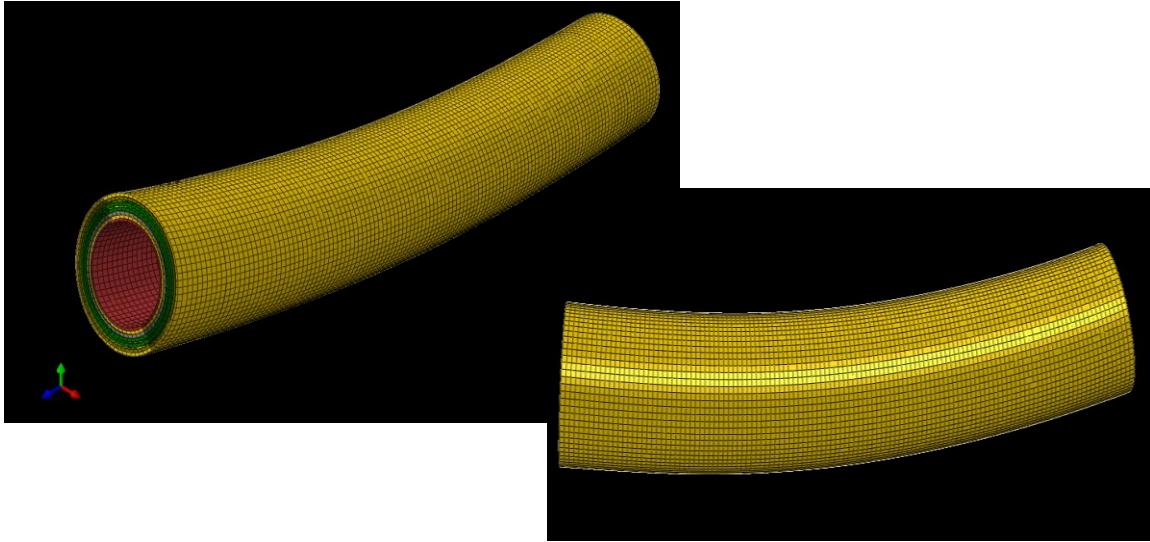


Figure 6-24. The pipe after imposing load condition.

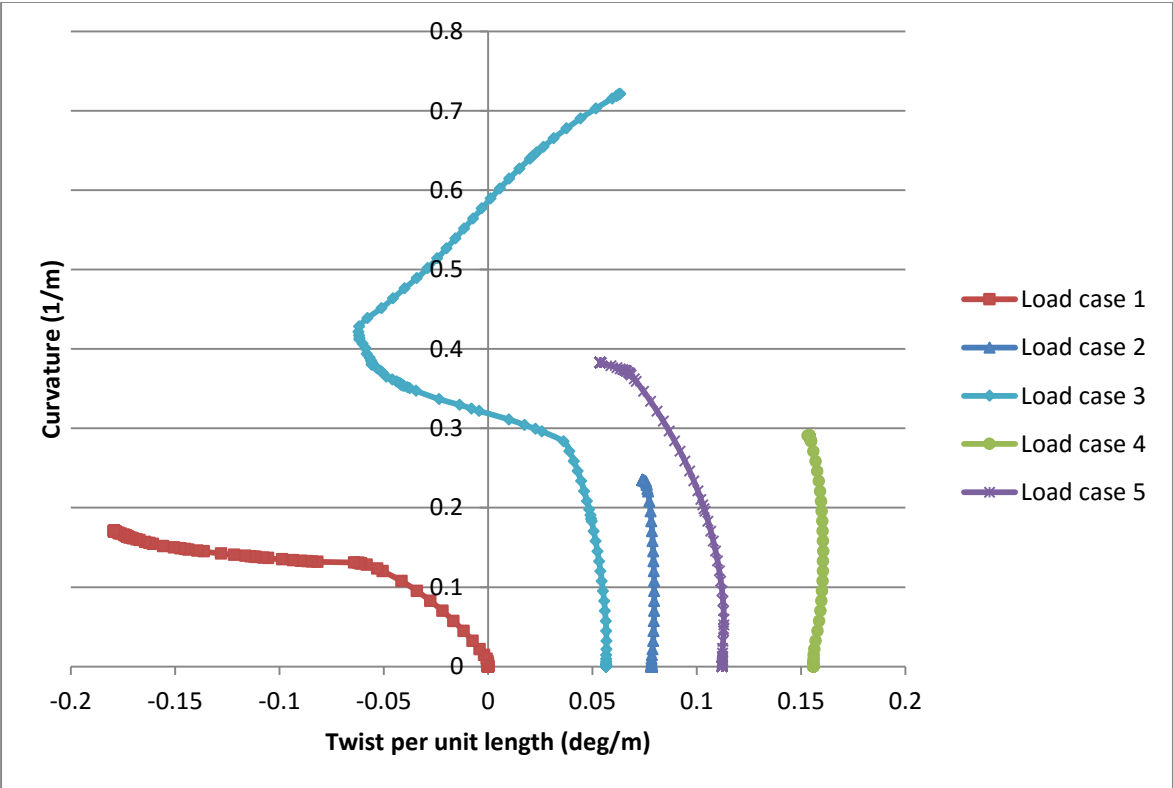


Figure 6-25. Curvature versus axial twist in different load cases.

Table 6-9. Critical curvature (i.e. buckling point) at the different load cases.

Load case #	Critical curvature (1/m)
1	0.133
2	0.235
3	0.271
4	0.291
5	0.383

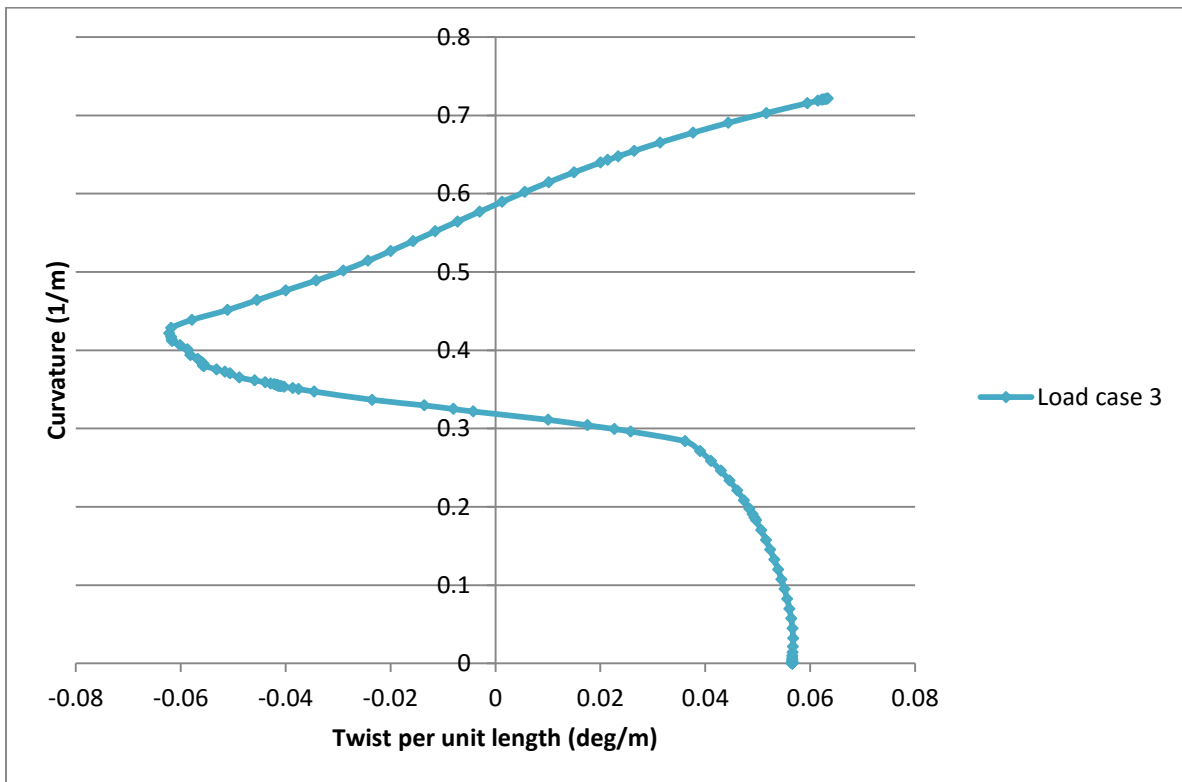


Figure 6-26. Curvature versus axial twist in load case 3.

## 6.5 Conclusion

Finite element investigation of lateral buckling in tensile armour wires of flexible pipe was implemented in this research paper to target deficiency of research in this field and examine the influencing parameters.

In this research 3D finite element model of subsea flexible pipe was developed which enjoys Implicit solver. The study was conducted in 4 different stages. In first stage a similar model with existing experimental and analytical model was developed to validate the outcome of FEM. The reasons of discrepancies have been talked through. After ascertaining on the result accuracy of FEM, a sensitivity study was carried out on the initial curvature of the pipe and it was concluded while the curvature caused minor changes on the buckling force, strain and axial stiffness of the 5m-length pipe, it did not change axial stiffness of 1.25m-length model. Also, it was concluded that, if no curvature is introduced in the pipe, the wires do not find chance to slip. In the parametric study on the friction coefficient which was conducted to address the “wet annulus” condition, it was concluded that reduction in friction coefficient, lower the axial stiffness, buckling force, strain and twist of the pipe. Furthermore, one of the model managed to reach post-buckling scope of the pipe, by which the statement that, axial stiffness of the pipe after lateral buckling of wires did not fail totally and just softened up after buckling point, is proven. Besides, the post-buckling of the FEM showed best-in-kind similarity with a real model. Last part of this research was dedicated to the assessment on the critical curvature of the flexible pipe which is a crucial parameter in installation. The results of this section can be more understandable by looking through [11]. As the critical bending curvature is the curvature in which the tensile wires start slipping, it is influenced remarkably by the imposing loads. In this study, it was deduced that axial tension and sea hydrostatic curvature prevent buckling and increase bending curvature limit (i.e. critical

bending curvature), while axial compression eases the lateral buckling and lowers the critical bending curvature.

This research paper is carried out to fill the gap between development of the application of flexible pipe in harsh conditions and flaws of the existing numerical and analytical simulations. This paper provides a reliable series of parametric studies for operation and installation of flexible pipe while it retains the time efficiency.

As recommendation for further study, a series of experimental or prototype tests are required to be carried out to complement the parametric studies of the current research. Since each individual cases of the parametric studies has its own challenges and they took few months to be implemented, a series of sensitivity study on the severe initial curvature (i.e. radius of curvature less than 11 m) is suggested to be done to complete this work and reaching a comprehensive guideline for industry. Relative displacement of the layers of flexible pipe and existing friction force between them, under each cycle of bending causes a hysteresis effect. Under few hundreds of bending cycles, these local misarrangements are accumulated and bring about substantial changes (i.e. imperfections) into the angle pitch of the wires. Because of this imperfections (i.e. misarrangements) the results of lateral buckling are expected to differ under cyclic bending with the constant bending curvature results. Hence, development of a FE model which would be able to execute cyclic bending analyses is recommended for future studies.

## **6.6 References**

[1]. Ostergaard, N.H., Lyckegaard, A., Andreasen, J. H., “On modeling of lateral buckling failure in flexible pipe tensile armour layers”, *Journal of Marine Structures*, Volume 22, 2012, Page 64-81.

- [2]. Neto, A.G., Martins, D.A., “Flexible pipes: influence of the pressure armor in the wet collapse”, *Journal of Offshore and Offshore Engineering*, Volume 136, May 19, 2016.
- [3]. Secher, Ph., Bectrate, F., Fleix-Henry, A., “Lateral buckling of armour wires in flexible pipes: reaching 3000m water depth”, *OMAE 2011, 30<sup>th</sup> International Conference on Offshore Mechanics and Arctic Engineering*, June 19-24, 211, Rotterdam, The Netherland.
- [4]. Braga M. P., Kallef P., “Flexible pipe sensitivity to birdcaging and armor wire lateral buckling”, *OMAE 2004, 23<sup>rd</sup> International Conference on Offshore Mechanics and Arctic Engineering*, June 20-25, 2004, Vancouver, BC, Canada.
- [5]. Tan, Z., Loper, C., Sheldrake, T., Karabelas, G., “Behaviour of tensile wires in unbounded flexible pipe under compression and design optimization for prevention”, *25<sup>TH</sup> International Conference on Offshore Mechanics and Arctic Engineering*, June 4-9, 2006, Hamburg, Germany.
- [6]. Perdrizet, T., Leroy, J.M., Barbin, N., Le-Corre, V., Charliac, D., Estrier, P., “Stresses in armour layers of flexible pipes: comparison of Abaqus model”, *SIMULIA Customer Conference*, 2011.
- [7]. Ebrahimi, A., Kenny, S., Hussein, A., “Radial instability of tensile armour wires in subsea flexible pipe-numerical assessment of key factors”, *Journal of Offshore Mechanics and Arctic Engineering*, Volume 138 (3), doi:10-1115/1.4032894.
- [8]. De Sousa, J.R.M., Magluta, C., Roitman, N., Londono, T. V., Campello, G.C, “A study on the response of a flexible pipe to combined axisymmetric loads”, *Proceedings of the ASME 2013 32<sup>nd</sup> International Conference on Ocean, Offshore and Arctic Engineering*, June 9-14, 2013, Nantes, France.
- [9]. Abaqus documentation 6.13.

- [10]. Ebrahimi, A., Kenny, S., Hussein, A., “Finite element simulation of flexible pipe: Challenges and Solutions”, Volume 14 (4), pages 275-287, 2015.
- [11]. Ebrahimi, A., Kenny, S., Hussein, A., “Finite element investigation on the tensile armour wire bifurcation response of flexible pipe for axisymmetric loading conditions using an implicit solver”, submitted to Journal of Offshore Mechanics and Arctic Engineering, July, 2015.
- [12]. Bai, Q., Yong, B., “Subsea pipeline design, analysis and installation”, Gulf Professional Publishing, 2011.

## **7 Conclusions and recommendations**

### **7.1 Overview**

Application of flexible pipe technology is being extended to deepwater and harsh environments and the operational envelope is being extended to higher temperatures and pressures. These places demand on the engineering tools for the design and analysis of flexible pipe to meet the demanding service conditions. The idealized analytical solutions are no longer trustworthy and sufficient for the current development in applications of flexible pipe. Early numerical simulation models that incorporated simplifications were able to extend knowledge, but those were constrained by hardware and software technology to incorporate a more realistic and accurate model. So, developing more realistic simulations of flexible pipe mechanical response through more detailed FE simulation is required to address complex interactions and deformation mechanism including radial and lateral buckling instability, and section response to combined loads. Wood Group Kenny Research Chair at Memorial University of Newfoundland decided to focus on the local buckling of flexible pipe by addressing the flaws of the previous methods and providing a model which can be enough reliable and dependable to be employed for simulations of local buckling of tensile wires of flexible pipe under different conditions, and also be extended to investigate other failure mechanisms of flexible pipe. On this basis this thesis can improve knowledge and current practice to meet future industry needs.

### **7.2 Conclusions**

This thesis investigates the local buckling of tensile wires in five major research activities to develop comprehensive numerical modelling procedures simulating the mechanical response and local instability of flexible pipe technology. In the following subsections, the fundamental

conclusions from the major research activities including the scope, outcomes and contributions are highlighted.

### **7.2.1 Literature review**

The first phase of the study provides information on the whole structure of the pipe; its application; reasons of applications; and extensive literature review of the researches have been implemented on mechanical behavior of flexible pipe and particularly local buckling in tensile wires of flexible pipe by now.

### **7.2.2 General modelling procedures**

Since the procedure of the modeling of flexible pipe by Implicit method faces many issues, the second chapter presents the general perspective over challenges and issues associated with finite element modeling of flexible pipe. The challenges for modelling flexible pipe have been discussed and solutions are provided through general finite element and mechanics of material approaches. This work tries to explain modeling challenges for each stage of modeling through elasticity, mechanics of material and finite element method concepts, while the goal is not to provide universal modelling strategy applicable to all situations, but high level guidance that addresses most issues, despite any specific software.

### **7.2.3 Radial buckling or birdcaging**

The third chapter focuses radial buckling (i.e. birdcaging instability) of flexible pipe. The strategy for this part is that, at the first stage a model which is similar to the only in-access experimental test is developed and the same physical model test procedure is duplicated. The results shows excellent consistency with the physical model test one and reasons causing minor differences are discussed and the evaluation of some parameters, which are supposed to influence the radial

buckling (i.e. external and internal pressure, and damage) is carried out. Also, key factors influencing the radial buckling response, including internal and external pressure, and damage level in the anti-birdcaging tape and plastic sheath, were examined through a parameter study. The results from parametric study suggest the radial buckling mechanism and characteristic parameters (e.g., global or local force, deformation) are mainly under influence by the normal contact pressure and shear stress between the layers. The external hydrostatic pressure and level of damage influence the inter-layer contact stress state that affects the buckling mechanism with respect to the limit load, and the axial strain and angle of twist prior to the onset of local buckling instability (i.e., bird caging response).

The radial buckling (i.e. birdcaging) which was investigated in chapter three, is complemented in chapter five by substituting the imperfection of the anti-birdcaging tape by a rupture in three difference length to emphasize the role of the imperfection of anti-birdcaging onto the radial buckling.

#### **7.2.4 Elastic instability**

The fourth step of this thesis is dedicated to investigation of the pipe under axisymmetric load combinations. The main goal of this section is the determination of the pipe mechanical response toward load cases (i.e. tension and torsion and their combination) which are assumed as the load cases that cannot arouse instability in tensile wires. The study is implemented for different key factors (i.e. friction coefficient, boundary conditions and hydrostatic pressure). The use of an implicit integration scheme was shown to improve confidence in the simulation of the existing bifurcation points in the mechanical response, which may not be captured by analytical solutions or finite element procedures using explicit schemes. This instability under torsion is due to separation of layers, which is caused by the direction of torsion trying to create gap between layers.

The parameter study demonstrates that this instability is independent of the interface friction coefficient, while it can be curbed by sea hydrostatic pressure. Furthermore, it is concluded axial tension loads restrict the radial displacement of external tensile wires by tightening up both layers of tensile wires. This results in a linear pipe response for both directions of applied rotation.

The effects of internal pressure on the tensile armour wire response was negligible where the pressure load was carried by the high radial strength pressure armour with negligible radial expansion. The response was similar to the unpressurized pipe load case.

### **7.2.5 Lateral buckling**

The last stage of this thesis is assigned to lateral buckling of tensile wires. Same as the other parts of this thesis, a similar model with existing experimental and analytical model is developed to validate the outcome of FEM. The reasons of discrepancies have been talked through and the investigation is extended on evaluation of key parameters (i.e. wet annulus condition, different initial curvatures and critical curvature). The sensitivity study on initial curvature show that, the initial curvature of the pipe causes minor changes on the buckling force, strain and axial stiffness of the 5m-length pipe and if no curvature is introduced in the pipe, the wires do not find chance to slip. In the parametric study on the friction coefficient which is conducted to address the “wet annulus” condition, it is concluded that reduction in friction coefficient, lower the axial stiffness, buckling force, strain and twist of the pipe. Furthermore, one of a model with wet annulus condition managed to reach post-buckling scope of the pipe, by which the statement that, axial stiffness of the pipe after lateral buckling of wires does not fail totally and just soften up after buckling point, is proven. Besides, the post-buckling of the FEM shows best-in-kind similarity with a real model. At the last stage of this research paper the critical curvature of the flexible pipe which is a crucial parameter in installation is determined in different cases. As the critical bending

curvature is the curvature in which the tensile wires start slipping, it is influenced remarkably by the imposing loads. In this study, it is deduced that axial tension and sea hydrostatic curvature prevent buckling and increase bending curvature limit (i.e. critical bending curvature), while axial compression eases the lateral buckling and lowers the critical bending curvature.

Different studies which were carried out in this thesis conclude that the instability or buckling in tensile wires can occur due to, 1) loss of radial confinement of tensile wires, 2) elimination of shear stress between tensile wires and other layers, or 3) separation between wires and adjacent layers (i.e. elimination of contact pressure). The buckling of tensile wire leads to abrupt changes in axial stiffness, severe twist of the pipe and local deformation while the wires are still in elastic region.

### **7.3 Recommendation for future studies**

This thesis is accomplished as a first step of finite element modeling of local buckling in tensile wires of flexible pipe by using Implicit solver to target accuracy and time efficiency of the previous studies, while further studies are still required to complement current work. For further study the recommendations are, investigation on the imperfection which shapes through manufacturing, operation and installation, and determination of its types and amplitudes on the lateral and radial buckling; development of an exact material degradation model of the anti-birdcaging tape which is a key factor on the radial buckling; advancement on the frictional behaviour pattern between layers which causes the different mode shapes of lateral buckling and it is expected to be non-uniform through the layers; execution of longer pipe segments and examination of the role of number of pitch on the buckling of the layers.

The test expense and manufacturer confidentiality did not allow this author to execute the similar parametric studies on physical model tests. The duplication of the sensitivity studies of this thesis

as the first study concerning these key parameters is a crucial matter to have more confidence on the current research.

For further studies, the imperfections should be taken into account as ovality or skew angle of wire pitches. The ovality seems to arouse radial buckling and the latter one may ease the lateral buckling of the wires.

Material degradation of anti-birdcaging tape or manufacturing defect can be measured through physical model test and be taken into account in numerical tools by developing user-subroutine (e.g. UMAT in Abaqus). Advancement of frictional pattern between layers, asks for precise local measurement of contact status in physical model test and development of user-subroutine for different status of normal contact pressures and friction directions (e.g. VFRIC in Abaqus).

Implementation of the same series of studies in this thesis with a model in which the tensile wires are simplified while the accuracy can be sustained, seems to be necessary. The wires can be modeled with beam element although that there is limitation on the type and number of the outputs which can be extracted from beam element.

The effect of the end-fitting was considered in the chapter 6 by reducing the effective length of the pipe. This assumption is considered to eliminate the numerical issues caused by simulation of end-fitting. Similar studies for each individual case of this thesis can be carried out by consideration of contact interaction of end-fittings on the pipe and the clamping area which is made for the tensile wires by the end-fitting.

Implementation of study on hysteresis effect remained uncompleted for this thesis as the data for validation could not be found. The angle of wires is susceptible to skew under cyclic loading and

study of the hysteresis effect may lead to gaining a mathematical formulation for estimation of skew of angle which can benefit both buckling and fatigue life of the pipe.

Boundary condition can change buckling pattern (i.e. mode shape, buckling force and etc.) and in some application of flexible pipe, the pipe is laid on the ground (e.g. connection of PLET and PLEM). The author made some analyses to investigate the effect of the ground on the birdcaging but due to lack of validation the results are not published. So, implementation of the same type of de Sousa's experiments with new type of boundary condition seems to be necessary. Also, the pipe segment can be considered as part of long length pipe instead of a short pipe in which the end-fittings are installed at the both ends. The implementation of this part requires modification on type of the BCs and coupling in numerical simulation and also execution of experiments on a long length pipe.

## **8 Appendix A: General Python Code**

```

# -*- coding: mbc -*-

from part import *

from material import *

from section import *

from assembly import *

from step import *

from interaction import *

from load import *

from mesh import *

from optimization import *

from job import *

from sketch import *

from visualization import *

from connectorBehavior import *

mdb.models['Model-1'].ConstrainedSketch(name='__profile__', sheetSize=10.0)

mdb.models['Model-1'].sketches['__profile__'].CircleByCenterPerimeter(center=(
    0.0, 0.0), point1=(0.0, 0.06))

mdb.models['Model-1'].sketches['__profile__'].ObliqueDimension(textPoint=(0.0,
    0.06), value=0.0811, vertex1=
    mdb.models['Model-1'].sketches['__profile__'].vertices[0], vertex2=
    mdb.models['Model-1'].sketches['__profile__'].vertices[1])

```

```

mdb.models['Model-1'].Part(dimensionality=THREE_D, name='Carcass', type=
    DEFORMABLE_BODY)

mdb.models['Model-1'].parts['Carcass'].BaseShellExtrude(depth=5.0, sketch=
    mdb.models['Model-1'].sketches['__profile__'])

del mdb.models['Model-1'].sketches['__profile__']

mdb.models['Model-1'].ConstrainedSketch(name='__profile__', sheetSize=1.0)

mdb.models['Model-1'].sketches['__profile__'].CircleByCenterPerimeter(center=(
    0.0, 0.0), point1=(0.0, 0.06))

mdb.models['Model-1'].sketches['__profile__'].ObliqueDimension(textPoint=(0.0,
    0.06), value=0.0856, vertex1=
    mdb.models['Model-1'].sketches['__profile__'].vertices[0], vertex2=
    mdb.models['Model-1'].sketches['__profile__'].vertices[1])

mdb.models['Model-1'].Part(dimensionality=THREE_D, name=
    'Interior-Plastic-Sheath', type=DEFORMABLE_BODY)

mdb.models['Model-1'].parts['Interior-Plastic-Sheath'].BaseShellExtrude(depth=
    5.0, sketch=mdb.models['Model-1'].sketches['__profile__'])

del mdb.models['Model-1'].sketches['__profile__']

mdb.models['Model-1'].ConstrainedSketch(name='__profile__', sheetSize=1.0)

mdb.models['Model-1'].sketches['__profile__'].CircleByCenterPerimeter(center=(
    0.0, 0.0), point1=(0.0, 0.06))

mdb.models['Model-1'].sketches['__profile__'].ObliqueDimension(textPoint=(0.0,

```

```

0.06), value=0.0911, vertex1=
mdb.models['Model-1'].sketches['__profile__'].vertices[0], vertex2=
mdb.models['Model-1'].sketches['__profile__'].vertices[1])
mdb.models['Model-1'].Part(dimensionality=THREE_D, name='Pressure-Armour',
type=DEFORMABLE_BODY)
mdb.models['Model-1'].parts['Pressure-Armour'].BaseShellExtrude(depth=5.0,
sketch=mdb.models['Model-1'].sketches['__profile__'])
del mdb.models['Model-1'].sketches['__profile__']
mdb.models['Model-1'].ConstrainedSketch(name='__profile__', sheetSize=1.0)
mdb.models['Model-1'].sketches['__profile__'].CircleByCenterPerimeter(center=(
0.0, 0.0), point1=(0.0, 0.06))
mdb.models['Model-1'].sketches['__profile__'].ObliqueDimension(textPoint=(0.0,
0.06), value=0.0966, vertex1=
mdb.models['Model-1'].sketches['__profile__'].vertices[0], vertex2=
mdb.models['Model-1'].sketches['__profile__'].vertices[1])
mdb.models['Model-1'].Part(dimensionality=THREE_D, name=
'Interior-Anti-Wear-Tape', type=DEFORMABLE_BODY)
mdb.models['Model-1'].parts['Interior-Anti-Wear-Tape'].BaseShellExtrude(depth=
5.0, sketch=mdb.models['Model-1'].sketches['__profile__'])
del mdb.models['Model-1'].sketches['__profile__']
mdb.models['Model-1'].ConstrainedSketch(name='__profile__', sheetSize=1.0)

```

```

del mdb.models['Model-1'].sketches['__profile__']

mdb.models['Model-1'].ConstrainedSketch(name='__profile__', sheetSize=1.0)

mdb.models['Model-1'].sketches['__profile__'].ConstructionLine(point1=(0.0,
    -0.5), point2=(0.0, 0.5))

mdb.models['Model-1'].sketches['__profile__'].FixedConstraint(entity=
    mdb.models['Model-1'].sketches['__profile__'].geometry[2])

mdb.models['Model-1'].sketches['__profile__'].Line(point1=(0.04, 0.06), point2=
    (0.04, 0.05))

mdb.models['Model-1'].sketches['__profile__'].VerticalConstraint(addUndoState=
    False, entity=mdb.models['Model-1'].sketches['__profile__'].geometry[3])

mdb.models['Model-1'].sketches['__profile__'].Line(point1=(0.04, 0.06), point2=
    (0.0, 0.06))

mdb.models['Model-1'].sketches['__profile__'].HorizontalConstraint(
    addUndoState=False, entity=
    mdb.models['Model-1'].sketches['__profile__'].geometry[4])

mdb.models['Model-1'].sketches['__profile__'].PerpendicularConstraint(
    addUndoState=False, entity1=
    mdb.models['Model-1'].sketches['__profile__'].geometry[3], entity2=
    mdb.models['Model-1'].sketches['__profile__'].geometry[4])

mdb.models['Model-1'].sketches['__profile__'].CoincidentConstraint(
    addUndoState=False, entity1=

```

```

mdb.models['Model-1'].sketches['__profile__'].vertices[2], entity2=
mdb.models['Model-1'].sketches['__profile__'].geometry[2])
mdb.models['Model-1'].sketches['__profile__'].HorizontalDimension(textPoint=(
0.0397995710372925, 0.0728996396064758), value=0.1006, vertex1=
mdb.models['Model-1'].sketches['__profile__'].vertices[2], vertex2=
mdb.models['Model-1'].sketches['__profile__'].vertices[0])
mdb.models['Model-1'].sketches['__profile__'].VerticalDimension(textPoint=(
0.117357641458511, 0.0512543618679047), value=0.01, vertex1=
mdb.models['Model-1'].sketches['__profile__'].vertices[0], vertex2=
mdb.models['Model-1'].sketches['__profile__'].vertices[1])
mdb.models['Model-1'].sketches['__profile__'].delete(objectList=(
mdb.models['Model-1'].sketches['__profile__'].geometry[4], ))
mdb.models['Model-1'].Part(dimensionality=THREE_D, name='Interior-Tensile-Wire'
, type=DEFORMABLE_BODY)
mdb.models['Model-1'].parts['Interior-Tensile-Wire'].BaseShellRevolve(angle=
1421.0, flipPitchDirection=OFF, flipRevolveDirection=OFF,
moveSketchNormalToPath=OFF, pitch=1.263, sketch=
mdb.models['Model-1'].sketches['__profile__'])
del mdb.models['Model-1'].sketches['__profile__']
mdb.models['Model-1'].ConstrainedSketch(name='__profile__', sheetSize=1.0)
mdb.models['Model-1'].sketches['__profile__'].CircleByCenterPerimeter(center=(

```

```

0.0, 0.0), point1=(0.0, 0.06))

mdb.models['Model-1'].sketches['__profile__'].ObliqueDimension(textPoint=(0.0,
0.06), value=0.1046, vertex1=
mdb.models['Model-1'].sketches['__profile__'].vertices[0], vertex2=
mdb.models['Model-1'].sketches['__profile__'].vertices[1])

mdb.models['Model-1'].Part(dimensionality=THREE_D, name=
'Exterior-Anti-Wear-Tape', type=DEFORMABLE_BODY)

mdb.models['Model-1'].parts['Exterior-Anti-Wear-Tape'].BaseShellExtrude(depth=
5.0, sketch=mdb.models['Model-1'].sketches['__profile__'])

del mdb.models['Model-1'].sketches['__profile__']

mdb.models['Model-1'].ConstrainedSketch(name='__profile__', sheetSize=1.0)

mdb.models['Model-1'].sketches['__profile__'].ConstructionLine(point1=(0.0,
-0.5), point2=(0.0, 0.5))

mdb.models['Model-1'].sketches['__profile__'].FixedConstraint(entity=
mdb.models['Model-1'].sketches['__profile__'].geometry[2])

mdb.models['Model-1'].sketches['__profile__'].Line(point1=(0.04, 0.06), point2=
(0.04, 0.0549999999674037))

mdb.models['Model-1'].sketches['__profile__'].VerticalConstraint(addUndoState=
False, entity=mdb.models['Model-1'].sketches['__profile__'].geometry[3])

mdb.models['Model-1'].sketches['__profile__'].ObliqueDimension(textPoint=(
0.0573521852493286, 0.0549299865961075), value=0.01, vertex1=

```

```

mdb.models['Model-1'].sketches['__profile__'].vertices[0], vertex2=
mdb.models['Model-1'].sketches['__profile__'].vertices[1])
mdb.models['Model-1'].sketches['__profile__'].Line(point1=(0.04,
0.0649999999674037), point2=(0.0, 0.06499999997759))
mdb.models['Model-1'].sketches['__profile__'].HorizontalConstraint(
addUndoState=False, entity=
mdb.models['Model-1'].sketches['__profile__'].geometry[4])
mdb.models['Model-1'].sketches['__profile__'].CoincidentConstraint(
addUndoState=False, entity1=
mdb.models['Model-1'].sketches['__profile__'].vertices[2], entity2=
mdb.models['Model-1'].sketches['__profile__'].geometry[2])
mdb.models['Model-1'].sketches['__profile__'].HorizontalDimension(textPoint=(
0.038166731595993, 0.0773920565843582), value=0.1086, vertex1=
mdb.models['Model-1'].sketches['__profile__'].vertices[2], vertex2=
mdb.models['Model-1'].sketches['__profile__'].vertices[0])
mdb.models['Model-1'].sketches['__profile__'].delete(objectList=(
mdb.models['Model-1'].sketches['__profile__'].geometry[4],
mdb.models['Model-1'].sketches['__profile__'].dimensions[1],
mdb.models['Model-1'].sketches['__profile__'].constraints[8]))
mdb.models['Model-1'].Part(dimensionality=THREE_D, name='Exterior-Tensile-Wire'
, type=DEFORMABLE_BODY)

```

```

mdb.models['Model-1'].parts['Exterior-Tensile-Wire'].BaseShellRevolve(angle=
    1362.0, flipPitchDirection=ON, flipRevolveDirection=OFF,
    moveSketchNormalToPath=OFF, pitch=1.318, sketch=
        mdb.models['Model-1'].sketches['__profile__'])
del mdb.models['Model-1'].sketches['__profile__']
mdb.models['Model-1'].ConstrainedSketch(name='__profile__', sheetSize=1.0)
mdb.models['Model-1'].sketches['__profile__'].CircleByCenterPerimeter(center=(
    0.0, 0.0), point1=(0.0, 0.06))
mdb.models['Model-1'].sketches['__profile__'].ObliqueDimension(textPoint=(0.0,
    0.06), value=0.1176, vertex1=
        mdb.models['Model-1'].sketches['__profile__'].vertices[0], vertex2=
            mdb.models['Model-1'].sketches['__profile__'].vertices[1])
mdb.models['Model-1'].Part(dimensionality=THREE_D, name='Anti-Birdcaging-Tape',
    type=DEFORMABLE_BODY)
mdb.models['Model-1'].parts['Anti-Birdcaging-Tape'].BaseShellExtrude(depth=5.0,
    sketch=mdb.models['Model-1'].sketches['__profile__'])
del mdb.models['Model-1'].sketches['__profile__']
mdb.models['Model-1'].ConstrainedSketch(name='__profile__', sheetSize=1.0)
mdb.models['Model-1'].sketches['__profile__'].CircleByCenterPerimeter(center=(
    0.0, 0.0), point1=(0.0, 0.06))
del mdb.models['Model-1'].sketches['__profile__']

```

```

del mdb.models['Model-1'].parts['Anti-Birdcaging-Tape']

mdb.models['Model-1'].ConstrainedSketch(name='__profile__', sheetSize=1.0)

mdb.models['Model-1'].sketches['__profile__'].CircleByCenterPerimeter(center=(
    0.0, 0.0), point1=(0.0, 0.06))

mdb.models['Model-1'].sketches['__profile__'].ObliqueDimension(textPoint=(0.0,
    0.06), value=0.1176, vertex1=
    mdb.models['Model-1'].sketches['__profile__'].vertices[0], vertex2=
    mdb.models['Model-1'].sketches['__profile__'].vertices[1])

mdb.models['Model-1'].Part(dimensionality=THREE_D, name=
    'External-Plastic-Sheath', type=DEFORMABLE_BODY)

mdb.models['Model-1'].parts['External-Plastic-Sheath'].BaseShellExtrude(depth=
    5.0, sketch=mdb.models['Model-1'].sketches['__profile__'])

del mdb.models['Model-1'].sketches['__profile__']

mdb.models['Model-1'].ConstrainedSketch(name='__profile__', sheetSize=1.0)

mdb.models['Model-1'].sketches['__profile__'].CircleByCenterPerimeter(center=(
    0.0, 0.0), point1=(0.0, 0.06))

mdb.models['Model-1'].sketches['__profile__'].ObliqueDimension(textPoint=(0.0,
    0.06), value=0.1126, vertex1=
    mdb.models['Model-1'].sketches['__profile__'].vertices[0], vertex2=
    mdb.models['Model-1'].sketches['__profile__'].vertices[1])

mdb.models['Model-1'].Part(dimensionality=THREE_D, name='Anti-Birdcaging-Tape',

```

```

type=DEFORMABLE_BODY)

mdb.models['Model-1'].parts['Anti-Birdcaging-Tape'].BaseShellExtrude(depth=5.0,

    sketch=mdb.models['Model-1'].sketches['__profile__'])

del mdb.models['Model-1'].sketches['__profile__']

mdb.models['Model-1'].parts['Carcass'].Surface(name='Carcass-Inside',

    side2Faces=

        mdb.models['Model-1'].parts['Carcass'].faces.getSequenceFromMask(([#1 ]',

        ), ))

mdb.models['Model-1'].parts['Carcass'].Surface(name='Carcass-Outside',

    side1Faces=

        mdb.models['Model-1'].parts['Carcass'].faces.getSequenceFromMask(([#1 ]',

        ), ))

mdb.models['Model-1'].parts['Anti-Birdcaging-Tape'].Surface(name=

    'Anti-Birdcaging-Inside', side2Faces=

        mdb.models['Model-1'].parts['Anti-Birdcaging-Tape'].faces.getSequenceFromMask(

            ([#1 ]', ), ))

mdb.models['Model-1'].parts['Anti-Birdcaging-Tape'].Surface(name=

    'Anti-Birdcaging-Outside', side1Faces=

        mdb.models['Model-1'].parts['Anti-Birdcaging-Tape'].faces.getSequenceFromMask(

            ([#1 ]', ), ))

mdb.models['Model-1'].parts['Exterior-Anti-Wear-Tape'].Surface(name=

```

```

'Ext-anti-wear-inside', side2Faces=
mdb.models['Model-1'].parts['Exterior-Anti-Wear-Tape'].faces.getSequenceFromMask(
(['#1 '], ), )
mdb.models['Model-1'].parts['Exterior-Anti-Wear-Tape'].Surface(name=
'Ext-anti-wear-outside', side1Faces=
mdb.models['Model-1'].parts['Exterior-Anti-Wear-Tape'].faces.getSequenceFromMask(
(['#1 '], ), )
mdb.models['Model-1'].parts['Exterior-Tensile-Wire'].Surface(name=
'ext-tensile-inside', side1Faces=
mdb.models['Model-1'].parts['Exterior-Tensile-Wire'].faces.getSequenceFromMask(
(['#1 '], ), )
mdb.models['Model-1'].parts['Exterior-Tensile-Wire'].Surface(name=
'ext-tensile-outside', side2Faces=
mdb.models['Model-1'].parts['Exterior-Tensile-Wire'].faces.getSequenceFromMask(
(['#1 '], ), )
mdb.models['Model-1'].parts['External-Plastic-Sheath'].Surface(name=
'ext-plastic-inside', side2Faces=
mdb.models['Model-1'].parts['External-Plastic-Sheath'].faces.getSequenceFromMask(
(['#1 '], ), )
mdb.models['Model-1'].parts['External-Plastic-Sheath'].Surface(name=
'ext-plastic-outside', side1Faces=

```

```

mdb.models['Model-1'].parts['External-Plastic-Sheath'].faces.getSequenceFromMask(
    ([#1 ]), )
)

mdb.models['Model-1'].parts['Interior-Anti-Wear-Tape'].Surface(name=
    'int-anti-wear-inside', side2Faces=
        mdb.models['Model-1'].parts['Interior-Anti-Wear-Tape'].faces.getSequenceFromMask(
            ([#1 ]), )
        )

mdb.models['Model-1'].parts['Interior-Anti-Wear-Tape'].Surface(name=
    'int-anti-wear-outside', side1Faces=
        mdb.models['Model-1'].parts['Interior-Anti-Wear-Tape'].faces.getSequenceFromMask(
            ([#1 ]), )
        )

mdb.models['Model-1'].parts['Interior-Plastic-Sheath'].Surface(name=
    'Int-plastic-inside', side2Faces=
        mdb.models['Model-1'].parts['Interior-Plastic-Sheath'].faces.getSequenceFromMask(
            ([#1 ]), )
        )

mdb.models['Model-1'].parts['Interior-Plastic-Sheath'].Surface(name=
    'Int-plastic-outside', side1Faces=
        mdb.models['Model-1'].parts['Interior-Plastic-Sheath'].faces.getSequenceFromMask(
            ([#1 ]), )
        )

mdb.models['Model-1'].parts['Interior-Tensile-Wire'].Surface(name=
    'Int-tensile-inside', side1Faces=
        mdb.models['Model-1'].parts['Interior-Tensile-Wire'].faces.getSequenceFromMask(

```

```

([#1 ], ), ))
mdb.models['Model-1'].parts['Interior-Tensile-Wire'].Surface(name=
'Int-tensile-outside', side2Faces=
mdb.models['Model-1'].parts['Interior-Tensile-Wire'].faces.getSequenceFromMask(
([#1 ], ), ))
mdb.models['Model-1'].parts['Pressure-Armour'].Surface(name='Pressure-Armour',
side2Faces=
mdb.models['Model-1'].parts['Pressure-Armour'].faces.getSequenceFromMask((
[#1 ], ), ))
mdb.models['Model-1'].parts['Pressure-Armour'].Surface(name=
'Pressure-armour-outside', side1Faces=
mdb.models['Model-1'].parts['Pressure-Armour'].faces.getSequenceFromMask((
[#1 ], ), ))
mdb.models['Model-1'].parts['Pressure-Armour'].surfaces.changeKey(fromName=
'Pressure-Armour', toName='Pressure-Armour-inside')

mdb.models['Model-1'].Material(name='Tensile-Wires')
mdb.models['Model-1'].materials['Tensile-Wires'].Density(table=((7850.0, ), ))
mdb.models['Model-1'].materials['Tensile-Wires'].Elastic(table=((
210000000000.0, 0.3), ))
mdb.models['Model-1'].materials['Tensile-Wires'].Plastic(table=((765000000.0,

```

```

0.0), (770000000.0, 0.001), (850000000.0, 0.1), (870000000.0, 0.2)))

mdb.models['Model-1'].Material(name='Plastic-Sheath')

mdb.models['Model-1'].materials['Plastic-Sheath'].Density(table=((500.0, ), ))

mdb.models['Model-1'].materials['Plastic-Sheath'].Elastic(table=((800000000.0,
0.4), ))

mdb.models['Model-1'].materials['Plastic-Sheath'].Plastic(table=((50000000.0,
0.0), (60000000.0, 0.001)))

mdb.models['Model-1'].Material(name='Anti-wear')

mdb.models['Model-1'].materials['Anti-wear'].Density(table=((500.0, ), ))

mdb.models['Model-1'].materials['Anti-wear'].Elastic(table=((350000000.0,
0.45), ))

mdb.models['Model-1'].materials['Anti-wear'].Plastic(table=((20000000.0, 0.0),
(21000000.0, 0.001), (25000000.0, 0.1)))

mdb.models['Model-1'].Material(name='Anti-Birdcaging')

mdb.models['Model-1'].materials['Anti-Birdcaging'].Density(table=((500.0, ), ))

mdb.models['Model-1'].materials['Anti-Birdcaging'].Elastic(table=((750000000.0,
0.4), ))

mdb.models['Model-1'].materials['Anti-Birdcaging'].Plastic(table=((100000000.0,
0.0), (110000000.0, 0.001), (150000000.0, 0.1)))

mdb.models['Model-1'].Material(name='Pressure-armour')

mdb.models['Model-1'].materials['Pressure-armour'].Density(table=((7850.0, ),

```

```

))

mdb.models['Model-1'].materials['Pressure-armour'].Elastic(table=((
    200000000000.0, 1000000000.0, 3000000000.0, 70000000000.0, 1000000000.0,
    200000000000.0, 500000000.0, 70000000000.0, 500000000.0), ), type=
    ORTHOTROPIC)

mdb.models['Model-1'].Material(name='Carcass', objectToCopy=
    mdb.models['Model-1'].materials['Pressure-armour'])

mdb.models['Model-1'].materials['Carcass'].elastic.setValues(table=((
    193000000000.0, 1000000000.0, 3000000000.0, 69000000000.0, 1000000000.0,
    193000000000.0, 500000000.0, 69000000000.0, 500000000.0), ))

mdb.models['Model-1'].parts['Pressure-Armour'].DatumCsysByThreePoints(
    coordSysType=CYLINDRICAL, name='Material-ASSIGNMENT-pPRESSURE-aRMOUR',
    origin=(0.0, 0.0, 0.0), point1=(1.0, 0.0, 0.0), point2=(1.0, 1.0, 0.0))

mdb.models['Model-1'].parts['Pressure-Armour'].MaterialOrientation(
    additionalRotationField="", additionalRotationType=ROTATION_ANGLE, angle=
    3.0, axis=AXIS_1, fieldName="", localCsys=
    mdb.models['Model-1'].parts['Pressure-Armour'].datums[4], orientationType=
    SYSTEM, region=Region(
    faces=mdb.models['Model-1'].parts['Pressure-Armour'].faces.getSequenceFromMask(
    mask=('[#1 ]', ), )))

```

```

mdb.models['Model-1'].parts['Carcass'].DatumCsysByThreePoints(coordSysType=
    CYLINDRICAL, name='Material-Assignment-carcass', origin=(0.0, 0.0, 0.0),
    point1=(1.0, 0.0, 0.0), point2=(1.0, 1.0, 0.0))
mdb.models['Model-1'].parts['Carcass'].MaterialOrientation(
    additionalRotationField="", additionalRotationType=ROTATION_ANGLE, angle=
    5.0, axis=AXIS_1, fieldName="", localCsys=
    mdb.models['Model-1'].parts['Carcass'].datums[4], orientationType=SYSTEM,
    region=Region(
    faces=mdb.models['Model-1'].parts['Carcass'].faces.getSequenceFromMask(
    mask=('[#1 ]', ), )))
mdb.models['Model-1'].HomogeneousShellSection(idealization=NO_IDEALIZATION,
    integrationRule=SIMPSON, material='Carcass', name='carcass', numIntPts=11,
    poissonDefinition=DEFAULT, preIntegrate=OFF, temperature=GRADIENT,
    thickness=0.004, thicknessField="", thicknessModulus=None, thicknessType=
    UNIFORM, useDensity=OFF)
mdb.models['Model-1'].HomogeneousShellSection(idealization=NO_IDEALIZATION,
    integrationRule=SIMPSON, material='Pressure-armour', name='Pressure-armour'
    , numIntPts=11, poissonDefinition=DEFAULT, preIntegrate=OFF, temperature=
    GRADIENT, thickness=0.006, thicknessField="", thicknessModulus=None,
    thicknessType=UNIFORM, useDensity=OFF)
mdb.models['Model-1'].HomogeneousShellSection(idealization=NO_IDEALIZATION,

```

```

integrationRule=SIMPSON, material='Tensile-Wires', name='Tensile-wires',
numIntPts=11, poissonDefinition=DEFAULT, preIntegrate=OFF, temperature=
GRADIENT, thickness=0.003, thicknessField="", thicknessModulus=None,
thicknessType=UNIFORM, useDensity=OFF)

mdb.models['Model-1'].HomogeneousShellSection(idealization=NO_IDEALIZATION,
integrationRule=SIMPSON, material='Anti-wear', name='anti-wear-tape',
numIntPts=11, poissonDefinition=DEFAULT, preIntegrate=OFF, temperature=
GRADIENT, thickness=0.005, thicknessField="", thicknessModulus=None,
thicknessType=UNIFORM, useDensity=OFF)

mdb.models['Model-1'].HomogeneousShellSection(idealization=NO_IDEALIZATION,
integrationRule=SIMPSON, material='Anti-Birdcaging', name='anti-birdcaging'
, numIntPts=11, poissonDefinition=DEFAULT, preIntegrate=OFF, temperature=
GRADIENT, thickness=0.005, thicknessField="", thicknessModulus=None,
thicknessType=UNIFORM, useDensity=OFF)

mdb.models['Model-1'].HomogeneousShellSection(idealization=NO_IDEALIZATION,
integrationRule=SIMPSON, material='Plastic-Sheath', name='Plastic-sheath',
numIntPts=11, poissonDefinition=DEFAULT, preIntegrate=OFF, temperature=
GRADIENT, thickness=0.005, thicknessField="", thicknessModulus=None,
thicknessType=UNIFORM, useDensity=OFF)

mdb.models['Model-1'].parts['Carcass'].Set(faces=
mdb.models['Model-1'].parts['Carcass'].faces.getSequenceFromMask(('[#1 ]',

```

```

), ), name='Set-2')

mdb.models['Model-1'].parts['Carcass'].SectionAssignment(offset=0.0,
    offsetField="", offsetType=MIDDLE_SURFACE, region=
    mdb.models['Model-1'].parts['Carcass'].sets['Set-2'], sectionName='carcass'
    , thicknessAssignment=FROM_SECTION)

mdb.models['Model-1'].parts['Pressure-Armour'].Set(faces=
    mdb.models['Model-1'].parts['Pressure-Armour'].faces.getSequenceFromMask((
    ['#1 ]', ), ), name='Set-2')

mdb.models['Model-1'].parts['Pressure-Armour'].SectionAssignment(offset=0.0,
    offsetField="", offsetType=MIDDLE_SURFACE, region=
    mdb.models['Model-1'].parts['Pressure-Armour'].sets['Set-2'], sectionName=
    'Pressure-armour', thicknessAssignment=FROM_SECTION)

mdb.models['Model-1'].parts['Interior-Plastic-Sheath'].Set(faces=
    mdb.models['Model-1'].parts['Interior-Plastic-Sheath'].faces.getSequenceFromMask(
    (['#1 ]', ), ), name='Set-1')

mdb.models['Model-1'].parts['Interior-Plastic-Sheath'].SectionAssignment(
    offset=0.0, offsetField="", offsetType=MIDDLE_SURFACE, region=
    mdb.models['Model-1'].parts['Interior-Plastic-Sheath'].sets['Set-1'],
    sectionName='Plastic-sheath', thicknessAssignment=FROM_SECTION)

mdb.models['Model-1'].parts['Interior-Anti-Wear-Tape'].Set(faces=
    mdb.models['Model-1'].parts['Interior-Anti-Wear-Tape'].faces.getSequenceFromMask(

```

```

([#1 ], ), ), name='Set-1')

mdb.models['Model-1'].parts['Interior-Anti-Wear-Tape'].SectionAssignment(
    offset=0.0, offsetField="", offsetType=MIDDLE_SURFACE, region=
    mdb.models['Model-1'].parts['Interior-Anti-Wear-Tape'].sets['Set-1'],
    sectionName='anti-wear-tape', thicknessAssignment=FROM_SECTION)

mdb.models['Model-1'].parts['External-Plastic-Sheath'].Set(faces=
    mdb.models['Model-1'].parts['External-Plastic-Sheath'].faces.getSequenceFromMask(
    ([#1 ], ), ), name='Set-1')

mdb.models['Model-1'].parts['External-Plastic-Sheath'].SectionAssignment(
    offset=0.0, offsetField="", offsetType=MIDDLE_SURFACE, region=
    mdb.models['Model-1'].parts['External-Plastic-Sheath'].sets['Set-1'],
    sectionName='Plastic-sheath', thicknessAssignment=FROM_SECTION)

mdb.models['Model-1'].parts['Exterior-Tensile-Wire'].Set(faces=
    mdb.models['Model-1'].parts['Exterior-Tensile-Wire'].faces.getSequenceFromMask(
    ([#1 ], ), ), name='Set-1')

mdb.models['Model-1'].parts['Exterior-Tensile-Wire'].SectionAssignment(offset=
    0.0, offsetField="", offsetType=MIDDLE_SURFACE, region=
    mdb.models['Model-1'].parts['Exterior-Tensile-Wire'].sets['Set-1'],
    sectionName='Tensile-wires', thicknessAssignment=FROM_SECTION)

mdb.models['Model-1'].parts['Exterior-Anti-Wear-Tape'].Set(faces=
    mdb.models['Model-1'].parts['Exterior-Anti-Wear-Tape'].faces.getSequenceFromMask(

```

```

([#1 ], ), ), name='Set-1')

mdb.models['Model-1'].parts['Exterior-Anti-Wear-Tape'].SectionAssignment(
    offset=0.0, offsetField="", offsetType=MIDDLE_SURFACE, region=
    mdb.models['Model-1'].parts['Exterior-Anti-Wear-Tape'].sets['Set-1'],
    sectionName='anti-wear-tape', thicknessAssignment=FROM_SECTION)

mdb.models['Model-1'].parts['Anti-Birdcaging-Tape'].Set(faces=
    mdb.models['Model-1'].parts['Anti-Birdcaging-Tape'].faces.getSequenceFromMask(
    ([#1 ], ), ), name='Set-1')

mdb.models['Model-1'].parts['Anti-Birdcaging-Tape'].SectionAssignment(offset=
    0.0, offsetField="", offsetType=MIDDLE_SURFACE, region=
    mdb.models['Model-1'].parts['Anti-Birdcaging-Tape'].sets['Set-1'],
    sectionName='anti-birdcaging', thicknessAssignment=FROM_SECTION)

mdb.models['Model-1'].parts['Interior-Tensile-Wire'].Set(faces=
    mdb.models['Model-1'].parts['Interior-Tensile-Wire'].faces.getSequenceFromMask(
    ([#1 ], ), ), name='Set-1')

mdb.models['Model-1'].parts['Interior-Tensile-Wire'].SectionAssignment(offset=
    0.0, offsetField="", offsetType=MIDDLE_SURFACE, region=
    mdb.models['Model-1'].parts['Interior-Tensile-Wire'].sets['Set-1'],
    sectionName='Tensile-wires', thicknessAssignment=FROM_SECTION)

mdb.models['Model-1'].rootAssembly.DatumCsysByDefault(CARTESIAN)

```

```
mdb.models['Model-1'].rootAssembly.Instance(dependent=ON, name='Carcass-1',  
    part=mdb.models['Model-1'].parts['Carcass'])  
  
mdb.models['Model-1'].rootAssembly.Instance(dependent=ON, name=  
    'Interior-Plastic-Sheath-1', part=  
    mdb.models['Model-1'].parts['Interior-Plastic-Sheath'])  
  
mdb.models['Model-1'].rootAssembly.Instance(dependent=ON, name=  
    'Pressure-Armour-1', part=mdb.models['Model-1'].parts['Pressure-Armour'])  
  
mdb.models['Model-1'].rootAssembly.Instance(dependent=ON, name=  
    'Interior-Anti-Wear-Tape-1', part=  
    mdb.models['Model-1'].parts['Interior-Anti-Wear-Tape'])  
  
mdb.models['Model-1'].rootAssembly.Instance(dependent=ON, name=  
    'Interior-Tensile-Wire-1', part=  
    mdb.models['Model-1'].parts['Interior-Tensile-Wire'])  
  
mdb.models['Model-1'].rootAssembly.Instance(dependent=ON, name=  
    'Exterior-Anti-Wear-Tape-1', part=  
    mdb.models['Model-1'].parts['Exterior-Anti-Wear-Tape'])  
  
mdb.models['Model-1'].rootAssembly.Instance(dependent=ON, name=  
    'Exterior-Tensile-Wire-1', part=  
    mdb.models['Model-1'].parts['Exterior-Tensile-Wire'])  
  
mdb.models['Model-1'].rootAssembly.Instance(dependent=ON, name=  
    'Anti-Birdcaging-Tape-1', part=
```

```

mdb.models['Model-1'].parts['Anti-Birdcaging-Tape'])
mdb.models['Model-1'].rootAssembly.Instance(dependent=ON, name=
'External-Plastic-Sheath-1', part=
mdb.models['Model-1'].parts['External-Plastic-Sheath'])
mdb.models['Model-1'].rootAssembly.Coaxial(fixedAxis=
mdb.models['Model-1'].rootAssembly.instances['External-Plastic-Sheath-1'].faces[0]
, flip=OFF, movableAxis=
mdb.models['Model-1'].rootAssembly.instances['Interior-Tensile-Wire-1'].faces[0])
mdb.models['Model-1'].rootAssembly.Coaxial(fixedAxis=
mdb.models['Model-1'].rootAssembly.instances['Anti-Birdcaging-Tape-1'].faces[0]
, flip=OFF, movableAxis=
mdb.models['Model-1'].rootAssembly.instances['Exterior-Tensile-Wire-1'].faces[0])
mdb.models['Model-1'].rootAssembly.translate(instanceList=(
'Interior-Tensile-Wire-1', ), vector=(-0.1006, -0.1046, 0.145337))
mdb.models['Model-1'].rootAssembly.translate(instanceList=(
'Exterior-Tensile-Wire-1', ), vector=(-0.022579, 0.001627, 4.841064))
mdb.models['Model-1'].rootAssembly.RadialInstancePattern(axis=(0.0, 0.0, -1.0),
instanceList=('Interior-Tensile-Wire-1', ), number=52, point=(0.0, 0.0,
4.986433), totalAngle=360.0)
mdb.models['Model-1'].rootAssembly.RadialInstancePattern(axis=(0.0, 0.0, 1.0),
instanceList=('Exterior-Tensile-Wire-1', ), number=54, point=(0.0, 0.0,

```

```

    0.0), totalAngle=360.0)

mdb.models['Model-1'].rootAssembly.DatumPointByCoordinate(coords=(0.0, 0.0,
    0.0))

mdb.models['Model-1'].rootAssembly.DatumPointByCoordinate(coords=(0.0, 0.0,
    5.0))

mdb.models['Model-1'].rootAssembly.ReferencePoint(point=
    mdb.models['Model-1'].rootAssembly.datums[230])

mdb.models['Model-1'].rootAssembly.ReferencePoint(point=
    mdb.models['Model-1'].rootAssembly.datums[231])

mdb.models['Model-1'].parts['Pressure-Armour'].setElementType(elemTypes=(
    ElemType(elemCode=S4R, elemLibrary=STANDARD, secondOrderAccuracy=OFF,
    hourglassControl=DEFAULT), ElemType(elemCode=S3, elemLibrary=STANDARD)),
    regions=(
    mdb.models['Model-1'].parts['Pressure-Armour'].faces.getSequenceFromMask((
    ['#1 ]', ), ), ))

mdb.models['Model-1'].parts['Pressure-Armour'].seedPart(deviationFactor=0.1,
    minSizeFactor=0.1, size=0.005)

mdb.models['Model-1'].parts['Pressure-Armour'].generateMesh()

mdb.models['Model-1'].parts['Pressure-Armour'].deleteMesh()

mdb.models['Model-1'].parts['Pressure-Armour'].seedPart(deviationFactor=0.1,

```

```

minSizeFactor=0.1, size=0.0075)

mdb.models['Model-1'].parts['Pressure-Armour'].generateMesh()

mdb.models['Model-1'].parts['Interior-Tensile-Wire'].setElementType(elemTypes=(
    ElemType(elemCode=S4R, elemLibrary=STANDARD, secondOrderAccuracy=OFF,
    hourglassControl=DEFAULT), ElemType(elemCode=S3, elemLibrary=STANDARD)),
    regions=(
        mdb.models['Model-1'].parts['Interior-Tensile-Wire'].faces.getSequenceFromMask(
            ([#1 ], ), ), ))

mdb.models['Model-1'].parts['Interior-Tensile-Wire'].seedPart(deviationFactor=
    0.1, minSizeFactor=0.1, size=0.005)

mdb.models['Model-1'].parts['Interior-Tensile-Wire'].generateMesh()

mdb.models['Model-1'].parts['Interior-Tensile-Wire'].deleteMesh()

mdb.models['Model-1'].parts['Interior-Tensile-Wire'].setMeshControls(regions=
    mdb.models['Model-1'].parts['Interior-Tensile-Wire'].faces.getSequenceFromMask(
        ([#1 ], ), ), technique=SWEEP)

mdb.models['Model-1'].parts['Interior-Tensile-Wire'].generateMesh()

mdb.models['Model-1'].parts['Interior-Plastic-Sheath'].setElementType(
    elemTypes=(ElemType(elemCode=S4R, elemLibrary=STANDARD,
    secondOrderAccuracy=OFF, hourglassControl=DEFAULT), ElemType(elemCode=S3,
    elemLibrary=STANDARD)), regions=(
        mdb.models['Model-1'].parts['Interior-Plastic-Sheath'].faces.getSequenceFromMask(

```

```

([#1 ], ), ), ))

mdb.models['Model-1'].parts['Interior-Plastic-Sheath'].seedPart(
    deviationFactor=0.1, minSizeFactor=0.1, size=0.0075)

mdb.models['Model-1'].parts['Interior-Plastic-Sheath'].generateMesh()

mdb.models['Model-1'].parts['Interior-Anti-Wear-Tape'].seedPart(
    deviationFactor=0.1, minSizeFactor=0.1, size=0.0075)

mdb.models['Model-1'].parts['Interior-Anti-Wear-Tape'].generateMesh()

mdb.models['Model-1'].parts['External-Plastic-Sheath'].setElementType(
    elemTypes=(ElemType(elemCode=S4R, elemLibrary=STANDARD,
        secondOrderAccuracy=OFF, hourglassControl=DEFAULT), ElemType(elemCode=S3,
        elemLibrary=STANDARD))), regions=(
    mdb.models['Model-1'].parts['External-Plastic-Sheath'].faces.getSequenceFromMask(
        ([#1 ], ), ), ))

mdb.models['Model-1'].parts['External-Plastic-Sheath'].seedPart(
    deviationFactor=0.1, minSizeFactor=0.1, size=0.0075)

mdb.models['Model-1'].parts['External-Plastic-Sheath'].generateMesh()

mdb.models['Model-1'].parts['Exterior-Tensile-Wire'].setElementType(elemTypes=(
    ElemType(elemCode=S4R, elemLibrary=STANDARD, secondOrderAccuracy=OFF,
        hourglassControl=DEFAULT), ElemType(elemCode=S3, elemLibrary=STANDARD))),
    regions=(
    mdb.models['Model-1'].parts['Exterior-Tensile-Wire'].faces.getSequenceFromMask(

```

```

([#1 ], ), ), ))

mdb.models['Model-1'].parts['Exterior-Tensile-Wire'].setMeshControls(regions=

mdb.models['Model-1'].parts['Exterior-Tensile-Wire'].faces.getSequenceFromMask(

([#1 ], ), ), technique=SWEEP)

mdb.models['Model-1'].parts['Exterior-Tensile-Wire'].seedPart(deviationFactor=

0.1, minSizeFactor=0.1, size=0.0075)

mdb.models['Model-1'].parts['Exterior-Tensile-Wire'].generateMesh()

mdb.models['Model-1'].parts['Exterior-Tensile-Wire'].deleteMesh()

mdb.models['Model-1'].parts['Exterior-Tensile-Wire'].seedPart(deviationFactor=

0.1, minSizeFactor=0.1, size=0.005)

mdb.models['Model-1'].parts['Exterior-Tensile-Wire'].generateMesh()

mdb.models['Model-1'].parts['Exterior-Anti-Wear-Tape'].setElementType(

elemTypes=(ElemType(elemCode=S4R, elemLibrary=STANDARD,

secondOrderAccuracy=OFF, hourglassControl=DEFAULT), ElemType(elemCode=S3,

elemLibrary=STANDARD)), regions=(

mdb.models['Model-1'].parts['Exterior-Anti-Wear-Tape'].faces.getSequenceFromMask(

([#1 ], ), ), ))

mdb.models['Model-1'].parts['Exterior-Anti-Wear-Tape'].seedPart(

deviationFactor=0.1, minSizeFactor=0.1, size=0.005)

mdb.models['Model-1'].parts['Exterior-Anti-Wear-Tape'].generateMesh()

mdb.models['Model-1'].parts['Carcass'].setElementType(elemTypes=(ElemType(

```

```

elemCode=S4R, elemLibrary=STANDARD, secondOrderAccuracy=OFF,
hourglassControl=DEFAULT), ElemType(elemCode=S3, elemLibrary=STANDARD)),
regions=(mdb.models['Model-1'].parts['Carcass'].faces.getSequenceFromMask((
'#1 ]', ), ), ))
mdb.models['Model-1'].parts['Carcass'].seedPart(deviationFactor=0.1,
minSizeFactor=0.1, size=0.0075)
mdb.models['Model-1'].parts['Carcass'].generateMesh()
mdb.models['Model-1'].parts['Anti-Birdcaging-Tape'].setElementType(elemTypes=(
ElemType(elemCode=S4R, elemLibrary=STANDARD, secondOrderAccuracy=OFF,
hourglassControl=DEFAULT), ElemType(elemCode=S3, elemLibrary=STANDARD)),
regions=(
mdb.models['Model-1'].parts['Anti-Birdcaging-Tape'].faces.getSequenceFromMask(
('#1 ]', ), ), ))
mdb.models['Model-1'].parts['Anti-Birdcaging-Tape'].seedPart(deviationFactor=
0.1, minSizeFactor=0.1, size=0.0075)
mdb.models['Model-1'].parts['Anti-Birdcaging-Tape'].generateMesh()
mdb.models['Model-1'].rootAssembly.regenerate()

```

```

#####Step
Generation#####

```

```
mdb.models['Model-1'].StaticStep(initialInc=0.001, maxInc=0.5, maxNumInc=1000,  
    minInc=1e-32, name='Initial-Curvature', nlgeom=ON, previous='Initial')
```

```
mdb.models['Model-1'].StaticStep(initialInc=1e-07, maxInc=0.5, maxNumInc=1000,  
    minInc=1e-35, name='Compression', previous='Initial-Curvature')
```

```
#####Contact
```

Property

```
Definition#####
```

```
mdb.models['Model-1'].ContactProperty('IntProp-1')
```

```
mdb.models['Model-1'].interactionProperties['IntProp-1'].TangentialBehavior(  
    dependencies=0, directionality=ISOTROPIC, elasticSlipStiffness=None,  
    formulation=PENALTY, fraction=0.005, maximumElasticSlip=FRACTION,  
    pressureDependency=OFF, shearStressLimit=None, slipRateDependency=OFF,  
    table=((0.1, ), ), temperatureDependency=OFF)
```

```
mdb.models['Model-1'].interactionProperties['IntProp-1'].tangentialBehavior.setValues(  
    dependencies=0, directionality=ISOTROPIC, elasticSlipStiffness=None,  
    formulation=PENALTY, fraction=0.005, maximumElasticSlip=FRACTION,  
    pressureDependency=OFF, shearStressLimit=None, slipRateDependency=OFF,  
    table=((0.1, ), ), temperatureDependency=OFF)
```

```
mdb.models['Model-1'].interactionProperties['IntProp-1'].NormalBehavior(  
    allowSeparation=ON, clearanceAtZeroContactPressure=0.0,  
    constraintEnforcementMethod=AUGMENTED_LAGRANGE, contactStiffness=DEFAULT,  
    contactStiffnessScaleFactor=1.0, pressureOverclosure=HARD)
```

```

mdb.models['Model-1'].parts['Interior-Tensile-Wire'].Set(edges=
    mdb.models['Model-1'].parts['Interior-Tensile-Wire'].edges.getSequenceFromMask(
        ('[#20000 ]', ), ), name='int-part-end')
mdb.models['Model-1'].rootAssembly.regenerate()
#####Defining Surface and Sets for
Coupling#####
mdb.models['Model-1'].rootAssembly.Set(name='RF-Moving', referencePoints=(
    mdb.models['Model-1'].rootAssembly.referencePoints[233], ))
mdb.models['Model-1'].rootAssembly.Set(name='RF-Fixed', referencePoints=(
    mdb.models['Model-1'].rootAssembly.referencePoints[232], ))
mdb.models['Model-1'].rootAssembly.Surface(name='Ext-Moving', side1Edges=
    mdb.models['Model-1'].rootAssembly.instances['Exterior-Tensile-Wire-1-rad-
53'].edges.getSequenceFromMask(
    mask=('[#20000 ]', ), )+\
    mdb.models['Model-1'].rootAssembly.instances['Exterior-Tensile-Wire-1-rad-
54'].edges.getSequenceFromMask(
    mask=('[#20000 ]', ), )+\
    mdb.models['Model-1'].rootAssembly.instances['Exterior-Tensile-Wire-
1'].edges.getSequenceFromMask(
    mask=('[#20000 ]', ), )+\
    mdb.models['Model-1'].rootAssembly.instances['Exterior-Tensile-Wire-1-rad-
2'].edges.getSequenceFromMask(
    mask=('[#20000 ]', ), )+\

```

```
mdb.models['Model-1'].rootAssembly.instances['Exterior-Tensile-Wire-1-rad-3'].edges.getSequenceFromMask(  
  
mask=(['#20000 ], ), )+\
```

```
mdb.models['Model-1'].rootAssembly.instances['Exterior-Tensile-Wire-1-rad-4'].edges.getSequenceFromMask(  
  
mask=(['#20000 ], ), )+\
```

```
mdb.models['Model-1'].rootAssembly.instances['Exterior-Tensile-Wire-1-rad-5'].edges.getSequenceFromMask(  
  
mask=(['#20000 ], ), )+\
```

```
mdb.models['Model-1'].rootAssembly.instances['Exterior-Tensile-Wire-1-rad-6'].edges.getSequenceFromMask(  
  
mask=(['#20000 ], ), )+\
```

```
mdb.models['Model-1'].rootAssembly.instances['Exterior-Tensile-Wire-1-rad-7'].edges.getSequenceFromMask(  
  
mask=(['#20000 ], ), )+\
```

```
mdb.models['Model-1'].rootAssembly.instances['Exterior-Tensile-Wire-1-rad-8'].edges.getSequenceFromMask(  
  
mask=(['#20000 ], ), )+\
```

```
mdb.models['Model-1'].rootAssembly.instances['Exterior-Tensile-Wire-1-rad-9'].edges.getSequenceFromMask(  
  
mask=(['#20000 ], ), )+\
```

```
mdb.models['Model-1'].rootAssembly.instances['Exterior-Tensile-Wire-1-rad-10'].edges.getSequenceFromMask(  
  
mask=(['#20000 ], ), )+\
```

```
mdb.models['Model-1'].rootAssembly.instances['Exterior-Tensile-Wire-1-rad-11'].edges.getSequenceFromMask(
```

```
mask=(['#20000 ], ), )+\
```

```
mdb.models['Model-1'].rootAssembly.instances['Exterior-Tensile-Wire-1-rad-12'].edges.getSequenceFromMask(
```

```
mask=(['#20000 ], ), )+\
```

```
mdb.models['Model-1'].rootAssembly.instances['Exterior-Tensile-Wire-1-rad-13'].edges.getSequenceFromMask(
```

```
mask=(['#20000 ], ), )+\
```

```
mdb.models['Model-1'].rootAssembly.instances['Exterior-Tensile-Wire-1-rad-14'].edges.getSequenceFromMask(
```

```
mask=(['#20000 ], ), )+\
```

```
mdb.models['Model-1'].rootAssembly.instances['Exterior-Tensile-Wire-1-rad-15'].edges.getSequenceFromMask(
```

```
mask=(['#20000 ], ), )+\
```

```
mdb.models['Model-1'].rootAssembly.instances['Exterior-Tensile-Wire-1-rad-16'].edges.getSequenceFromMask(
```

```
mask=(['#20000 ], ), )+\
```

```
mdb.models['Model-1'].rootAssembly.instances['Exterior-Tensile-Wire-1-rad-17'].edges.getSequenceFromMask(
```

```
mask=(['#20000 ], ), )+\
```

```
mdb.models['Model-1'].rootAssembly.instances['Exterior-Tensile-Wire-1-rad-18'].edges.getSequenceFromMask(
```

```
mask=(['#20000 ], ), )+\
```

```
mdb.models['Model-1'].rootAssembly.instances['Exterior-Tensile-Wire-1-rad-52'].edges.getSequenceFromMask(
```

```
mask=(['#20000 ], ), )+\
```

```
mdb.models['Model-1'].rootAssembly.instances['Exterior-Tensile-Wire-1-rad-43'].edges.getSequenceFromMask(
```

```
mask=(['#20000 ], ), )+\
```

```
mdb.models['Model-1'].rootAssembly.instances['Exterior-Tensile-Wire-1-rad-42'].edges.getSequenceFromMask(
```

```
mask=(['#20000 ], ), )+\
```

```
mdb.models['Model-1'].rootAssembly.instances['Exterior-Tensile-Wire-1-rad-41'].edges.getSequenceFromMask(
```

```
mask=(['#20000 ], ), )+\
```

```
mdb.models['Model-1'].rootAssembly.instances['Exterior-Tensile-Wire-1-rad-40'].edges.getSequenceFromMask(
```

```
mask=(['#20000 ], ), )+\
```

```
mdb.models['Model-1'].rootAssembly.instances['Exterior-Tensile-Wire-1-rad-39'].edges.getSequenceFromMask(
```

```
mask=(['#20000 ], ), )+\
```

```
mdb.models['Model-1'].rootAssembly.instances['Exterior-Tensile-Wire-1-rad-38'].edges.getSequenceFromMask(
```

```
mask=(['#20000 ], ), )+\
```

```
mdb.models['Model-1'].rootAssembly.instances['Exterior-Tensile-Wire-1-rad-37'].edges.getSequenceFromMask(
```

```
mask=(['#20000 ], ), )+\
```

```
mdb.models['Model-1'].rootAssembly.instances['Exterior-Tensile-Wire-1-rad-36'].edges.getSequenceFromMask(
```

```
mask=(['#20000 ], ), )+\
```

```
mdb.models['Model-1'].rootAssembly.instances['Exterior-Tensile-Wire-1-rad-35'].edges.getSequenceFromMask(
```

```
mask=(['#20000 ], ), )+\
```

```
mdb.models['Model-1'].rootAssembly.instances['Exterior-Tensile-Wire-1-rad-34'].edges.getSequenceFromMask(
```

```
mask=(['#20000 ], ), )+\
```

```
mdb.models['Model-1'].rootAssembly.instances['Exterior-Tensile-Wire-1-rad-33'].edges.getSequenceFromMask(
```

```
mask=(['#20000 ], ), )+\
```

```
mdb.models['Model-1'].rootAssembly.instances['Exterior-Tensile-Wire-1-rad-32'].edges.getSequenceFromMask(
```

```
mask=(['#20000 ], ), )+\
```

```
mdb.models['Model-1'].rootAssembly.instances['Exterior-Tensile-Wire-1-rad-31'].edges.getSequenceFromMask(
```

```
mask=(['#20000 ], ), )+\
```

```
mdb.models['Model-1'].rootAssembly.instances['Exterior-Tensile-Wire-1-rad-30'].edges.getSequenceFromMask(
```

```
mask=(['#20000 ], ), )+\
```

```
mdb.models['Model-1'].rootAssembly.instances['Exterior-Tensile-Wire-1-rad-29'].edges.getSequenceFromMask(
```

```
mask=(['#20000 ], ), )+\
```

```
mdb.models['Model-1'].rootAssembly.instances['Exterior-Tensile-Wire-1-rad-28'].edges.getSequenceFromMask(
```

```
mask=(['#20000 ], ), )+\
```

```
mdb.models['Model-1'].rootAssembly.instances['Exterior-Tensile-Wire-1-rad-27'].edges.getSequenceFromMask(
```

```
mask=(['#20000 ], ), )+\
```

```
mdb.models['Model-1'].rootAssembly.instances['Exterior-Tensile-Wire-1-rad-26'].edges.getSequenceFromMask(
```

```
mask=(['#20000 ], ), )+\
```

```
mdb.models['Model-1'].rootAssembly.instances['Exterior-Tensile-Wire-1-rad-25'].edges.getSequenceFromMask(
```

```
mask=(['#20000 ], ), )+\
```

```
mdb.models['Model-1'].rootAssembly.instances['Exterior-Tensile-Wire-1-rad-24'].edges.getSequenceFromMask(
```

```
mask=(['#20000 ], ), )+\
```

```
mdb.models['Model-1'].rootAssembly.instances['Exterior-Tensile-Wire-1-rad-23'].edges.getSequenceFromMask(
```

```
mask=(['#20000 ], ), )+\
```

```
mdb.models['Model-1'].rootAssembly.instances['Exterior-Tensile-Wire-1-rad-19'].edges.getSequenceFromMask(
```

```
mask=(['#20000 ], ), )+\
```

```
mdb.models['Model-1'].rootAssembly.instances['Exterior-Tensile-Wire-1-rad-20'].edges.getSequenceFromMask(
```

```
mask=(['#20000 ], ), )+\
```

```
mdb.models['Model-1'].rootAssembly.instances['Exterior-Tensile-Wire-1-rad-21'].edges.getSequenceFromMask(
```

```
mask=(['#20000 ], ), )+\
```

```
mdb.models['Model-1'].rootAssembly.instances['Exterior-Tensile-Wire-1-rad-22'].edges.getSequenceFromMask(
```

```
mask=(['#20000 ], ), )+\
```

```
mdb.models['Model-1'].rootAssembly.instances['Exterior-Tensile-Wire-1-rad-44'].edges.getSequenceFromMask(
```

```
mask=(['#20000 ], ), )+\
```

```
mdb.models['Model-1'].rootAssembly.instances['Exterior-Tensile-Wire-1-rad-45'].edges.getSequenceFromMask(
```

```
mask=(['#20000 ], ), )+\
```

```
mdb.models['Model-1'].rootAssembly.instances['Exterior-Tensile-Wire-1-rad-46'].edges.getSequenceFromMask(
```

```
mask=(['#20000 ], ), )+\
```

```
mdb.models['Model-1'].rootAssembly.instances['Exterior-Tensile-Wire-1-rad-47'].edges.getSequenceFromMask(
```

```
mask=(['#20000 ], ), )+\
```

```
mdb.models['Model-1'].rootAssembly.instances['Exterior-Tensile-Wire-1-rad-48'].edges.getSequenceFromMask(
```

```
mask=(['#20000 ], ), )+\
```

```
mdb.models['Model-1'].rootAssembly.instances['Exterior-Tensile-Wire-1-rad-49'].edges.getSequenceFromMask(
```

```
mask=(['#20000 ], ), )+\
```

```

mdb.models['Model-1'].rootAssembly.instances['Exterior-Tensile-Wire-1-rad-
50'].edges.getSequenceFromMask(
    mask=('[#20000 ]', ), )+\

mdb.models['Model-1'].rootAssembly.instances['Exterior-Tensile-Wire-1-rad-
51'].edges.getSequenceFromMask(
    mask=('[#20000 ]', ), ))

mdb.models['Model-1'].rootAssembly.Surface(name='Ext-Fixed', side1Edges=
    mdb.models['Model-1'].rootAssembly.instances['Exterior-Tensile-Wire-1-rad-
12'].edges.getSequenceFromMask(
    mask=('[#100 ]', ), )+\

    mdb.models['Model-1'].rootAssembly.instances['Exterior-Tensile-Wire-1-rad-
11'].edges.getSequenceFromMask(
    mask=('[#100 ]', ), )+\

    mdb.models['Model-1'].rootAssembly.instances['Exterior-Tensile-Wire-1-rad-
10'].edges.getSequenceFromMask(
    mask=('[#100 ]', ), )+\

    mdb.models['Model-1'].rootAssembly.instances['Exterior-Tensile-Wire-1-rad-
13'].edges.getSequenceFromMask(
    mask=('[#100 ]', ), )+\

    mdb.models['Model-1'].rootAssembly.instances['Exterior-Tensile-Wire-1-rad-
14'].edges.getSequenceFromMask(
    mask=('[#100 ]', ), )+\

    mdb.models['Model-1'].rootAssembly.instances['Exterior-Tensile-Wire-1-rad-
15'].edges.getSequenceFromMask(

```

```

mask=(['#100 '], ), )+\

mdb.models['Model-1'].rootAssembly.instances['Exterior-Tensile-Wire-1-rad-
16'].edges.getSequenceFromMask(

mask=(['#100 '], ), )+\

mdb.models['Model-1'].rootAssembly.instances['Exterior-Tensile-Wire-1-rad-
17'].edges.getSequenceFromMask(

mask=(['#100 '], ), )+\

mdb.models['Model-1'].rootAssembly.instances['Exterior-Tensile-Wire-1-rad-
18'].edges.getSequenceFromMask(

mask=(['#100 '], ), )+\

mdb.models['Model-1'].rootAssembly.instances['Exterior-Tensile-Wire-1-rad-
19'].edges.getSequenceFromMask(

mask=(['#100 '], ), )+\

mdb.models['Model-1'].rootAssembly.instances['Exterior-Tensile-Wire-1-rad-
20'].edges.getSequenceFromMask(

mask=(['#100 '], ), )+\

mdb.models['Model-1'].rootAssembly.instances['Exterior-Tensile-Wire-1-rad-
21'].edges.getSequenceFromMask(

mask=(['#100 '], ), )+\

mdb.models['Model-1'].rootAssembly.instances['Exterior-Tensile-Wire-1-rad-
22'].edges.getSequenceFromMask(

mask=(['#100 '], ), )+\

mdb.models['Model-1'].rootAssembly.instances['Exterior-Tensile-Wire-1-rad-
23'].edges.getSequenceFromMask(

```

```

mask=(['#100 '], ), )+\

mdb.models['Model-1'].rootAssembly.instances['Exterior-Tensile-Wire-1-rad-
24'].edges.getSequenceFromMask(

mask=(['#100 '], ), )+\

mdb.models['Model-1'].rootAssembly.instances['Exterior-Tensile-Wire-1-rad-
25'].edges.getSequenceFromMask(

mask=(['#100 '], ), )+\

mdb.models['Model-1'].rootAssembly.instances['Exterior-Tensile-Wire-1-rad-
26'].edges.getSequenceFromMask(

mask=(['#100 '], ), )+\

mdb.models['Model-1'].rootAssembly.instances['Exterior-Tensile-Wire-1-rad-
27'].edges.getSequenceFromMask(

mask=(['#100 '], ), )+\

mdb.models['Model-1'].rootAssembly.instances['Exterior-Tensile-Wire-1-rad-
37'].edges.getSequenceFromMask(

mask=(['#100 '], ), )+\

mdb.models['Model-1'].rootAssembly.instances['Exterior-Tensile-Wire-1-rad-
38'].edges.getSequenceFromMask(

mask=(['#100 '], ), )+\

mdb.models['Model-1'].rootAssembly.instances['Exterior-Tensile-Wire-1-rad-
39'].edges.getSequenceFromMask(

mask=(['#100 '], ), )+\

mdb.models['Model-1'].rootAssembly.instances['Exterior-Tensile-Wire-1-rad-
40'].edges.getSequenceFromMask(

```

```

mask=(['#100 '], ), )+\

mdb.models['Model-1'].rootAssembly.instances['Exterior-Tensile-Wire-1-rad-
41'].edges.getSequenceFromMask(

mask=(['#100 '], ), )+\

mdb.models['Model-1'].rootAssembly.instances['Exterior-Tensile-Wire-1-rad-
42'].edges.getSequenceFromMask(

mask=(['#100 '], ), )+\

mdb.models['Model-1'].rootAssembly.instances['Exterior-Tensile-Wire-1-rad-
43'].edges.getSequenceFromMask(

mask=(['#100 '], ), )+\

mdb.models['Model-1'].rootAssembly.instances['Exterior-Tensile-Wire-1-rad-
44'].edges.getSequenceFromMask(

mask=(['#100 '], ), )+\

mdb.models['Model-1'].rootAssembly.instances['Exterior-Tensile-Wire-1-rad-
45'].edges.getSequenceFromMask(

mask=(['#100 '], ), )+\

mdb.models['Model-1'].rootAssembly.instances['Exterior-Tensile-Wire-1-rad-
46'].edges.getSequenceFromMask(

mask=(['#100 '], ), )+\

mdb.models['Model-1'].rootAssembly.instances['Exterior-Tensile-Wire-1-rad-
47'].edges.getSequenceFromMask(

mask=(['#100 '], ), )+\

mdb.models['Model-1'].rootAssembly.instances['Exterior-Tensile-Wire-1-rad-
48'].edges.getSequenceFromMask(

```

```

mask=(['#100 '], ), )+\

mdb.models['Model-1'].rootAssembly.instances['Exterior-Tensile-Wire-1-rad-
49'].edges.getSequenceFromMask(

mask=(['#100 '], ), )+\

mdb.models['Model-1'].rootAssembly.instances['Exterior-Tensile-Wire-1-rad-
50'].edges.getSequenceFromMask(

mask=(['#100 '], ), )+\

mdb.models['Model-1'].rootAssembly.instances['Exterior-Tensile-Wire-1-rad-
51'].edges.getSequenceFromMask(

mask=(['#100 '], ), )+\

mdb.models['Model-1'].rootAssembly.instances['Exterior-Tensile-Wire-1-rad-
52'].edges.getSequenceFromMask(

mask=(['#100 '], ), )+\

mdb.models['Model-1'].rootAssembly.instances['Exterior-Tensile-Wire-1-rad-
53'].edges.getSequenceFromMask(

mask=(['#100 '], ), )+\

mdb.models['Model-1'].rootAssembly.instances['Exterior-Tensile-Wire-1-rad-
54'].edges.getSequenceFromMask(

mask=(['#100 '], ), )+\

mdb.models['Model-1'].rootAssembly.instances['Exterior-Tensile-Wire-
1'].edges.getSequenceFromMask(

mask=(['#100 '], ), )+\

mdb.models['Model-1'].rootAssembly.instances['Exterior-Tensile-Wire-1-rad-
2'].edges.getSequenceFromMask(

```

```
mask=('[#100 ]', ), )+\

mdb.models['Model-1'].rootAssembly.instances['Exterior-Tensile-Wire-1-rad-3'].edges.getSequenceFromMask(

mask=('[#100 ]', ), )+\

mdb.models['Model-1'].rootAssembly.instances['Exterior-Tensile-Wire-1-rad-4'].edges.getSequenceFromMask(

mask=('[#100 ]', ), )+\

mdb.models['Model-1'].rootAssembly.instances['Exterior-Tensile-Wire-1-rad-5'].edges.getSequenceFromMask(

mask=('[#100 ]', ), )+\

mdb.models['Model-1'].rootAssembly.instances['Exterior-Tensile-Wire-1-rad-28'].edges.getSequenceFromMask(

mask=('[#100 ]', ), )+\

mdb.models['Model-1'].rootAssembly.instances['Exterior-Tensile-Wire-1-rad-30'].edges.getSequenceFromMask(

mask=('[#100 ]', ), )+\

mdb.models['Model-1'].rootAssembly.instances['Exterior-Tensile-Wire-1-rad-29'].edges.getSequenceFromMask(

mask=('[#100 ]', ), )+\

mdb.models['Model-1'].rootAssembly.instances['Exterior-Tensile-Wire-1-rad-31'].edges.getSequenceFromMask(

mask=('[#100 ]', ), )+\

mdb.models['Model-1'].rootAssembly.instances['Exterior-Tensile-Wire-1-rad-32'].edges.getSequenceFromMask(
```

```

mask=(['#100 '], ), )+\

mdb.models['Model-1'].rootAssembly.instances['Exterior-Tensile-Wire-1-rad-
33'].edges.getSequenceFromMask(

mask=(['#100 '], ), )+\

mdb.models['Model-1'].rootAssembly.instances['Exterior-Tensile-Wire-1-rad-
34'].edges.getSequenceFromMask(

mask=(['#100 '], ), )+\

mdb.models['Model-1'].rootAssembly.instances['Exterior-Tensile-Wire-1-rad-
35'].edges.getSequenceFromMask(

mask=(['#100 '], ), )+\

mdb.models['Model-1'].rootAssembly.instances['Exterior-Tensile-Wire-1-rad-
36'].edges.getSequenceFromMask(

mask=(['#100 '], ), )+\

mdb.models['Model-1'].rootAssembly.instances['Exterior-Tensile-Wire-1-rad-
6'].edges.getSequenceFromMask(

mask=(['#100 '], ), )+\

mdb.models['Model-1'].rootAssembly.instances['Exterior-Tensile-Wire-1-rad-
7'].edges.getSequenceFromMask(

mask=(['#100 '], ), )+\

mdb.models['Model-1'].rootAssembly.instances['Exterior-Tensile-Wire-1-rad-
8'].edges.getSequenceFromMask(

mask=(['#100 '], ), )+\

mdb.models['Model-1'].rootAssembly.instances['Exterior-Tensile-Wire-1-rad-
9'].edges.getSequenceFromMask(

```

```

mask=(['#100 '], ), )
del mdb.models['Model-1'].parts['Interior-Tensile-Wire'].sets['int-part-end']
mdb.models['Model-1'].rootAssembly.regenerate()
mdb.models['Model-1'].rootAssembly.Surface(name='Int-Fixed', side1Edges=
    mdb.models['Model-1'].rootAssembly.instances['Interior-Tensile-Wire-1-rad-
35'].edges.getSequenceFromMask(
    mask=(['#20000 '], ), )+\
    mdb.models['Model-1'].rootAssembly.instances['Interior-Tensile-Wire-1-rad-
34'].edges.getSequenceFromMask(
    mask=(['#20000 '], ), )+\
    mdb.models['Model-1'].rootAssembly.instances['Interior-Tensile-Wire-1-rad-
33'].edges.getSequenceFromMask(
    mask=(['#20000 '], ), )+\
    mdb.models['Model-1'].rootAssembly.instances['Interior-Tensile-Wire-1-rad-
31'].edges.getSequenceFromMask(
    mask=(['#20000 '], ), )+\
    mdb.models['Model-1'].rootAssembly.instances['Interior-Tensile-Wire-1-rad-
32'].edges.getSequenceFromMask(
    mask=(['#20000 '], ), )+\
    mdb.models['Model-1'].rootAssembly.instances['Interior-Tensile-Wire-1-rad-
30'].edges.getSequenceFromMask(
    mask=(['#20000 '], ), )+\

```

```
mdb.models['Model-1'].rootAssembly.instances['Interior-Tensile-Wire-1-rad-29'].edges.getSequenceFromMask(
```

```
mask=(['#20000 ], ), )+\
```

```
mdb.models['Model-1'].rootAssembly.instances['Interior-Tensile-Wire-1-rad-28'].edges.getSequenceFromMask(
```

```
mask=(['#20000 ], ), )+\
```

```
mdb.models['Model-1'].rootAssembly.instances['Interior-Tensile-Wire-1-rad-27'].edges.getSequenceFromMask(
```

```
mask=(['#20000 ], ), )+\
```

```
mdb.models['Model-1'].rootAssembly.instances['Interior-Tensile-Wire-1-rad-26'].edges.getSequenceFromMask(
```

```
mask=(['#20000 ], ), )+\
```

```
mdb.models['Model-1'].rootAssembly.instances['Interior-Tensile-Wire-1-rad-25'].edges.getSequenceFromMask(
```

```
mask=(['#20000 ], ), )+\
```

```
mdb.models['Model-1'].rootAssembly.instances['Interior-Tensile-Wire-1-rad-36'].edges.getSequenceFromMask(
```

```
mask=(['#20000 ], ), )+\
```

```
mdb.models['Model-1'].rootAssembly.instances['Interior-Tensile-Wire-1-rad-37'].edges.getSequenceFromMask(
```

```
mask=(['#20000 ], ), )+\
```

```
mdb.models['Model-1'].rootAssembly.instances['Interior-Tensile-Wire-1-rad-38'].edges.getSequenceFromMask(
```

```
mask=(['#20000 ], ), )+\
```

```
mdb.models['Model-1'].rootAssembly.instances['Interior-Tensile-Wire-1-rad-39'].edges.getSequenceFromMask(
```

```
mask=(['#20000 '], ), )+\
```

```
mdb.models['Model-1'].rootAssembly.instances['Interior-Tensile-Wire-1-rad-40'].edges.getSequenceFromMask(
```

```
mask=(['#20000 '], ), )+\
```

```
mdb.models['Model-1'].rootAssembly.instances['Interior-Tensile-Wire-1-rad-41'].edges.getSequenceFromMask(
```

```
mask=(['#20000 '], ), )+\
```

```
mdb.models['Model-1'].rootAssembly.instances['Interior-Tensile-Wire-1-rad-42'].edges.getSequenceFromMask(
```

```
mask=(['#20000 '], ), )+\
```

```
mdb.models['Model-1'].rootAssembly.instances['Interior-Tensile-Wire-1-rad-43'].edges.getSequenceFromMask(
```

```
mask=(['#20000 '], ), )+\
```

```
mdb.models['Model-1'].rootAssembly.instances['Interior-Tensile-Wire-1-rad-44'].edges.getSequenceFromMask(
```

```
mask=(['#20000 '], ), )+\
```

```
mdb.models['Model-1'].rootAssembly.instances['Interior-Tensile-Wire-1-rad-49'].edges.getSequenceFromMask(
```

```
mask=(['#20000 '], ), )+\
```

```
mdb.models['Model-1'].rootAssembly.instances['Interior-Tensile-Wire-1-rad-50'].edges.getSequenceFromMask(
```

```
mask=(['#20000 '], ), )+\
```

```
mdb.models['Model-1'].rootAssembly.instances['Interior-Tensile-Wire-1-rad-51'].edges.getSequenceFromMask(
```

```
mask=(['#20000 ], ), )+\
```

```
mdb.models['Model-1'].rootAssembly.instances['Interior-Tensile-Wire-1-rad-52'].edges.getSequenceFromMask(
```

```
mask=(['#20000 ], ), )+\
```

```
mdb.models['Model-1'].rootAssembly.instances['Interior-Tensile-Wire-1'].edges.getSequenceFromMask(
```

```
mask=(['#20000 ], ), )+\
```

```
mdb.models['Model-1'].rootAssembly.instances['Interior-Tensile-Wire-1-rad-2'].edges.getSequenceFromMask(
```

```
mask=(['#20000 ], ), )+\
```

```
mdb.models['Model-1'].rootAssembly.instances['Interior-Tensile-Wire-1-rad-3'].edges.getSequenceFromMask(
```

```
mask=(['#20000 ], ), )+\
```

```
mdb.models['Model-1'].rootAssembly.instances['Interior-Tensile-Wire-1-rad-4'].edges.getSequenceFromMask(
```

```
mask=(['#20000 ], ), )+\
```

```
mdb.models['Model-1'].rootAssembly.instances['Interior-Tensile-Wire-1-rad-5'].edges.getSequenceFromMask(
```

```
mask=(['#20000 ], ), )+\
```

```
mdb.models['Model-1'].rootAssembly.instances['Interior-Tensile-Wire-1-rad-6'].edges.getSequenceFromMask(
```

```
mask=(['#20000 ], ), )+\
```

```
    mdb.models['Model-1'].rootAssembly.instances['Interior-Tensile-Wire-1-rad-7'].edges.getSequenceFromMask(  
    mask=('[#20000 ]', ), )+\n  
    mdb.models['Model-1'].rootAssembly.instances['Interior-Tensile-Wire-1-rad-8'].edges.getSequenceFromMask(  
    mask=('[#20000 ]', ), )+\n  
    mdb.models['Model-1'].rootAssembly.instances['Interior-Tensile-Wire-1-rad-9'].edges.getSequenceFromMask(  
    mask=('[#20000 ]', ), )+\n  
    mdb.models['Model-1'].rootAssembly.instances['Interior-Tensile-Wire-1-rad-10'].edges.getSequenceFromMask(  
    mask=('[#20000 ]', ), )+\n  
    mdb.models['Model-1'].rootAssembly.instances['Interior-Tensile-Wire-1-rad-11'].edges.getSequenceFromMask(  
    mask=('[#20000 ]', ), )+\n  
    mdb.models['Model-1'].rootAssembly.instances['Interior-Tensile-Wire-1-rad-12'].edges.getSequenceFromMask(  
    mask=('[#20000 ]', ), )+\n  
    mdb.models['Model-1'].rootAssembly.instances['Interior-Tensile-Wire-1-rad-13'].edges.getSequenceFromMask(  
    mask=('[#20000 ]', ), )+\n  
    mdb.models['Model-1'].rootAssembly.instances['Interior-Tensile-Wire-1-rad-14'].edges.getSequenceFromMask(  
    mask=('[#20000 ]', ), )+\n
```

```
mdb.models['Model-1'].rootAssembly.instances['Interior-Tensile-Wire-1-rad-45'].edges.getSequenceFromMask(
```

```
mask=(['#20000 ], ), )+\
```

```
mdb.models['Model-1'].rootAssembly.instances['Interior-Tensile-Wire-1-rad-46'].edges.getSequenceFromMask(
```

```
mask=(['#20000 ], ), )+\
```

```
mdb.models['Model-1'].rootAssembly.instances['Interior-Tensile-Wire-1-rad-47'].edges.getSequenceFromMask(
```

```
mask=(['#20000 ], ), )+\
```

```
mdb.models['Model-1'].rootAssembly.instances['Interior-Tensile-Wire-1-rad-48'].edges.getSequenceFromMask(
```

```
mask=(['#20000 ], ), )+\
```

```
mdb.models['Model-1'].rootAssembly.instances['Interior-Tensile-Wire-1-rad-15'].edges.getSequenceFromMask(
```

```
mask=(['#20000 ], ), )+\
```

```
mdb.models['Model-1'].rootAssembly.instances['Interior-Tensile-Wire-1-rad-16'].edges.getSequenceFromMask(
```

```
mask=(['#20000 ], ), )+\
```

```
mdb.models['Model-1'].rootAssembly.instances['Interior-Tensile-Wire-1-rad-17'].edges.getSequenceFromMask(
```

```
mask=(['#20000 ], ), )+\
```

```
mdb.models['Model-1'].rootAssembly.instances['Interior-Tensile-Wire-1-rad-18'].edges.getSequenceFromMask(
```

```
mask=(['#20000 ], ), )+\
```

```

mdb.models['Model-1'].rootAssembly.instances['Interior-Tensile-Wire-1-rad-
19'].edges.getSequenceFromMask(
    mask=('[#20000 ]', ), )+\

mdb.models['Model-1'].rootAssembly.instances['Interior-Tensile-Wire-1-rad-
20'].edges.getSequenceFromMask(
    mask=('[#20000 ]', ), )+\

mdb.models['Model-1'].rootAssembly.instances['Interior-Tensile-Wire-1-rad-
21'].edges.getSequenceFromMask(
    mask=('[#20000 ]', ), )+\

mdb.models['Model-1'].rootAssembly.instances['Interior-Tensile-Wire-1-rad-
22'].edges.getSequenceFromMask(
    mask=('[#20000 ]', ), )+\

mdb.models['Model-1'].rootAssembly.instances['Interior-Tensile-Wire-1-rad-
23'].edges.getSequenceFromMask(
    mask=('[#20000 ]', ), )+\

mdb.models['Model-1'].rootAssembly.instances['Interior-Tensile-Wire-1-rad-
24'].edges.getSequenceFromMask(
    mask=('[#20000 ]', ), ))

mdb.models['Model-1'].rootAssembly.Surface(name='Int-Moving', side1Edges=

    mdb.models['Model-1'].rootAssembly.instances['Interior-Tensile-Wire-1-rad-
34'].edges.getSequenceFromMask(
    mask=('[#100 ]', ), )+\

    mdb.models['Model-1'].rootAssembly.instances['Interior-Tensile-Wire-1-rad-
35'].edges.getSequenceFromMask(

```

```
mask=('[#100 ]', ), )+\

mdb.models['Model-1'].rootAssembly.instances['Interior-Tensile-Wire-1-rad-
36'].edges.getSequenceFromMask(

mask=('[#100 ]', ), )+\

mdb.models['Model-1'].rootAssembly.instances['Interior-Tensile-Wire-1-rad-
37'].edges.getSequenceFromMask(

mask=('[#100 ]', ), )+\

mdb.models['Model-1'].rootAssembly.instances['Interior-Tensile-Wire-1-rad-
38'].edges.getSequenceFromMask(

mask=('[#100 ]', ), )+\

mdb.models['Model-1'].rootAssembly.instances['Interior-Tensile-Wire-1-rad-
39'].edges.getSequenceFromMask(

mask=('[#100 ]', ), )+\

mdb.models['Model-1'].rootAssembly.instances['Interior-Tensile-Wire-1-rad-
40'].edges.getSequenceFromMask(

mask=('[#100 ]', ), )+\

mdb.models['Model-1'].rootAssembly.instances['Interior-Tensile-Wire-1-rad-
41'].edges.getSequenceFromMask(

mask=('[#100 ]', ), )+\

mdb.models['Model-1'].rootAssembly.instances['Interior-Tensile-Wire-1-rad-
42'].edges.getSequenceFromMask(

mask=('[#100 ]', ), )+\

mdb.models['Model-1'].rootAssembly.instances['Interior-Tensile-Wire-1-rad-
43'].edges.getSequenceFromMask(
```

```
mask=(['#100 '], ), )+\

mdb.models['Model-1'].rootAssembly.instances['Interior-Tensile-Wire-1-rad-44'].edges.getSequenceFromMask(

mask=(['#100 '], ), )+\

mdb.models['Model-1'].rootAssembly.instances['Interior-Tensile-Wire-1-rad-45'].edges.getSequenceFromMask(

mask=(['#100 '], ), )+\

mdb.models['Model-1'].rootAssembly.instances['Interior-Tensile-Wire-1-rad-46'].edges.getSequenceFromMask(

mask=(['#100 '], ), )+\

mdb.models['Model-1'].rootAssembly.instances['Interior-Tensile-Wire-1-rad-47'].edges.getSequenceFromMask(

mask=(['#100 '], ), )+\

mdb.models['Model-1'].rootAssembly.instances['Interior-Tensile-Wire-1-rad-48'].edges.getSequenceFromMask(

mask=(['#100 '], ), )+\

mdb.models['Model-1'].rootAssembly.instances['Interior-Tensile-Wire-1-rad-49'].edges.getSequenceFromMask(

mask=(['#100 '], ), )+\

mdb.models['Model-1'].rootAssembly.instances['Interior-Tensile-Wire-1-rad-33'].edges.getSequenceFromMask(

mask=(['#100 '], ), )+\

mdb.models['Model-1'].rootAssembly.instances['Interior-Tensile-Wire-1-rad-32'].edges.getSequenceFromMask(
```

```
mask=(['#100 '], ), )+\

mdb.models['Model-1'].rootAssembly.instances['Interior-Tensile-Wire-1-rad-31'].edges.getSequenceFromMask(

mask=(['#100 '], ), )+\

mdb.models['Model-1'].rootAssembly.instances['Interior-Tensile-Wire-1-rad-23'].edges.getSequenceFromMask(

mask=(['#100 '], ), )+\

mdb.models['Model-1'].rootAssembly.instances['Interior-Tensile-Wire-1-rad-22'].edges.getSequenceFromMask(

mask=(['#100 '], ), )+\

mdb.models['Model-1'].rootAssembly.instances['Interior-Tensile-Wire-1-rad-21'].edges.getSequenceFromMask(

mask=(['#100 '], ), )+\

mdb.models['Model-1'].rootAssembly.instances['Interior-Tensile-Wire-1-rad-20'].edges.getSequenceFromMask(

mask=(['#100 '], ), )+\

mdb.models['Model-1'].rootAssembly.instances['Interior-Tensile-Wire-1-rad-19'].edges.getSequenceFromMask(

mask=(['#100 '], ), )+\

mdb.models['Model-1'].rootAssembly.instances['Interior-Tensile-Wire-1-rad-18'].edges.getSequenceFromMask(

mask=(['#100 '], ), )+\

mdb.models['Model-1'].rootAssembly.instances['Interior-Tensile-Wire-1-rad-17'].edges.getSequenceFromMask(
```

```

mask=(['#100 '], ), )+\

mdb.models['Model-1'].rootAssembly.instances['Interior-Tensile-Wire-1-rad-
16'].edges.getSequenceFromMask(

mask=(['#100 '], ), )+\

mdb.models['Model-1'].rootAssembly.instances['Interior-Tensile-Wire-1-rad-
15'].edges.getSequenceFromMask(

mask=(['#100 '], ), )+\

mdb.models['Model-1'].rootAssembly.instances['Interior-Tensile-Wire-1-rad-
14'].edges.getSequenceFromMask(

mask=(['#100 '], ), )+\

mdb.models['Model-1'].rootAssembly.instances['Interior-Tensile-Wire-1-rad-
13'].edges.getSequenceFromMask(

mask=(['#100 '], ), )+\

mdb.models['Model-1'].rootAssembly.instances['Interior-Tensile-Wire-1-rad-
12'].edges.getSequenceFromMask(

mask=(['#100 '], ), )+\

mdb.models['Model-1'].rootAssembly.instances['Interior-Tensile-Wire-1-rad-
11'].edges.getSequenceFromMask(

mask=(['#100 '], ), )+\

mdb.models['Model-1'].rootAssembly.instances['Interior-Tensile-Wire-1-rad-
10'].edges.getSequenceFromMask(

mask=(['#100 '], ), )+\

mdb.models['Model-1'].rootAssembly.instances['Interior-Tensile-Wire-1-rad-
9'].edges.getSequenceFromMask(

```

```

mask=(['#100 '], ), )+\

mdb.models['Model-1'].rootAssembly.instances['Interior-Tensile-Wire-1-rad-
8'].edges.getSequenceFromMask(

mask=(['#100 '], ), )+\

mdb.models['Model-1'].rootAssembly.instances['Interior-Tensile-Wire-1-rad-
7'].edges.getSequenceFromMask(

mask=(['#100 '], ), )+\

mdb.models['Model-1'].rootAssembly.instances['Interior-Tensile-Wire-1-rad-
6'].edges.getSequenceFromMask(

mask=(['#100 '], ), )+\

mdb.models['Model-1'].rootAssembly.instances['Interior-Tensile-Wire-1-rad-
5'].edges.getSequenceFromMask(

mask=(['#100 '], ), )+\

mdb.models['Model-1'].rootAssembly.instances['Interior-Tensile-Wire-1-rad-
4'].edges.getSequenceFromMask(

mask=(['#100 '], ), )+\

mdb.models['Model-1'].rootAssembly.instances['Interior-Tensile-Wire-1-rad-
50'].edges.getSequenceFromMask(

mask=(['#100 '], ), )+\

mdb.models['Model-1'].rootAssembly.instances['Interior-Tensile-Wire-1-rad-
51'].edges.getSequenceFromMask(

mask=(['#100 '], ), )+\

mdb.models['Model-1'].rootAssembly.instances['Interior-Tensile-Wire-1-rad-
52'].edges.getSequenceFromMask(

```

```
mask=(['#100 '], ), )+\

mdb.models['Model-1'].rootAssembly.instances['Interior-Tensile-Wire-
1'].edges.getSequenceFromMask(

mask=(['#100 '], ), )+\

mdb.models['Model-1'].rootAssembly.instances['Interior-Tensile-Wire-1-rad-
2'].edges.getSequenceFromMask(

mask=(['#100 '], ), )+\

mdb.models['Model-1'].rootAssembly.instances['Interior-Tensile-Wire-1-rad-
3'].edges.getSequenceFromMask(

mask=(['#100 '], ), )+\

mdb.models['Model-1'].rootAssembly.instances['Interior-Tensile-Wire-1-rad-
30'].edges.getSequenceFromMask(

mask=(['#100 '], ), )+\

mdb.models['Model-1'].rootAssembly.instances['Interior-Tensile-Wire-1-rad-
29'].edges.getSequenceFromMask(

mask=(['#100 '], ), )+\

mdb.models['Model-1'].rootAssembly.instances['Interior-Tensile-Wire-1-rad-
28'].edges.getSequenceFromMask(

mask=(['#100 '], ), )+\

mdb.models['Model-1'].rootAssembly.instances['Interior-Tensile-Wire-1-rad-
27'].edges.getSequenceFromMask(

mask=(['#100 '], ), )+\

mdb.models['Model-1'].rootAssembly.instances['Interior-Tensile-Wire-1-rad-
26'].edges.getSequenceFromMask(
```

```

mask=('[#100 ]', ), )+\

mdb.models['Model-1'].rootAssembly.instances['Interior-Tensile-Wire-1-rad-
25'].edges.getSequenceFromMask(

mask=('[#100 ]', ), )+\

mdb.models['Model-1'].rootAssembly.instances['Interior-Tensile-Wire-1-rad-
24'].edges.getSequenceFromMask(

mask=('[#100 ]', ), ))

mdb.models['Model-1'].rootAssembly.Surface(name='Cyl-Moving', side1Edges=

mdb.models['Model-1'].rootAssembly.instances['External-Plastic-Sheath-
1'].edges.getSequenceFromMask(

mask=('[#1 ]', ), )+\

mdb.models['Model-1'].rootAssembly.instances['Anti-Birdcaging-Tape-
1'].edges.getSequenceFromMask(

mask=('[#1 ]', ), )+\

mdb.models['Model-1'].rootAssembly.instances['Exterior-Anti-Wear-Tape-
1'].edges.getSequenceFromMask(

mask=('[#1 ]', ), )+\

mdb.models['Model-1'].rootAssembly.instances['Interior-Anti-Wear-Tape-
1'].edges.getSequenceFromMask(

mask=('[#1 ]', ), )+\

mdb.models['Model-1'].rootAssembly.instances['Pressure-Armour-
1'].edges.getSequenceFromMask(

mask=('[#1 ]', ), )+\

```

```

mdb.models['Model-1'].rootAssembly.instances['Interior-Plastic-Sheath-
1'].edges.getSequenceFromMask(
    mask=('[#1 ]', ), )+\
mdb.models['Model-1'].rootAssembly.instances['Carcass-1'].edges.getSequenceFromMask(
    mask=('[#1 ]', ), ))
mdb.models['Model-1'].rootAssembly.Surface(name='Cyl-Fixed', side1Edges=
    mdb.models['Model-1'].rootAssembly.instances['Carcass-1'].edges.getSequenceFromMask(
        mask=('[#2 ]', ), )+\
        mdb.models['Model-1'].rootAssembly.instances['Interior-Plastic-Sheath-
1'].edges.getSequenceFromMask(
            mask=('[#2 ]', ), )+\
            mdb.models['Model-1'].rootAssembly.instances['Pressure-Armour-
1'].edges.getSequenceFromMask(
                mask=('[#2 ]', ), )+\
                mdb.models['Model-1'].rootAssembly.instances['Interior-Anti-Wear-Tape-
1'].edges.getSequenceFromMask(
                    mask=('[#2 ]', ), )+\
                    mdb.models['Model-1'].rootAssembly.instances['Exterior-Anti-Wear-Tape-
1'].edges.getSequenceFromMask(
                        mask=('[#2 ]', ), )+\
                        mdb.models['Model-1'].rootAssembly.instances['Anti-Birdcaging-Tape-
1'].edges.getSequenceFromMask(
                            mask=('[#2 ]', ), )+\

```

```
mdb.models['Model-1'].rootAssembly.instances['External-Plastic-Sheath-1'].edges.getSequenceFromMask(  
    mask=('#2 ], ), )
```

```
#####Coupling
```

```
Definition#####
```

```
mdb.models['Model-1'].Coupling(controlPoint=  
    mdb.models['Model-1'].rootAssembly.sets['RF-Moving'], couplingType=  
    KINEMATIC, influenceRadius=WHOLE_SURFACE, localCsys=None, name=  
    'Constraint-1', surface=  
    mdb.models['Model-1'].rootAssembly-surfaces['Cyl-Moving'], u1=ON, u2=ON,  
    u3=ON, ur1=ON, ur2=ON, ur3=ON)
```

```
mdb.models['Model-1'].Coupling(controlPoint=  
    mdb.models['Model-1'].rootAssembly.sets['RF-Moving'], couplingType=  
    KINEMATIC, influenceRadius=WHOLE_SURFACE, localCsys=None, name=  
    'Constraint-2', surface=  
    mdb.models['Model-1'].rootAssembly-surfaces['Int-Moving'], u1=ON, u2=ON,  
    u3=ON, ur1=ON, ur2=ON, ur3=ON)
```

```
mdb.models['Model-1'].Coupling(controlPoint=  
    mdb.models['Model-1'].rootAssembly.sets['RF-Moving'], couplingType=  
    KINEMATIC, influenceRadius=WHOLE_SURFACE, localCsys=None, name=  
    'Constraint-3', surface=  
    mdb.models['Model-1'].rootAssembly-surfaces['Ext-Moving'], u1=ON, u2=ON,
```

u3=ON, ur1=ON, ur2=ON, ur3=ON)

```
mdb.models['Model-1'].Coupling(controlPoint=  
    mdb.models['Model-1'].rootAssembly.sets['RF-Fixed'], couplingType=KINEMATIC  
    , influenceRadius=WHOLE_SURFACE, localCsys=None, name='Constraint-4',  
    surface=mdb.models['Model-1'].rootAssembly-surfaces['Cyl-Fixed'], u1=ON,  
    u2=ON, u3=ON, ur1=ON, ur2=ON, ur3=ON)
```

```
mdb.models['Model-1'].Coupling(controlPoint=  
    mdb.models['Model-1'].rootAssembly.sets['RF-Fixed'], couplingType=KINEMATIC  
    , influenceRadius=WHOLE_SURFACE, localCsys=None, name='Constraint-5',  
    surface=mdb.models['Model-1'].rootAssembly-surfaces['Ext-Fixed'], u1=ON,  
    u2=ON, u3=ON, ur1=ON, ur2=ON, ur3=ON)
```

```
mdb.models['Model-1'].Coupling(controlPoint=  
    mdb.models['Model-1'].rootAssembly.sets['RF-Fixed'], couplingType=KINEMATIC  
    , influenceRadius=WHOLE_SURFACE, localCsys=None, name='Constraint-6',  
    surface=mdb.models['Model-1'].rootAssembly-surfaces['Int-Fixed'], u1=ON,  
    u2=ON, u3=ON, ur1=ON, ur2=ON, ur3=ON)
```

```
#####  
#####
```

```
#####General  
Definition#####
```

Contact

```

mdb.models['Model-1'].ContactStd(createStepName='Initial', name='Int-1')

mdb.models['Model-1'].interactions['Int-1'].includedPairs.setValuesInStep(
    stepName='Initial', useAllstar=ON)

mdb.models['Model-1'].interactions['Int-1'].contactPropertyAssignments.appendInStep(
    assignments=((GLOBAL, SELF, 'IntProp-1'), ), stepName='Initial')

```

```

#####Interior    Tensile    wires    contact    definition
#####

```

```
n=0
```

```
for n in range(51):
```

```
    n=n+2
```

```

mdb.models['Model-1'].SurfaceToSurfaceContactStd(adjustMethod=OVERCLOSED,
    clearanceRegion=None, createStepName='Initial', datumAxis=None,
    initialClearance=OMIT, interactionProperty='IntProp-1', master=
    mdb.models['Model-1'].rootAssembly.instances['Interior-Anti-Wear-Tape-1'].surfaces['int-
anti-wear-outside']
    , name='Int-Wires-Inside-'+str(n), slave=
    mdb.models['Model-1'].rootAssembly.instances['Interior-Tensile-Wire-1-rad-
'+str(n)].surfaces['Int-tensile-inside']

```

```
, sliding=FINITE, thickness=ON, tied=OFF)
```

```
mdb.models['Model-1'].SurfaceToSurfaceContactStd(adjustMethod=OVERCLOSED,  
clearanceRegion=None, createStepName='Initial', datumAxis=None,  
initialClearance=OMIT, interactionProperty='IntProp-1', master=  
mdb.models['Model-1'].rootAssembly.instances['Interior-Anti-Wear-Tape-1'].surfaces['int-  
anti-wear-outside']  
, name='Int-Wires-Inside-0', slave=  
mdb.models['Model-1'].rootAssembly.instances['Interior-Tensile-Wire-1'].surfaces['Int-  
tensile-inside']  
, sliding=FINITE, thickness=ON, tied=OFF)
```

```
p=0
```

```
for p in range(51):
```

```
    p=p+2
```

```
mdb.models['Model-1'].SurfaceToSurfaceContactStd(adjustMethod=OVERCLOSED,  
clearanceRegion=None, createStepName='Initial', datumAxis=None,  
initialClearance=OMIT, interactionProperty='IntProp-1', master=  
mdb.models['Model-1'].rootAssembly.instances['Exterior-Anti-Wear-Tape-1'].surfaces['Ext-  
anti-wear-inside']  
, name='Int-Wires-Outside-'+str(p), slave=
```

```

        mdb.models['Model-1'].rootAssembly.instances['Interior-Tensile-Wire-1-rad-
'+str(p)].surfaces['Int-tensile-outside']

        , sliding=FINITE, thickness=ON, tied=OFF)

mdb.models['Model-1'].SurfaceToSurfaceContactStd(adjustMethod=OVERCLOSED,

        clearanceRegion=None, createStepName='Initial', datumAxis=None,

        initialClearance=OMIT, interactionProperty='IntProp-1', master=

        mdb.models['Model-1'].rootAssembly.instances['Exterior-Anti-Wear-Tape-1'].surfaces['Ext-
anti-wear-inside']

        , name='Int-Wires-Outside-0', slave=

        mdb.models['Model-1'].rootAssembly.instances['Interior-Tensile-Wire-1'].surfaces['Int-
tensile-outside']

        , sliding=FINITE, thickness=ON, tied=OFF)

```

```

#####Exterior      Tensile      wires      Contact
Definition#####
#####

```

T=0

for T in range(53):

T=T+2

```

        mdb.models['Model-1'].SurfaceToSurfaceContactStd(adjustMethod=OVERCLOSED,

        clearanceRegion=None, createStepName='Initial', datumAxis=None,

        initialClearance=OMIT, interactionProperty='IntProp-1', master=

```

```
    mdb.models['Model-1'].rootAssembly.instances['Exterior-Anti-Wear-Tape-1'].surfaces['Ext-  
anti-wear-outside']
```

```
    , name='Ext-Wires-Inside-'+str(T), slave=
```

```
    mdb.models['Model-1'].rootAssembly.instances['Exterior-Tensile-Wire-1-rad-  
'+str(T)].surfaces['ext-tensile-inside']
```

```
    , sliding=FINITE, thickness=ON, tied=OFF)
```

```
mdb.models['Model-1'].SurfaceToSurfaceContactStd(adjustMethod=OVERCLOSED,
```

```
    clearanceRegion=None, createStepName='Initial', datumAxis=None,
```

```
    initialClearance=OMIT, interactionProperty='IntProp-1', master=
```

```
    mdb.models['Model-1'].rootAssembly.instances['Exterior-Anti-Wear-Tape-1'].surfaces['Ext-  
anti-wear-outside']
```

```
    , name='Ext-Wires-Inside-0', slave=
```

```
    mdb.models['Model-1'].rootAssembly.instances['Exterior-Tensile-Wire-1'].surfaces['ext-  
tensile-inside']
```

```
    , sliding=FINITE, thickness=ON, tied=OFF)
```

```
k=0
```

```
for k in range(53):
```

```
    k=k+2
```

```
    mdb.models['Model-1'].SurfaceToSurfaceContactStd(adjustMethod=OVERCLOSED,
```

```
        clearanceRegion=None, createStepName='Initial', datumAxis=None,
```

```
initialClearance=OMIT, interactionProperty='IntProp-1', master=
mdb.models['Model-1'].rootAssembly.instances['Anti-Birdcaging-Tape-1'].surfaces['Anti-
Birdcaging-Inside']
, name='Ext-Wires-Outside-'+str(k), slave=
mdb.models['Model-1'].rootAssembly.instances['Exterior-Tensile-Wire-1-rad-
'+str(k)].surfaces['ext-tensile-outside']
, sliding=FINITE, thickness=ON, tied=OFF)
```

```
mdb.models['Model-1'].SurfaceToSurfaceContactStd(adjustMethod=OVERCLOSED,
clearanceRegion=None, createStepName='Initial', datumAxis=None,
initialClearance=OMIT, interactionProperty='IntProp-1', master=
mdb.models['Model-1'].rootAssembly.instances['Anti-Birdcaging-Tape-1'].surfaces['Anti-
Birdcaging-Inside']
, name='Ext-Wires-Outside-0', slave=
mdb.models['Model-1'].rootAssembly.instances['Exterior-Tensile-Wire-1'].surfaces['ext-
tensile-outside']
, sliding=FINITE, thickness=ON, tied=OFF)
```

```
#####
#####
```

#####Boundary COndition

Definition#####  
#####

```
mdb.models['Model-1'].DisplacementBC(amplitude=UNSET, createStepName='Initial-Curvature', distributionType=UNIFORM, fieldName="", fixed=OFF, localCsys=None, name='BC-1', region=mdb.models['Model-1'].rootAssembly.sets['RF-Fixed'], u1=0.0, u2=0.19, u3=0.0, ur1=0.155, ur2=0.0, ur3=0.0)
```

```
mdb.models['Model-1'].DisplacementBC(amplitude=UNSET, createStepName='Initial-Curvature', distributionType=UNIFORM, fieldName="", fixed=OFF, localCsys=None, name='BC-2', region=mdb.models['Model-1'].rootAssembly.sets['RF-Moving'], u1=0.0, u2=0.19, u3=UNSET, ur1=0.155, ur2=0.0, ur3=UNSET)
```

```
mdb.models['Model-1'].boundaryConditions['BC-2'].setValuesInStep(stepName='Compression', u3=-0.1)
```

#####Job

Definition#####  
#####

```
mdb.Job(atTime=None, contactPrint=OFF, description="", echoPrint=OFF, explicitPrecision=SINGLE, getMemoryFromAnalysis=True, historyPrint=OFF, memory=90, memoryUnits=PERCENTAGE, model='Model-1', modelPrint=OFF,
```

```
multiprocessingMode=DEFAULT, name='Lateral-Buckling-General-Model',  
nodalOutputPrecision=SINGLE, numCpus=4, numDomains=4, numGPUs=0, queue=None  
, scratch="", type=ANALYSIS, userSubroutine="", waitHours=0, waitMinutes=0)
```